A finger function simulator and surface replacement prosthesis for the metacarpophalangeal joint

Susan Marie Stokoe

A FINGER FUNCTION SIMULATOR AND SURFACE REPLACEMENT PROSTHESIS FOR THE METACARPOPHALANGEAL JOINT

by

Susan Marie Stokoe

Thesis submitted for the degree of

Doctor of Philosophy

at the

University of Durham

School of Engineering and Applied Science

University of Durham

Science Site

South Road

Durham City

DH1 3LE

September 1990

"The hand is more than a tool: it is a means of expression - Man's second face"

Schilling

To Ian

with gratitude

xxxx

CONTENTS

ABSTRACT

"A finger function simulator and surface replacement prosthesis for the metacarpophalangeal joint"

Susan Marie Stokoe

Joint replacement surgery in the treatment of arthritic disease is now commonplace and on the whole very successful. Research into the design and development of prostheses has made major advances since the 1940s resulting in complex devices for almost all articulating joints of the body. In this thesis, a programme of work to design and test a surface replacement prosthesis for the metacarpophalangeal joint is presented. The anatomy and kinematics of the MCP joint are discussed for both normal and abnormal joint function and, based on these considerations, the design of a new surface replacement prosthesis is described. Various materials are explored with respect to their biocompatibility, durability and ease of fabrication with special attention being paid to one material - a new cross linked ultra-high molecular weight polyethylene - which is tested for wear and assessed for durability in long-term prototype tests. A finger function simulator is detailed which was designed and developed during this research programme, and results of tests on bone replicas, Swanson Silastic implants and prototypes of the new design are presented. The simulator can be easily modified to accept any MCP joint prosthesis for bench testing. Finally the stress response of the prototype design is studied using finite element analysis and modifications to the implant design and bone preparation are suggested.

DECLARATION

The work presented in this thesis was carried out in the School of Engineering and Applied Science at the University of Durham between October 1985 and September 1988. This material has not been submitted previously for any degree in this or any other university.

No claim of originality is made for Chapter 1 but the remaining Chapters 2 to 8 are claimed as original, except where authors have been specifically acknowledged in the text. Material from Chapters 3 & 4 is to be published in Engineering in Medicine: Part H of the Proceedings of the Institution of Mechanical Engineers.

ACKNOWLEDGEMENTS

The author would like to thank all the staff of the School of Engineering and Applied Science for their help and advice, in particular Professor A Unsworth for his role as supervisor and Mr G Turnbull for his excellent craftsmanship. The author also acknowledges useful discussions with Dr C Woodford of the Computing Department at the University of Newcastle and the co-operation of Mr G Manders at Chas F Thackray & Sons Ltd. The author is very grateful for the electron microscopy work done by Mr W H Chatwin, and the photographic work by Dr T L Shaw and Mrs M Ford at AEA Windscale. Thanks are due to the UK Science and Engineering Research Council for their financial support (Studentship No. 85302660). Finally the author wishes to thank sincerely her husband, Ian, for typing this thesis and for his patience and understanding during its completion.

CHAPTER 1

INTRODUCTION AND LITERATURE REVIEW

1.1 INTRODUCTION

Rheumatoid arthritis is a chronic progressive disease which can affect both males and females at any stage in their lives. Often the small joints of the hand are affected and sufferers have their quality of life severely impaired due to the pain, deformity and loss of dexterity. There is no cure for this crippling disease and treatment is conservative, usually involving a combination of drugs, physiotherapy and surgery. During the last thirty years engineers and surgeons have worked hard to develop joint replacement prostheses for the rheumatoid hand, spurred on by the successes in hip and knee implant surgery. This thesis describes a programme of work to develop a novel surface replacement prosthesis for the metacarpophalangeal (MCP) joint.

The essential stages for the design of any surgical joint implant are as follows:

i) A detailed study of both normal and abnormal joint function.

ii) Analysis of the material properties of the prosthetic device.

iii) The design of a prototype on the basis of experience gained in i) & ii).

iv) Testing of the artificial joint in the laboratory before clinical use and modification of the prototype.

v) The analysis of stress responses in the implanted joint and the investigation into possible failure mechanisms (again making necessary modifications to the prototype).

vi) The clinical assessment of the functional result by objective measurements.

vii) The review of post-operative complications in order to define defects in material, design or surgical technique.

The work presented in this thesis covers stages i) - v) and research is continuing at the University of Durham to progress to clinical trials.

The thesis opens with an historical look at finger implant surgery and related fields of interest, along with a review of the available literature, though it is true to say that very little has been published during the last decade. For this reason it was necessary to enter into private communication with surgeons and designers internationally to effect a survey of current trends in surgical treatment of the rheumatoid hand. This correspondence has proved very fruitful and, while being mentioned here in Chapter 1, current philosophy is discussed in more detail in Chapter 8.

In the opening review five topics are discussed which are essential to the understanding of the problems involved in the treatment of the MCP joint and it is intended that within this discussion some justification shall be given for the paths taken in the course of the research programme. Two topics which might also have been reviewed in Chapter 1 were biotribology and finite element analysis. However, it was felt that these might be more helpful in context and hence they are included in the introductory sections of the relevant chapters.

Chapter 2 comprises a description of the early design stages of the Durham surface replacement prosthesis based on information obtained from the literature. A programme of metrology performed on the bones of five hands is described in detail along with the preliminary assessment of

hand-made model implants. The design of a finger function simulator in which the prototypes were tested is discussed in Chapter 3, and an evaluation of its performance through commissioning trials and tests on the Swanson Silastic implant is presented in Chapter 4. Also in Chapter 4 is a more detailed look at the mechanics and function of the MCP joint. The crucial bench testing of the prototype implant is related in Chapter 6 with a critical assessment of damage mechanisms and the implications for implant integrity.

The implant material, prior to cross linking, was studied in wear tests described in Chapter 5, and finite element analyses, to highlight stress concentrations in the implanted joint under a heavy static load, are presented in Chapter 7. Chapter 8 concludes the thesis with a summary of the main results of the work and a general discussion about the achievements of the research, with recommendations concerning the continued development of this prosthesis in the light of current philosophy on the treatment of the rheumatoid hand.

1.2 ANATOMY

1.2.1 Osteology

The bones of the hand comprise the carpals, metacarpals and phalanges. The wrist or carpus consists of eight small bones arranged in two rows. The bones are named in order from the lateral (radial) side to the medial (ulnar) side.

Proximal row	Scaphoid (articulates with radius)
	Lunate
	Triquetral
	Pisiform (smallest carpal bone)
Distal row	Trapezium (articulates with the metacarpal on the thumb side)
	Trapezoid
	Capitate (largest carpal bone)
	Hamate (bears the hamulus, a hook-like process projecting toward the volar surface)

The bones of the palm are called metacarpals and are numbered I to V. The base of each is irregular in shape and articulates with the proximal phalanx of the corresponding digit. Each of the three bones in the finger (two in a thumb) is called a phalanx, the base of which is concave to receive the head of the metacarpal, and the head of which forms a pulley-like surface called the trochlea.

The skeletal structure of the hand is illustrated in Figs 1.1 & 1.2.

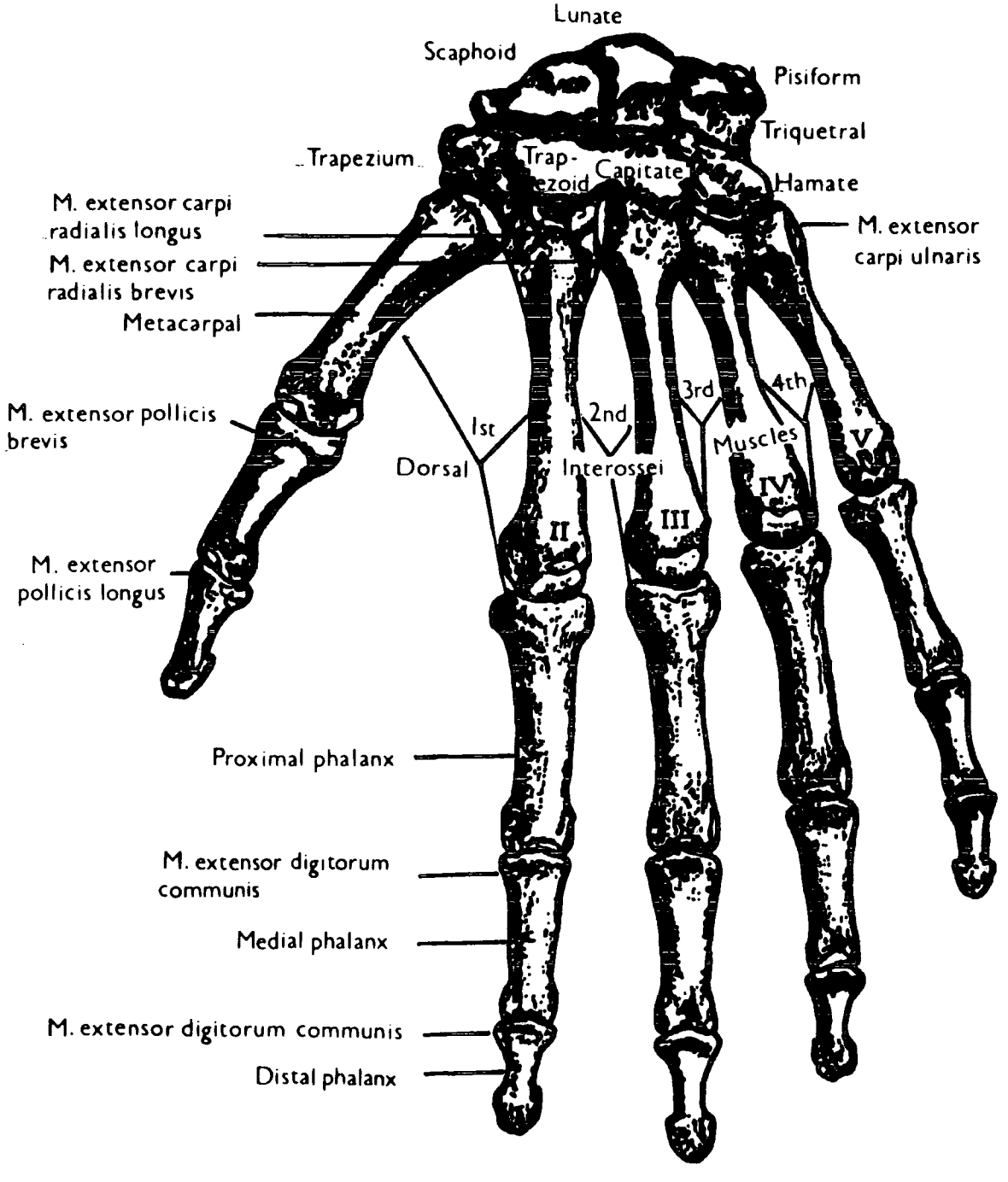

Left hand, dorsal surface.

Fig 1.1 The skeletal structure of the hand (1).

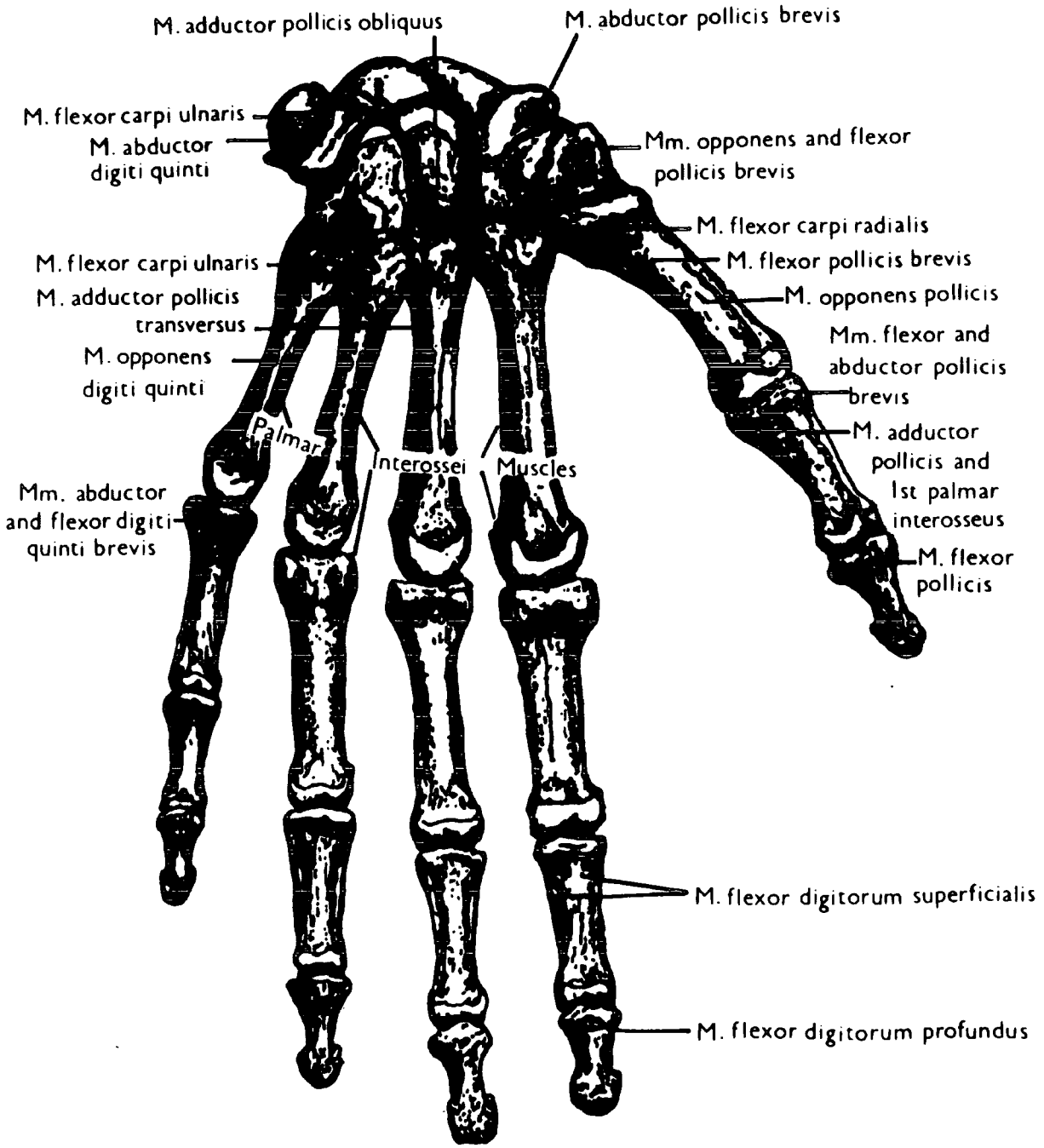

Left hand, palmar surface.

Fig 1.2 The skeletal structure of the hand (2).

1.2.2 Articulations

The articulations of the hand are diarthrodal. A typical diarthrosis consists of: articular cartilage, which covers the articulating surfaces; an articular capsule, completely enveloping the joint and having two layers (an outer fibrous and an inner synovial); a joint cavity, a space within the capsule lined with the synovial membrane and containing a small quantity of synovial fluid; and ligaments, bands of connective tissue which bind the bones together, not generally very elastic but permitting movement and at the same time acting to limit the degree of movement.

1.2.3 The Metacarpophalangeal Joint

The articulation of the hand that is the focus of the research reported in this thesis is the metacarpophalangeal joint. This joint (Fig 1.3) is of the condyloid type with movements about two axes at right-angles (flexion/extension in the sagittal plane and abduction/adduction in the frontal plane).

The metacarpal head is an approximately spherical articular surface which is broader anteriorly than posteriorly, and the base of the proximal phalanx has an ellipsoidal articular surface with spherical curvature. Attached to the palmar surface of the base of the phalanx is the 'volar plate' or ligament. Its attachment to the articular cartilage of the phalanx is formed by a small fibrous band called the 'incisura' (Fig 1.3(3)) which acts like a hinge. During extension the medial cartilaginous half of the volar plate articulates with the metacarpal head. During flexion the plate moves past the metacarpal

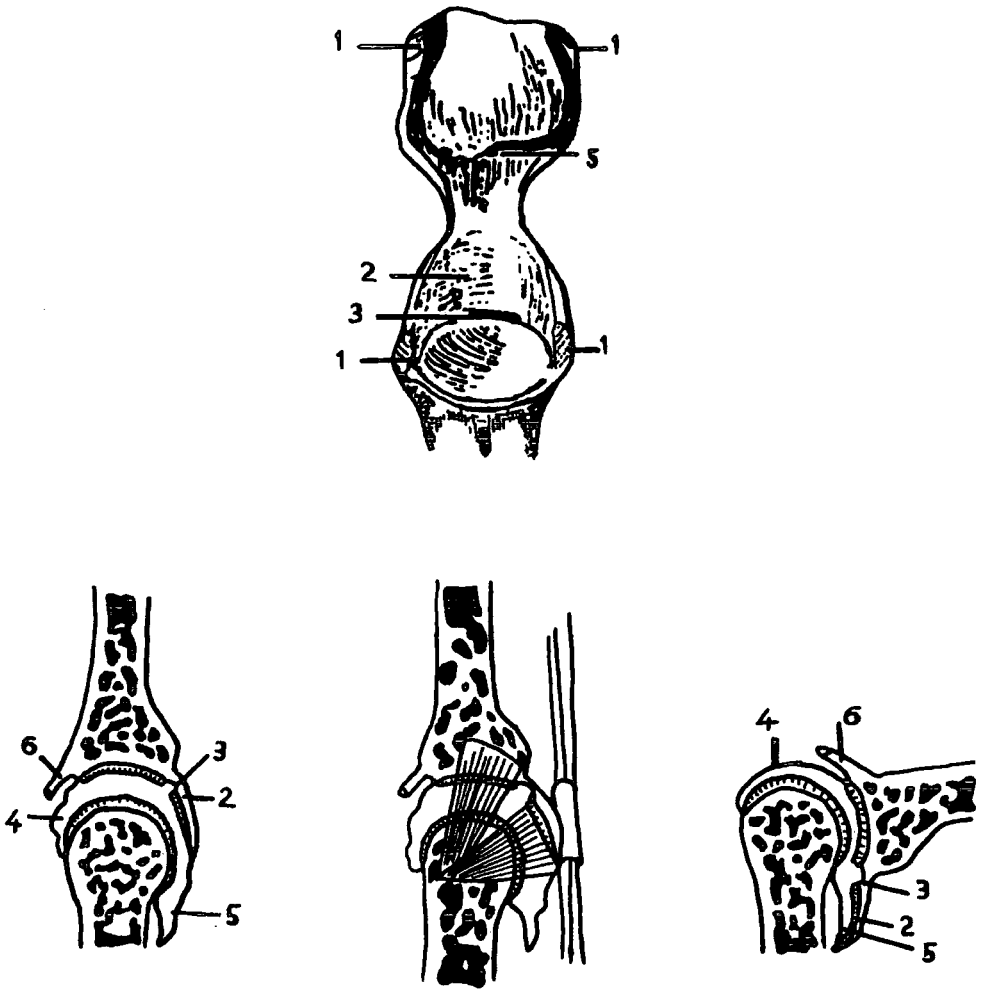

Fig 1.3 The metacarpophalangeal joint.

head and glides along the palmar surface of the metacarpal. The flexor tendon sheath is attached to the palmar surface of the plate.

An essential condition for the freedom of movement in this joint is a certain degree of flexibility in the joint capsule and synovium. This is provided by the 'dorsal' (Fig 1.3(4)) and 'palmar' (Fig 1.3(5)) recesses of the joint capsule. Also the presence of the palmar recess is essential for the gliding movement of the volar plate during flexion. On the dorsal surface of the base of the phalanx is inserted the 'deep attachment' (Fig 1.3(6)) of the extensor tendon. On each side of the joint there are two types of ligament (Fig 1.3): the 'glenoidal' ligament, joining the metacarpal to the volar plate and controlling the movements of the latter, and the 'collateral' ligament, joining the metacarpal head to the phalanx base, which keeps the articular surfaces together and restrains their movements. The insertion of the ligaments into the metacarpal head is slightly dorsal to its centre of curvature. Thus they become lax in extension and taut in flexion.

Abduction and adduction become more difficult when the MCP joint is flexed and in full extension. The maximum ranges are 20° to 30° either side. In the sagittal plane the MCP has a range of about 20° hyperextension to 90° flexion for the index which increases progressively to the little finger. Being a condyloid joint the MCP joint does not normally show active axial rotation. However, owing to laxity of the ligaments, a measure of passive rotation is possible with a range of about 60°.

1.2.4 The Flexor Tendons of the Fingers

The muscles of the digital flexors lie in the anterior compartment of the forearm and are thus considered extrinsic muscles in relation to the hand. The tendons of these muscles pass across the hand and attach to the fingers.

There are two main flexors of the fingers. The most superficial tendon is the 'flexor digitorum sublimis' (FDS) which has its insertion on the middle phalanx proximal to that of the deep tendon or 'flexor digitorum profundus' (FDP) which attaches to the base of the distal phalanx. Obviously then, the two tendons must cross each other and do this symmetrically to avoid any unwanted lateral force. To achieve this the profundus passes through the sublimis (Fig 1.4). Why is it that the attachments of the two tendons are this way round, necessitating such a crossing? By staying superficial to its insertion the sublimis maintains a greater angle of contact with the bone which enhances its efficiency.

The action of the two flexors can be deduced from their points of insertion: the FDS is inserted into the middle phalanx thus flexing the proximal IP joint (Fig 1.4(3)). It is a weak flexor of the MCP joint when the proximal IP joint is flexed and has no effect on the distal IP joint. It has maximum efficiency when the MCP joint is extended by the synergistic action of the 'extensor digitorum communis' (EDC). The FDP (Fig 1.4(4)) is inserted into the distal phalanx and thus flexes the distal IP joint. It too flexes the proximal IP joint and is a weak flexor of the MCP joint. If the MCP and proximal IP joints are passively flexed the profundus cannot flex the distal IP joint because

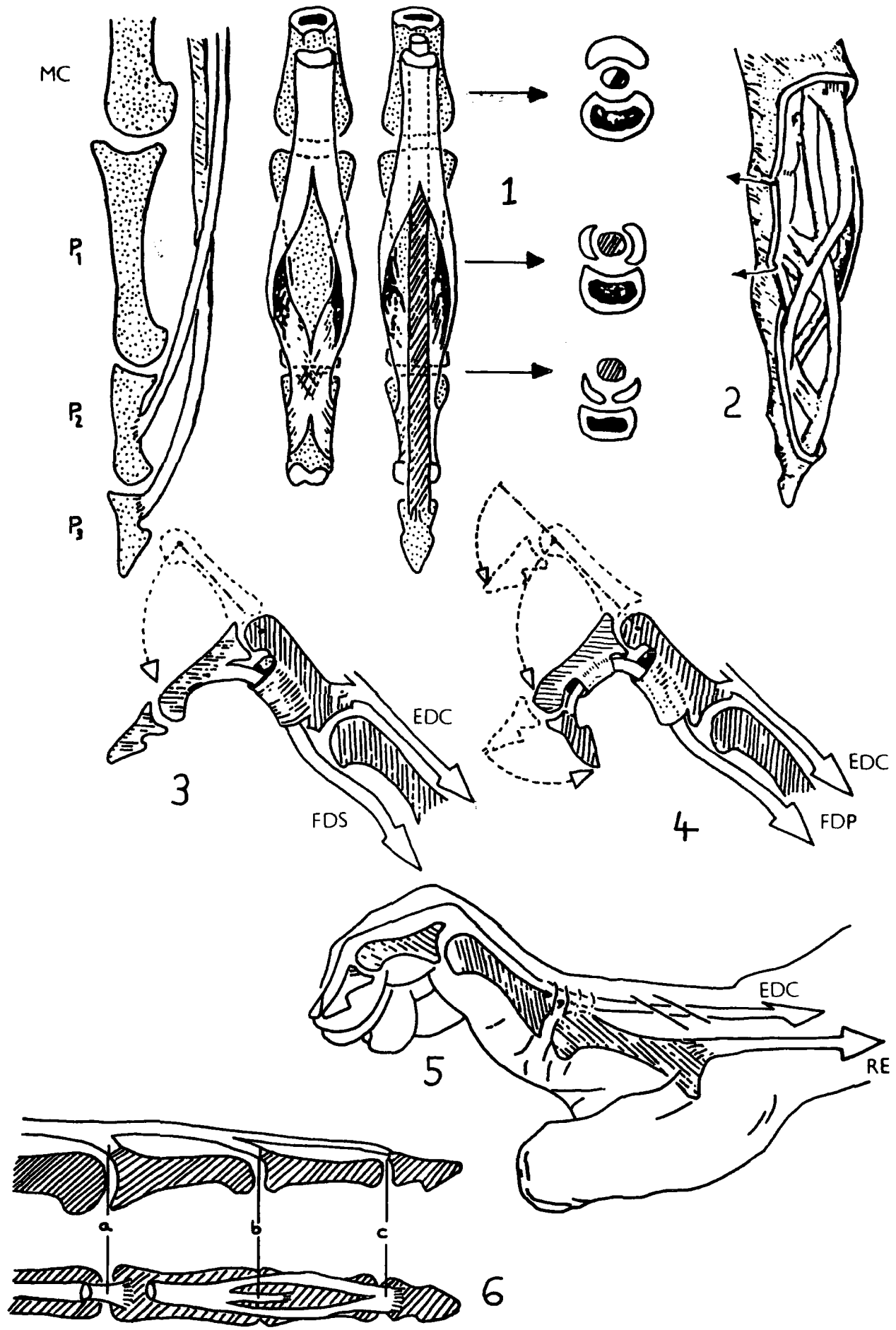

Fig 1.4 The tendons of the fingers.

it is too slack. Again it works to best advantage when the MCP joint is extended.

1.2.5 The Extensor Tendons of the Fingers

The extensors too are extrinsic muscles of the hand but having, on the whole, a convex path through the hand, they need fewer tunnels than the flexors. The extensor tendons passing through the wrist to the digits, medio-laterally, are:

i) The 'extensor digiti minimi' which more distally joins the extensor digitorum communis for the little finger.
ii) The four tendons of the 'extensor digitorum communis' (EDC).
iii) The 'extensor indicis' which more distally joins the EDC for the index.

The EDC is a powerful extensor of the MCP joint and active in any wrist position. Extension of the MCP joint is via the extensor expansion, which is about 10 mm long, arising from the deep surface of the tendon, crossing the joint capsule and inserting into the base of the proximal phalanx (Fig 1.4(6a)). Its action on the proximal IP joint is through the median band (Fig 1.4(6b)), and on the distal IP joint is through the two lateral bands (Fig 1.4(6c)). This action, however, does depend on the degree of tension in the ligament, and thus the position of the wrist: appreciable when the wrist is flexed, weak when the wrist is straight, and negligible when the wrist is extended. Also the degree of tension in the digital flexors is important.

The tendons of the extensor indicis and the extensor digiti minimi

behave in the same way as EDC but allow the index and little finger to move independently.

1.2.6 The Interosseous and Lumbrical Muscles

The interosseous and lumbrical muscles are intrinsic muscles of the hand which essentially act as synergists and antagonists to the actions of the flexors and extensors as well as producing movements of abduction and adduction. The interossei have two functions: abduction/adduction and flexion/extension. The ability to abduct and adduct arises from the attachment of part of their tendon insertion into the lateral tuberosity at the base of the proximal phalanx. The dorsal interossei (Fig 1.5(1&3)) run towards the axis of the hand, thus producing abduction. The middle finger will not move if the second and third interossei contract simultaneously. Abduction of the little finger is by the abductor digiti minimi (Fig 1.5(2)). The volar interossei are larger and more powerful than the dorsal interossei. The four lumbrical muscles (Fig 1.5(4)) arise from the radial aspects of the tendons of the FDP. Their tendons run distally then curve in medially and are at first separated from the tendons of the interossei by the deep transverse palmar ligament. Finally they blend with the third interosseous expansion distal to the extensor expansion.

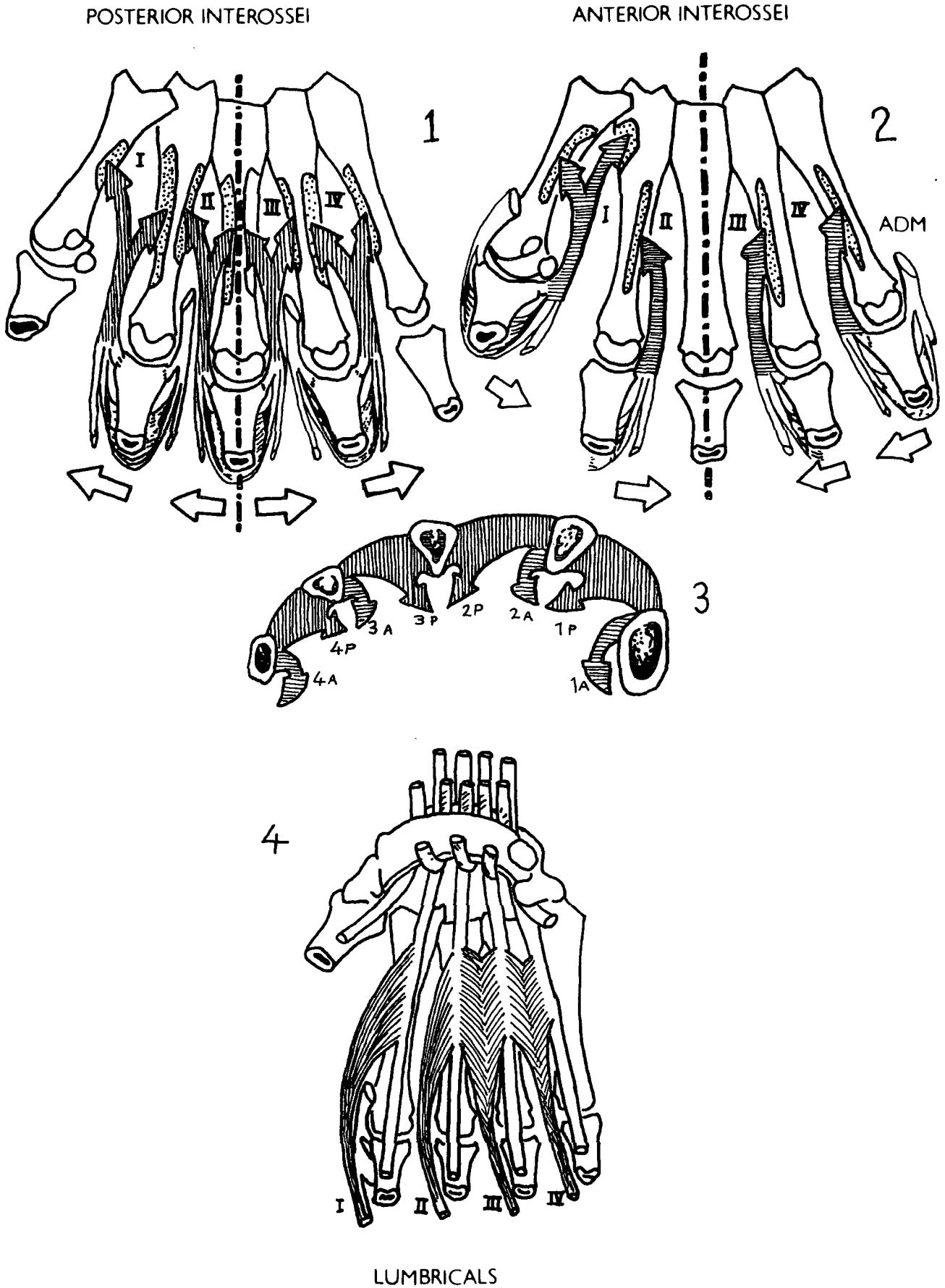

Fig 1.5 The intrinsic muscles of the fingers.

1.3 BIOMECHANICS

The MCP joint is by no means a simple structure anatomically. The relative importance of local soft tissue structures in joint function and stability, and the magnitude of forces in ligaments, tendons and the joint itself must be known before its action can be successfully simulated.

Research has dealt extensively with the analysis of MCP joint mechanics but the few attempts made to quantify joint forces have resulted in very different values, largely as a result of the variation in simplifying assumptions.

One of the most informative pieces of work in this field was published by Weightman & Amis in 1982 (1) which presented a review of several biomechanical models and, by reconciling the differences between them, gave a guide as to which data are the most reliable. The paper went on to describe a new model, based on the successful elements of the reviewed models, and this will be discussed later in this section. An early paper written on this subject was by Smith et al in 1964 (2). The authors dissected a cadaveric index finger fixed in an unspecified tip pinch position, and from it measured moment arms which they then used in a two-dimensional model of the finger. They were able to work out a force polygon for the MCP joint and concluded that for a force P acting at the finger tip, the force at the joint due to the flexors would be 7.5 P. Since no detailed description of finger position was given the results are unclear, but seem to differ considerably from results of other authors (as will be demonstrated). The answer to this may lie in

the fact that the assumptions of the model greatly simplified the contribution of the intrinsic muscles and ignored the capsulo-ligamentous structures surrounding the joint altogether. This is rather surprising in view of the fact that the authors went on to consider the aetiology of rheumatoid deformities and stressed the importance of the collateral ligaments and the presence of the volar plate for stability of the joint. In pinch action the long extensors were assumed to be relaxed. This assumption was based on evidence from electromyographic traces, as demonstrated by Long et al in 1970 (3), and is common to many biomechanical models of the MCP joint. The radial and ulnar interossei were treated as a single force - half acting on the proximal and half on the distal interphalangeal (IP) joint. The lumbrical muscle was assumed to exert a force equal to one sixth of the interosseous force.

In 1968 Flatt & Fischer (4) published a very brief report which presented a graph showing the variation of forces acting on the MCP joint and its surrounding structures for a range of joint positions during finger tip action. Their results were very odd indeed, showing compressive ligament actions and joint forces varying from 0.8 P to 8 P (where P is the force applied at the finger tip) with the resultant force always acting 70° to 80° to the axis of the proximal phalanx. No explanation for these results can be found in the original paper but in a private communication from G W Fischer in 1976 a more detailed description of the model was given. The authors had treated the MCP joint as a free body in two dimensions with no consideration of the more distal joints of the finger. The long extensor tendon was assumed to be relaxed and the intrinsic muscles were ignored completely, leaving only a single flexor tendon force which was taken to equal 6 P. The actions of soft tissue structures were invoked to establish static equilibrium

in the joint and these were described in great detail, including contributions from the collateral ligaments, the glenoidal ligaments, the volar plate and the joint capsule itself. Clearly the problems of the model arise from the gross over-simplification of the major load carrying components of the finger and the misplaced emphasis on the soft tissue structures, commonly absent in other models. It is unlikely that any of the results in this report are of use.

Berme, Paul & Purves (5) were dissatisfied with previous two-dimensional treatments of the MCP joint and criticised the fact that other models were not based on experimental measurements of external force, nor did they generally include consideration of ligamentous structures. In 1977 the authors studied index finger MCP joint forces using a three-dimensional model. Six female cadaver specimens were dissected and photographed from various angles to identify the dimensions and lines of action of the major load-carrying components within the MCP joint at four positions of flexion. Four healthy females were asked to perform tap turning and tip pinch actions on transducer devices and they were filmed from two orthogonal directions for skeletal geometrical information. The authors recognised the importance of finger posture in the assessment of these tests. Their model included consideration of the collateral ligaments and the intrinsic muscles and the flexor apparatus was simplified to a single force. Equilibrium of the PIP and MCP joints was considered with lateral moments and torsion being balanced by the intrinsic muscles and ligaments. Moment equations were solved using the constraint that no compressive forces could exist in muscle or ligament, and sometimes required long extensor activity. They revealed a mean MCP joint force of 5.5 P for an average tip pinch position. This is somewhat lower than the value reported by Smith et al

(2). In a later paper by Purves et al in 1978 (6) this work was extended and the model was modified to include a more detailed description of the PIP joint. However, for this joint the model was statically indeterminate (a problem common to three-dimensional models) and this forced further assumptions that the long extensor and also the collateral ligaments were relaxed.

The other main champions of the three-dimensional approach were researchers from the Mayo Clinic who felt that simplified planar analysis was insufficient to provide quantitative data for the purpose of joint reconstructive surgery. In 1976 Chao et al (7) dissected fresh cadaveric fingers and manipulated the specimens to mimic pinch and grasp configurations. The tendons were marked with Kirschner wires and bi-planar radiographs were taken for the determination of tendon geometries. The authors then devised a three-dimensional model of the finger in which no attempt was made to describe the stabilising effect of soft tissue structures. Rather, for this role, passive action of the long extensor was invoked. The function of the intrinsic muscles was fully described. Free body analysis was applied at each of the three joints from which were obtained nineteen equations with twenty-three unknowns. To solve this statically indeterminate problem the authors systematically relaxed sets of tendons to produce one hundred and twenty-six possible solutions. Those solutions giving compressive tendon forces, tensile joint forces or excessive extensor force magnitudes, were rejected and an average was calculated from the remaining solutions. Because of the unfortunate subjectivity of this method, and the fact that the results presented included three different types of pinch grip, the authors presented an MCP joint force prediction of 8.8 P which is rather higher than might be expected. It perhaps

would have been more appropriate if the authors had systematically applied constant, non-zero tensions to sets of tendons making the problem determinate, since there is no reason to relax anything other than the long extensors.

This team published a further three papers in the following two years, all based on the same model but considering only tip pinch action. The first of these by Chao & An in 1978 (8) described new, more complex, relationships between the forces developed by the extensor and the intrinsic muscle structures, and an alternative method to the solution of the redundant problem using linear programming. This report gives similar muscle and joint force predictions to those of the first paper, quoting the MCP joint force to be 8.6 P. However this work was based on a rather more extended finger posture. In the same year Chao & An (9) published another paper, this time using the same finger posture as in the first report (7) but employing yet another method of solution involving graphical techniques. In this case the extensor contribution was concluded to be 4.1 P which is very much higher than any previously seen. Again in 1978 An et al (10) predicted no extensor action for tip pinch and joint forces at half the levels seen in their previous publications. Later, in 1985, An et al (11) used their model to compare forces in the normal and abnormal hand for various everyday activities and also to evaluate various treatment modes. In this paper the normal MCP joint force for tip pinch grip lay in the range 3.5 - 3.9 P. It is apparent that the considerable differences between the results of these reports, which employ basically the same model, raise serious doubts as to the validity of this method.

In 1982 Weightman & Amis (1) looked very closely at all the models

described here in order to facilitate the formulation of a new model that was well defined and not over-simplified. The report attempted to reconcile the differences between the models and to give some indication of their overall validity. The authors did acknowledge that to model complex activities, such as lateral pinch and tap turning, a three-dimensional model would be needed. They also, however, expressed serious reservations as to the accuracy of the predictions of these in view of the problems apparent in the Mayo Clinic models. As a result, Weightman & Amis reasoned that a two-dimensional model was sufficient to describe pinch grip and, if applied to assess force responses for several finger postures, would provide a great deal of information on finger function. They felt that previous models, which concentrated on a single posture, were lacking in their facility to aid joint designers.

As in all the models described here, the authors assumed a pin-jointed model. All three joints of the finger were included and the intrinsic muscle relations were taken to be identical to those of Chao & An (8) in that:

(a) one-third of the radial interosseous tension acts on the extensor slip and two-thirds on the proximal phalanx,

(b) one-third of the ulnar interosseous tension acts on the extensor slip, one-third on the ulnar band, and one-third on the proximal phalanx, and

(c) one-third of the lumbrical tension acts on the extensor slip and two-thirds on the radial band.

However, they assumed the long extensor tendons to be relaxed where Chao & An did not. It was pointed out that the assumptions of the model were only valid in mid-range positions since tension proportions depend on

angles of flexion. In the first instance there was no consideration of ligamentous structures but later it was realised that the shear components of joint forces increase with flexion and that the predicted joint force acted at or outside the edge of the articular contact of the joint. This was a clear indication of the importance of capsulo-ligamentous support in preventing volar subluxation (the palmar dislocation deformity commonly seen in arthritis sufferers). The original model was modified to take account of the collateral ligaments making the following assumptions:

(a) the lines of action of the collateral ligaments pass through the centre of rotation of the joint at a fixed angle of 45° to the axis of the proximal phalanx, originating from a dorsal position on the metacarpal head and inserting on the volar tip of the phalanx, and

(b) the tension in the ligaments would not significantly affect the tendon tensions, since the moment arms of the collateral ligaments about the joint are very much smaller than those of the tendons.

The ligaments were invoked to hold the angle of the resultant force at 20° to the axis of the proximal phalanx thus stabilising the joint by keeping the resultant within the concavity of the articulation (as described by Walker & Erkman in 1975 (12)). The authors did not examine the capacity of the metacarpoglenoidal ligaments to absorb some of the shearing component of the joint force although this mechanism will be described briefly in Chapter 4 along with a more detailed review of the Weightman & Amis model. Generally, over the range of postures described in this work MCP joint forces were predicted to lie between 3.6 P and 5.6 P, with the subluxing component of the force increasing with increased flexion. The model embodies the successful elements of the

previous models and has been carefully thought out. In this thesis no attempt has been made to formulate yet another MCP joint model but rather results are assessed in terms of their agreement with Weightman & Amis where it has been practical to do so.

In the discussion of biomechanical models for the finger all MCP joint forces were expressed merely as a factor of P (the force applied at the finger tip) but, for the purposes of building a finger function simulator, pinch grip strength must be quantified. Many methods have been used for this purpose with varying results and measurements from some of the more recent strain-gauged devices are reviewed here.

In 1974 Swanson et al (13) measured normal grip strength in a group of one hundred healthy subjects (fifty males and fifty females) who were asked to apply pulp pinch grip to a disc measuring 2.2 cm diameter and 0.5 cm thick, being allowed to adopt their preferred posture (not recorded). The average tip pinch strength in the index fingers was found to be 53 N for males and 36 N for females.

In 1977 Berme et al (5) measured four normal female subjects performing pinch grip with the index finger and thumb on a 45 mm diameter cylinder. Again the subjects used their preferred grip posture but were filmed doing so, that the postures might be recorded. The forces applied to the cylinder were in the range 18 - 21 N which is rather lower than the results of other authors. This may have been due to a fault in the apparatus or just a consequence of the small population tested.

Also in 1977, Walker & Erkman (14) reported an average maximum pinch strength of 74 N in male index fingers and 56 N in females. Their

population consisted of sixty-five male and eighty female subjects. The apparatus used was not described in great detail but appeared to consist of two cantilevers separated by ~1 cm, the idea being to close the gap. Tests on pre-operative arthritic patients revealed a maximum pinch strength of only 13 N (some 20% of normal). The authors reported that strengths after implant surgery were not markedly improved though no figures were given. The same conclusion was reached by Opitz & Linscheid (15) in 1978 when they compared hand function in rheumatoid patients before and after MCP joint replacement with the Swanson silastic spacer. Tests were performed on a three-jaw chuck pinch.

An et al in 1978 (10) modified the Walker & Erkman apparatus and used it on forty normal subjects (eighteen male and twenty-two female) to measure tip and pulp pinch forces. They found little difference between the two types of pinch and reported an average maximum strength of 65 N in male and 47 N in female index fingers (a little lower than the earlier results obtained using the same equipment).

Again using similar apparatus, Weightman & Amis in 1982 (1) asked eleven healthy young female subjects to apply a pinch grip and obtained a mean value of 35 N for the strength in the index finger. In this report the authors compared strengths for different postures and observed no difference between them. This is in agreement with An et al (10).

In 1985 Jones et al (16) measured pulp pinch strength in fifty-eight subjects (twenty normal and thirty-eight patients, sex not listed) as part of a programme of work to devise a comprehensive set of tests for hand assessment. For normals they measured a strength of 57 N in the index finger compared with 19 N for patients. In 1979 Linscheid &

Dobyns (17) reported pinch strength in the pre-operative rheumatoid patient to lie in the range 5 - 20 N.

In all the papers described here the authors reported a large scatter in the data (~25% standard deviation) and it is not surprising therefore that the results obtained, using different equipment and sample populations, are quite varied.

To sum up, the healthy male can exert a force of around 65 N in pulp pinch and the female some 72% of this. The force resulting at the level of the MCP joint due to this pinch is 3.6 - 5.6 times greater, that is, up to 364 N. In pre-operative arthritic patients strength is very poor (5 - 20 N) and it is not clear that there is much improvement after implant surgery. However, in 1978 Hagert (18) described reports of 100% increase in strength for the Flatt and Swanson models - in other words, a possible joint force of 224 N. The finger function simulator, described in Chapter 3, was designed with the specification that it should periodically apply a static joint force of 200 N with the joint at 30° flexion to simulate pinch action.

The limiting factor in strength improvement will always be the condition of the soft tissue structures, particularly for implants with little inherent stability, and unless techniques to repair the soft tissues improve greatly there can be little hope of vast improvements in strength or joint stability. The reasons for this will become more apparent in the next section.

The biomechanical models described in this section have all treated the finger as a pin-jointed structure with the joints having constant

centres of rotation. It should be recognised, however, that this is not an undisputed assumption - around 50% of researchers would disagree. It is therefore worth considering here since it must affect the design of the implant. For example, many elbow prostheses are hinge joints and hip replacements are ball and sockets. Both types indicate circular or spherical motion and hence fixed centres of rotation. On the other hand, many unconstrained knee prostheses are based on a moving centre of rotation concept.

In 1971 Unsworth et al (19) and later in 1979 Unsworth & Alexander (20) reported very detailed measurements on the metacarpal and proximal phalanx. Their main conclusions were that the articulating surfaces of both the metacarpal and phalanx were spherical to within six percent, and specifically in the sagittal plane, the radius of the phalanx was generally a little larger than that of the corresponding metacarpal (the converse was true in the transverse plane). The authors stated that the geometry of the joints implied a constant centre of rotation. The spherical nature of the bones is not generally contested but, in their experiments to locate the centre of rotation of the MCP joint, Aleksandrowicz et al in 1974 (21) and Walker & Erkman in 1975 (12) concluded that not only does the phalanx slide around the metacarpal head but that it also rocks by virtue of the difference in radius between the bones and the action of the ligamentous structures. In other words, the point of contact moves from the dorsal side of the phalanx to the palmar side during flexion, which in turn implies that the centre of rotation must move. These studies both involved the passive movement of a relaxed cadaveric joint which makes them rather subject to error. In 1977 Pagowski & Piekarski (22) gave a mechanical description of this sliding and rolling action concluding that the

centre of rotation must move on an arc of radius 1.5 mm about the radius of curvature of the metacarpal head.

Earlier in 1968 Bartel et al (23) performed an experiment in which subjects actively flexed the MCP joint with tracings of the motion being made on X-ray film. Using a method of over-determined collocation the authors concluded that the centre of rotation is fixed to within 0.25% of the radius. These results were confirmed in 1978 by Youm (24) using the far more sophisticated three-dimensional sonic digitiser on passively moved cadaveric fingers. In this case all the tendons were loaded to simulate physiological muscle tone.

With the conflicting evidence it is difficult to say whether or not the described rocking motion occurs. Certainly, if it does occur it is a small effect and may have little significance on the function of the joint. Supporters of this idea suggest that the motion is important for movement of synovial fluid between the cartilage surfaces and also that wear will be more evenly distributed if the point of contact changes. The author finds it difficult to comment on the first point, this again being a large area of disagreement. The second point is hardly valid since the conforming radii are really very similar and cartilage is not rigid, thus the load is distributed over a reasonable area preventing localised wear.

With these arguments in mind, the Durham surface replacement was designed to have exactly conforming surfaces. The advantages in doing this are as follows:

i) Both surfaces being spherical sections are far easier to manufacture than trying to accommodate the 6% non-sphericity found

in some, but not all, bones.

ii) The area of contact is maximal and hence local surface stresses are minimised - this will help reduce penetration.

iii) A totally conforming joint has more resistance against subluxation - though admittedly only marginally so.

In this way a constant centre of rotation is built into the design. It is of course possible to use different sizes of component thereby re-introducing the propensity to rocking (if such exists) though it is difficult to see how complex motion of this nature can be assured after the disturbance of the soft tissue structures through disease and surgery.

1.4 THE AETIOLOGY OF RHEUMATOID DEFORMITIES OF THE MCP JOINT AND THEIR SURGICAL TREATMENT

Rheumatoid arthritis has a predilection for attacking the wrist and finger joints, severely limiting hand function. The synovial membranes of the joints and tendons become inflamed and thickened, secreting enzymes and this results in secondary changes in the surrounding structures which can cause near total destruction of the joint. The joint is distended by the proliferation of the pannus which causes severe pain and a reduction in movement. Secondly, the peripheral cartilage adjacent to the thickened synovium is eroded, exposing subchondral bone which is itself further eroded, causing large bony defects and skeletal shortening. Thus the basic factor for deformity at a joint is the loss of capsulo-ligamentous support through hyperlaxity of the ligaments, tendon rupture and progressive degeneration of diseased tissues. Detailed descriptions of how these processes affect all the joints of the hand and wrist were given by Tubiana & Toth (25) and also by Burke (26) in 1984.

As damage to surrounding soft tissue structures occurs the unopposed action of adjacent muscles and tendons results in characteristic deformities such as volar subluxation (Fig 1.6) and ulnar drift (Fig 1.7). The interossei and long flexors have both been incriminated as causing volar subluxation due to their natural line of action. This action is accentuated when contractures develop in these muscles holding the joint in flexion and luxation (Beckenbaugh, 1989 (27)). There is a clear indication that in normal action the MCP joint relies on ligamentous support to prevent volar subluxation: thus if the ligaments

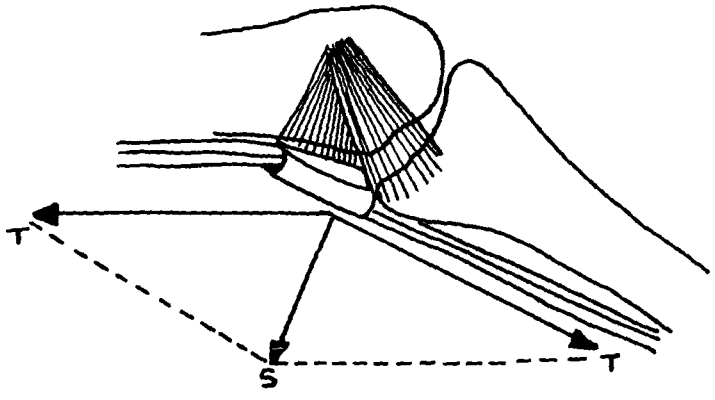

Fig 1.6 Volar subluxation.

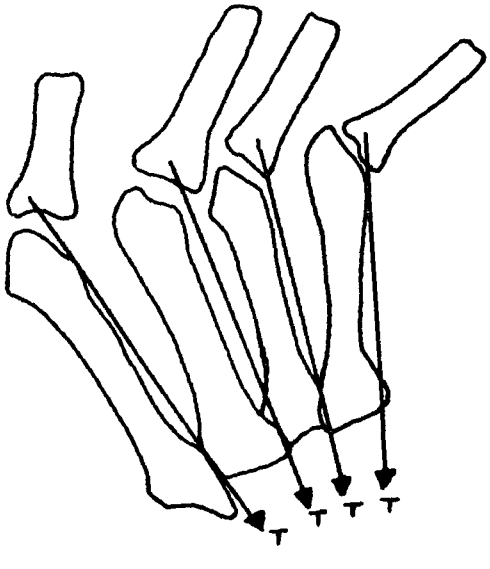

Fig 1.7 Ulnar drift.

are stretched or damaged then deformity will result.

In 1984 and 1985 Minami et al (28,29) investigated capsulo-ligamentous contributions to joint stability through load displacement tests on the MCP joints of fifteen human cadavers. The contribution of each ligament was quantified by measuring the reduction of load that induced a given joint displacement after sequential ligamentous sectioning. Their studies concluded that both the radial and ulnar collateral ligaments play primary roles in stabilising the joint against distal distraction, dorso-palmar dislocation, abduction-adduction rotations, and supination-pronation rotations. The glenoidal ligaments were found to contribute primarily to abduction-adduction rotational stability, but contribute little to stabilising dorso-palmar dislocation or axial rotations. The palmar plate was seen to prevent dorsal dislocation at full extension. Smith et al in 1964 (2) and Linscheid & Chao in 1973 (30) also pointed out the importance of the action of the volar plate, the surface of which glides along the metacarpal head and beneath which is suspended the tendon sheath (the arrangement acting like a mobile pulley).

Ulnar deviation of the fingers again appears to derive from a natural tendency towards this state arising both as a result of asymmetries within the MCP joint itself (Hakstian & Tubiana, 1967 (31)) and also the fact that the lines of action of the extrinsic tendons cross into the hand on the ulnar side of its axis. Normally the tendency is limited by the capsulo-ligamentous structures and the action of the interosseous muscles but if the radial collateral ligament is damaged and the extensor tendon is dislocated medially then ulnar deviation must result (Smith & Kaplan, 1967 (32) and Harrison, 1978 (33)). Often the flexor tendon imbalance problem is exacerbated by instability and deformity in

the wrist which must be corrected before the problem can be addressed.

The rheumatoid process is often one of gradual deterioration but the resulting disability can, on occasions, be reversed and maintained by well-timed appropriate surgery. It is important to note that surgery is only one of many methods of treatment for the rheumatoid hand and in general the most successful approach is one of collaboration between surgeons, rheumatologists and physiotherapists (Gschwend, 1987 (34)). The aims of surgery are to treat pain, improve function, prevent destruction, correct deformities and improve appearance. To this end the main surgical alternatives available at present are synovectomy, arthrodesis and arthroplasty (with or without implants). None of these operations is suitable in all conditions and varying combinations are used according to the circumstances.

1.4.1 Synovectomy

Despite scepticism about the long-term benefits of synovectomy, this is the most common surgery performed on the rheumatoid hand. This procedure reduces pain very effectively by relieving joint distension, and slows further articular and tendonous erosion, thus delaying destruction and deformity (Gschwend, 1987 (34)). The patients who most benefit from the operation are those in whom a small number of joints are involved with little or no deformity, but where persistent localised synovitis is present (Urbaniak et al, 1970 (35)). However, most patients present too late for synovectomy alone to be sufficient and thus it is usually performed in association with joint reconstructive surgery (Nalebuff, 1983 (36)). Early synovectomy is regarded as an absolute requirement if there is evidence of restricted tendon gliding

or nerve compression (Burke, 1984 (26)). Long-standing synovitis of the MCP joint may result in what has been described as a 'cup and saucer' deformity, the joint being relatively stable and mobile (Fig 1.8).

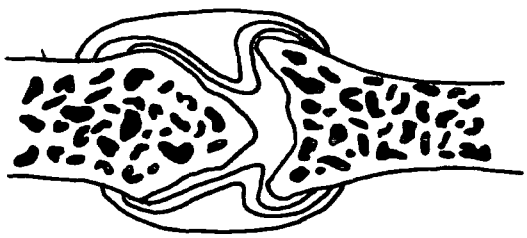

Fig 1.8 The 'cup and saucer' deformity.

If the motion is adequate and the joints are pain-free no further surgery is indicated (Swanson & de Groot Swanson, 1984 (37)).

1.4.2 Arthrodesis

Arthrodesis is commonly indicated for the proximal and distal interphalangeal joints and for the MCP joint of the thumb. It is performed on the MCP joints of the fingers only when there is good mobility at both IP joints and even then only as a last resort since it is obviously very limiting functionally (Flatt, 1983 (38)). Progress in joint arthroplasty has given surgeons the opportunity to avoid arthrodesis generally but it remains, on occasions, indispensable since any procedure designed to restore mobility must not sacrifice stability in the process. Arthrodesis reliably produces stability and a pain-free joint.

1.4.3 Arthroplasty

Arthroplasty is the surgical remodelling of a diseased joint. To prevent the ends of the bones fusing after the operation, a large gap may be created between them (resection arthroplasty), a barrier of tissue or artificial material may be inserted (interposition arthroplasty), or one or both ends may be replaced by a prosthesis.

The earliest and simplest of these procedures was the resection arthroplasty. For a stiffened, contracted joint surgical resection of the metacarpal was often successful in improving motion by shortening skeletal structures and relatively lengthening softened parts. A new joint space was developed with a supportive fibrous joint capsule and the method worked well if the joint space and alignment could be maintained. The procedure almost always relieved pain but range of motion and stability were very unpredictable. For this reason various methods of interpositional arthroplasty have been developed and have greatly improved in reliability over the years (Nalebuff, 1983 (36)). Fowler & Vainio use the dorsal extrinsic extensor hood as a supporting mechanism against dorso-palmar instability. Another approach, favoured by Tupper, is to provide a sling from the palmar surface of the phalanx by attaching the volar plate to the dorsum of the shortened metacarpal. In both procedures there is a good interpositional barrier to prevent bony contact (Flatt, 1983 (38)).

Resection arthroplasty is an uncertain procedure with recurrent deformity and limited motion as common complications. Because of this unpredictability attempts were made to develop replacement prostheses for the MCP joint. Researchers were encouraged by the success of

prostheses in restoring function to the larger joints of the lower limbs and could be forgiven for believing that the problems of the MCP joint would be far less. This has turned out not to be the case.

1.5 MCP JOINT PROSTHESES

The development of MCP prostheses has now included three generations of design. The first generation was introduced in 1959 when Brannon & Klein, and later Flatt, developed rigid, single axis, metallic hinge implants based on the philosophy that a prosthesis should provide the stability of arthrodesis combined with the movement of an arthroplasty. The second generation was introduced in the early 1960's when Swanson & Niebauer developed silicone rubber prostheses. These were based on the 'spacer' concept which provides an MCP joint arthroplasty that maintains length and provides some degree of initial stability, with long-term stability improving with the development of a suitable soft tissue capsule. Second generation devices are flexible one-piece implants, often freely movable within the medullary canal. Encouraged by Charnley's success with a cemented endoprosthesis in the hip, researchers tried to produce prostheses which would better imitate the physiology of the MCP joint. The first of these was introduced in 1973 by Steffee et al. The third generation designs are articulated joints made of dissimilar materials. They provide much more stability than the second generation implants and usually require cement fixation of the stems.

The first generation implants are no longer available. The second generation, and in particular the Swanson design, has experienced widespread use, continuing to the present day. They remain the most accepted implant at this time. Design of third generation implants has been prolific with many designs having been introduced and withdrawn in the last decade. There hasn't yet been sufficient time to assess

properly the results of this type of prosthesis and it is unclear whether any will yet become established. To do so they would have to demonstrate significant advantages over the Swanson design (which holds by far the greatest proportion of the market) and at the moment this seems unlikely. Some of the more prominent designs of each generation are reviewed below so that the problems associated with MCP joint replacement might be highlighted.

1.5.1 First Generation

The two pronged metal hinge of Flatt (Flatt, 1973 (39) and 1974 (40)) was designed to be a very stable joint replacement to be used for totally destroyed MCP joints (Fig 1.9).

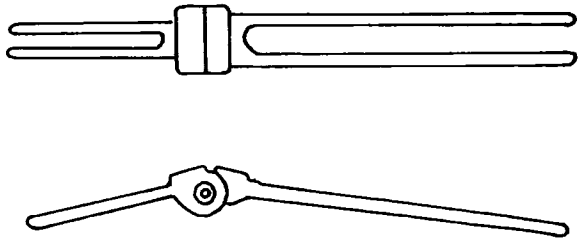

Fig 1.9 The Flatt metallic hinge.

It consisted of two components of 18/8 stainless steel linked together by a screw which formed a fixed axis of rotation for flexion and extension. The stems were two pronged to combat the problem of rotational instability evident with the Brannon & Klein implant (41).

In the original design the axis of the hinge was in line with the stem axes but in later developments the axis was lowered relative to the

stems to improve active extension and better restoration of function was achieved. This is not surprising in the light of a later report by Unsworth & Alexander in 1979 (20) which concluded that the centre of rotation of the MCP joint lies 2.6 mm below the centre-line of the medullary cavity.

In several long-term follow-up studies the Flatt metallic hinge was seen to have reduced pain and considerably increased strength (Girzadas & Clayton, 1969 (42)). The range of motion, although tending to decrease in time, was more favourably placed in extension (Flatt & Ellison, 1972 (43)). However, there was almost invariably bone resorption accompanied by stem loosening and implant migration. Large subluxing and ulnar deviating forces led to metal fatigue fractures at the screw and stems which in turn led to recurrent deformity (Blair et al, 1984 (44)). Also there was growing concern over long-term metallic wear and corrosion often resulting in black staining of the tissues. After the introduction of the second generation implants the unforgiving metallic hinge could not compete and has been withdrawn but it did provide some valuable lessons for the third generation designs.

1.5.2 Second Generation

In the late 1960's Calnan developed a polypropylene integral hinge at the Hammersmith Hospital in London (Fig 1.10 a)). The intramedullary stems were of a tapered square cross-section and required fixation with cement to maintain the hinge position (Calnan & Reis, 1968 (45)).

After problems with tissue interposition of the hinge and resulting loss of motion, Calnan & Nicolle modified the design and encapsulated the

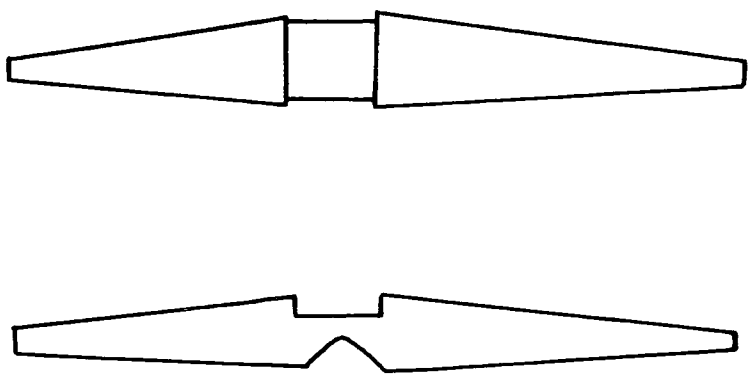

Fig 1.10 a) The Calnan polypropylene integral hinge.

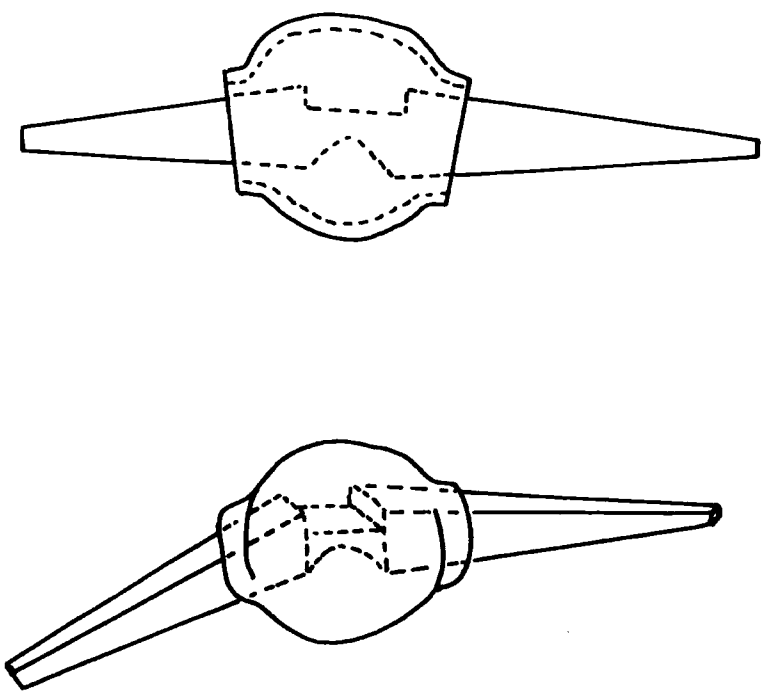

Fig 1.10 b) The Calnan hinge with encapsulation.

hinge in a ball of silicone elastomer (Fig 1.10 b)). The purpose of the capsule was to alleviate interposition problems, allow smooth gliding of adjacent tissues and give a good cosmetic appearance (Nicolle & Calnan, 1972 (46)). Since it also maintained the joint space effectively, the capsule negated the need for cement fixation. However the capsule was sometimes seen to cause ulnar dislocation of the extensor tendon (Walker & Erkman, 1975 (12)) and the built-in 35° flexion contracture was felt to imply an imbalance in joint forces (Flatt, 1974 (40)). Problems with the joint were mainly associated with failure of the capsule due to the poor tear resistance of silicone rubber but stem fractures and recurrent ulnar deviation also occurred (Hagert, 1978 (18)).

In 1977 Nicolle (47) described a further development of this implant by Griffiths & Nicolle. In this the polypropylene hinge has been replaced by a stainless steel cylindrical bearing, moving away from the spacer concept back to the metallic hinge. The capsule is still present and durability has improved somewhat but similar problems remain. In England this design did fairly well in the 1970's because it was relatively very cheap but the high complication rate has seen a reduction in usage (Evans, 1989 (48)). There is no indication that the implant is available in America.

Another design that has been used very widely since 1968 is the Niebauer-Cutter silicone-Dacron implant (Fig 1.11) and it was first described in detail in 1969 by Niebauer et al (49). The device, produced by the Sutter Company, is made of silicone rubber and has a core of Dacron tricot mesh moulded within it in the frontal plane to reinforce the rubber. The stems are also surrounded by the Dacron fibre and intramedullary fixation of the stems is achieved by fibrous and bony

ingrowth into the mesh. The midsection consists of two blocks of equal size and shape, connected by a thin hinge which has a low centre of rotation with respect to the stems. Bending was designed to occur only at the hinge though this has clearly not been the case. Bending at the stems has been found to cause serious bone resorption often leading to joint buckling under load (Hagert, 1975 (50)). In common with the original Calnan hinge, the bending of the central hinge is often impaired due to interposition of tissue. This may occur in the early stages of healing or as a result of tissue passage over the implant being difficult. Failure of the hinge has been a common problem although the presence of a fracture does not preclude a good functional result (Urbaniak et al, 1970 (35)). The material strength has improved 270% since the first release. The average range of motion for this implant is 51° (Goldner & Urbaniak, 1973 (51)) which is not significantly greater than the pre-operative range but the arc of motion has moved to a position of greater extension. There is some moderate recurrence of deformity after ~5 years but generally the performance of the implant is good (Derkash et al, 1986 (52)). However, the Niebauer implant fell into disfavour in the 1970's when it was seen to be less reliable than the Swanson design (Beckenbaugh et al, 1976 (53)). It is still available but not really utilised.

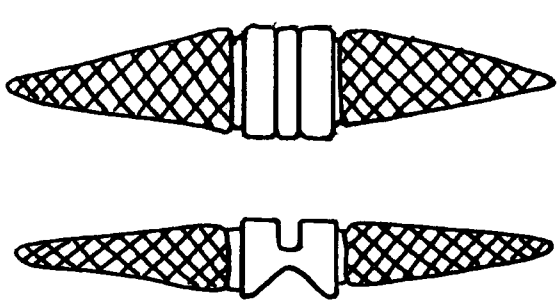

Fig 1.11 The Niebauer-Cutter implant.

In the early 1980's the Sutter Company developed a new silicone hinge based on the Niebauer design which has better flexibility and more stability against rotation (Fig 1.12). So far it has no known advantages over the Swanson implant but there has been insufficient time for evaluation.

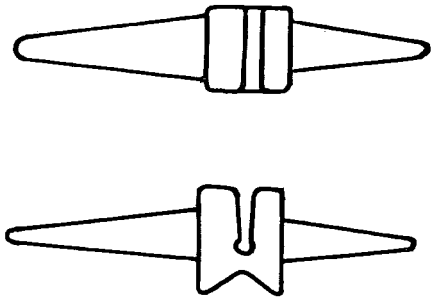

Fig 1.12 The Sutter implant.

Still the most widely used and the most successful MCP joint prosthesis is the Swanson Silastic implant manufactured by Dow-Corning since 1966 (Fig 1.13). The implant is of one piece and moulded from silicone rubber. The stems are of rectangular cross-section to resist rotation and are allowed to slide in the medullary canals.

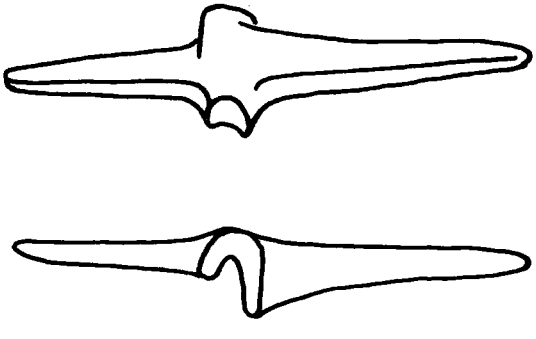

Fig 1.13 The Swanson Silastic implant.

The midsection is a transverse block which bears against the two bone ends to keep them apart, and bending of the implant takes place both at the midsection and in the stems. The implant acts as a dynamic spacer which maintains joint separation and alignment after a resection arthroplasty until the joint is stabilised by a new capsule. Stability depends on proper tendon balance and the development of a firm new capsule in the early stages of healing (Swanson & de Groot Swanson, 1984 (37)).

The performance of the Swanson prosthesis has been the subject of very many articles in the literature. Overall the results are pleasing and the Swanson implant has established a standard against which the performance of other designs is assessed. Only by improving on the Swanson can any new implant do well on the market.

The post-operative range of motion for this implant, reported to be around 45° (Blair et al, 1984 (54), and Fleming & Hay, 1984 (55)), is only a marginal improvement on the pre-operative range but again is better placed functionally. Often there is a steady decrease in mobility due to fibrosis around the implant or migration of the prosthesis into the bone (Hagert et al, 1975 (56)). In time bony resorption is a severe problem with this device. The reduction of deformity is generally very good but there is a tendency for recurrent ulnar drift because of the inherent flexibility of the implant and some propensity to cold flow (Walker et al, 1983 (57), also Vahvanen & Viljakka, 1986 (58)). There remains a substantial rate of prosthetic fracture despite continual improvements in the material's tear strength. These fractures commonly occur at the junction of the phalangeal stem when a small nick produced by a sharp bone edge results in a stress

concentration and hence fracture. In their paper reviewing silicone rubber implants, Beckenbaugh et al in 1976 (53) reported a fracture rate of 26.2% compared with 7.5% reported by Swanson et al in 1986 (59) - Swanson has consistently reported better results than any other surgeon. Most patients with fractured implants have suffered no functional loss but there is a greater tendency to recurrent deformity. In order to combat fracture problems and also to try to reduce bone resorption, Swanson introduced a titanium hemi-grommet in the early 1980's. In this country these were not widely utilised since they doubled the cost of the operation which is already considerable (Evans, 1989 (48)). They were used to some extent in America but had considerable rotation problems and thus have been discontinued. Now there is a new rectangular total grommet in the early stages of clinical trials (Beckenbaugh, 1989 (60)). Though it would appear to give little strength increase (Bieber et al, 1986 (61), also Mannerfelt & Andersson, 1975 (62)), the Swanson implant has consistently given good cosmetic results and pain-free joints. It is also relatively simple to replace since it employs no bone cement for fixation and it seems set to remain on the market for the foreseeable future. However not all researchers are supporters of the spacer concept and a great deal of effort has gone into the third generation devices.

1.5.3 Third Generation

The earliest third generation implant was the Steffee design from the Mayo Clinic which was developed in the late 1960's. Very little has been published on the performance of this implant in the open literature and this is a problem common to all the third generation prostheses. The Steffee Mark I was made from two components which snapped together

to form a two-piece hinge with some lateral mobility in extension (Fig 1.14). The metacarpal component had a cobalt-chrome alloy stem with a plastic head. The all-metal phalangeal component comprised a T-piece to snap into the plastic housing of the metacarpal component. It had a relatively short stem. The centre of rotation of the joint was fixed and level with the stems (Walker & Erkman, 1975 (12)).

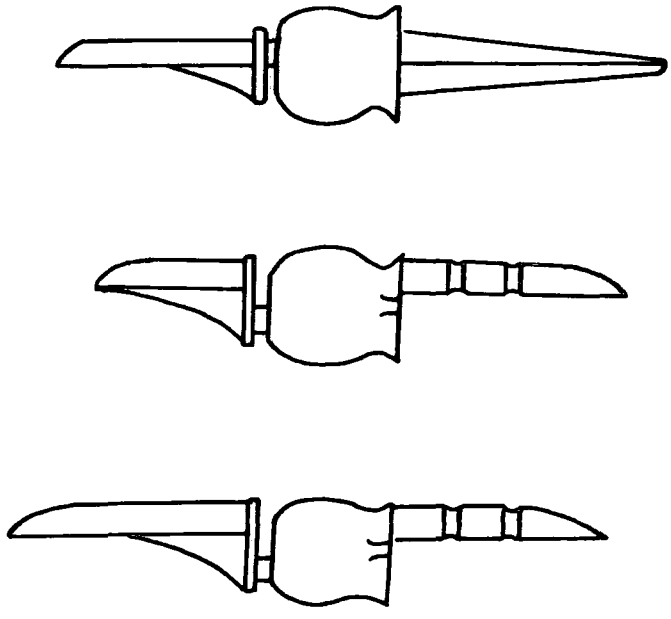

Fig 1.14 The Steffee implants I, II & III.

The greatest problem with the Mark I design was the severe reduction in the range of motion caused by extensor lag. This occurred as a result of the dorsal placement of the centre of rotation and this was lowered in 1974 when the Mark II version was introduced. Also at this time the metacarpal component was made wholly of polyethylene (Linscheid, 1989 (63)). The range of motion was improved and was comparable with other designs at 42° flexion, but there was recurrent stem loosening and perforation of the cortex by the distal stems due to bone resorption and

implant migration. In 1977 the Mark III version was released with rather longer distal stems (Fig 1.14) to disperse the intramedullary force and to project into thicker cortical bone. At the stem heads there were thin collars to locate against the bone ends which would prevent cement from welling out and also restrict implant migration. Unfortunately, while relief of pain was reliable there was inconsistent correction of deformity and frequent stem loosening. There was no measurable improvement in grip strength post-operatively which was disappointing, this being one of the main aims of the third generation designs. Complications included bone resorption, infection, fracture of the plastic housing and dislocation of the trunion bar. Because of the large amount of resection performed in the operation, revision was very difficult and this made the implant unattractive, thus it has been withdrawn from the market but development is continuing at the Mayo Clinic (Flatt, 1983 (38)).

In 1971 Stellbrink et al (64) described the St Georg prosthesis which is rather like the Steffee design but with a hinge more akin to the Flatt implant. The metacarpal component is made of plastic with a grooved stem attached to a hollow sphere into which is machined a midline slot to accommodate the distal component. The phalangeal component is made of metal and has a ball end which pops into the metacarpal component. The two parts are connected by a transverse pin (Fig 1.15). The phalangeal component comes in two forms - the first is flat and rectangular and allows some lateral movement in extension; the second is triangular and permits no lateral movement. The device is cemented and has a fixed centre of rotation volar to the stems.

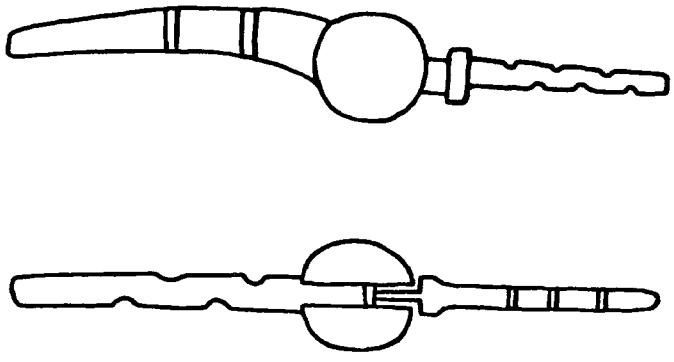

Fig 1.15 The St Georg prosthesis.

The large lateral stresses seen to cause failure in the Flatt prosthesis are also a problem here and tend to distort the metacarpal component. In experiments to assess implant performance, Gillespie et al in 1979 (65) placed the St Georg prosthesis into cadaveric finger rays and artificially loaded the tendons. They reported evidence of cold flow in the plastic stem of the proximal component. In 1973 and 1975 Englert published reports on the performance of the St Georg (66,67) describing a general loss of motion due to fibrosis caused by soft tissue interference in the mobile parts. A similar problem was seen in the Niebauer and Calnan designs. By 1983 it was evident that this implant suffered an especially high rate of loosening and that the benefits of high stability were outweighed by mechanical failures (Flatt, 1983 (38)).

Two rather similar designs are the Link arthroplasty, described in only one report by Devas & Shah in 1975 (68), and the Schetrumpf implant, also introduced in 1975 (69). The Link arthroplasty (Fig 1.16) is in two parts and made entirely of chrome-cobalt alloy.

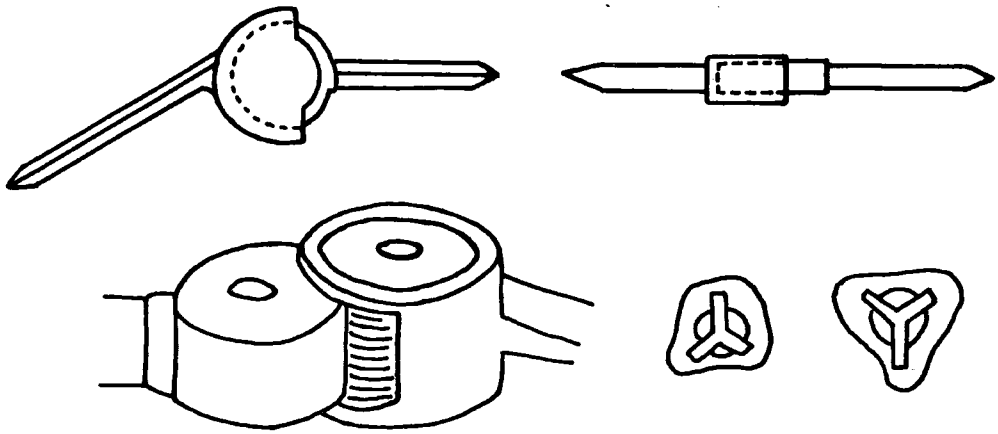

Fig 1.16 The Link and Schetrumpf designs.

The metacarpal component is a hollowed flat cylinder into which the flat disk of the phalangeal part is linked. The stems are cemented and movement is strictly in one plane. The only report available describes a 40° range of flexion with some stem loosening and weld failures in the metacarpal part. One point in favour of this design is that very little resection is needed. It is very unclear how well this design is doing or indeed if it is still available - it has never been mentioned in American reviews.

J Schetrumpf presented a two-component implant similar to the Link prosthesis but with both parts being made of plastic. No cement is used and fixation to the bone is considered to be achieved by three wings on each stem cutting into cortical bone. There was no real description of performance.

More recently another implant emerged from Japan (Doi et al, 1984 (70)) called the Alumina ceramic prosthesis (Fig 1.17). This is a hinge in three parts - a proximal stem of polycrystal alumina, the proximal part of the hinge joint of high density polyethylene, and a distal stem of

single crystal alumina. The proximal stem and the polyethylene screw into each other. In the latest version some 20° of lateral movement is allowed and the stems fit tightly into the medullary canals with no bone cement. This is indicative of current moves away from bone cement in all joint replacement surgery and brings a new set of problems. The choice of ceramic was to reduce the risk of stem fracture and, indeed, in a four-year follow-up study no failures of this nature were recorded (Minami et al, 1988 (71)).

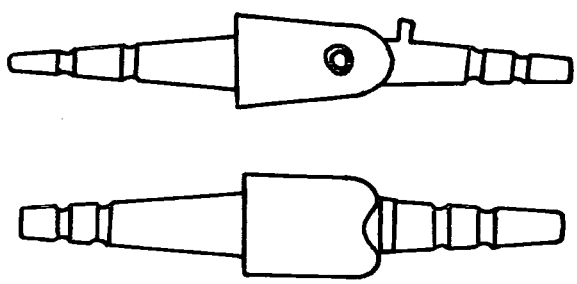

Fig 1.17 The Alumina ceramic implant.

The average range of motion for the metacarpophalangeal joint was seen to be 36.5° and lack of extension was evident. The authors acknowledge a need to modify the design to bring the axis of rotation more volar to the stems. Radiographs of patients showed severe implant migration and perforation of the cortex.

Other third generation designs not described here are those by Schultz, Strickland, Mathys GSB, Hagert and Weightman. One of the most unusual was the biomeric design by Kingsbury Heiple marketed by the Johnson company. It used a synthetic polymer polyafin secured to two titanium stems by a proprietary glue originally used in the manufacture of helicopter hubs. This design is no longer manufactured.

1.5.4 The Way Forward

The attempts to provide MCP joint stability using constrained or semi-constrained devices have placed impossible demands on the implants in-vivo. All the third generation designs have suffered common, seemingly unconquerable, problems of stem loosening, bone resorption and implant fracture. It is perhaps time that the prostheses were regarded as complementary to, rather than an integral feature of, rheumatoid hand surgery with surgeons concentrating more on precise rebalancing of tendon and soft tissue support. In the early days of excisional arthroplasty greater reliability was often achieved by the introduction of interpositional materials such as polyethylene as sheets or cups and much can be learnt from this. In the past few years a small number of fourth generation implants have been developed based on the surface replacement concept that has been so successful in knee and elbow arthroplasty. These are not yet marketed but are generally used and developed at the site of origin.

The problem of resurfacing the metacarpophalangeal joint was addressed by Welsh et al in 1982 (72). A contoured stainless steel metacarpal component is matched with a phalangeal component (also of stainless steel) with a high density polyethylene button inset to articulate with the metacarpal component (Fig 1.18) - opposing surfaces are exactly conforming. It is interesting to note that the metacarpal head has not been designed necessarily to mimic closely the anatomical shape, but provides a broad articulating surface with a large volar protrusion to aid in stability against volar subluxation.

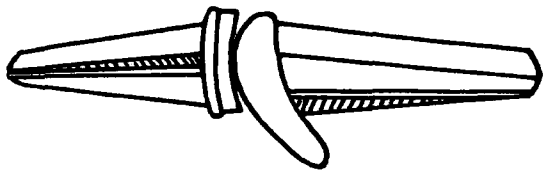

Fig 1.18 The WEL resurfacing arthroplasty.

The implant needs very minimal bone resection; only a squaring off of the metacarpal head. The stems are pressed into the medullary cavity and need no cement. This early report described the case of a 17 year old girl who had a stable and pain-free joint four years after surgery.

At the Mayo clinic, R D Beckenbaugh has designed a non-cemented two-component surface replacement prosthesis, the components in this case being made of pyrolytic carbon (Fig 1.19). The conforming surfaces are spheroidal.

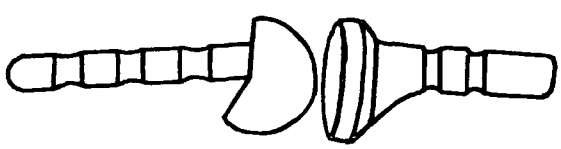

Fig 1.19 The pyrolytic carbon implant.

From 1983 one hundred and twenty of these devices were implanted and over three years they demonstrated good biological fixation and mobility. Problems occurring were ulnar instability and carbon deposition around the synovial tissues and gradually their use was

discontinued in the Mayo clinic. However, only last year, the manufacturers restarted the development programme and there are several carbon designs under consideration (Beckenbaugh & Linscheid, 1989 (27)). There is no intrinsic stability of these joints except the anterioposterior support provided by the deep ball and socket joint. In this case some resection of the metacarpal head is necessary, incurring the loss of the collateral ligament attachments.

It is believed that there are two other teams in the UK working on surface replacement designs - in Leeds and in Scotland - though there would appear to have been nothing published in the open literature at this time.

It should be understood that a resurfacing arthroplasty is not to be used on grossly deformed joints or in cases where soft tissue rebalancing cannot be achieved. For this reason the surgery needs to be undertaken considerably earlier than it would for any other type of implant and thus minimal bone resection and ease of recovery are essential to make replacement with a more constrained device possible at a later stage should this prove necessary.

The type of prosthesis considered in this thesis is a resurfacing arthroplasty since it would seem that all possibilities for constrained devices have been explored and this is therefore the best way forward. Soft tissue repair techniques stand the best chance of success given an improved articulation. In the next section the suitability of certain implant materials is discussed and their performance in joint applications is described.

1.6 BIOMATERIALS

In choosing a material for a new surgical implant many things must be taken into consideration. The most important of these is the effect the material will have on the body and also the effect that the body will have on it. If it is established that a material would be well tolerated, it must be clear that its mechanical properties within the body (not necessarily the same as outside) are such that it can reliably perform the task intended for it. While the material properties may not be affected, the action of a device may be impeded by the ingrowth of tissue into any interstices or by deposition of tissue onto its surface. This was seen to occur in the St Georg MCP prosthesis and was reported by Englert in 1973 and 1975 (66,67).

For joint replacement prostheses a wide variety of different materials have been employed. Metallic materials such as titanium, stainless steel and cobalt-chromium alloys (eg. vitallium) are used, as are softer polymeric materials such as polyethylene, silicone rubber, polypropylene and polyester (eg. Dacron) and, more recently, ceramics and composite materials. With the form of prostheses changing from mechanical hinges towards surface replacements, wear properties have become as important a consideration as strength and durability. In the knee, two component surface replacements employing dissimilar materials have been particularly successful - for example, the Leeds knee (Seedhom et al, 1975 (73)) and the Total Condylar implant (Insall et al, 1976 (74)). They are also becoming more popular in the elbow with, for example the Ewald and Lowe designs (Ewald et al, 1980 (75) and Lowe et al, 1984 (76)) and even in the shoulder with the Neer design (Cofield,

1984 (77)).

Of course the fixation of a prosthesis is an important issue also and the mechanical loosening of cemented implants remains the number one complication to date. The generally poor performance of polymethylmethacrylate bone cement has fuelled efforts to produce a prosthetic implant with a surface potentially capable of enhancing a living ingrowth of tissue (Williams, 1971 (78)). In weight-bearing joints a tiny motion of the implant within its skeletal bed can give rise to considerable pain: hence the degree of rigidity of fixation eventually achieved by a porous surface is a critical issue.

This review of the performance of some of the more common biomaterials will put these considerations into perspective and provide some justification for the choice of material made for the MCP surface replacement described in this thesis.

1.6.1 Metallic Materials

Metals and alloys are very strong but with some ductility which means that they are eligible to be used for structural purposes. Of the metallic materials used for prosthetic implants the most common are cobalt-chrome-molybdenum alloys, stainless steel and pure titanium. In general they are very expensive. Cobalt-chrome alloys are extremely hard and resistant to wear but are difficult to fabricate except through precision casting using the lost wax technique. Their poor ductility has sometimes proved a disadvantage (Williams, 1971 (79)). Stainless steel provides a compromise between wear properties and machinability. It too is a high modulus material and has excellent ductility but it is

the least inert of the implantable metals. Titanium is chemically the most inert but is more subject to wear and has a rather lower modulus.

In using metals, great care must be taken in designing the component where in critical areas very high cyclic stresses may arise, since fatigue failure is common. In the body, locomotion is a prime cause of prosthetic cycling fatigue. In a review by Galante et al in 1975 (80) metal fatigue was seen to cause failure in the femoral stems of six total hip prostheses. Five showed metallurgical defects and only one did not. In this case, loosening of the prosthesis had led to overstressing. A similar review by Cahoon & Paxton in 1968 (81) also concluded that material defects or the occurrence of abnormal stresses due to poor design, malposition or loosening had caused fatigue failure of implants. This is particularly true for stainless steel and cobalt-chrome alloys which are often subject to inclusions, porosity and surface cracks at manufacture. Metal implants, being very hard, can cause severe damage to the bone at any point of contact where there are high stresses. This is especially true if the implant has loosened and the ensuing bone resorption results in further loosening and implant migration. This was seen to occur with the Steffee MCP prosthesis (Linscheid, 1989 (63)).

The human body is a very hostile environment for most metals. Body fluids are principally saline, and only the most corrosion-resistant materials can survive. Metals such as aluminium, chromium and titanium, which rely on a surface oxide film for protection, were initially used for implants and only recently was stainless steel included. Corrosion can take several forms:

1) Uniform attack over the whole surface of a metal causing rusting or fogging.

2) Pitting - local attack resulting in deep pits sometimes filled with metal oxide debris. This can be aggravated by fretting due to disruption of the protective surface layer.

3) Intergranular attack - attack on the grain boundaries of a metal. These may be deep and rapid leading to abrupt failure - stress corrosion cracking.

Corrosion may be initiated if the implant comes into contact with haematomas or infected tissue after surgery since these have a very low pH (Laing, 1973 (82)). Cobalt-chrome has a low reaction to tissue unless wear occurs, when the wear particles will corrode. Titanium has excellent corrosion resistance but it is more subject to wear and again the wear particles will readily corrode. Stainless steel is the least corrosion resistant, often due to poor material quality on manufacture, and is subject to pitting though this may be alleviated to some extent by the addition of molybdenum. Dissimilar metals in close proximity will enhance corrosion electrochemically and this is generally to be avoided. Surface finish is very important for metals and high polish tolerances can now be achieved to reduce wear and inhibit corrosion.

The presence of an implant can impair the body's natural ability to fight infection - thus if an infection does occur at the joint it is often necessary to remove the implant. Infection can exacerbate corrosion by altering the local pH (Laing, 1973 (82)). Tissue reaction to implants is time-related and the severity is linked to the size and shape of the implant, movement between the implant and the tissues, the amount of degradation/corrosion of the implant and the biological

activity of the by-products of corrosion and wear. Tissue response to metallic corrosion is inflammatory and results in implant loosening. Pigmentation of the tissues surrounding implants is commonly seen and must be attributable to metallic dissolution, either by corrosion or slow ionic transfer. Absorbed metals can be transported around the body to various organs and, indeed, cobalt and nickel, which appear to be the most active, have been observed to accumulate mainly in the spleen (Ferguson et al, 1962 (83)). Though this has caused some concern there have been no reported ill effects in patients to date. Pigmentation is greatest with titanium and is not associated with corrosion. This may be due to a slow rate of removal rather than to a high dissolution rate. In some patients there has been evidence of metal sensitivity, demonstrated in skin tests, especially to chrome, cobalt and nickel. In these patients metal absorption was thought to have caused bone necrosis and stem loosening resulting in the necessary removal of the implant (Evans et al, 1974 (84)).

One important consideration for any material is carcinogenesis and almost all materials have been shown to induce tumour formation in rats, the occurrence being related to particle size and not to chemical activity. Until recently there had been only one confirmed case of a primary malignant tumour in man due to metallic implants and this occurred after thirty years of implant with dissimilar materials (Williams, 1971 (85)). In 1984 three cases of malignancy adjacent to metallic implants were reported (Hamblin & Carter, 1984 (86), Penman & Ring, 1984 (87), and Swann, 1984 (88)).

1.6.2 Cement

In 1946 the Judet brothers introduced their acrylic femoral head prosthesis made of polymethylmethacrylate, heat cured. This material is now advocated as a bone cement for prosthesis fixation. The exothermic reaction, reaching up to 90°C, can result in damage to adjacent tissues and permanent scarring. There is some toxicity during the curing reaction from the excess liquid curing agent and this has a hypotensive effect which has been known to cause cardiac arrest during surgery (Cohen & Smith, 1971 (89)). In addition this material has been found to be unreliable under stress, resulting in loss of fixation, and cement debris entering the joint cavity causes tissue reaction which leads to bone destruction. Not surprisingly there is a strong move to design prostheses with an alternative mode of fixation, though this has proved rather difficult. One promising area has been in the development of new materials which will permit the ingrowth of bone into the surface thereby providing a natural bond between the implant and its host. Porous ceramic materials were the ideal candidate for this purpose and their use has increased during the last decade. Some porous metals are beginning to emerge and in 1975 Judet et al (90) described a new hip using porous cobalt-chrome alloy and no cement. In clinical trials new-formed bone had completely filled the irregularities of the surface in ten weeks. In 828 operations there were only two displacements after one year with almost complete removal of pain. One disadvantage envisaged is that the surface area of a porous material, being four to ten times greater than a non-porous one, would greatly enhance toxic metallic ion leeching to the surrounding tissues.

1.6.3 Ceramics

Ceramics are even stronger than metals in compression but, having no ductility, they are poor in tension and are usually used for large structures subject to static compressive stresses. Having a high bond strength they are far more resistant to attack than other materials and if the cost and mechanical properties of ceramics matched their inertness they would be used much more. Porous ceramics encourage bony ingrowth and hence promote a strong mechanical fixation between the bone and the implant but they may be more useful as porous coatings on a metal base. In this way the problem of brittleness is obviated. Dense alumina is the most commonly used ceramic and has been particularly popular in Japan, being used for hip, knee and finger prostheses (Hamaguchi et al, 1981 (91), Oonishi et al, 1981 (92), and Doi et al, 1984 (70)). Its use in the finger, where stresses are relatively very low, seems excessive and the choice would seem to have been made for reasons of inertness and fatigue resistance. The device is expensive and unfortunately, only one year after surgery, evidence of bone resorption and implant migration can be seen caused by the extreme hardness of the material.

1.6.4 Polymers

Polymers have been used for surgical implants for many years. The inherent flexibility and inertness of these materials have been well exploited in the 'whole piece' prostheses of the finger, especially in the Swanson design (Swanson & de Groot Swanson, 1984 (37)). Molecular orientation can be controlled to increase polymer strength and this also has been used to great advantage, for example in the Calnan-Nicolle

finger implant (Calnan & Reis, 1968 (93)). They can be used alone or in conjunction with metals with no material incompatibility problems and this has been particularly popular in prosthetic design.

Polymers, being soft, do not have such an adverse effect on bone. They are inexpensive but sometimes do not have the durability to stand up to the demands placed upon them although they can be strengthened by attaching a metal backing. Polymers are not very strong but come in many forms from the brittle acrylic, used in bone cement, to the flexible silicone elastomer used in the Swanson design. The most important polymers used in joint replacement surgery are Ultra-High Molecular Weight Polyethylene (UHMWP), polypropylene and silicone rubber. Polymeric implants sometimes suffer from environmental stress cracking which is the apparent brittle failure of the material when subjected to the combination of stress and a hostile environment.

For some polymers the absorption of body fluids can be a problem. Polyethylene and polypropylene are not prone to this but nylon and polyurethanes are extensively degraded in the body - becoming very soft and losing up to 40% of their original strength due to hydrolysis of interatomic linkages (Williams, 1971 (78)). Silicone rubber also tends to absorb body lipids and this proved a very serious problem when encountered in prosthetic aortic valves in which the balls were found to become swollen (Bradley, 1969 (94)). Consequently these balls are now usually made of metal. It is debatable whether this is an important consideration in the performance of joint prostheses. For example silicone rubber is used very successfully in the Swanson MCP implant and it has been reported that surface damage from lipid absorption is not an important contributory factor in fatigue failure (Meester & Swanson,

1972 (95)). However, it has been seen to cause discolouration and also surface cracking, beginning at the point of maximum stress concentration (Weightman et al, 1972 (96) and Homsey, 1970 (97)). In spite of this silicone rubber is well tolerated in the body and produces a minimal reaction. Although its propensity to tearing has been a disappointment over the years improvements have been made in this area (Amstutz, 1973 (98)).

UHMWP is a highly crystalline polymer with a modulus twice that of other polyethylenes and it is thermoplastic which means that it can be moulded. However, this is rather difficult so it is often machined from blocks. It is inexpensive, has a high impact strength and can be prepared to have a very low coefficient of friction, hence its popularity as a bearing material, being used most commonly against metal. The coupling of metal against polyethylene was pioneered by Sir John Charnley in the design of his Low Friction Arthroplasty for the hip (Charnley, 1967 (99)) and has been very successful in all joints. The wear properties of UHMWP against metal are very good but against itself it does not perform so well. Indeed, in 1976 Atkinson (100) reported that the wear rate of polyethylene against polyethylene is some 700 times worse than that of the polyethylene/metal system. His experiments were aimed at investigating the feasibility of an all-plastic surface replacement for the MCP joint which is under relatively light loading and this will be looked at more closely in Chapters 5 & 6.

One problem encountered with UHMWP, common in polymers, is its propensity to creep and deform under large loads, such that it may only serve in the weight-bearing joints if there is enough area of contact, reasonable thickness of material and good bone support. The creep

properties can be improved by cross linking which makes the material more rigid. For polymers radiation sterilisation has been adopted since there is a risk that chemicals, used in manufacturing sterilisation processes, which are toxic to man, could be absorbed by the implant and leeched out later. Bulk polymer is irradiated in the presence of a gaseous cross linking agent (eg. acetylene), resulting in highly cross linked polymer at the surface while the bulk material is largely unaffected. The new surface restricts cold flow, improves surface hardness and wear properties though some impact strength is lost. The effect is rather like the case-hardening of steel (Bruck & Mueller, 1988 (101)).

Surface damage, associated with fatigue, is quite often seen in UHMWP especially in non-conforming prostheses such as the knee. Fatigue is manifested as crack growth due to cyclic loading - as the contact zone moves, a point on the surface may be in compression in the centre of the contact zone and in tension when it is at the periphery - and this leads to surface pitting. This problem is more severe in knees than hips since the contact zone is smaller and the relative movement is larger. While surface damage does not in itself imply early failure, it is known that debris in the joint capsule can cause an inflammatory tissue reaction leading to prosthetic loosening (Skinner & Mabey, 1987 (102), and Wright & Bartel, 1986 (103)). If debris from wear and surface degradation can be kept to a minimum, the block material is very inert in the body with only a slight discolouration seen sometimes, and being much softer than metal, it produces minimal bone reaction. For these reasons this is the material chosen for the conforming, two-part MCP surface prosthesis described in this thesis. It is not anticipated that wear will prove a problem since in the finger there is unlikely to be

very much relative movement of the surfaces under a large load. Nevertheless this is not taken for granted and the wear performance of the implant is assessed carefully. The implant design is such that, should it prove necessary later, the metacarpal component can be switched to stainless steel. This is to be avoided since bone resorption and implant migration constitute a very serious problem in the finger and also the cost would be increased.

CHAPTER 2

THE MCP SURFACE REPLACEMENT PROSTHESIS

2.1 MOTIVATION

Metacarpophalangeal joint implants have been in existence for many years though it is true to say that they still enjoy only limited success. Many different designs have been published but these have aimed mainly at providing joint stability by means of the prosthesis rather than the natural joint structures. Indeed the collateral ligaments are often sacrificed during the surgical procedure. A limited amount of soft tissue reconstruction is performed at present but following the success of surface replacement knee joints, it was felt that fingers could also benefit from a similar approach. Since hand surgery is often performed by plastic surgeons as well as orthopaedic surgeons, soft tissue reconstruction is a natural approach to solving the stability problem if the architecture can be restored by means of artificial surfaces. The intention, then, is to re-model the natural joint removing only the diseased surfaces, reshaping the bone ends, and inserting replacement surfaces which closely follow the topography of the healthy joint. Effectively the bones and capsulo-ligamentous structures of the joint will be left intact. Of course such a surface replacement could offer no contribution to joint stability and would be of little or no help to the surgeon in his battle against volar subluxation and ulnar drift; however, neither would it be a hindrance to the surgeon's soft tissue repair techniques where procedures involving gross bone resection almost certainly are.

The procedure would undoubtedly have to be performed rather earlier than at present but this could be advantageous since surgical intervention may be delayed until the latest possible moment, when it is clear that

the patient requires joint reconstruction. As a result there is an increased risk of restricting tendon gliding and nerve compression. Also if a surface replacement proved unsuccessful for reasons of infection, recurrent deformity etc., the implant could be removed and replaced later with a different design of prosthesis such as the Swanson, giving the surgeon a welcome opportunity of revision.

The design of the Durham surface replacement was undertaken on the basis of the considerations detailed below. There were obviously many choices to be made and it is intended that the account in this chapter will outline the options, detail the advantages and disadvantages of each, and justify the direction taken.

2.2 SPECIFICATION

A successful MCP prosthesis needs to have a good range of motion. This is an inherent quality of a two component surface replacement which has no linkage restrictions to compromise natural motion. This is not true of 'pop-in' designs such as the Link arthroplasty in which lateral movement is lost or limited, and dissociation of the components is possible if hyperflexion occurs (Devas & Shah, 1975 (68)). On the other hand, with the surface replacement, hyperextension and rotational instability could be a problem.

The aim is to retain as much of the natural joint structure as possible. This poses quite a problem since, if the implant is not to impede the range of joint movement or the actions of the ligaments and tendons etc., there is very little space left in which to accommodate the prosthesis. Only the space originally occupied by the articular cartilage is available.

The mode of fixation for a prosthesis is an important consideration since not only does it resist stresses which would tend to dislocate the implant but also largely determines the distribution of stress along the bone/implant interface. Conventional single component designs have commonly used cemented intramedullary stems designed to form a rigid link with the bone. This is important particularly for uni-planar designs since the restriction placed on joint movement results in large shear stresses across the implant. Often an implant has to be removed not because of implant failure but through failure at the bone/cement interface. For a surface replacement prosthesis there is little or no

pull-out force and only small rotational and shear forces due to friction. Fixation requirements are therefore minimal as with the Swanson Silastic implant. Certainly cement is not necessary and should be avoided since cement left during surgery can cause infection and implant damage. Also, removal of the prosthesis, should this prove necessary, would be considerably more difficult.

The use of intramedullary stems, even without cement, would mean drilling holes in the bone-ends which is something that ideally should be avoided. However, a short well-designed stem would not interfere with joint function and would help to distribute large compressional joint forces more evenly through the prosthesis to the bone. To resist rotation a stem can be made with square cross-section and to resist pull-out it can have fins although the latter is only really feasible when using a flexible material. The stem itself is sufficient to hold the component against shear stress. The alternative to an intramedullary stem for the metacarpal component would be to extend the implant past a hemisphere and 'snap' the component over the bone head. Again this would only be feasible if using a flexible material and there is a risk of interfering with tendon movement. Gripping ridges could be incorporated in the dorsal and volar edges of the component to engage in grooves cut into the bone head. These would necessarily need to be small and would result in large stress concentrations. If the bone is in poor condition or the material is particularly hard the link would quickly fail. Because of the shape of the phalanx head, the phalangeal component could be simply seated inside a recess cut into the bone during surgery. In this case there is no real need for a stem but it can be used as an added precaution if bone resorption should occur at a later stage. Also if the component is held this way there is less risk

of it slipping out of position during surgery. The implant design must lend itself to a quick and simple insertion procedure - a surgeon has only a limited amount of time for the operation, most of which will be taken up in soft tissue repairs.

The choice of material is one of the most important decisions to be made in prosthesis design since it is on the durability and suitability of this material, in its given application, that the success of the implant depends. The first consideration is one of biocompatibility and in the light of many years research a large number of materials (metallic, polymeric and ceramic) are available which are well tolerated in the body. For a surface replacement prosthesis it is necessary for the two components to be made of materials with good wear properties. They need not necessarily be made of the same materials provided the two materials are chemically compatible. They must also be strong enough to withstand the largest predicted joint forces and be fatigue resistant. Seemingly an ideal candidate for these requirements would be stainless steel. This is a material often used in joint replacement surgery for the hip and knee and has proved very satisfactory. However, these are weight bearing joints which require very much greater material strength than the finger joint and also have ample bone stock so that bone resorption (occurring as a result of hard material impinging on the bone) is far less of a problem.

A polymeric material such as Ultra-High Molecular Weight Polyethylene (UHMWP) would be sufficiently strong for a finger prosthesis and would also be rather less expensive to manufacture. The softer material would result in less bone resorption but may suffer cuts initiating a possible fatigue failure mechanism. Admittedly, in wear tests UHMWP against

itself has not compared favourably with UHMWP against stainless steel: indeed it has been reported to be 700 times worse in reciprocating pin on plate experiments (Atkinson, 1976 (100)). A rather better wear performance could be expected in-vivo if fluid film lubrication is present. This has been proposed for the MCP joint by virtue of its geometry, light loading and fast movement. It may be that the wear properties of polymer against polymer in the finger are good enough for the implant to function for twenty years which would be an acceptable lifetime. If this were not the case the wear resistance could be improved by making one component (the metacarpal component) from stainless steel.

The properties of UHMWP can be improved by cross linking. Chas F Thackray & Sons Ltd of Leeds have a new medical grade cross linked UHMWP which they have proposed as a possible material for the Durham surface replacement. The wear characteristics of this material are the subject of Chapter 6.

The design of the surface replacement proceeded on the basis that it would be a two component polymeric implant with the proviso that, should the wear characteristics prove unsatisfactory, the metacarpal component may later be made from stainless steel or CoCrMo alloy. For such an implant a detailed knowledge of the bone topography is essential.

2.3 BONE MODELLING AND MEASUREMENTS

Many of the dimensions necessary in the design of a surface prosthesis are given in the papers by Unsworth & Alexander, 1979 (20) and Unsworth et al, 1971 (19). In addition the major and minor axes (R_w and R_h) of the ellipsoidal recess of the phalangeal articulating surface are needed and, for the metacarpal component, the lengths a & b and angles θ, ϕ & τ (Fig 2.1).

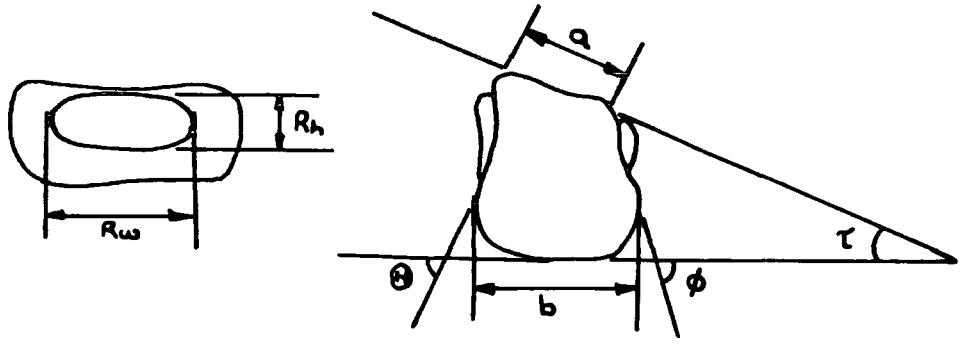

Fig 2.1 The articulating surfaces of the phalanx and metacarpal.

Measurement of these quantities was performed first using radiographs. Because of the limitations of a two-dimensional image, the measurements from the radiographs were not directly very useful but did demonstrate that different lengths could be simply related, and these relationships were used to scale the components over a range of sizes. Later more detailed measurements were taken from the matched clean bones of five hands using a toolmaker's microscope.

2.3.1 The Study of Radiographs

When a patient presents with arthritic disorders of the hand a control

bone for density comparison is included on the radiographs taken. This bone is embedded in a wax block which also appears clearly on the film and from which can be obtained the magnification of the image, its true size being known. In this way each film can be calibrated independently, hence accounting for film shrinkage (assumed linear) and source-to-plate distance.

The study was performed on radiographs from Middlesbrough General Hospital (Rheumatology Unit) taken during the period 1983 - 1986, during which time two blocks (1 & 2) were in use. The X-ray Department kindly provided two films (A & B) showing both blocks and incorporating a scale (Fig 2.2). The scale was of actual length 110 mm and had a mean length of 112.3 mm and 112.5 mm on films A & B respectively corresponding to a magnification of 1.02:1. Since radiographs of patients contain no scale it was necessary to measure the blocks in order to determine the magnification. A feasibility study was performed by calculating the magnification of films A & B from measurements taken of the blocks rather than the scales. A value of 1.03:1 for both films was obtained indicating that with care this method could be used with reasonable accuracy, only incurring an error of 0.1 mm in 10 mm. Measurements were taken from the radiographs of ten male and ten female hands, patients with severely degenerated joints being avoided to reduce error. Also, since angular measurements were not possible, only right hands were chosen.

From the radiographs the lengths a, b and R_w were measured and tabulated (Tables 3.1 - 3.4). In an attempt to relate the lengths a and b a graph of mean b against mean a was plotted (Fig 2.3). A least squares straight line fit is not valid in this case because the quantities of

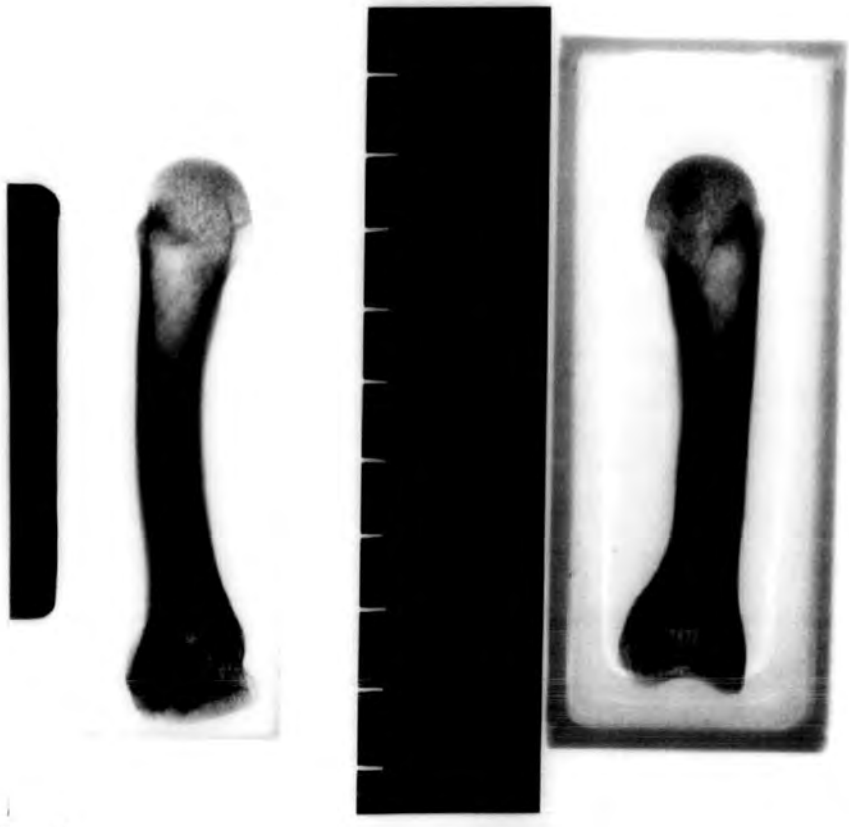

Film A

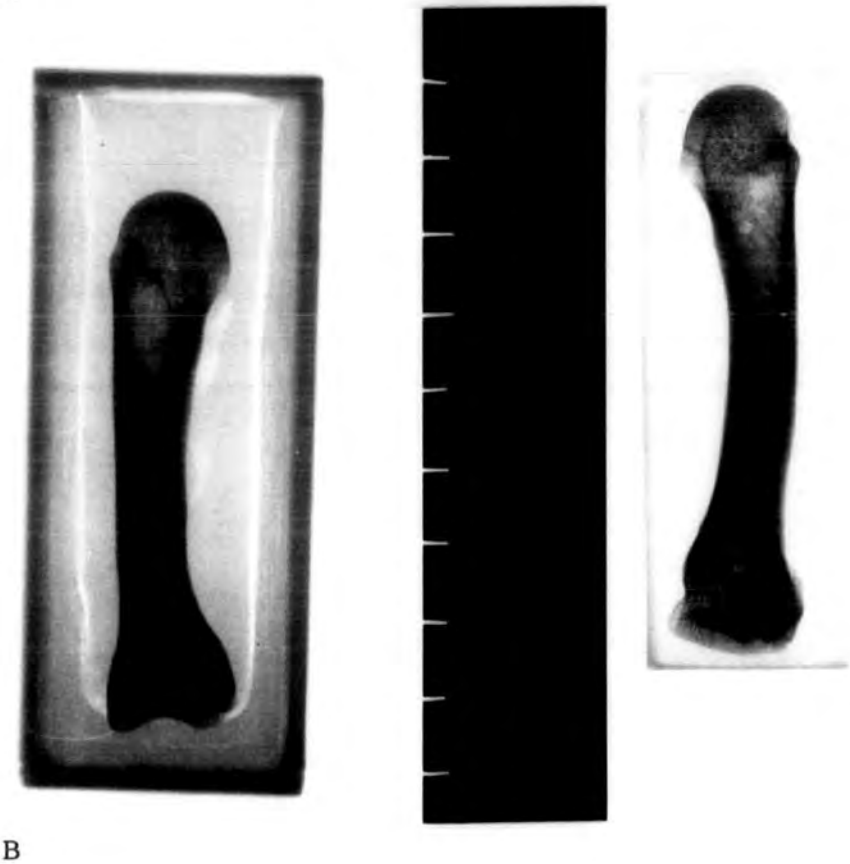

Film B

Fig 2.2 Calibration radiographs of standard blocks 1 and 2 with scale.

Index	$\overline{R_w}$ (mm)	$\bar{a}$ (mm)	$\bar{b}$ (mm)
M1	11.49	8.41	14.56
M2	10.84	8.74	12.46
M3	10.58	9.45	12.50
M4	11.43	8.89	12.70
M5	11.59	9.52	14.76
M6	11.27	9.05	11.90
M7	10.63	10.79	14.44
M8	13.17	8.89	15.08
M9	12.74	11.12	16.67
M10	12.34	10.73	14.74
F1	10.58	9.30	13.30
F2	9.38	7.28	12.78
F3	11.76	7.51	13.56
F4	11.33	5.99	9.87
F5	9.47	8.01	14.38
F6	10.48	7.94	9.52
F7	10.78	9.64	13.40
F8	11.11	8.73	13.97
F9	10.52	6.80	11.97
F10	11.43	8.33	12.74

Table 2.1 Index finger measurements from the radiographs of ten males and ten females.

Middle	$\overline{R_w}$ (mm)	$\bar{a}$ (mm)	$\bar{b}$ (mm)
M1	11.00	7.28	14.40
M2	10.84	9.38	11.97
M3	11.86	8.97	13.62
M4	12.38	9.36	14.92
M5	12.54	9.21	13.33
M6	11.90	8.41	16.51
M7	11.09	9.52	16.19
M8	11.75	8.73	15.87
M9	12.26	10.13	17.50
M10	12.17	9.61	16.99
F1	10.26	7.85	13.78
F2	10.19	7.12	13.43
F3	11.11	7.84	13.24
F4	11.49	8.89	12.30
F5	10.29	8.17	13.06
F6	10.16	7.94	11.90
F7	10.78	8.01	14.38
F8	11.59	7.62	14.76
F9	9.87	7.77	13.92
F10	12.09	8.82	14.70

Table 2.2 Middle finger measurements from the radiographs of ten males and ten females.

Ring	$\overline{R_w}$ (mm)	$\bar{a}$ (mm)	$\bar{b}$ (mm)
M1	9.55	6.96	11.97
M2	10.52	9.06	11.65
M3	11.54	9.61	12.50
M4	10.63	7.78	13.49
M5	10.79	8.57	13.33
M6	10.32	8.57	13.33
M7	11.75	9.05	14.44
M8	11.43	8.57	13.65
M9	9.80	8.82	14.86
M10	11.38	7.69	15.55
F1	8.20	5.92	11.70
F2	8.25	7.12	11.97
F3	9.64	7.57	10.94
F4	9.87	8.58	11.81
F5	9.31	7.51	12.58
F6	9.05	7.78	10.63
F7	9.15	7.35	12.74
F8	10.48	7.62	13.02
F9	8.25	7.12	11.00
F10	9.80	7.84	12.42

Table 2.3 Ring finger measurements from the radiographs of ten males and ten females.

Little	$\overline{R_w}$ (mm)	$\bar{a}$ (mm)	$\bar{b}$ (mm)
M1	8.09	7.28	11.97
M2	10.19	8.74	11.00
M3	9.30	8.12	11.22
M4	8.25	6.98	12.54
M5	9.36	8.41	10.63
M6	10.00	7.78	11.90
M7	9.52	7.62	12.06
M8	9.84	7.62	13.02
M9	9.80	7.84	13.06
M10	10.42	8.40	14.58
F1	8.81	5.92	10.89
F2	8.58	7.12	10.19
F3	8.49	7.35	10.94
F4	8.74	7.44	11.16
F5	8.49	8.49	10.78
F6	8.73	7.62	9.68
F7	8.82	6.05	11.44
F8	9.05	7.46	11.43
F9	8.25	6.31	9.71
F10	9.15	7.85	10.62

Table 2.4 Little finger measurements from the radiographs of ten males and ten females.

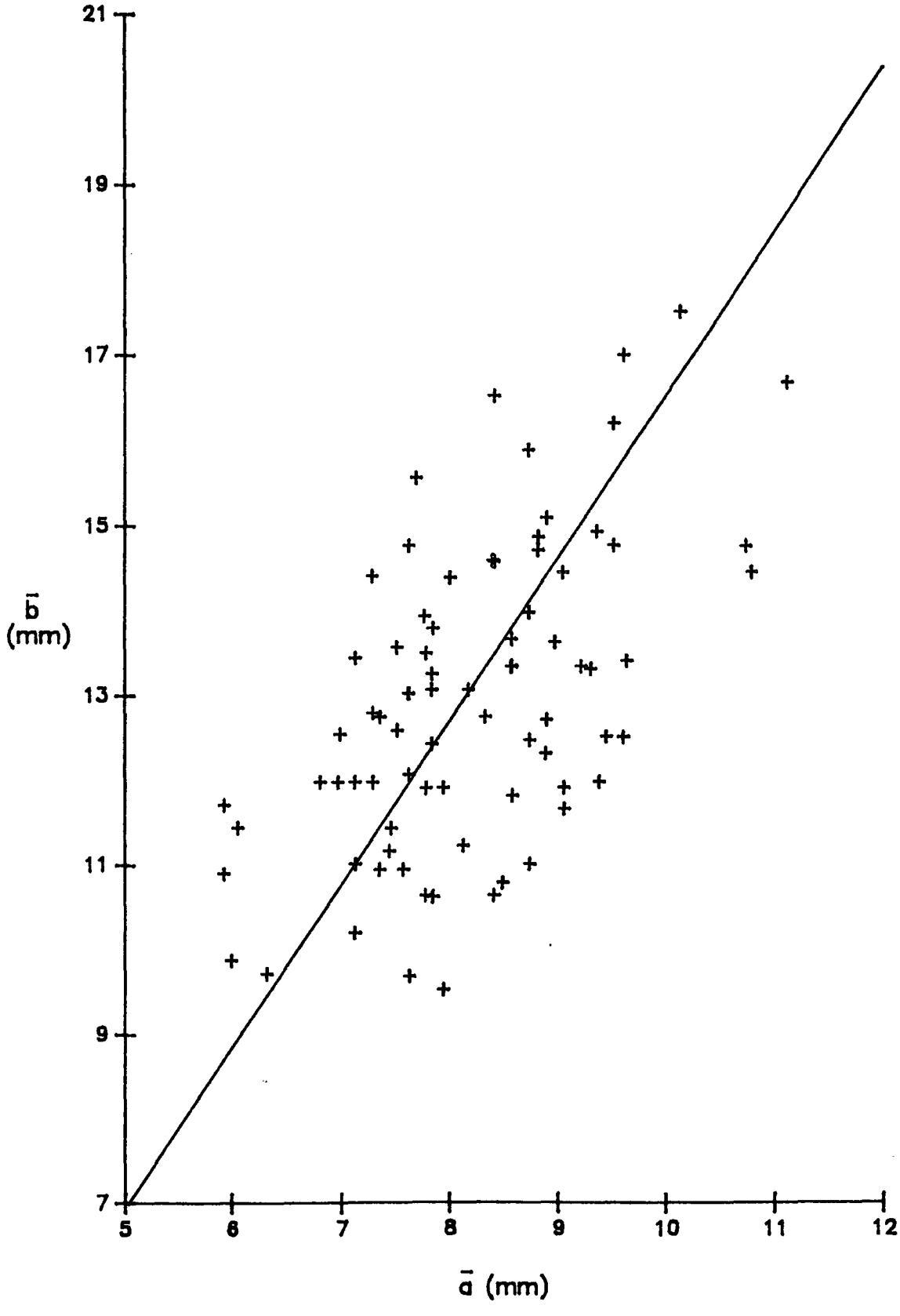

Fig 2.3 Graph of mean b against mean a for the metacarpal.

both axes are in error. However, in their paper giving linear correlations between sulphur-nitrogen bond distances and bond angles, Banister et al in 1985 (104) described a linear regression method which enabled them to deal with data from radiographs in much the same way as was required here. The model was adapted and used to give a straight line fit of b = 1.918a - 2.6601 which seems quite good despite the large scatter in data (19% in a and 12% in b). Polynomial and exponential regression fits were also tried but with far less success than the linear fit. The simplicity of the linear relationship encouraged investigation into other such simple relations during the more detailed study of bone topography, which proved fruitful.

2.3.2 The Study of Bone Heads

Clean matched bones of five hands were kindly lent by the Newcastle Medical School and measurements of the important lengths and angles were made using a toolmaker's microscope. This is an optical microscope incorporating a large illuminated specimen table which can be rotated and moved in the x, y & z directions using micrometer screw adjusters. Fine cross-hairs in the eyepiece enable the accurate measurement of 'landmark' positions, distances and angles. The results obtained from this investigation are given in Tables 2.5 & 2.6. It should be noted that the measurements - apparently small when compared to published data (Unsworth & Alexander, 1979 (20), and Unsworth et al, 1971 (19)) - are those of completely clean bones. During surgery it is anticipated that the diseased articular cartilage will largely be removed before the implant is fitted.

Phalanges				Metacarpals		
Finger	R_w (mm)	R_h (mm)	R_w/R_h	h (mm)	b (mm)	r (mm)
index 1	10.97	8.75	1.25	11.49	11.54	6.20
2	10.03	7.57	1.32	10.80	11.13	5.45
3	11.48	9.33	1.23	12.72	12.92	6.43
*4	12.46	11.10	1.12	14.26	12.65	7.50
*5	11.85	8.93	1.33	12.08	11.72	6.70
middle 1	10.68	8.77	1.22	13.90	11.13	7.00
2	10.10	8.39	1.20	11.10	9.94	5.55
3	12.23	10.13	1.21	14.67	13.33	7.55
*4	12.86	10.15	1.27	15.27	13.33	7.70
*5	11.89	8.93	1.33	12.36	10.72	6.50
ring 1	10.17	8.27	1.23	11.73	9.28	6.10
2	9.15	7.50	1.22	10.49	9.01	5.25
3	10.89	9.29	1.17	13.22	11.33	6.70
*4	11.53	9.65	1.19	13.73	10.76	6.90
*5	11.15	8.45	1.32	11.29	10.23	5.98
little 1	9.55	7.80	1.22	10.12	9.40	5.25
2	9.18	7.64	1.22	9.00	8.53	4.65
3	10.59	9.05	1.17	11.56	11.85	6.05
*4	11.19	8.96	1.25	11.64	10.84	6.10
*5	11.00	8.13	1.35	10.26	9.78	5.30

* - Right hand bones

Table 2.5 Length measurements from matched bones.

Finger	θ	ϕ	τ
index 1	58°18'	86°54'	+16°24'
2	46°03'	81°00'	+ 8°36'
3	51°33'	89°57'	+ 2°42'
*4	86°12'	63°42'	0°00'
*5	71°12'	50°06'	- 8°54'
middle 1	90°54'	72°06'	+18°24'
2	81°48'	74°06'	+10°36'
3	80°18'	71°42'	+19°30'
*4	70°48'	81°33'	-25°40'
*5	68°27'	76°12'	- 4°30'
ring 1	92°22'	75°06'	+ 4°24'
2	87°24'	67°36'	+ 0°12'
3	85°18'	76°00'	+11°00'
*4	79°00'	76°06'	- 2°54'
*5	64°18'	78°54'	-11°00'
little 1	84°36'	68°03'	- 6°48'
2	73°33'	60°30'	-20°36'
3	73°03'	66°03'	- 8°09'
*4	70°36'	81°54'	+10°27'
*5	59°30'	74°33'	+10°12'

* - Right hand bones

Table 2.6 Angular measurements from matched bones.

2.4 RESULTS

It is probably easier to inspect the results of the metacarpal and phalanx bones separately since the phalanx shape is far less complicated. The lengths taken from the phalanx were the major axis R_w and the minor axis R_h. It seemed reasonable to suppose that some relationship existed between the two and, indeed, the graph of R_w against R_h gives a good straight line $R_w = 0.9772R_h + 2.2982$ (Fig 2.4).

The graph showing the radius of curvature r against R_h also appears as a straight line $r = 0.84046R_h - 1.33145$ (Fig 2.5). The radius measurements taken were those of the respective metacarpal heads which may not necessarily be the same as those of the phalanges (Unsworth et al, 1971 (19)). Given the rather small number of data points, the straight line fits were remarkably good and it was a simple matter to produce a set of phalangeal component sizes based on a radius range of 7 mm - 10 mm (in increments of 0.5 mm), the results being displayed in Table 2.7.

Internal Radius (mm)	7.00	7.50	8.00	8.50	9.00	9.50	10.00
Minor Axis (mm)	8.72	9.32	9.91	10.51	11.10	11.70	12.29
Major Axis (mm)	10.82	11.40	11.98	12.56	13.14	13.73	14.31

Table 2.7 The range of phalanx sizes.

The lengths taken from the metacarpal were the height h, the base width b and the radius of curvature r. The angles measured were θ, ϕ and τ

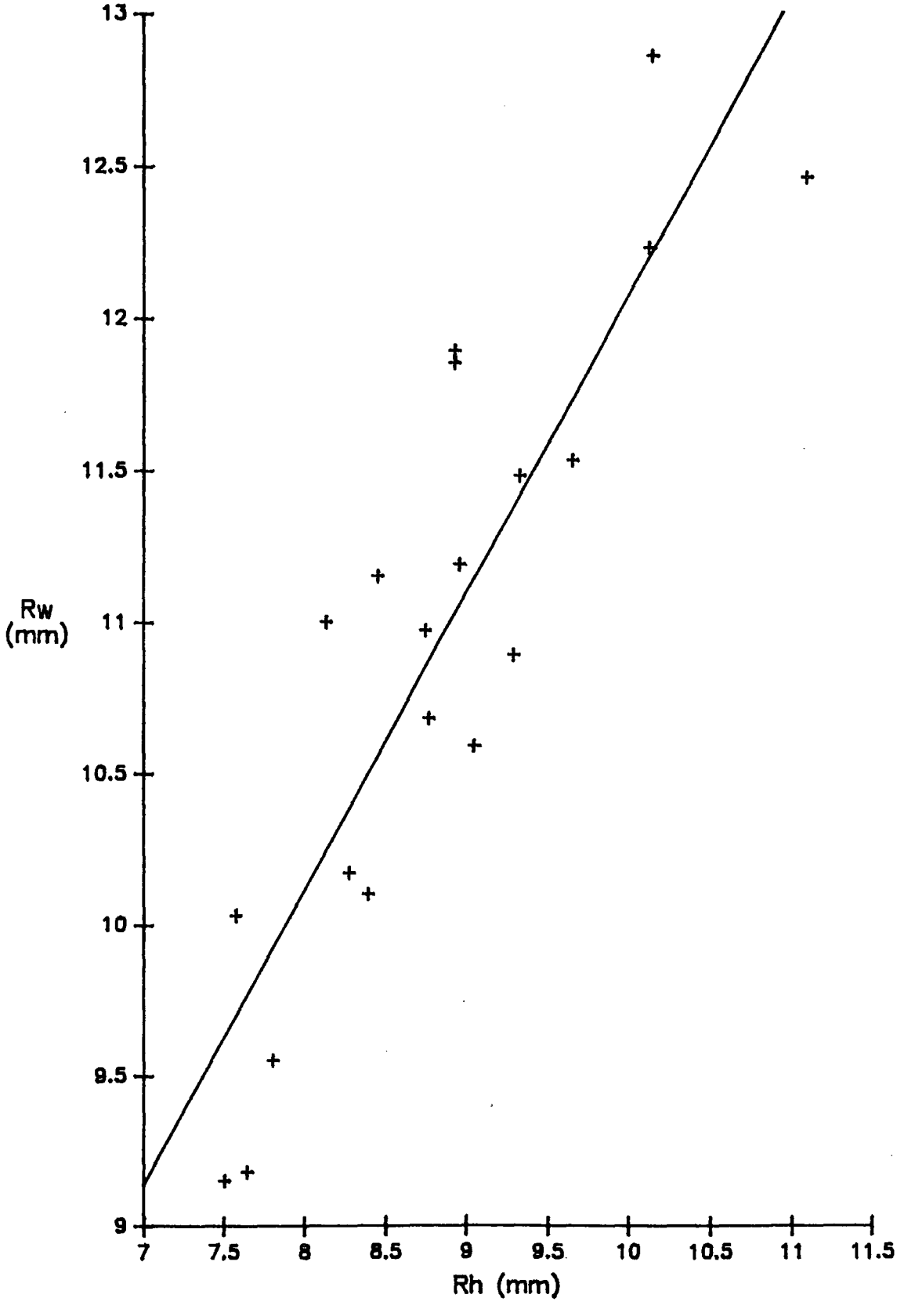

Fig 2.4 Graph of R_w against R_h for the phalanx.

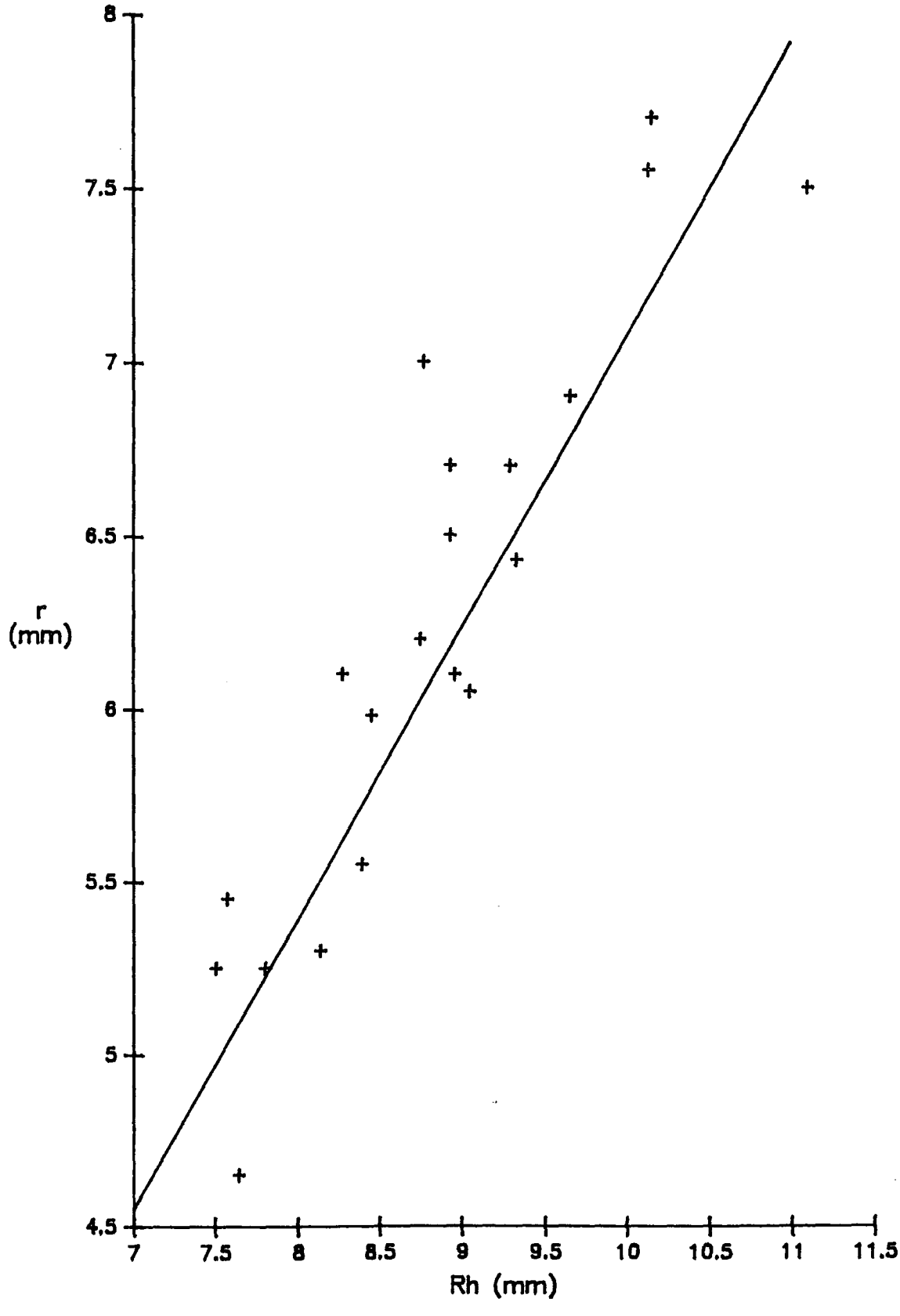

Fig 2.5 Graph of r against R_h for the phalanx.

(see Fig 2.1). As expected, the metacarpal proved rather more difficult to deal with than the phalanx. The shapes of the articulating surfaces for a typical right and left hand are shown in Fig 2.6 and can be seen to be non-symmetrical and rather complex. The index finger profile in particular is unusual.

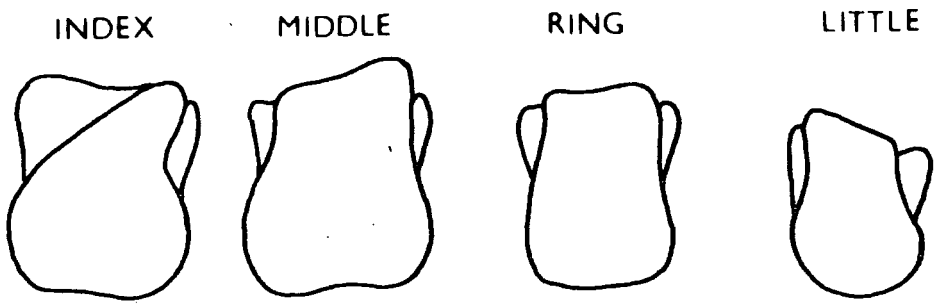

Fig 2.6 The articulating surface profiles of typical metacarpals.

It was discovered from the measurements that the base width b and the radius of curvature r were directly proportional, the ratio b/r being 1.75 with a standard deviation of 0.16. It is perhaps easier to see the similarities of the metacarpal heads through simple quadrilateral representations, obtained from the measurements (Figs 2.7 - 2.10). The superimposed circles are chosen to have the most suitable radii of the range defined previously (Table 2.7). In this way it is possible to envisage how a simplified articulating head can be modelled by cutting down a hemispherical shell.

Putting aside the index finger for a moment, the general shape of the metacarpal heads was observed to be fairly consistent. Thus the statistical averages of measurements θ, ϕ and r were calculated and a standard geometrical shape was adopted which could be scaled in size

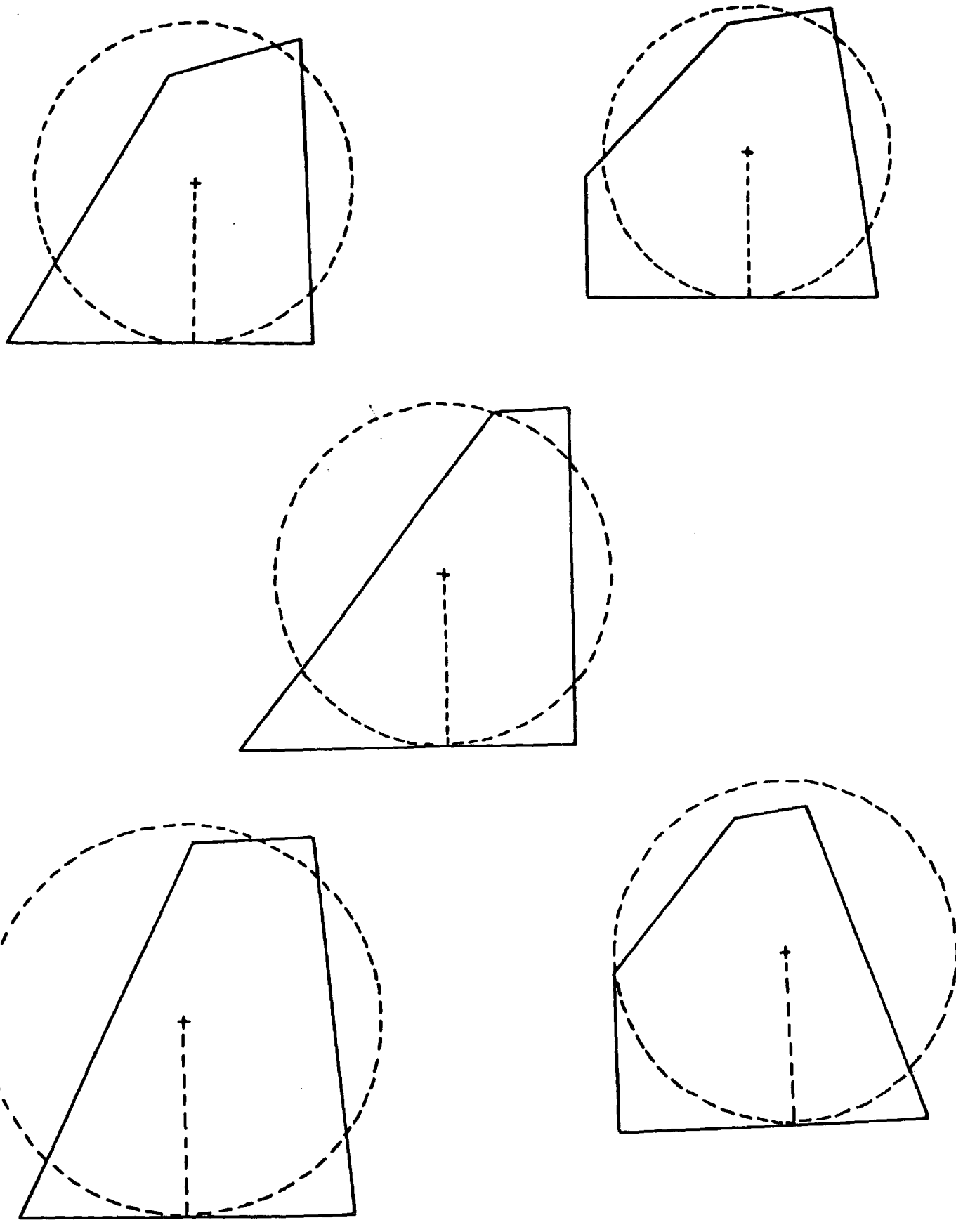

Fig 2.7 Quadrilateral representations of five left index fingers.

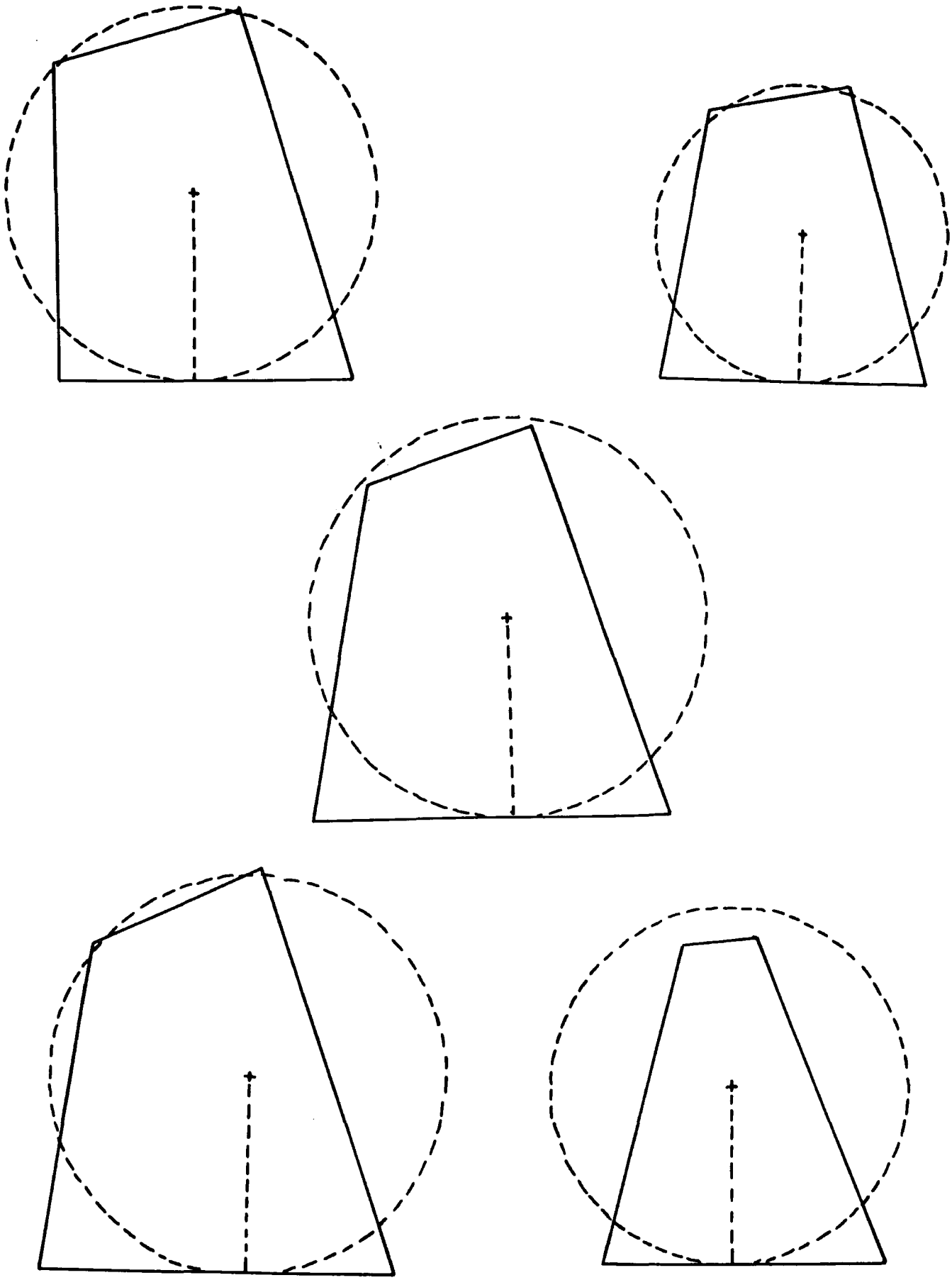

Fig 2.8 Quadrilateral representations of five left middle fingers.

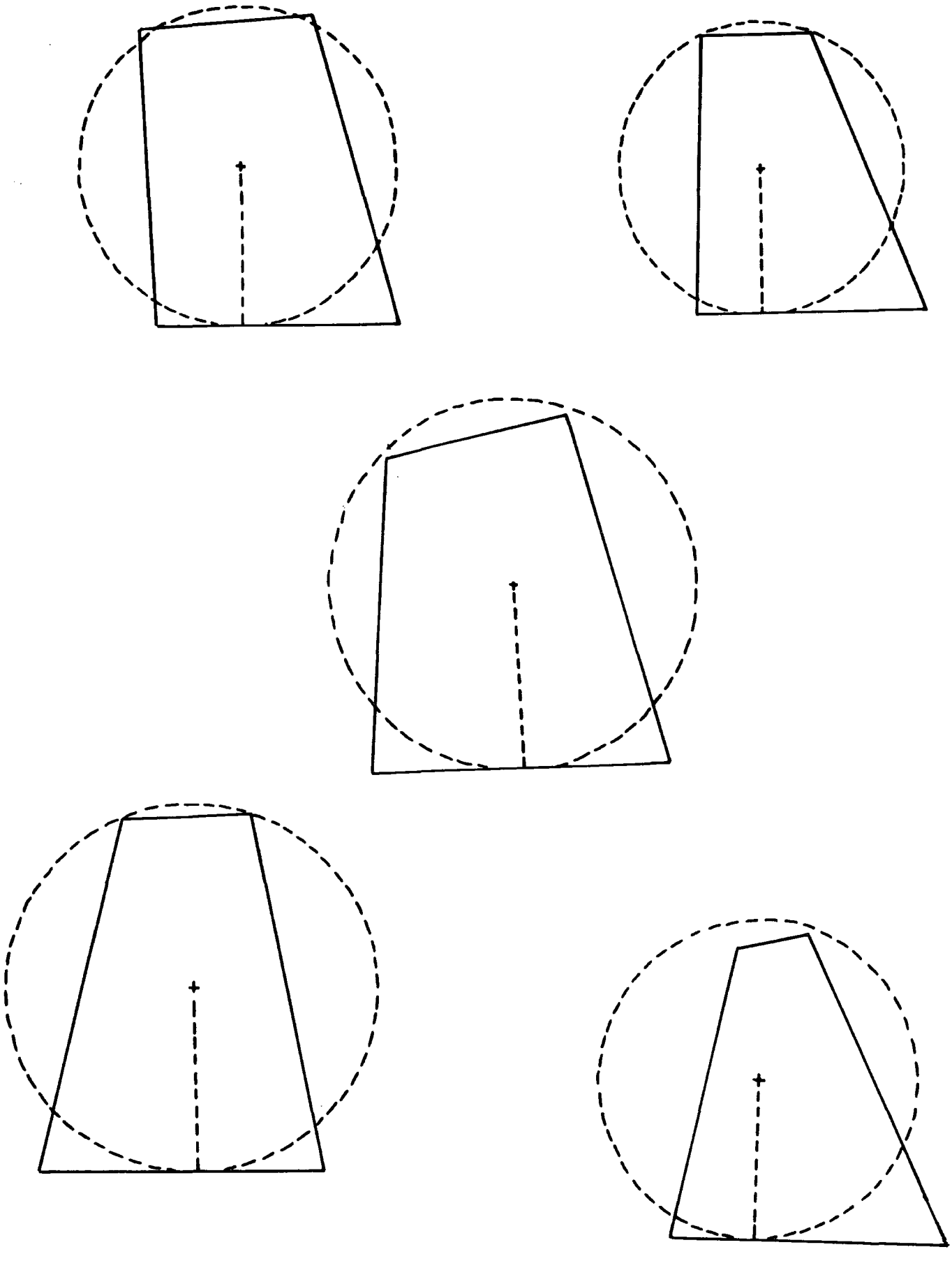

Fig 2.9 Quadrilateral representations of five left ring fingers.

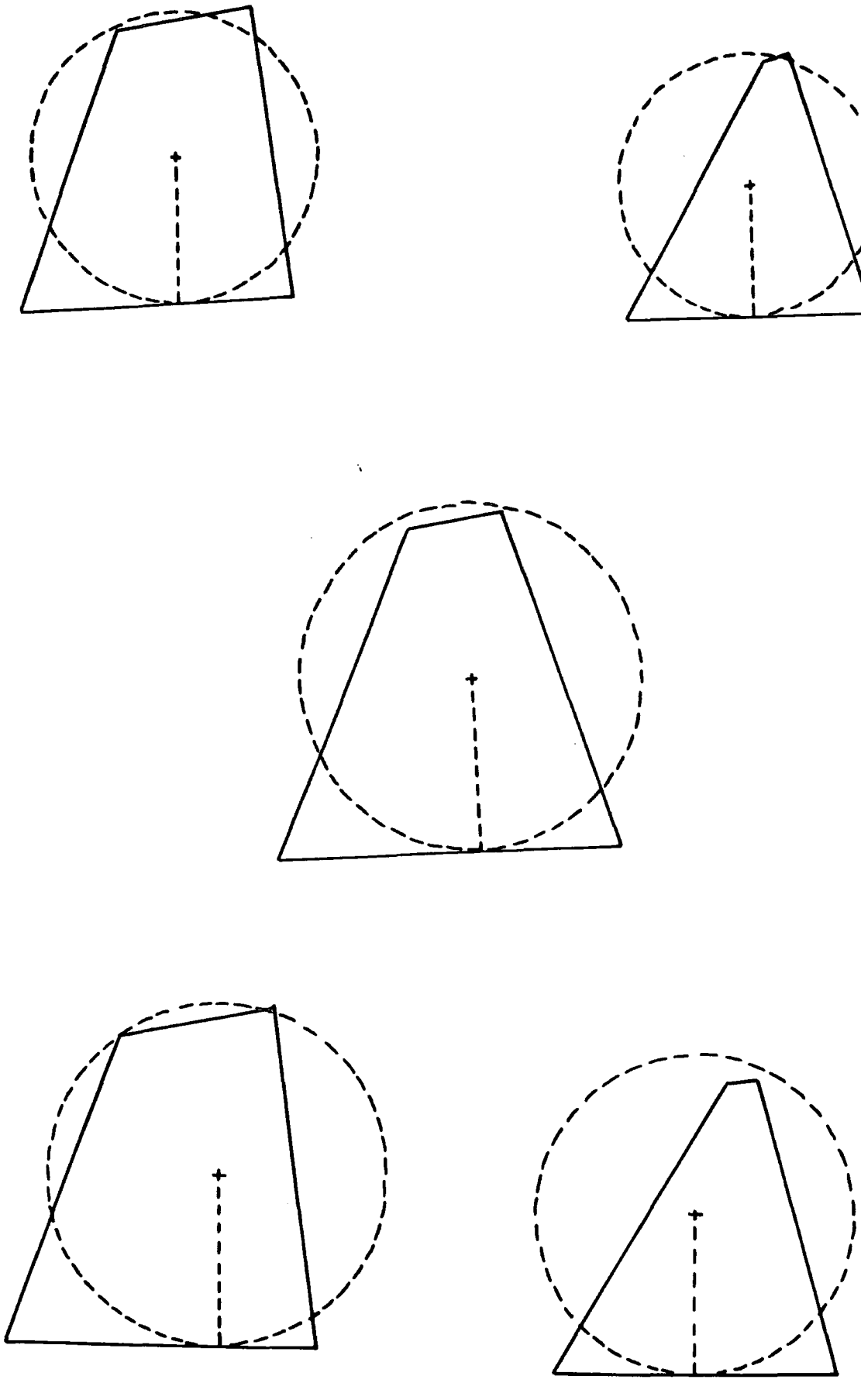

Fig 2.10 Quadrilateral representations of five left little fingers.

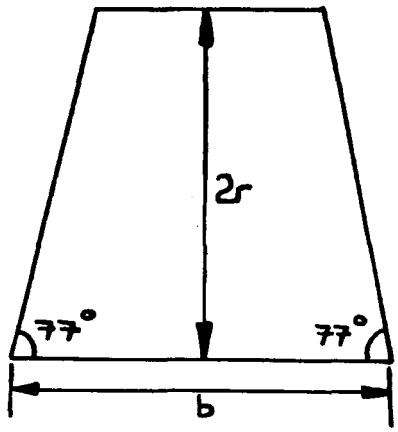

Fig 2.11 The standard shape of the metacarpal articulating surface.

according to the radius (Fig 2.11). Since this shape was symmetrical it could be used for both right and left hand bones, cutting down the number of components necessary. The index finger, although rather different in profile to the rest, was investigated for its suitability for this standard shape and was found to be quite acceptable. The problems associated with the index finger are detailed later. The size range is shown in Table 2.8.

External Radius (mm)	7.00	7.50	8.00	8.50	9.00	9.50	10.00
Base Width (mm)	10.79	11.69	12.60	13.50	14.40	15.29	16.20
Top Width (mm)	4.32	4.76	5.20	5.64	6.09	6.52	6.97

Table 2.8 The range of metacarpal sizes.

It may seem at first unreasonable to attempt to replace the natural articulating surface with components of such a simple form. It was apparent at an early stage that any form of surface replacement would be a compromise on the true shape of the bone head. If the shape were the only requirement the best approximation would be to take a series of

castings for each finger. This would result in at least 56 components for the metacarpal alone (7 sizes for each finger, both right and left). However, to do this would not only be expensive but would also limit the choice of material and serve to confuse the surgeon who undoubtedly would not wish to spend time searching through a large assortment of components to find a suitable one. Given that a simplification needed to be made, it was decided to employ a very practical design which would best satisfy the requirements of low cost, ease of manufacture, etc., without worrying unduly about the precise surface shape. After all, simplicity is so often the key to success as with the Swanson design for example.

By adopting a symmetrical shape suitable for both right and left hands the necessary number of components is halved. Since the adopted shape is also suitable for all four fingers the only remaining consideration is size, reducing the minimum range to just seven components each for the phalanx and the metacarpal. The proposed material is UHMWP which is cross linked after moulding. This suits these components, which need to be injection moulded due to their complex shape.

It was not easy to see exactly how good a covering could be achieved by such a component, particularly for the index finger, and so a series of acrylic models were made by hand for appraisal. The components for matching phalanx and metacarpal bones were cut from hemispheres of the same radius. The new joint, being totally conforming, would be a little more stable than the natural joint, and by increasing the surface contact the stresses transmitted across the joint are distributed more evenly. The models were made according to the following design. The modelling method and design improvements are described later.

2.5 DESIGN

The proposed component designs are shown in Figs 2.12 and 2.13. The phalangeal component has a simple ellipsoidal shape with spherical curvature which will fit into the natural articulating recess of the phalanx. If a shallow recess is cut into the bone the component will sit inside, being prevented from slipping by the surrounding bone. It is very unlikely that any significant 'pull-out' force will occur since the joint is normally in compression. The metacarpal component has the simple quadrilateral form adopted during the measurement stage which approximates to that of the articulating surface. This too has spherical curvature and was cut from a hemisphere originally (later a 20° extension on the volar aspect was found necessary to achieve full cover).

Since neither component must interfere with capsulo-ligamentous structures in any way it is essential that they do not protrude beyond the boundaries of the articulating surfaces and that any mode of fixation must be contained within these areas. In both cases the fixation comprises a short intramedullary stem. Frictional shear stresses and rotational forces should be well resisted by the geometry of the components but as an extra precaution the stems should be of square cross-section or contain fins. Certainly no cement is necessary and indeed is contra-indicated since the removal of the prosthesis (should this prove necessary) would then be difficult and damaging to the bone. Notice that the stem of the metacarpal component is offset dorsally from the centre of curvature: this is a very important consideration as discovered by Flatt in 1973 (39) who altered the design

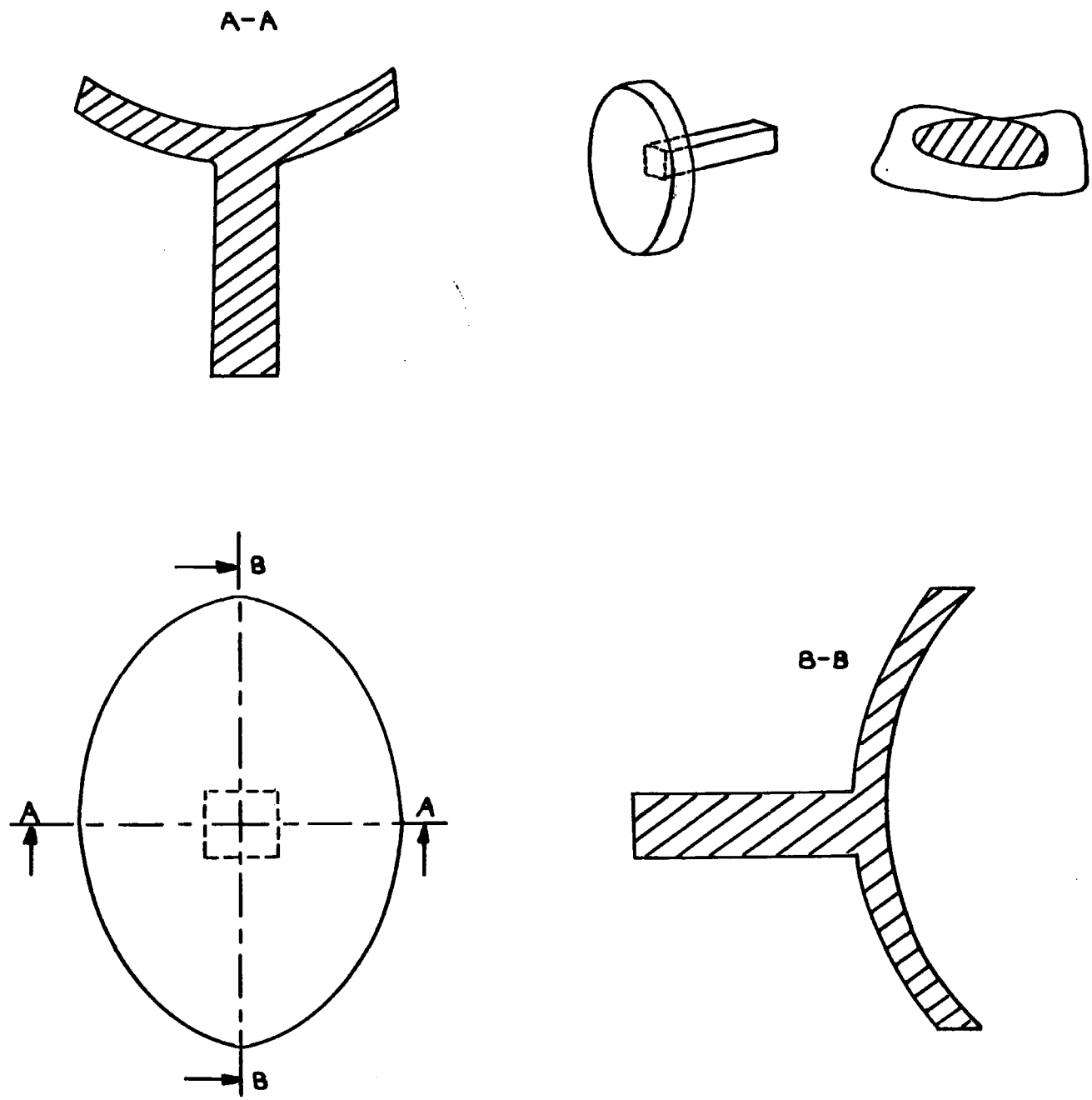

Fig 2.12 Proposed phalangeal component design.

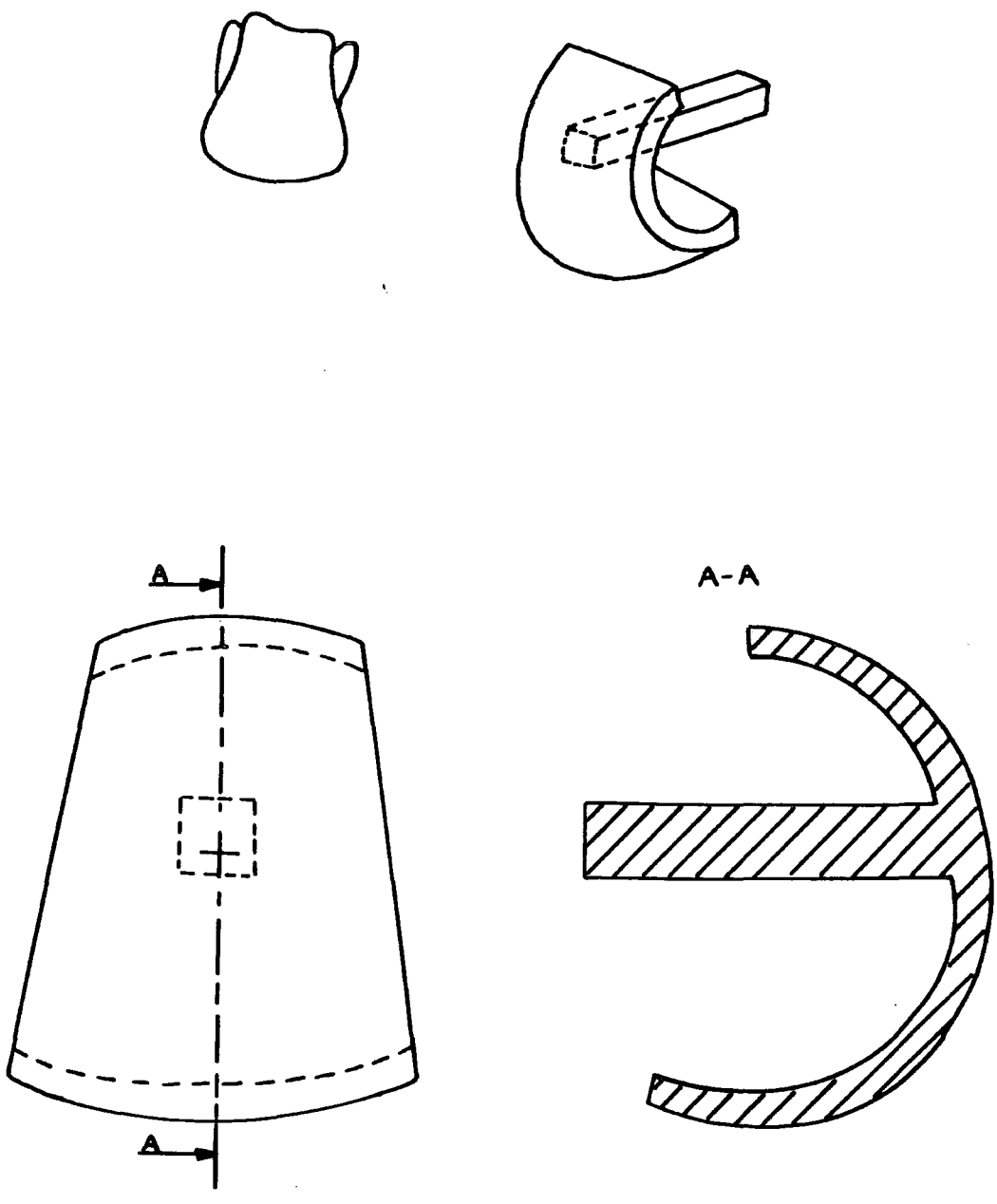

Fig 2.13 Proposed metacarpal component design.

of his metallic prosthesis to account for this. The amount of offset necessary is given in the paper by Unsworth & Alexander, 1979 (20).

Both components will be made from a cross linked polyethylene in the first instance for reasons stated previously. However,should it prove necessary at a later stage of development, the metacarpal component could be made from a castable metal such as CoCrMo alloy. Up to the completion of this thesis this has not been seen to be the case.

2.6 HAND-MADE MODELS & PROTOTYPE MANUFACTURE

Having put the basic design and size range on paper, the next stage was to make some first generation prototypes to assess feasibility. At this stage the mode of fastening was unimportant and could be omitted but the surface geometry was crucial, particularly for the index finger which might pose a problem. The first set of models was made to demonstrate how good a cover could be attained over the articulating surfaces of randomly chosen bones and to look at the suitability of the size range. The models were made from dental repair acrylic in the form of hemispherical shells and then cut down to the required shape. The method was as follows.

Seven blind holes were drilled into two perspex blocks. The holes in the first block had radii ranging from 6 - 9 mm in 0.5 mm intervals and in the second block they ranged from 7 - 10 mm. Stainless steel balls of matching radius were placed in each of the holes and fixed using loctite (Fig 2.14).

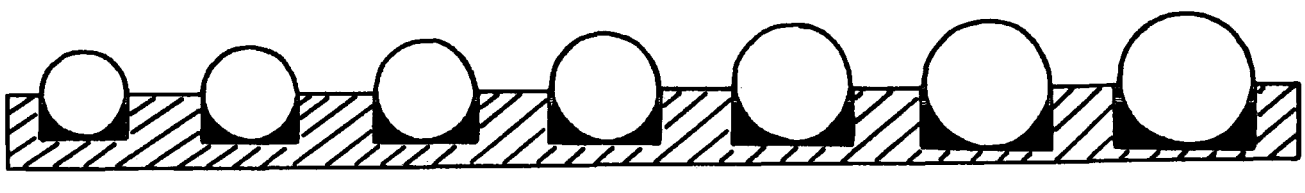

Fig 2.14 Perspex block with stainless steel balls.

The first block was placed in a deep box and plaster of Paris poured over. When the plaster was dry it was detached from the first block and placed in its own box to be covered with silicone rubber. The second

block was placed in a similar box and silicone rubber poured over. The resulting rubber former and die could then be used repeatedly for making hemispherical shells of 1 mm thickness over a range of radii (Fig 2.15).

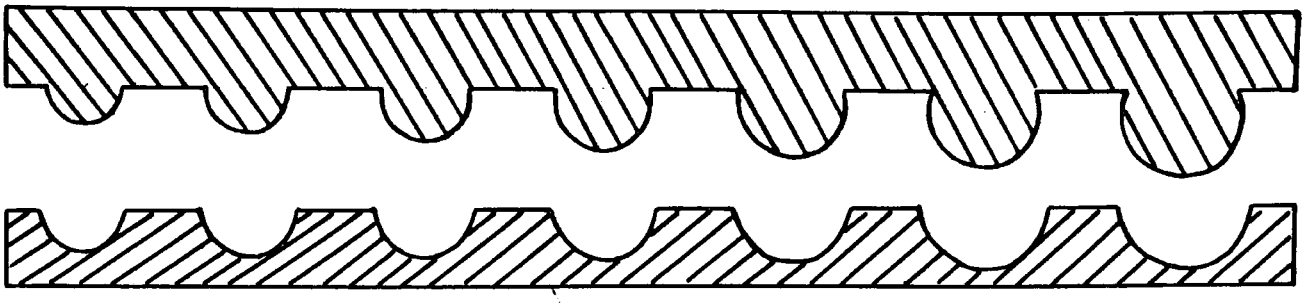

Fig 2.15 Rubber former and die for hemispherical shells.

A little dental acrylic was poured into each recess of the die then the former was lowered into place and weighted. When dry the shells were placed on the balls of the first block for support while the outline of the required component shape was drawn on in pencil. Lines were scored on the perspex block to help in this (Fig 2.16).

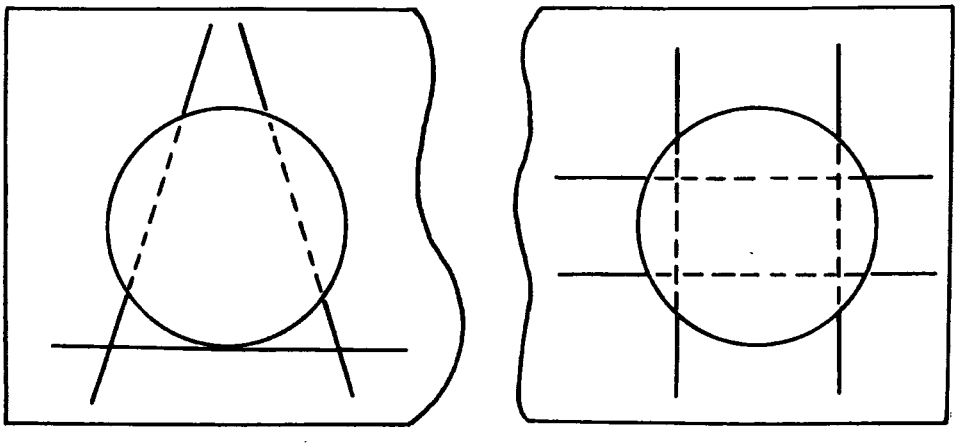

Fig 2.16 Scoring of the perspex block.

The drawn shapes were then cut out by using a fine piercing saw and a full set of phalanx and metacarpal components was made in this way.

When tested against several bones of different sizes the phalanx models appeared to cover the articulating surface very well indeed, as expected, and it was decided not to alter the profile at all. Second generation models were produced with 5 mm long intramedullary stems of square cross-section. The metacarpal shapes gave generally good cover of the articulating surfaces, for all non-index fingers, but tended to be rather short in the palmar aspect and sometimes left a narrow uncovered region medially. Contact was good in all places (Fig 2.17).

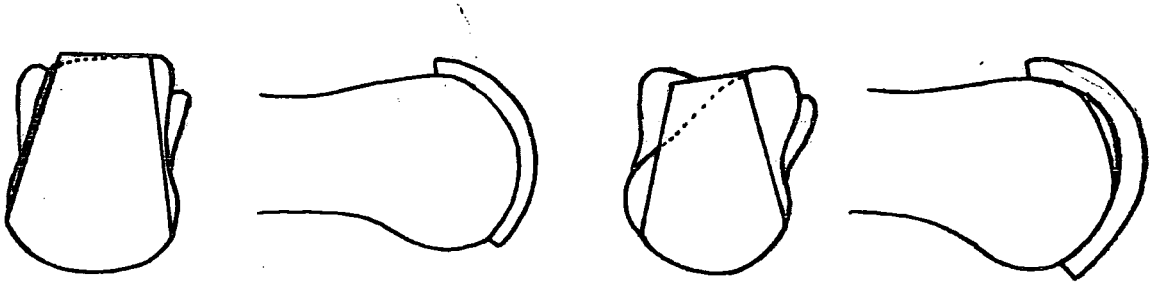

Fig 2.17 Testing the fit of the hand-made models.

For the index finger, again there was generally good cover for the articulating surface but there was consistently a large protrusion on the medial side. Contact was not always good everywhere and gaps occurred between the prosthesis and the bone head (Fig 2.17). In spite of these problems it was felt (because of the good cover) that it was not unreasonable to use this design for the index finger, particularly since it is intended that the implants will be sold with reamers and tools of the correct shape to prepare the bone surfaces. In this way problems of surface conformity are easily dealt with.

The design was improved by making an extension beyond the hemisphere of 20° on the volar aspect and decreasing the angle of the sides from 14° 36' to 13°. This would result in a slightly wider body and provide

improved coverage on the volar side.

The second generation of metacarpal models were produced, using a similar method to that previously described, and incorporating the design changes along with 5 mm intramedullary stems of square cross-section. These stems were offset dorsally from the centre of curvature by 2.63 mm (Unsworth & Alexander, 1979 (20)).

The new models were again tested against a selection of bones - this time with holes drilled to accept the stems and some surface preparation performed by hand with a file. The improvement was considerable.

After consultation with a plastic surgeon (Mr Charles Viva), it was agreed that the design was worth pursuing and a preference was expressed for a small intramedullary stem fixation. In this way, should it prove necessary to re-operate at a later stage, it would be a simple matter to insert the Swanson implant at revision. The stem, it was felt, should be rather longer than that of the second generation model - in the region of 15 mm in length. Fins on the stem should be considered but this may cause similar problems to cement should removal prove necessary and so work should continue using stems of square cross-section for the time being.

Contact was established with the company Chas F Thackray & Sons Ltd of Leeds who make a large range of medical equipment and also the Charnley hip prosthesis. They agreed to injection mould some prototypes in a new medical grade cross linked polyethylene that has been undergoing clinical trials for the past four years. Relatively little is known about the properties of this material though it would be expected to

behave in a similar way to normal UHMWP. It was decided that, along with fatigue and wear tests on the prototypes, an investigation into the wear properties of this new material and a brief stress analysis of the implant design should be carried out (Chapters 5 and 7).

The moulding tool was designed and made jointly in the workshops of Durham University and Chas F Thackray & Sons Ltd initially for one average-sized pair of components (size 4 - see Fig 2.18). The prototypes also fit very well onto the bones although it was noted that the flexibility of the material (not a property of dental acrylic) tended to make the implant 'bounce' off a bone which had a radius that was slightly bigger than its own. It is recommended that an implant slightly larger than necessary should be preferred over one smaller if an exact fit is not possible.

The cross linked prototypes have been assessed for durability in the finger function simulator and the results are very encouraging. The tests took place over a period of eight months and the results are discussed in Chapter 6.

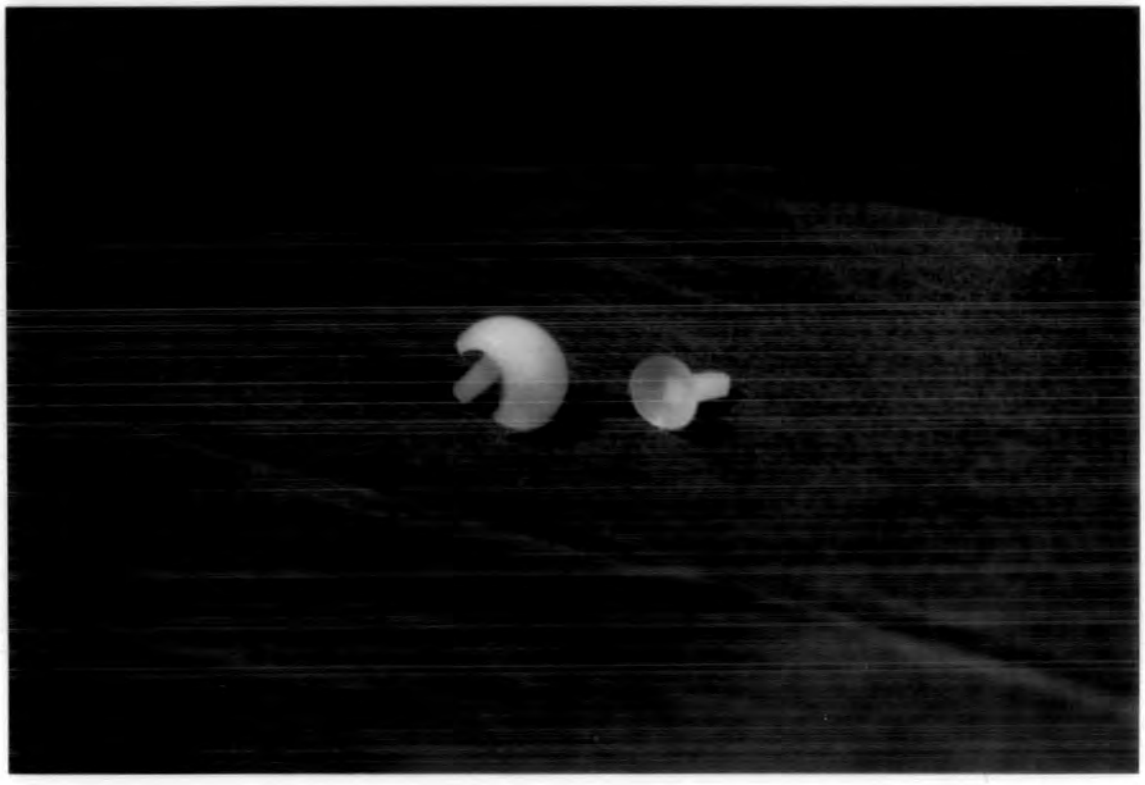

Fig 2.18 Photograph of the prototype components.

CHAPTER 3

THE FINGER FUNCTION SIMULATOR

3.1 MOTIVATION AND SPECIFICATION

Joint replacement surgery in the treatment of arthritic disease is now commonplace and on the whole very successful. Research into the design and development of prostheses has made major advances since the 1940's resulting in complex devices for almost all articulating joints of the body. Designers of such devices are increasingly using laboratory facilities to test their ideas before commencing clinical trials. In this way problems of wear and fatigue etc. can be monitored very closely. However, failure to simulate the situation pertaining in-vivo may leave one ignorant of inherent design problems however demanding the test procedures might be. As with, for example, the Swanson Silastic implant which, although it can be flexed several million times in the laboratory without failure, has commonly been prone to fracture in-vivo within a relatively short time of surgery. One device used to test this was built by Weightman et al in 1972 (96). Their machine used a form of scotch-yoke mechanism to flex the implants which were loosely held in Plexiglas blocks and immersed in serum. Although their tests revealed evidence of stress corrosion fatigue which would eventually cause failure, it is felt that this would have occurred rather sooner using a closer simulation. Some trials have been carried out using animals which are obviously helpful but also time consuming and lacking fine control. As part of the programme to design a new type of MCP joint replacement, a finger function simulator was designed to provide some method of realistic assessment. Several assumptions and simplifications had to be made to provide the closest simulation that could realistically be achieved mechanically.

If one considers the human hand in normal use there are really two modes of operation. Firstly, the finger should be capable of performing very delicate tasks needing dexterity of the fingers. An example of this is that when typing, the fingers will be moving quite quickly but are under very little load. Secondly, the hand may be required to apply a strong grip force when, for instance, turning a key or holding a pan. The movement of the fingers here is minimal but the joint force is very large. A successful MCP prosthesis needs to have a good range of motion and to be resistant to wear caused by sliding surfaces and to fatigue caused by cyclic flexion. It must also be able to withstand the stresses placed upon it during heavy loading. The simulator, then, must flex the MCP joint cyclically over the whole range of motion (0° - 90°) with very light loading and must also periodically apply a heavy static load to simulate grip.

The motion produced need only be uni-planar since flexion and extension of the finger is by far the predominant action and therefore of greatest concern. To try to reproduce circumduction of the finger would greatly complicate the simulator design for little reward. Undoubtedly in the past the natural ability of the finger to move laterally has caused prosthesis failure as with, for example, the Flatt metallic hinge which, having been designed to restrict joint movement to a single plane, suffered hinge fractures and stem fatigue due to large stresses from recurrent ulnar drift (Blair et al, 1984 (44) and also Flatt, 1983 (38)). However, for other designs, for example the Steffee prosthesis, in which some stability has been sacrificed in favour of increased freedom, the effects of lateral motion are similar to those of flexion/extension though to a lesser degree. This is particularly true in the case of a surface replacement prosthesis where the problems are

largely those of wear. It is possible, however, that stresses occurring due to persistent post-operative ulnar drift may combine with and accentuate the effects of stresses applied during flexion and extension. Some provision should be included in the simulator design to enable reproduction of this effect.

To test fully the prosthesis it is insufficient to place it in the simulator without first inserting it into finger bones. The interaction of the implant with the bone is an important consideration since cuts from bony spurs can accelerate fatigue as for example with the Swanson Silastic implant. If the bones were mounted independently in clamps then the plane of motion could be rotated through 90° if required in order to look at abduction and adduction. The clamps must be easily removable for regular inspection of the implant during long term testing, and adaptable to accept bones of different sizes.

The MCP joint is by no means a simple structure anatomically and it would be impractical to attempt to reproduce it exactly by mechanical means. This would not only be surplus to needs but also difficult to co-ordinate. The relative importance of local soft tissue structures in joint function and stability has been discussed in Chapter 1, and simplifications can be made in the light of information from the available literature. A single wire producing extension and one producing flexion is sufficient to represent the actions of all the muscles associated with the MCP joint since by far the greatest contribution to movement in this plane is made by the tendons of the FDP, FDS and EDC. Path restrictions normally imposed by the tendon sheaths can be provided by simple pulleys. The volar plate and metacarpoglenoidal ligament can be simulated using a mobile pulley

pivoted about the point of attachment of the ligaments just dorsally and distally from the centre of rotation of the joint. Stability against volar subluxation normally provided by the collateral ligaments must be included also. However, it should be remembered that the simulator needs to be capable of accommodating various designs of prosthesis in their normal mode of operation. In many cases the surgical procedure involves the resection of the metacarpal head and removal or relocation of ligamentous structures such as the volar plate. The function of the simulator must therefore not rely on their presence and they should be easily removable.

It has already been seen that there are two levels of loading at the joint. During cyclical motion the load required is less than 20 N and can easily be applied by increasing the working tension in the 'tendons'. In this way the load is also variable which is important since this affects the wear rate of sliding contacts. The application of a heavy static load is more complicated and must also be applied through the 'tendons' in some way. During pinch grip the majority of the force is carried through the flexor apparatus with the extensors relaxed (Smith et al, 1964 (2), Weightman & Amis, 1982 (1)) and this has been shown using electromyographic techniques (Long et al, 1970 (3)). Since this results in large subluxing forces at the MCP joint that are potentially damaging to an implant it is vital that the simulator produces the same kind of loading. Some method of releasing the extensor apparatus, or at least of greatly reducing its effect in comparison with the flexor, is needed. If the finger is pulled against a restraining pin, representing the thumb, at a position of about 30° flexion (the average pinch grip position (Weightman & Amis, 1982 (1))) then force conditions very similar to those found in-vivo should be

achievable. Pre-operative pinch grip strength has been measured to be between 5 N and 20 N (Linscheid & Dobyns, 1979 (17)) compared with the normal pinch grip strength of between 50 N and 70 N (Walker & Erkman, 1977 (14), Jones et al, 1985 (16)). Hagert in 1978 (18) reported that the strength of patients after joint replacement surgery was up to twice their pre-operative strength. 40 N would produce an MCP joint force of 184 N (40 x 4.6) (Weightman & Amis, 1982 (1)). The load can be applied pneumatically and varied as required by regulating the supply pressure. Obviously the force needs to be monitored using transducers and since fatigue tests may run for several weeks, an automatic control and data collection system must be incorporated. To further imitate conditions in-vivo the joint should be immersed in saline at 37°C.

By no means the least important consideration in the building of the simulator is cost, and the design must be kept as simple as possible without compromising its function. The following section describes the simulator as it now stands. It is a versatile machine and it is believed that it is one of the first devices of its kind, which hopefully will play an important role in the assessment and further development of finger joint prostheses.

3.2 THE SIMULATOR DESIGN

The simulator can be split into three main sections. The lower section (Fig 3.1) is a perspex bath containing saline solution held at 37°C in which the pulleys and clamps, holding the bones of the finger joint, are situated. The upper section is the drive and pinch force system through which the cyclical motion of the joint and the heavy static loading are achieved (Fig 3.2). The remainder of the rig (Fig 3.3) comprises the control and data collection circuitry.

The lower section consists of two stainless steel clamps in which the metacarpal and proximal phalanx are held. It is very important, since the finger bones are mounted separately, to ensure that their long axes are in line. Real bones are a rather difficult shape to hold but the outer profile of the shaft is irrelevant when testing MCP joint prostheses. It was decided, therefore, to set the shafts in acrylic cylinders of diameter 10 mm leaving the bone heads exposed. This enabled the clamp design to be kept very simple. The cylinder rests upon two v-shaped knife edges with a third in the middle being screwed down from above to give three-point fixing (Fig 3.4). In this way not only are the bones easily removable but are also certain to be properly aligned. Of course there is also the opportunity to alter the alignment of the bones and reproduce the effects of ulnar drift by putting a taper on the phalangeal cylinder.

The phalangeal clamp is free to pivot through a 100° arc about the centre of rotation of the joint. It is supported on a low friction UHMWP slide and guided by ball bearings moving in a semi-circular track.

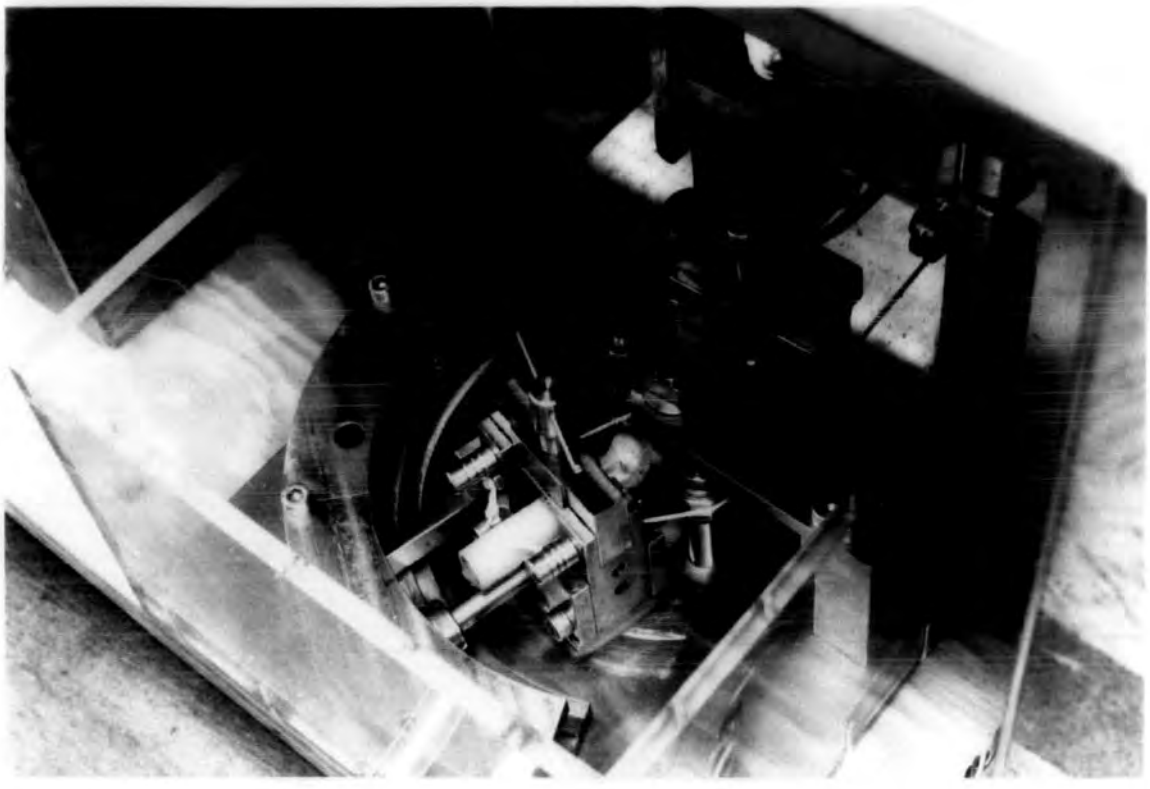

Fig 3.1 Clamp and pulley section of the simulator.

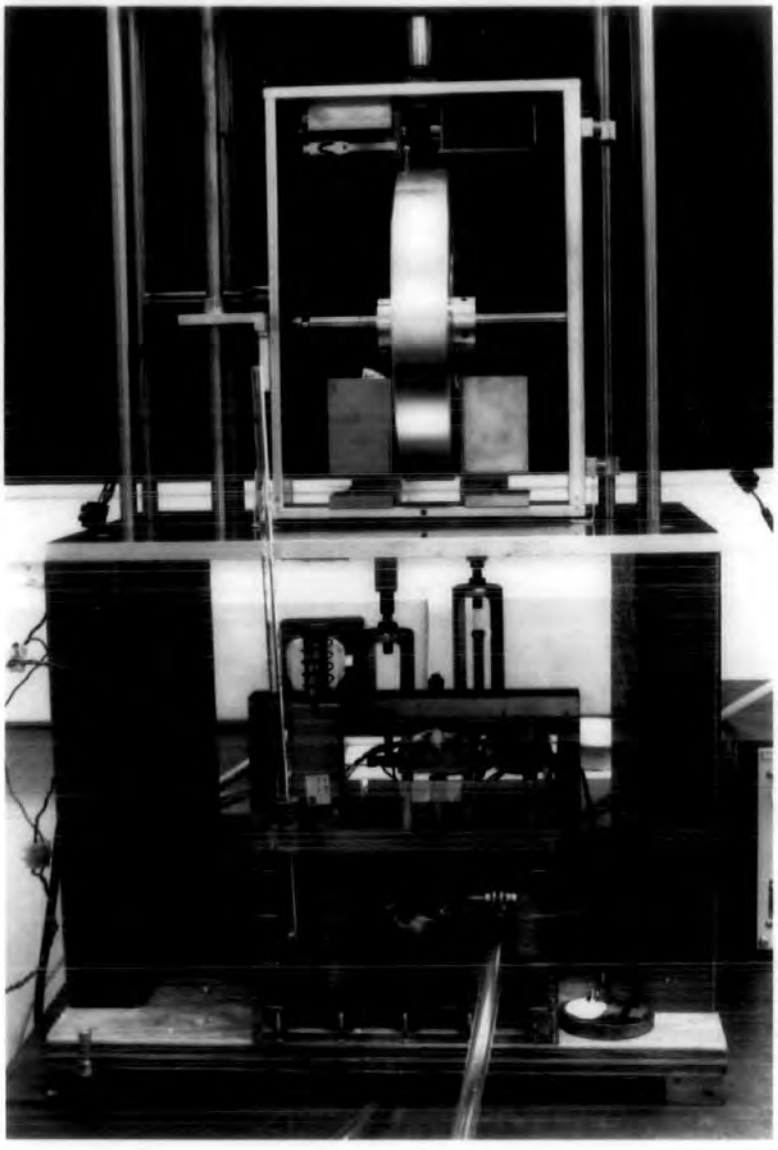

Fig 3.2 Drive and lift section of the simulator.

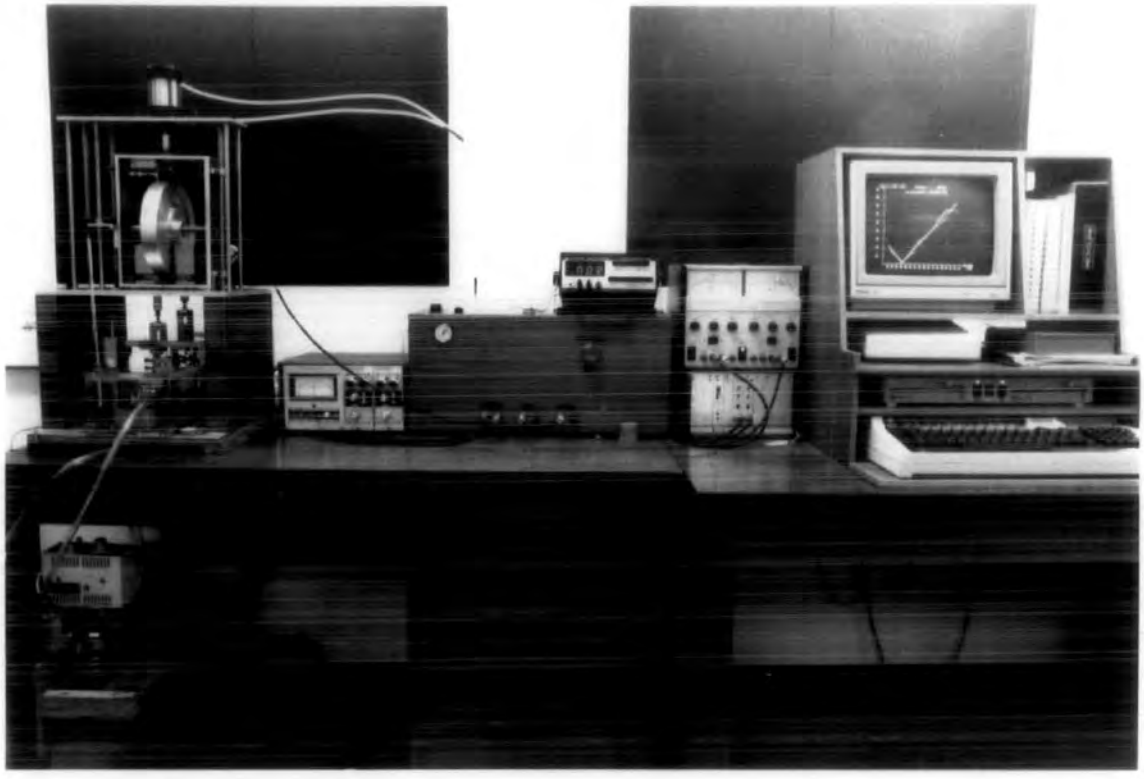

Fig 3.3 Control and data collection system
of the simulator.

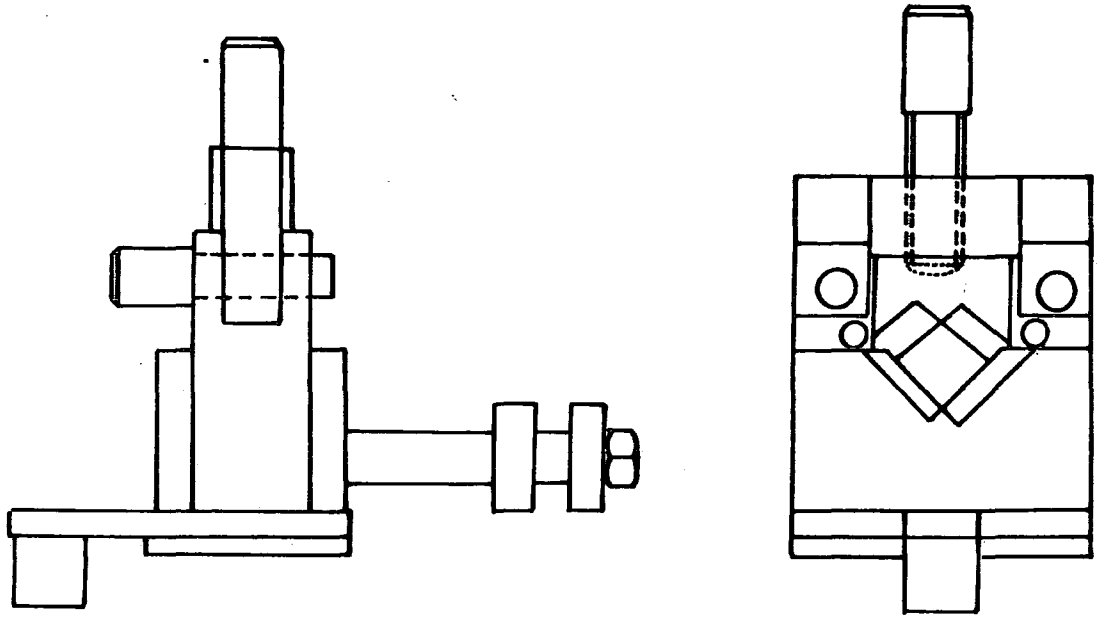

Fig 3.4 The phalangeal clamp.

The function of the ball bearings is to restrain the movement of the joint to a single plane, this plane being horizontal rather than vertical to eliminate any gravitational effects on the joint action. At the front of the phalangeal clamp there is a locating peg which rotates inside an oversize hole in the baseplate. This affords some 'ligamentous' stability to the joint by preventing the joint surfaces from separating. Because it is oversize it does not determine the centre of rotation of the joint and the loading passes through the joint rather than the baseplate. The metacarpal clamp remains stationary and is suspended from an overhead gantry by a strain-gauged cantilever beam through which force measurements in two directions can be made.

The two artificial 'tendons' used to represent the actions of all muscles associated with the MCP joint pass through holes in the phalangeal clamp close to the bone and are retained at the back by washers. They then follow separate pulley systems to the drive mechanism with their lines of action parallel to the centreline of the bone cylinders. During commissioning trials it was discovered that the subluxing force on the joint was not as large as expected. This was greatly improved by attaching the flexor 'tendon' to the proximal phalanx using a simple electrical cable tie to imitate the flexor tendon sheath. The 'tendons' themselves proved quite a problem initially since they need to be very flexible, strong enough to withstand forces of up to 200 N with minimal extension, and corrosion resistant. A form of braided nylon, although slightly extensible, has proved the most durable of all the materials tried.

The flexor system includes a small freely moving pulley mounted above the joint and pivoted about the point of attachment of the

metacarpoglenoidal ligaments. This 'volar plate' can be easily removed if desired.

The baseplate containing the clamp and pulley system fits into a perspex box filled with saline at 37°C. At a lower level is a thermostatically controlled tank containing a heater and stirrer. The saline is pumped from the lower tank to the upper one and returned by gravity through an overflow outlet at a level above the joint.

Obviously there were many ways in which cyclical motion could be imparted to the joint through the 'tendons' using servo-controlled hydraulics or stepper motors etc. but the simulator was designed on the basis of low cost and simplicity. To be effective in fatigue and wear testing, the drive mechanism must be very durable and reliable in order to run continuously for periods of several weeks. The idea of the final design was to reduce the number of possible areas of failure and to keep the cost of replacing worn or damaged components to a minimum. The two 'tendons' pass out of the bath and each is attached to a cam follower. The followers move in eccentric circular cam grooves cut into a Duralumin flywheel which is driven by a DC motor and gearbox at frequencies of up to 2 Hz. This converts the rotational motion of the disc to a linear displacement which is transmitted to the tendons. The motor is one which uses an ironless rotor and it is formed in three sections, the magnet, the ironless rotor and the endcap with carbon brushes. Motors of this kind have a unique linear characteristic and the advantage of low starting voltages.

Fig 3.5 shows a plan view of the clamp and pulley system at positions of 0° and 90° flexion. As the joint moves between these positions the

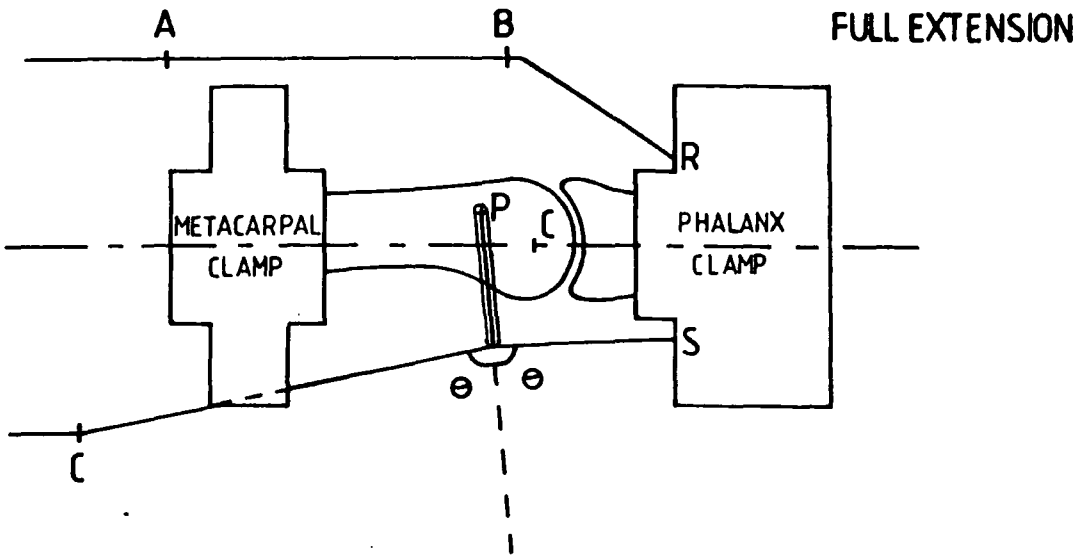

A, B AND C ARE THE PULLEYS WHICH ACT AS TENDON SHEATHS. R & S ARE THE POINTS OF ATTACHMENT OF THE TENDONS TO THE PHALANGEAL CLAMP

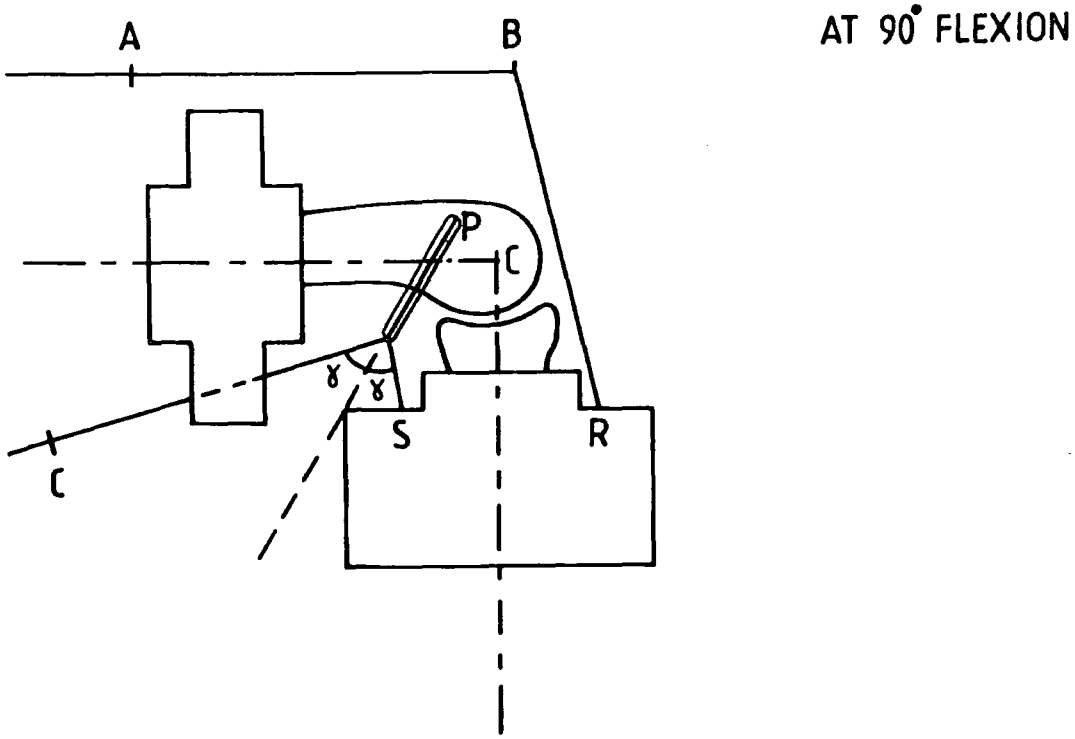

Fig 3.5 Plan view of the clamp and pulley system.

'volar plate' pulley must move round in an arc in order to preserve equilibrium of forces. Scale drawings were made of this system at 10° intervals of increasing flexion and accurate measurements made of the change in the 'tendon' lengths. In this way the eccentricity needed for the flexor cam grooves was found to be 11.75 mm off-centre and for the extensor cam groove 12.0 mm 180° out of phase.

The true shape of the cam grooves ought not to be circular but a very close approximation was achieved by choosing the groove radii such that the error in follower travel never exceeds 1 mm throughout the cycle (flexor groove radius = 52.5 mm and extensor groove radius = 44.5 mm). The cam disc has been designed in order that its flywheel effect will help to maintain uniform velocity during cyclical motion against transient effects such as water resistance and increased friction etc. Its weight was limited to 2 kg since it forms part of the assembly lifted pneumatically during heavy loading and its moment of inertia is well within the capabilities of the motor and gearbox. One problem observed during commissioning trials was the occurrence of unwanted lateral forces on the cam followers. The original follower guides were replaced by larger steel blocks which greatly reduce the moment arms and act also as heat sinks. Calculations used in the design of the cam disc and drive shaft are detailed in Appendix 1.

The speed of the motor, and hence cycle frequency, can be varied using a potentiometer. The motor and cam system is mounted in a light cage which is free to move vertically on rods which pass through brass brushes. During normal cyclical motion the cage rests on a lower shelf but is lifted vertically during simulation of tip pinch by a pneumatic cylinder which is flange mounted above the cage (Fig 3.6).

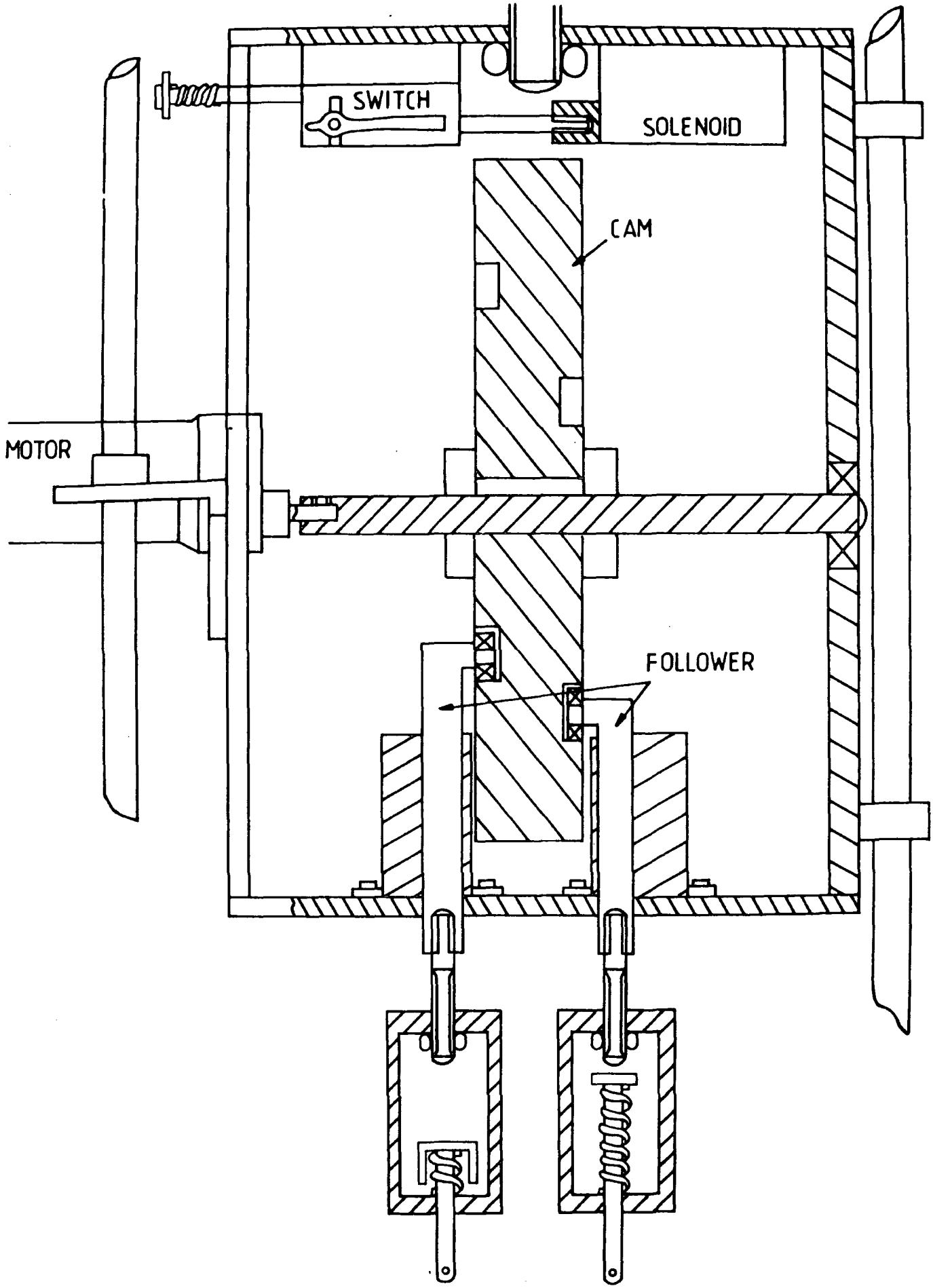

Fig 3.6 The drive and lift mechanism.

When the large static load is to be applied, a microswitch is pulled into the path of the flywheel by a solenoid. This deactivates the motor and activates another solenoid which prevents the flywheel from bouncing back off the microswitch (a problem initially encountered). In the lower section of the simulator a third solenoid is activated which then protrudes into the semi-circular track at a position of 30° flexion. A solenoid-operated pneumatic valve, controlling the air supply to the piston, then switches the air supply from the top of the cylinder to the bottom. The piston retracts pulling the drive cage vertically so that the phalangeal clamp is pulled hard against the restraining pin thus simulating tip pinch action. The tip pinch force is transmitted through the flexor 'tendon' and can be regulated by the supply pressure to up to 200 N.

Looking again at Fig 3.6 it can be seen that the 'tendons' are attached to the cam followers via two springs. In cyclical motion these act to smooth out any inaccuracies in cam position but play a rather more important role during heavy static loading. As the piston lifts the drive cage, the collar of the flexor 'tendon' spring is pressed hard against its base whereas the far longer spring of the extensor 'tendon' is hardly compressed at all. This means that all the force is carried through the flexor 'tendon' and this produces a force similar to that found in-vivo. In other words, a compressive force combined with a large subluxing force is applied to the joint. This force pattern can be very damaging to some designs of prosthesis.

So that the rig could be left running unattended for long periods of time a means of synchronising the actions of both the drive and pneumatic systems was included. A series of cam controlled

microswitches is used to effect the following:

i) The microswitch is pulled into the path of the flywheel.

ii) The motor is disconnected and the cam arrested.

iii) The restraining pin is activated.

iv) The air cylinder lifts the drive cage and the phalangeal clamp is pulled hard against the restraining pin.

v) After a pre-set time the air cylinder lowers the drive cage.

vi) The microswitch is released, deactivating the restraining pin and reconnecting the motor.

vii) Cyclical motion continues.

The control circuitry is shown in Fig 3.7.

In order to measure joint forces some form of strain-gauged transducer arrangement was needed. It was not considered possible to place the strain gauges on the joint itself in view of the obvious problems of attachment, the different geometries of prosthesis to be tested, and the corrosive environment. Rather, the joint force had to be measured remotely and a method of supporting the clamp such that **all** the joint force was transmitted through it to be detected by the gauges was devised. Lack of space beneath the clamp ruled out the use of any form of hydrostatic bearing and so a stainless steel beam was cantilevered down from a rigid overhead gantry into the bath to support the clamp (Fig 3.8). The cantilever beam contains two separate sets of strain gauges. This is necessary because of the very large difference in the magnitude of the forces involved. In addition, the direction of the force on the joint is continually changing during cyclical motion and it is necessary to measure the force in two perpendicular directions simultaneously. The beam itself is of square cross-section and is made up of two parts of different cross-sectional area. When a large static

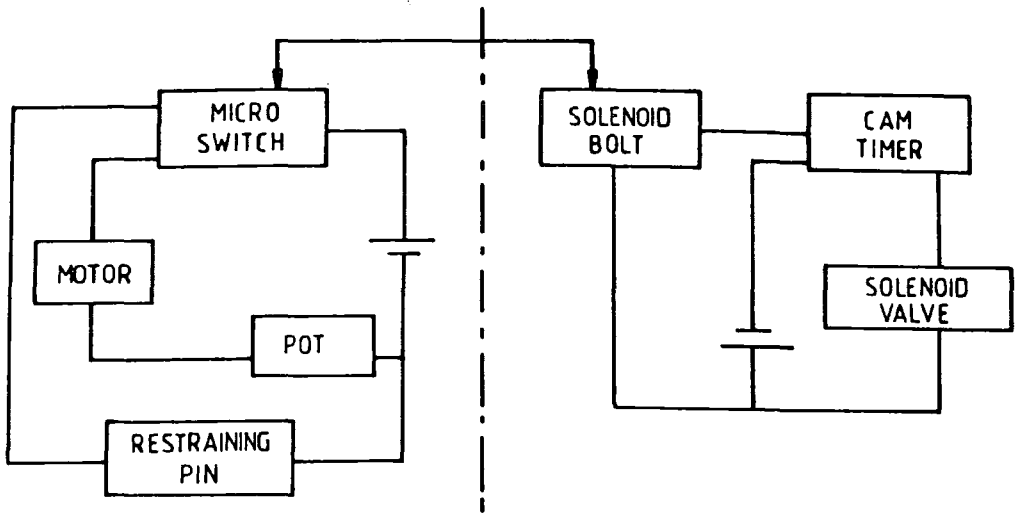

Fig 3.7 The control circuitry.

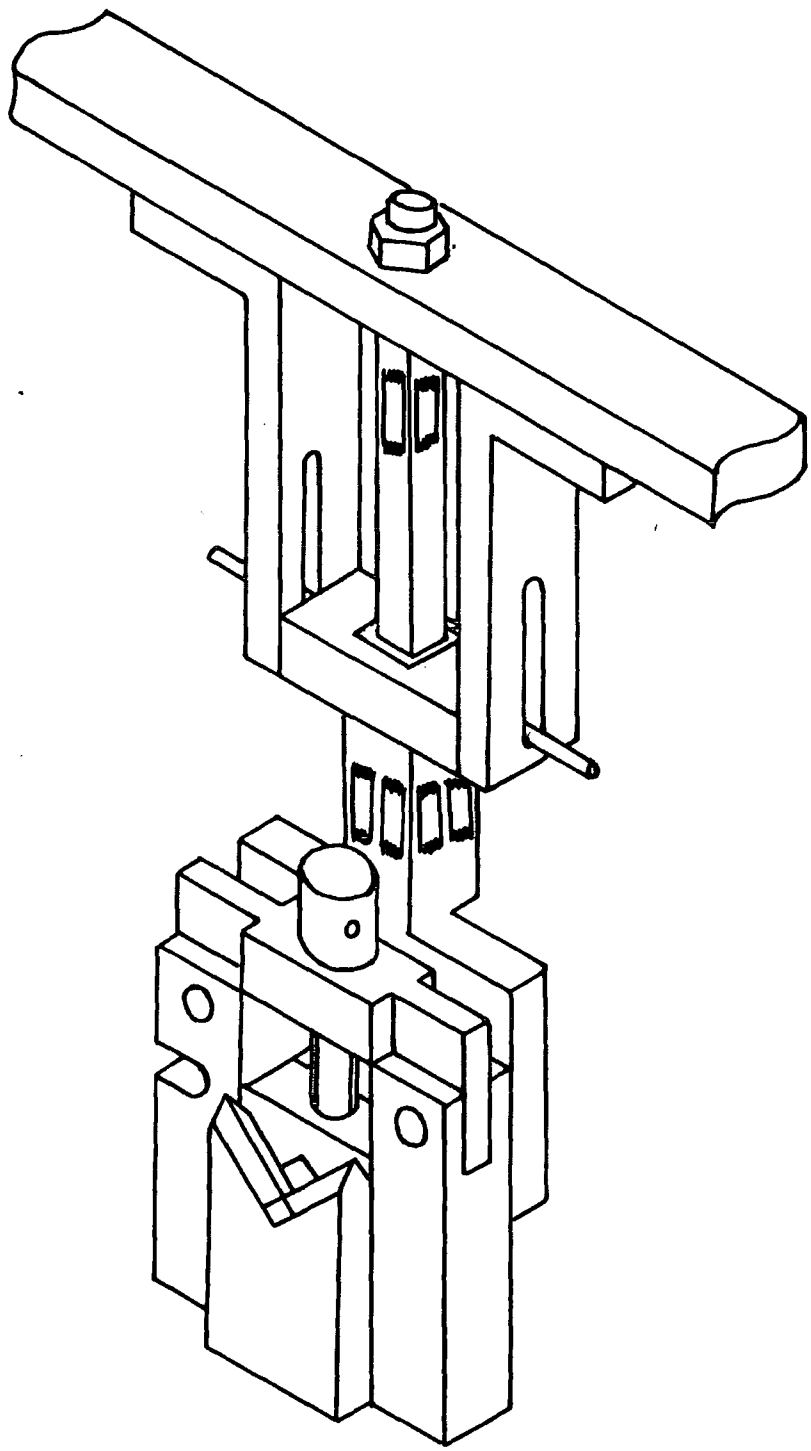

Fig 3.8 The metacarpal clamp and cantilever.

force is applied, the beam is clamped at the lower thicker section so that bending is restricted to this region. In this way the upper, more sensitive, section is protected. Measurement of large forces is achieved through two full strain gauge bridge arrangements. During light dynamic loading the clamp can be removed allowing bending to take place along the full length of the beam. The small forces are measured by means of two half bridge configurations mounted at the top of the beam. Here the cross-sectional area is too small for full bridges and dummy resistors are used to complete the arms.

Even though the strain gauges are protected by a plastic coating and are not, in fact, submerged in the saline environment, problems of electrical shorting were initially encountered during tests. After a short time the gauges came loose altogether and inspection revealed that saline, splashed onto the connecting wires, had seeped through the jacket and moved up underneath the plastic coating to the gauges. After their replacement the gauges and connecting wires were protected by a layer of silicone rubber. (For calculations concerning the strain gauge bridges see Appendix 1.)

The signals from the Wheatstone bridge arrangements are fed into two amplifier units which give a low noise calibrated output of 0 - 1 V representing 0 - 1000 $\mu\epsilon$. Since the two amplifiers are in close proximity they are connected in a master-slave configuration to eliminate the risk of beat frequencies being generated between the oscillators. As an early warning against bridge failure a digital voltmeter is connected to the amplifier outputs giving a continuous visual reading of strain. The analogue signals are passed from the amplifiers to voltage conditioner units ready for analogue to digital

conversion. The full scale voltage range for each unit is nominally 1 V but the gain and offset can be adjusted to suit the required peak input voltage (which in this case is 0.5 V). This facility greatly improves the digital resolution available. Each unit has its own secondary address for software scanning of the signals when the A-D converter accepts data from a conditioning module and converts it into a digital form for the IEEE-488 bus. Each reading is sent to the microcomputer as a code of three ASCII characters, representing a twelve bit number, plus a return marker. This can be decoded into a force reading in the software. The system has a sampling rate of 1 every 25 μs which is quite adequate for our purposes.

User friendly software has been developed in BASIC with menu options to facilitate the following:

i) Choose a bridge configuration and set up a data file containing details of the test.

ii) Take a set of force measurements and store them on disc.

iii) Review the data stored in numerical form and make a hard copy.

iv) Review the data stored in several graphical forms and make hard copies.

The program is listed in Appendix 2.

3.3 CALIBRATION

The strain gauges bonded to the metacarpal cantilever beam are connected as shown in Figs 3.9 & 3.10. The active gauges used are of 120 Ω and gauge factor = 2.12. The resistors used to complete the half bridges are also of 120 Ω with a tolerance of 0.01. The apex connections of either the half or full bridge arrangements are made at the rear of two amplifier modules via four 2 mm terminals. These modules, powered by a stabilised 18 V supply, energise and condition the signals from the bridges to give a calibrated low noise output of 1 V. The number of active gauges is set using a switch on the rear panel and, in order that the instrument can be read directly in strain, a scale factor control is provided where scale factor = 1/gauge factor. Since the two amplifier modules are in close proximity they are joined through the 7-pin DIN output connectors in a master-slave arrangement to eliminate the risk of beat frequencies being generated.

After a warm-up time of 15 minutes the amplifier modules were internally calibrated in the following way. The self-oscillating master unit was calibrated first since the oscillator amplitude affects the slave unit. With the mode switch in 'Cal' position, scale factor = 0.5 and 'Range' = LVDT the output signal was adjusted to give the full scale reading of 1 V. With the mode switch at 'R' the input was shorted out and the amplifier balanced to zero. The mode switch was then moved to 'X' and the quadrature control adjusted to compensate for cable capacitance etc. until a minimum output was obtained. With the mode switch at 'N' the correct scale factor was set and the range chosen to be 0 - 1000 $\mu\epsilon$ since the expected maximum strain for both static and

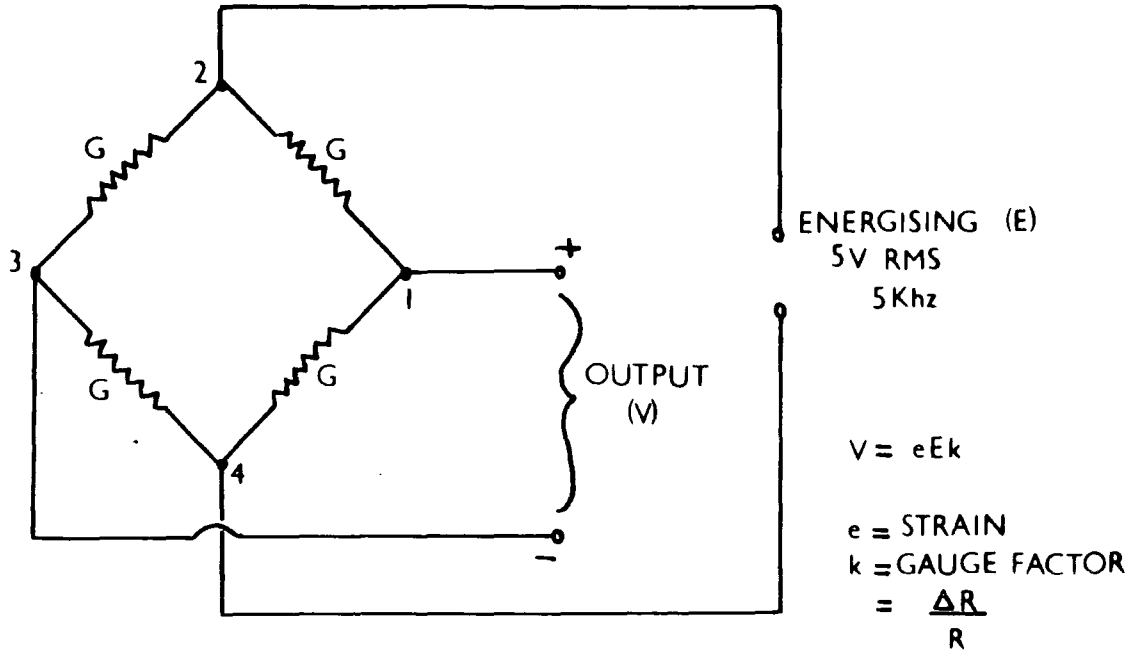

Fig 3.9 Full strain gauge bridge arrangement.

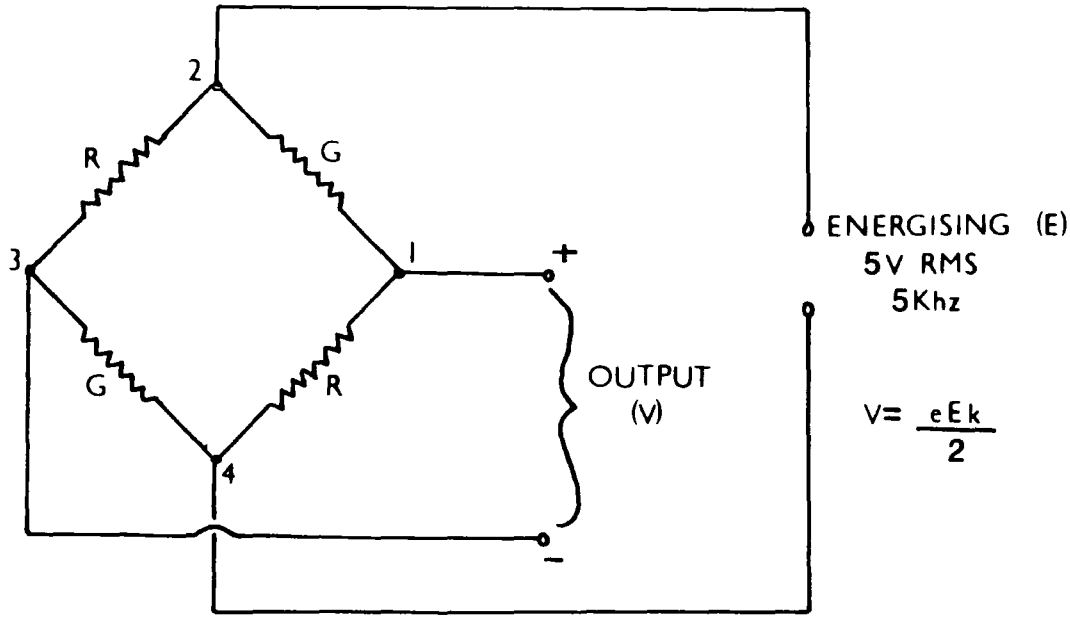

Fig 3.10 Half strain gauge bridge arrangement.

dynamic loading were calculated to lie within the range 300 - 400 $\mu\epsilon$ (Appendix 1). The same procedure was applied to the slave module after which both units were ready for normal use and it was then necessary to calibrate the strain-gauge bridges themselves to obtain a conversion factor from strain into joint force. This was effected in the following manner.

The perspex box and baseplate were removed leaving the metacarpal clamp suspended alone. A wire was attached to the clamp and passed over a pulley to hang over the edge of the bench such that when the wire was loaded the line of action of the force was the same as that of the 'tendon' force during normal use of the simulator. The strain gauges were connected to the amplifier modules with the output being fed to a digital voltmeter. The readings taken from the voltmeter were direct measurements of strain with 1000 mV = 1000 $\mu\epsilon$. The calibration graphs of strain against force for both full and half bridge arrangements in each direction are shown in Figs 3.11 & 3.12.

The conversion factors obtained were

	Forward ($\mu\epsilon$/N)	Lateral ($\mu\epsilon$/N)
Full Bridge	1.4	1.3
Half Bridge	13.9	18.3

These values have been incorporated into the software for data conversion (Appendix 2). Obviously it is not practical to use a digital voltmeter for data acquisition during simulator tests since the reading changes are rapid and written data storage is unwieldy. Rather, the

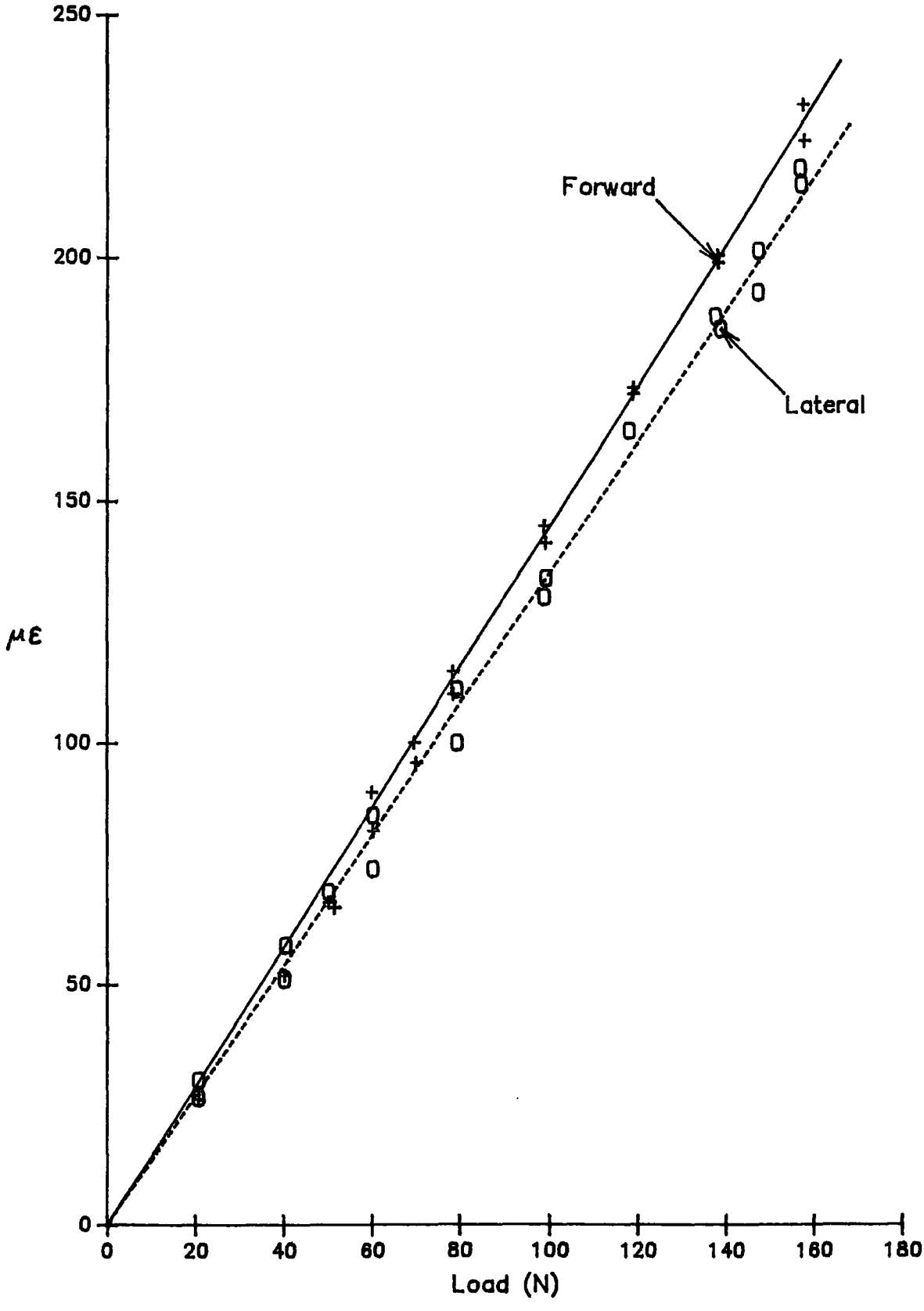

Fig 3.11 Calibration graphs for full bridge.

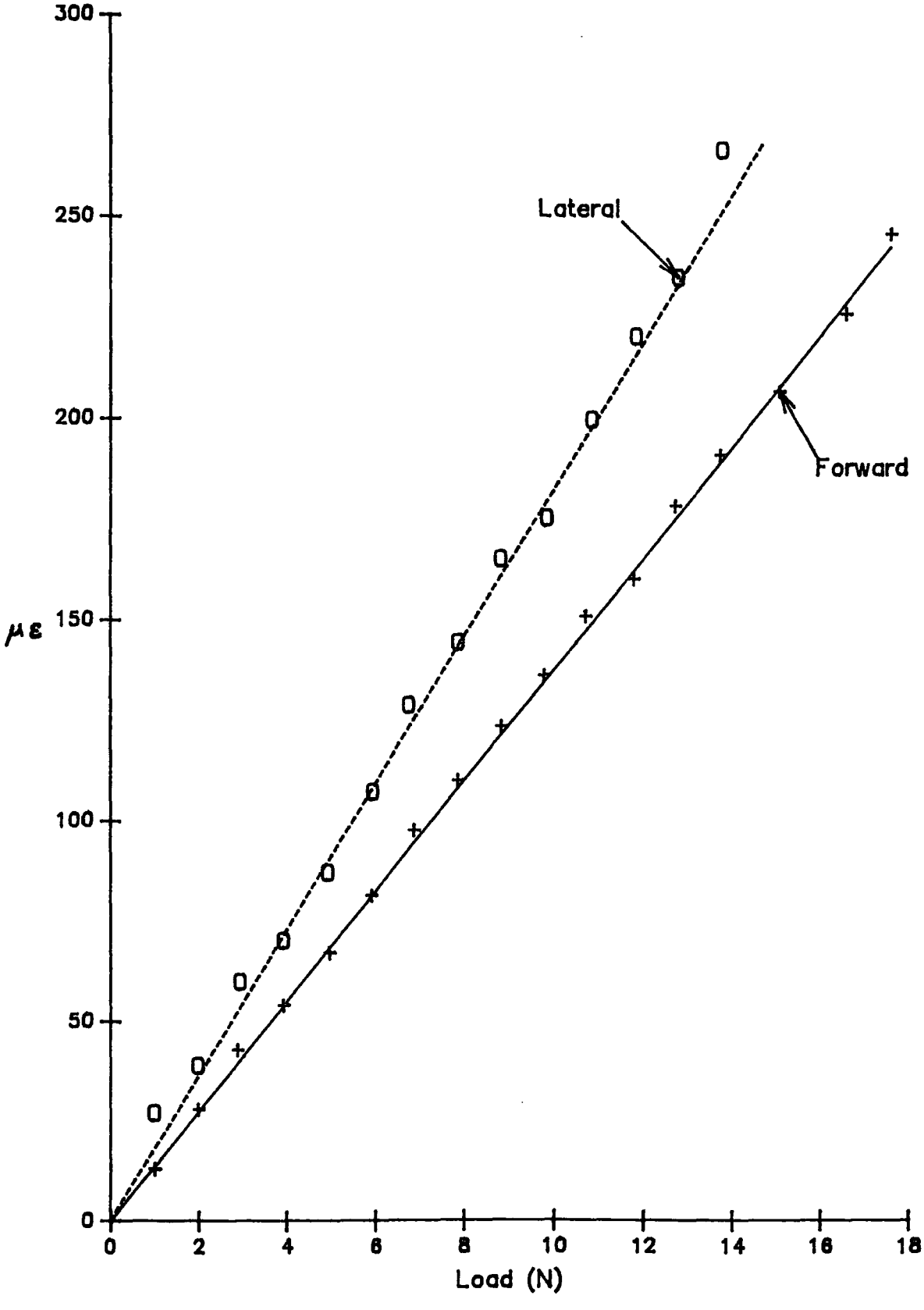

Fig 3.12 Calibration graphs for half bridge.

analogue signals are passed from the amplifiers through an interface system to be processed in a BBC microcomputer and stored on disc. The interface system comprises a mains-powered control frame containing the necessary circuitry for complete IEEE-488 bus operation, two input voltage conditioner units (one for each force direction) and a 12-bit A-D converter. The microcomputer communicates with the control frame through its primary address. Each conditioner module has its own secondary address and when called by the computer will pass its signal through the A-D converter to the IEEE-488 bus. The conversion time is less than 25 μs which is quite adequate for the purposes of the simulator. The input voltage conditioner units feature continuously variable gain and offset controls and a 3-position voltage switch which selects the maximum full scale voltage as 0.1 V, 1 V or 10 V. It was necessary to calibrate these units to obtain the desired digital resolution. A short calibration program, written in BASIC, allowed the gain and offset controls to be adjusted for the signal characteristics expected. The program displayed the reading through the A-D converter on the screen. The signals from the strain-gauge bridges were expected to be mono-polar 0 - 0.5 V and the following procedure was adopted.

The voltage switch was set to 1 V. The input leads were short-circuited and the 0 V level was set to the converted value of 0 using the offset control. It should be noted that too much offset would result in the A-D converter continuing to provide readings of 0 at voltages above 0 V. It was found better to set the 0 V level slightly inside the extreme reading. With an applied calibration voltage of 1 V the gain control was adjusted to give a converted reading just inside the 4095 extreme value. This gave a digital resolution of 0.25 N for heavy static loads and 0.025 N for light dynamic loads. Of course it would be possible to

double this resolution by setting 0.5 V equal to 4095 but this was considered unnecessary and would provide a sensitivity comparable to instrument error. Once the gain had been set the offset was readjusted to check the 0 V converted value.

Because of zero drift in the amplifier modules, recalibration of the equipment was performed at regular intervals. The simulator was then ready for the commissioning trials which are described in Chapter 4.

CHAPTER 4

COMMISSIONING TRIALS AND TESTS ON THE SWANSON SILASTIC IMPLANT

4.1 INTRODUCTION

It was felt necessary to perform extensive commissioning trials on the simulator before embarking on experiments to evaluate the prototype Durham surface replacement prosthesis. This was to enable the equipment to be 'run in', so that unforeseen problems, occurring as a consequence of continuous use or design short-comings, could be dealt with at this stage. Hopefully this would result in a reduction of undesirable operating interruptions during long-term wear and fatigue tests.

These trials were split into two sections. In the first part the capacity of the simulator to imitate the biomechanical situation in-vivo was fully investigated by obtaining both the dynamic and static force response curves for a normal joint and comparing them to published data. Based on this comparison further design changes were made to improve the subluxing force achieved by the rig. In the second part the well-established Swanson Silastic implant was tested to 10 million cycles. Fatigue failure of a type commonly seen in patients occurred at the shoulder of the phalangeal intramedullary stem. Failure of the Swanson implant has not previously been achieved in the laboratory and the results are therefore very encouraging since they would seem to validate the claim that the simulator successfully imitates the finger function.

The simulator has been developed such that it is possible to perform tests using cadaveric bones, and in this way problems of bone resorption, bone/cement interfacing strength and bone/prosthesis interaction can be investigated. In certain designs of prosthesis, eg. St Georg or the Link arthroplasty these would be very important

considerations. However the studies undertaken during this research programme have been involved with the Swanson Silastic implant and Durham surface replacement, neither of which are cemented, and being of such soft materials very little bone resorption is expected. In both cases the impingement of the prosthesis against the bone is an important factor in cycling and corrosion fatigue mechanisms but this can be similarly achieved using a hard material such as acrylic in place of bone. Weightman et al in 1972 (96) in their tests on the Swanson implant used Plexiglas blocks.

Experiments to investigate fatigue necessarily take around eight weeks to complete. At regular intervals of only a few days cadaveric bones would need to be replaced with fresh ones. Not only would this involve a lengthy stoppage for the sterilisation of the equipment but it would also mean that experimental conditions were constantly being changed since no two bones can be prepared identically. For this reason (and also to reduce the biohazard) acrylic model bones were used and were made in the following way.

Clean matched bones (kindly lent by the Newcastle Medical School) were thickly painted with silicone rubber and allowed to dry. A small plastic box was half filled with plaster of Paris and the coated bone pushed in up to half its depth, touching one end of the box. When the plaster was hard a coating of waterglass was applied to the surface and an upper layer of plaster poured into the box. The use of waterglass was to ensure that the two plaster layers could be easily separated, and careful slitting of the rubber released the bone. The rubber and plaster were put back together to serve as a re-usable mould for acrylic dental modelling plastic.

As mentioned previously, the outer profile of the bone shaft is irrelevant when testing an MCP joint prosthesis and it was decided to set the model shafts in acrylic cylinders of diameter 10 mm leaving the bone heads exposed. This was easily achieved by setting a brass cylinder in silicone rubber, inserting the bone replicas into the mould and pouring in acrylic. For the first part of the commissioning tests average sized models were used and thereafter a size was chosen suitable for the size of prosthesis under consideration.

4.2 RIG ASSESSMENT USING ACRYLIC REPLICA BONES

In Chapter 1 the biomechanical behaviour of the MCP joint was discussed in the light of theoretical models and published data. The model of Weightman & Amis in 1982 (1) was felt to be a reasonable standard by which to measure the performance of the simulator since it was statically determinate, well thought out, and embodied the successful elements of previous models. In trials using acrylic replica bones it was hoped to obtain force response curves which could be compared with the theoretical model, and to make design improvements as a result. It was also hoped to determine the consistency of performance over a long period of time. The experiments were all performed using the same matched pair of average sized, middle finger, acrylic replica bones with cylindrical stems as described previously. In placing the bones in their respective clamps great care was taken to ensure that they were correctly aligned. The tensions of the 'tendons' were then adjusted and balanced until the cyclical motion was smooth over a range of 90° flexion with a dynamic load of around 10 N. This process was actually quite difficult and it required some patience to achieve a good range of motion and the desired average load whilst maintaining a smooth cycle. This was particularly true at high cycling speeds when the springs attached to the wire fasteners could not smooth the directional changes as effectively. This resulted in jumping of the bones. Because of this it was sometimes necessary to use lower speeds.

The strain gauge amplifiers were switched on and saline at 37°C was cycled through the lower bath. The system was then allowed to reach steady state conditions over a period of two hours after which time the

data collection equipment was re-calibrated to allow for balance point drift of the temperature sensitive strain gauges. The motor and air supply were switched on and the cycle frequency (accurately measured over 500 cycles) was set to 2 Hz. Every 15 minutes joint force readings were gathered for several cycles and the motor speed was checked. However, when it became apparent that there was very good consistency in motor speed this check was discontinued. The force readings taken were stored on disc, which contained the joint force magnitude, joint force angle, angle of flexion and time. Static force readings were taken every 30 minutes and also stored on disc.

During the early trials there was some problem in obtaining force readings beyond two hours of starting up the simulator. Upon investigation this was seen to be due to electrical shorting across the strain gauge bridge arms. Even with a protective coating on the strain gauges the saline appeared to be penetrating the jacket of the connecting wires and seeping up the wires to the bridge. To alleviate this problem the strain gauges and their associated wires were coated with silicone rubber and the bridges re-calibrated. No further problem of this nature occurred.

Another problem encountered initially was that the simulator did not seem to apply enough subluxing force to the joint. This had apparently been compromised as a result of holding the finger bones in clamps which, although they were designed to be physically small, meant that the flexor 'tendon' remained at ~10 mm from the joint rather than running alongside. This reduced the moment arm considerably. In addition, the volar plate in-vivo is not only attached to the metacarpal head through the glenoidal ligaments but is also attached to the base of

the phalanx through a small fibrous band called the incisura (Chapter 1). It is through this attachment that the joint subluxing force results (Fig 4.1). In the simulator it was not possible to attach the mobile pulley to the phalanx base and there was no advantage in attaching it to the phalanx clamps so this link was omitted.

After identifying the problems resulting in the loss of subluxation it was a surprisingly simple matter to rectify the situation. A small plastic electric cable tie was placed around the flexor 'tendon' and the phalanx just behind the phalanx base. The 'tendon' was drawn tightly against the bone for its passage across the joint, relieving the first problem, and the cable tie acted as an effective link between the mobile pulley ('volar plate') and the phalanx base. Measurements then showed a subluxing component in the joint force and the replica test series continued.

4.2.1 Biomechanics

Before embarking on a discussion of the test results it is perhaps worthwhile to pause at this point to consider the forces in the MCP joint, for both the healthy and the diseased finger (to review the Weightman & Amis treatment of forces), and to look at how the simulator achieves the same behaviour. Fig 4.1 gives a representation of the forces produced in a finger during tip pinch due to the actions of the extrinsic flexor tendons alone. The EDP tendon is assumed to be relaxed and the intrinsic muscles have been omitted to simplify the diagram, although it is recognised that the interossei do contribute to a certain extent (Long et al, 1970 (3)). Fig 4.1 a) shows the distal IP joint under the action of the FDP tendon which attaches to the lip of the

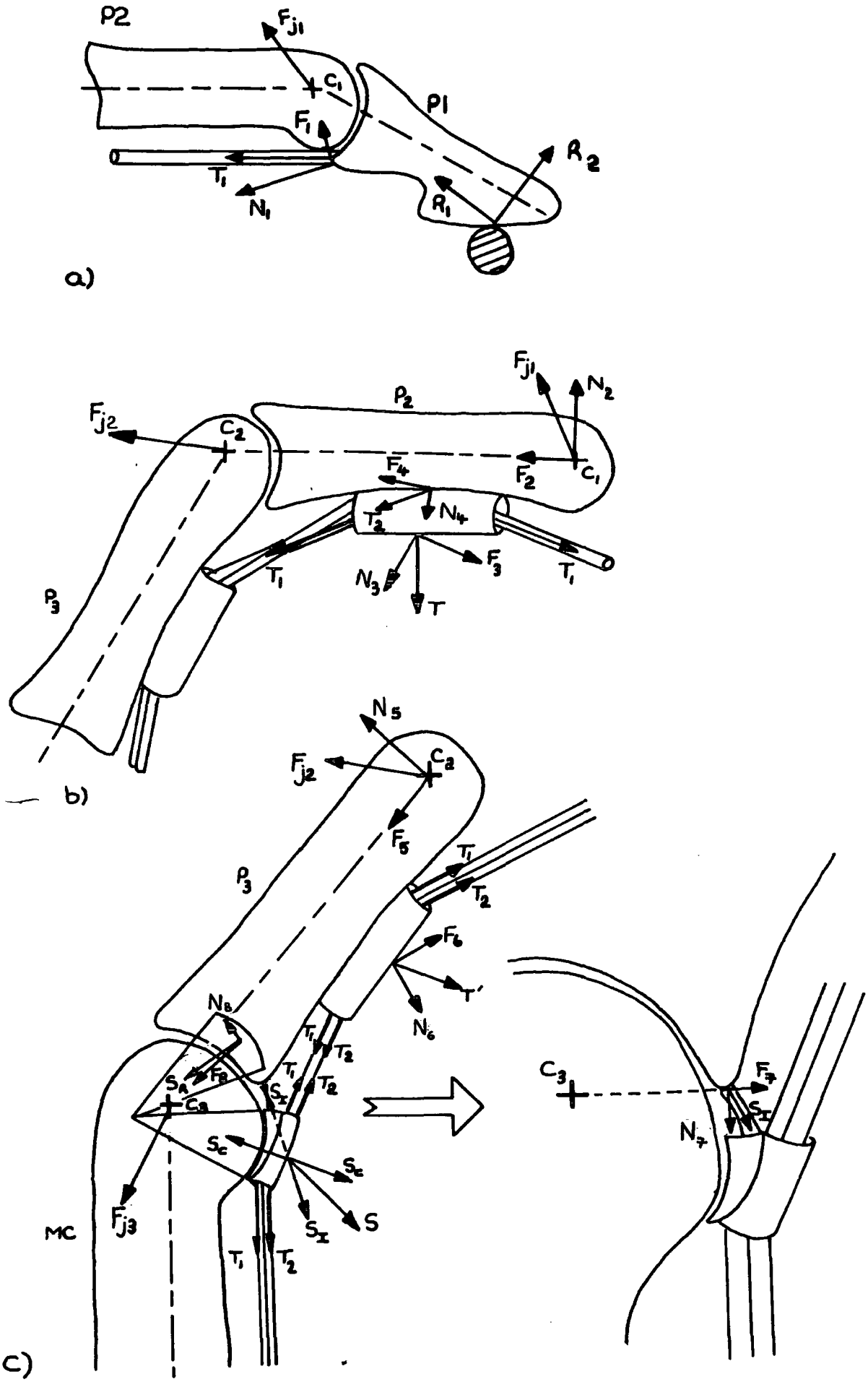

Fig 4.1 Force diagrams for the finger.

distal phalanx (P_1). In pinch action when the joint is in equilibrium the tension T_1 produces a moment about the centre of rotation C_1 which is balanced by a reactionary moment at the finger tip. There is a resultant compressive joint force F_{j1} exerted on the middle phalanx (P_2) by P_1 in the direction shown which is the vector sum of F_1 and R_1.

Fig 4.1 b) shows the proximal IP joint which is now under the action of both the FDP and FDS tendons. The FDS attachment is in the middle of P_2 exerting a force T_2 when under tension. The FDP passing through the tendon sheath produces a resultant force T. The moments produced by T and T_2 about C_2 must balance the moment produced by the joint force F_{j1} acting at C_1. The resultant joint force F_{j2} exerted by P_2 on the proximal phalanx (P_3) is the vector sum of F_2, F_3, and F_4.

Fig 4.1 c) shows the MCP joint which is complicated by the presence of the volar plate and its attachment to the lip of the proximal phalanx. The combined effects of the FDP and FDS tendons passing through the tendon sheath of the proximal phalanx result in a force T' acting at the middle of P_3. In a similar way as they pass through the volar plate sheath the tendons produce a resultant force S. Most of this force will be counteracted by tension in the metacarpoglenoidal ligaments S_C but there will still be a component S_I transmitted through the incisura to the proximal phalanx. Tension S_R in the collateral ligaments maintains joint stability against volar subluxation. Moments produced by S_I and T' about C_3 must balance with those produced by S_R and the joint force F_{j2} acting at C_2. The resulting joint force F_{j3} exerted by P_3 on the metacarpal is the vector sum of F_5, F_6, F_7, and F_8.

S_I constitutes the major part of the subluxing force acting on the

phalanx which presents a serious problem in the rheumatoid MCP joint. In a healthy joint most of the force S is resisted by the metacarpoglenoidal ligaments with the rest passing through the attachment to the phalanx. This in turn is resisted by the collateral ligaments which hold the phalanx and metacarpal bones together. When the joint is diseased, however, and both types of ligament are damaged, more of the force will be transmitted through the fibrous incisura which is not balanced by tension in the ligaments and eventually this causes dislocation of the joint.

It should be noted at this point that no importance has been given to the phalangeoglenoidal ligaments (not shown in Fig 4.1 c)) since in a study by Minami et al in 1984 & 1985 (28,29) they were found to contribute primarily to abduction-adduction rotational stability and do little to stabilise dorso-palmar dislocation or axial rotations.

The subluxing force S_I also depends on the angle of the MCP joint since this largely determines the magnitude and direction of S and governs the angle of the incisura to the phalanx. In addition, since the collateral ligaments are attached dorsally and distally from the centre of rotation of the joint they become more taut with increased flexion, thus enhancing stability. This is sufficient to counteract the joint subluxing force which also increases with increased flexion.

Consider the MCP joint force F_{j3} - during static loading its magnitude and direction are governed by the posture of the interphalangeal joints. For example if the IP joints were less flexed the joint forces F_{j1} and F_{j2} would be larger and directed more axially along their respective proximal bone. In turn F_{j3} would be directed more axially along the

metacarpal even though the MCP joint angle may have remained the same. Thus for one MCP joint position there are a range of possible joint force angles and magnitudes depending on the degree of flexion in the other joints of the finger. Unfortunately this is not a facility which is available with the finger function simulator since it contains only the MCP joint. There are some difficulties, then, in comparing the simulator behaviour with a model such as that proposed by Weightman & Amis in 1982 (1) which of course deals with all three joints. However, it is hoped to show in the commissioning trials that during its flexion cycle the simulator produces joint forces F_{j3} that are **typical** of the range predicted for each angle of the MCP joint. In particular as the angle of flexion increases so too should the magnitude of the joint force.

Using a similar approach to that outlined above Weightman & Amis developed their two dimensional model to analyse a range of finger configurations from pulp to tip pinch. A pin-jointed model was assumed which included the intrinsic muscles. The tensions developed in these muscles were taken to be in proportion to their physiological cross-sectional areas and the long extensor tendons were assumed to be relaxed. In its original form the model predicted that the resultant MCP joint force acted at or outside the edge of the articular contact of the joint. This highlighted the importance of soft tissue structures for joint support and the model was modified to include the effect of the collateral ligaments to reduce the volar shear component of the joint force. This treatment was rather simplified and the contribution of the metacarpoglenoidal ligaments was not considered at all, although their importance was recognised. Very generally the model predicted that joint force magnitudes increase with the finger extending towards

the cantilever position and shear forces increase as joints are flexed. Figs 4.2 & 4.3 show how the joint force magnitude and direction vary with angle of flexion for the MCP joint. The results shown are for the case where there is no ligamentous support for comparison with the simulator behaviour since it is important that in fatigue tests the simulator can apply forces which will severely test a prosthesis. In Figs 4.2 & 4.3 posture 1 is highlighted since, although it gives one possible force response for 20° flexion in the MCP joint, it is by no means the only one (as discussed previously) and therefore does not necessarily represent a stage in the force change progression as the joint flexion is increased. This is the difficulty associated with trying to compare a dynamic system with a static model. However, bearing in mind the limitations, it is still instructive to do so.

Fig 4.4 is a schematic diagram of the way in which the simulator applies the correct force to the MCP joint. In normal dynamic motion there is a tension of relatively even magnitude in both 'tendons'. The tensions are adjusted by applying compression to the smoothing springs described in Chapter 3. The attachment of the 'tendons' to the phalangeal clamp produces the forces T_1 and T_2 but these alone would give little or no shear component to the joint force. This was evident at an early stage in the simulator trials and a simple cable tie was employed to attach the flexor 'tendon' to the phalanx. The resulting tendon angle at the point of attachment produces the force S which exerts the majority of the subluxing force on the joint. The joint force F_j is given by the vector sum of F_1, F_2, and F_3 and increases in magnitude as the joint flexes due to the action of the springs. The shear component of F_j also increases with flexion because the angle at the cable tie becomes more and more acute, hence increasing the magnitude of S.

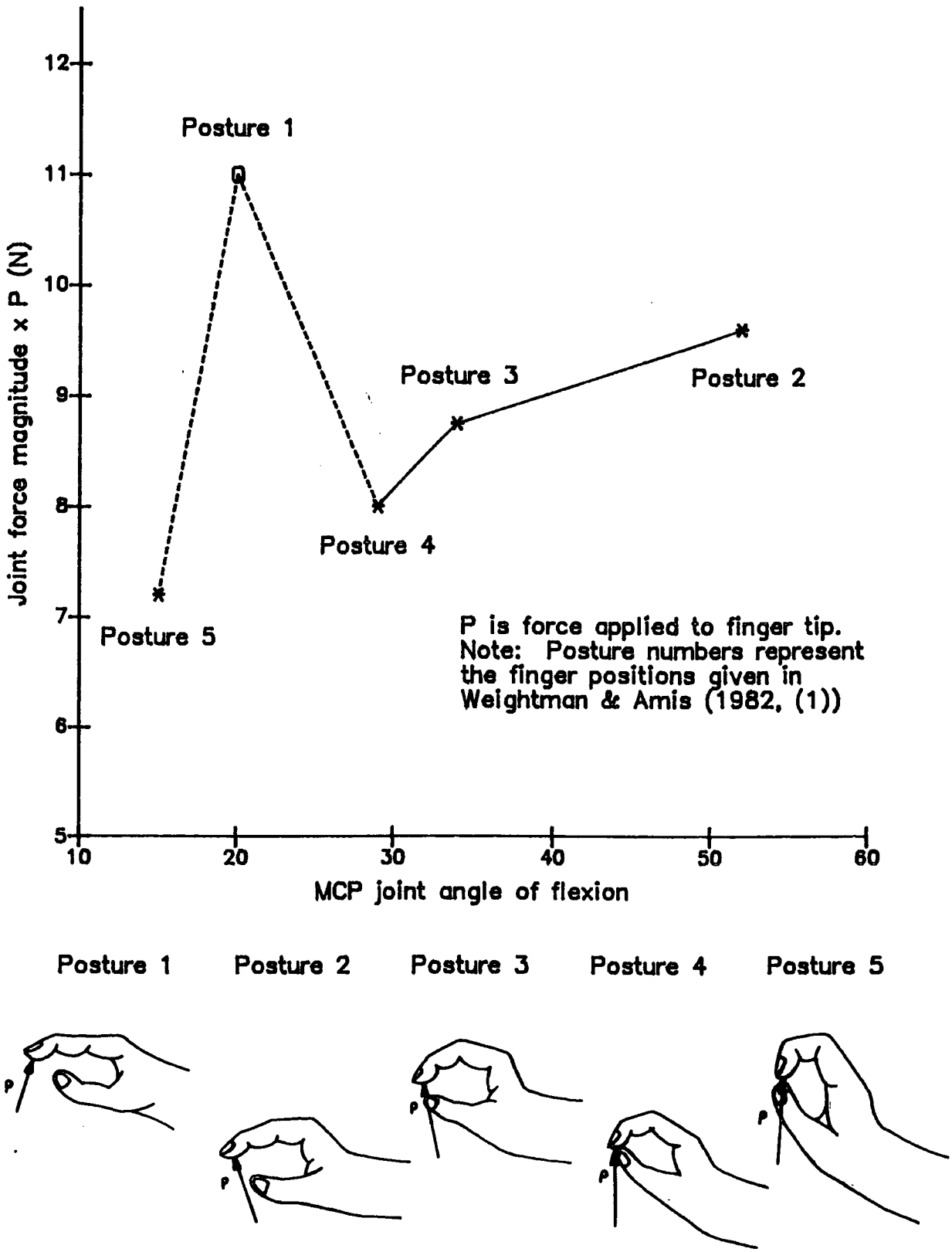

Fig 4.2 Joint force magnitude against angle of flexion as predicted by Weightman and Amis in 1982 (1)

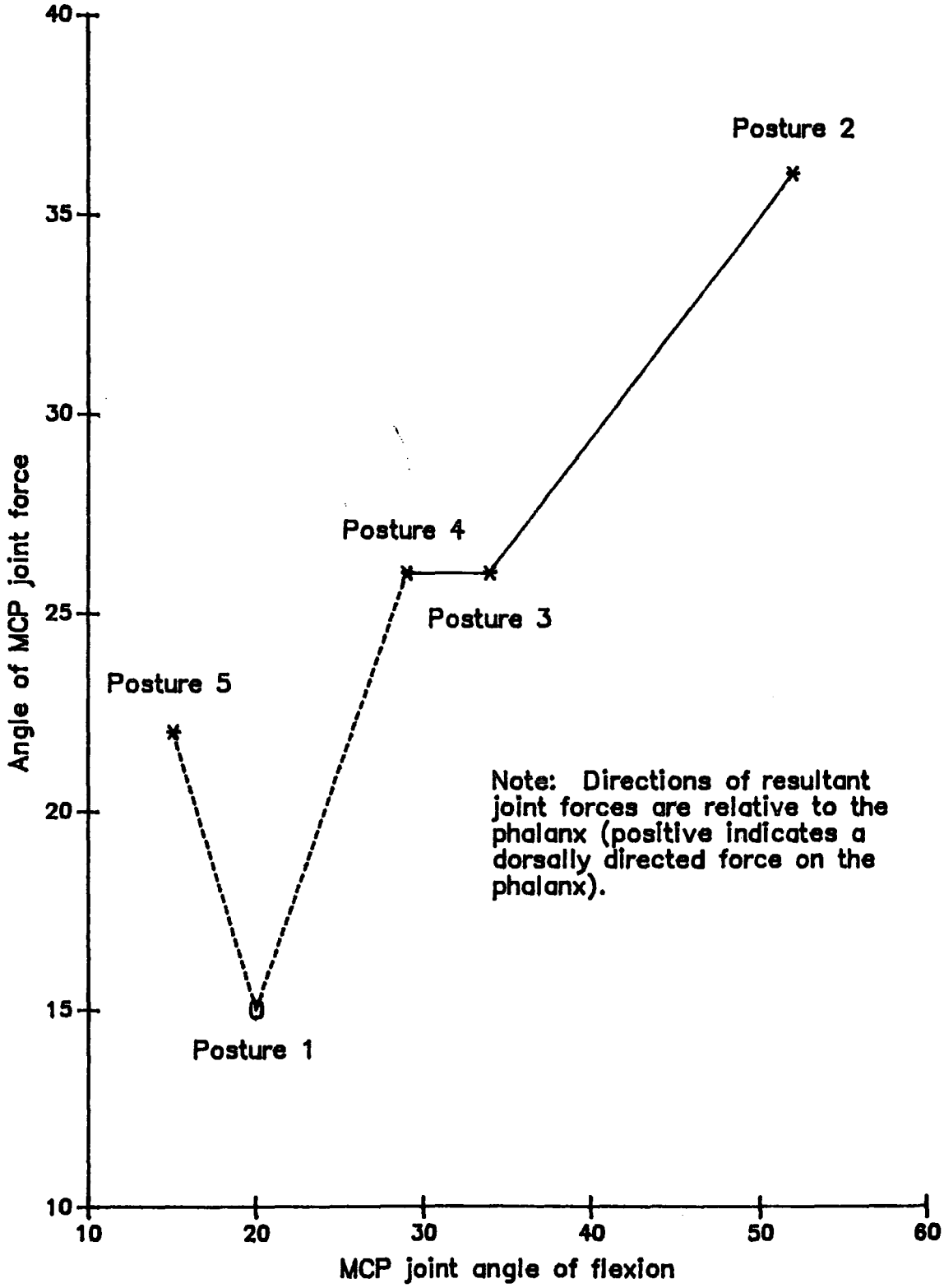

Fig 4.3 Joint force direction against angle of flexion as predicted by Weightman and Amis in 1982 (1)

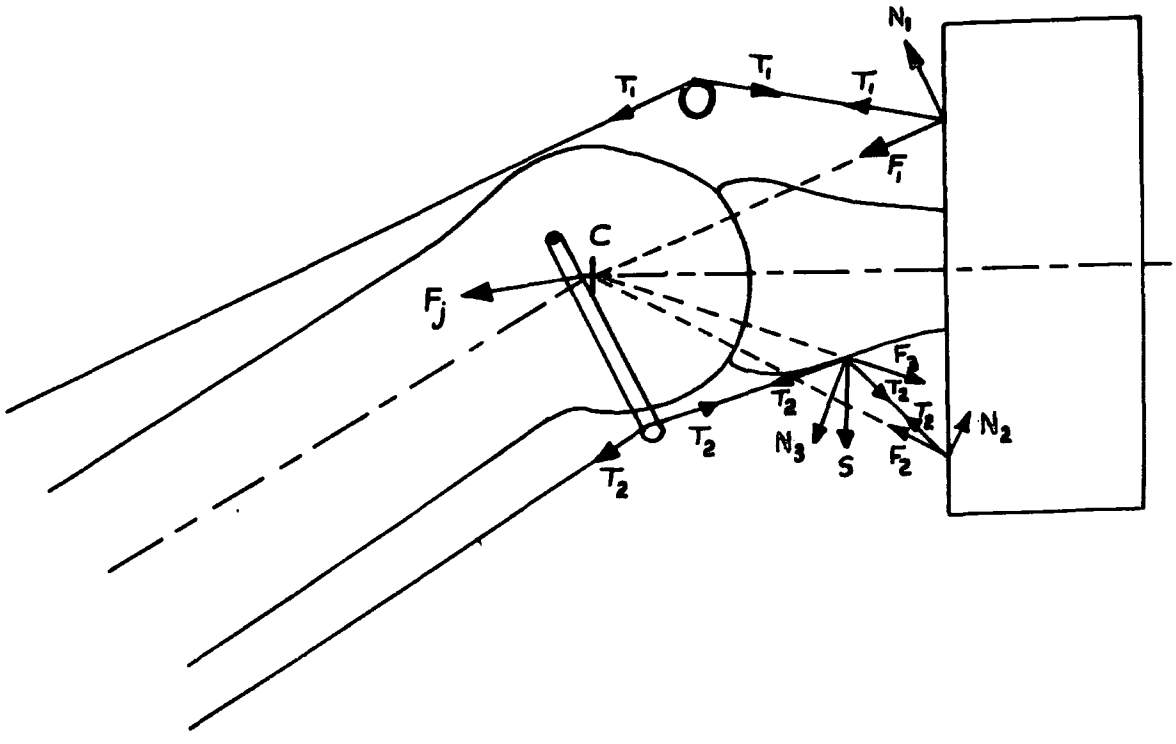

Fig 4.4 Force diagram for the simulator.

The heavy static load applied by the simulator acts for a joint position of 30° (the average position for pinch grip) when the majority of the load passes through the flexor tendon.

4.2.2 Replica Test Results

The series of tests performed on replica bones is given in Table 4.1. The duration of each test was three hours with dynamic force readings being taken at 15 minute intervals and static readings every 30 minutes. The latter results are given in Table 4.1; the former results are summarised in the following discussions.

Test number 1 was performed to investigate the consistency of the simulator over a long period of time. An average load of 12 N was

Test Number	Dynamic load (average)(N)	Speed (Hz)	Static load (N) and angle
1	12	1.92	184.2 30°
2	12	2.08	180.4 25°
3	12	1.78	184.0 30°
4	12	1.67	186.1 32°
5	8	1.92	189.9 34°
6	10	1.92	182.9 28°
7	14	1.92	187.8 32°

Table 4.1 The series of tests.

applied at a cycle rate of 1.92 Hz. Figs 4.5 a) & b) show how the joint force angle and magnitude vary with the angle of joint flexion for each time point of dynamic results recorded. The angle of the force is given relative to the phalanx and when above 20° indicates a significant shear force in the joint. During the early stages of the test it is evident that a drop in joint force magnitude has occurred, probably due to stretching in the 'tendons' and tightening of the knots. Between the first two time points there is a fall of ~0.75 N but thereafter there is little change and a steady state is reached by the sixth time point with a total loss in joint force magnitude of ~1 N. Looking at Fig 4.5 a), it can be seen that not only have the 'tendons' stretched but also the balance between them has changed during the early part of the test. Some of the subluxing component of the force has been lost, which implies that the flexor tendon has stretched more than the extensor. This is to be expected since during heavy static loading the majority of the force is applied through the flexor tendon. This would also explain why there is very little difference between time points 2 and 3 since the heavy static load occurs between time points 1 & 2, 3 & 4, 5 & 6 etc. The extensor is only stretched during the light dynamic loading and therefore takes longer to reach its final state. Generally the

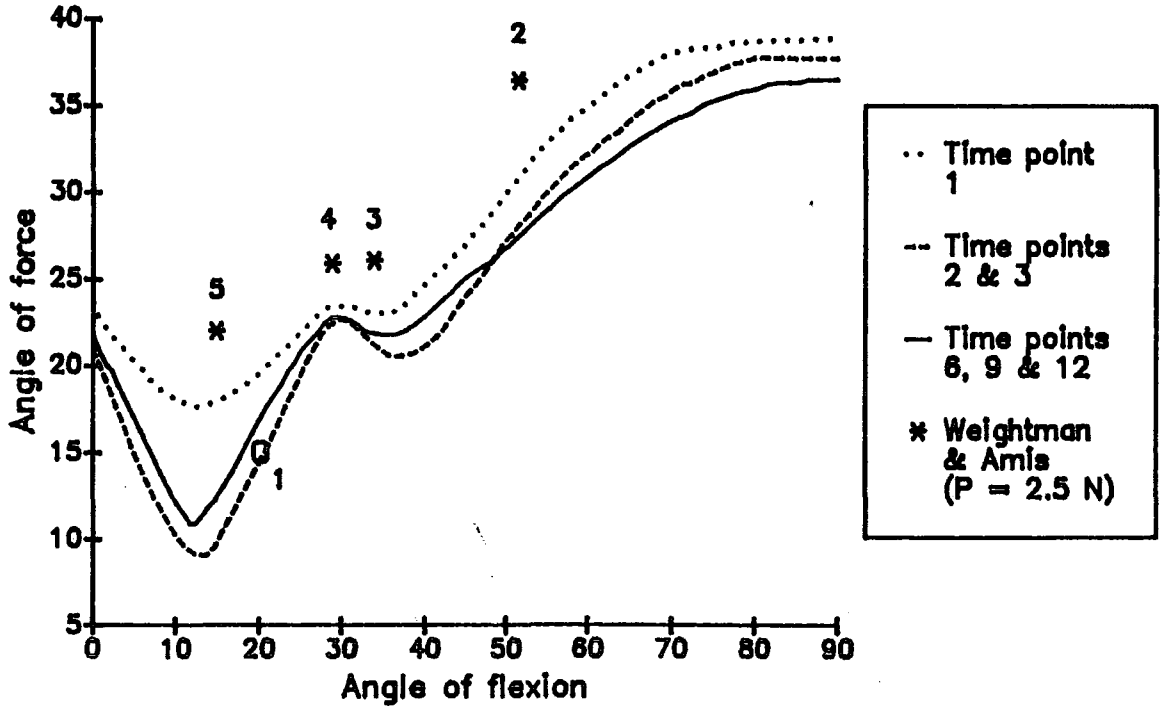

Fig 4.5 a) Test number 1, variation of angle of force with time.

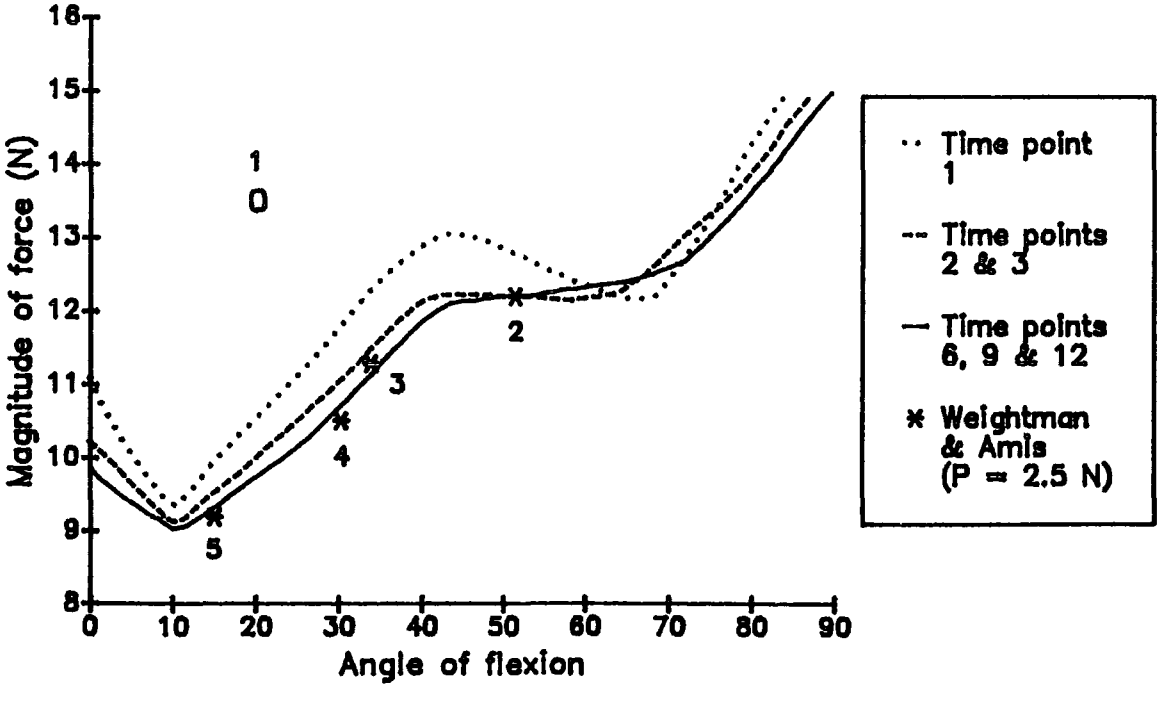

Fig 4.5 b) Test number 1, variation of magnitude of force with time.

graphs show an increase in force magnitude and subluxing component between 15° - 75° flexion. Towards the ends of the cycle (0° - 15° & 75° - 90°) both 'tendons' are acting and the springs act to smooth the motion during the change of direction, which causes the deviation of the curves from the expected trend.

Also shown on Figs 4.5 a) & b) are the Weightman & Amis predictions for a finger tip force P of 2.5 N. Again posture 1 is shown separately for the reasons discussed previously: it is reasonable to suppose that a natural dynamic progression would follow the path 5-4-3-2. The simulator results seem to be in very good agreement with the predicted values although some shear force was sacrificed to preserve cycle stability. This is very encouraging if consistency of operation can be confirmed for other loads and cycle rates.

Tests 2 to 4 were performed as an extension to test 1 to investigate the effect of changing the cycle rate within the range anticipated for use. Test 2 had a cycle rate of 2.08 Hz, on the limit of the possible speed range before the smoothing effect of the springs was badly compromised. Test 4 had a cycle rate of 1.67 Hz which, while not appearing particularly slow, would unnecessarily increase the duration of a fatigue test by several days. Since steady state had already been achieved in test 1 and no alteration was made to the 'tendon' balance for tests 2 to 4 the only effects seen in the force response curves for the four tests should be solely due to the change in speed. Figs 4.6 a) & b) show the direction and magnitude of the joint force against angle of flexion. Test 2 is beginning to show some deviation due to the failure of the smoothing mechanism but tests 1, 3 and 4 all have very similar response curves. As the cycle rate is increased there

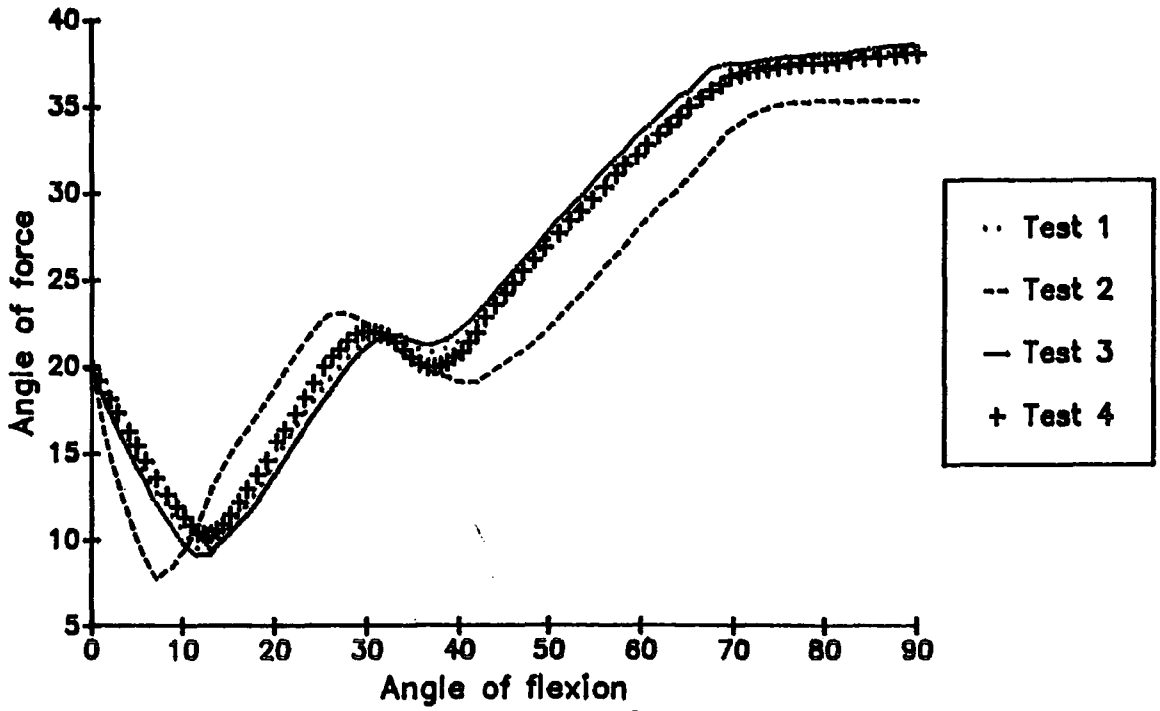

Fig 4.6 a) Variation of angle of force with speed.

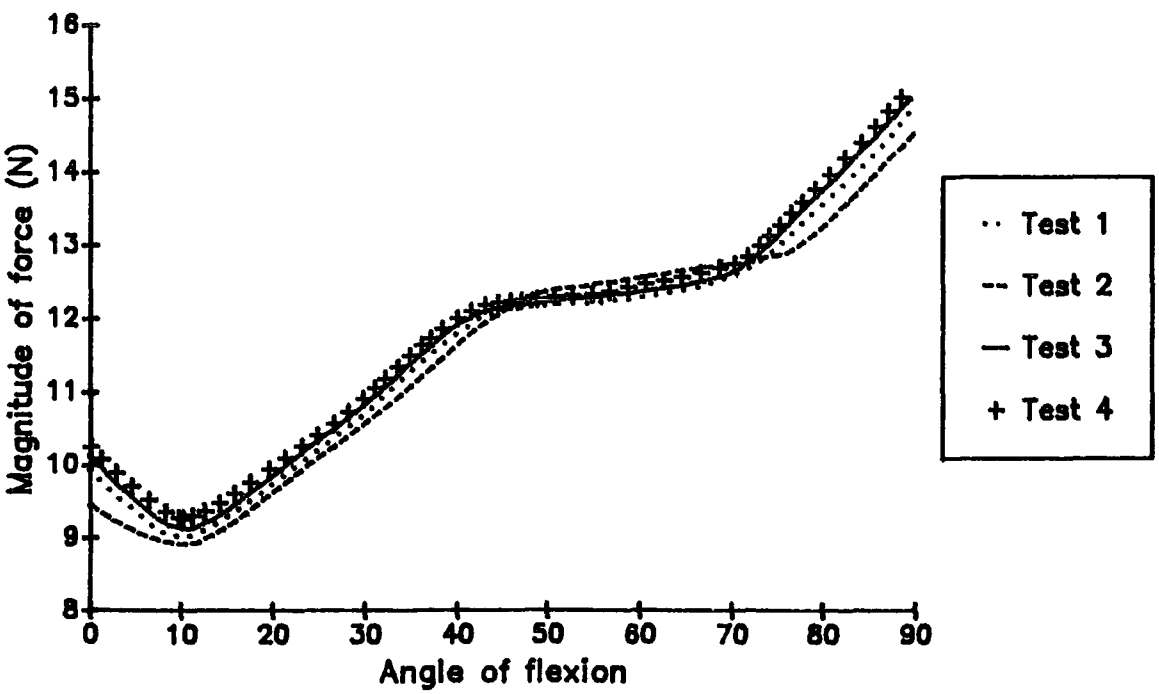

Fig 4.6 b) Variation of magnitude of force with speed.

is a slight fall in joint force magnitude. The origin of this drop is unclear but it may be due to the fact that proportionately more of the 'tendon' force is needed to maintain the necessary accelerations for the motion. It would appear, then, that the simulator behaviour is very consistent with speed changes provided the cycle rate does not exceed around 1.92 Hz.

Tests 5, 6 and 7 were performed to look at the effects of changing the load. The steady state results of these three tests, along with test 1, are shown in Figs 4.7 a) & b). The first thing that is apparent is the variability in the angle of force curve (Fig 4.7 a)). The general shape of the curves is maintained but there are modifications rather like those seen during the settling period of test 1 (Fig 4.5 a)). For each test in this series, unlike the previous series, the simulator 'tendon' tensions had to be adjusted and rebalanced. The balance between the tendons is important and it is evident that there is a range of relative tensions within which a smooth cycle can be obtained. Since the force response, and in particular the subluxing force, is very sensitive to this balance, a method had to be found by which to ensure consistency in simulator behaviour after stoppages. One way of doing this is to measure the length of the smoothing springs at rest and under tension. This method was employed for all ensuing tests. Fig 4.7 b) shows how the force magnitude curve is affected by an increase in the joint loading generally. The trend is very much as expected with the gradient of the curves gradually increasing with load and the initial dip becoming more and more pronounced.

From the stage 1 commissioning trials it may be concluded that the dynamic behaviour of the simulator is consistent (if care is taken to

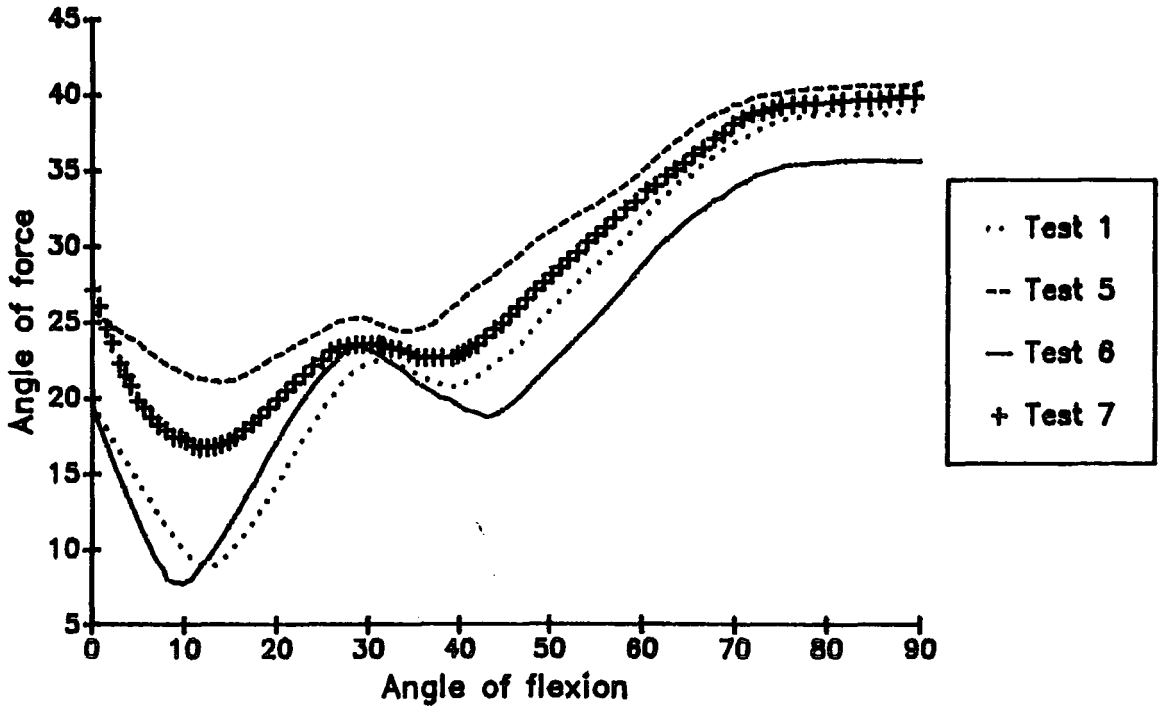

Fig 4.7 a) Variation of angle of force with load.

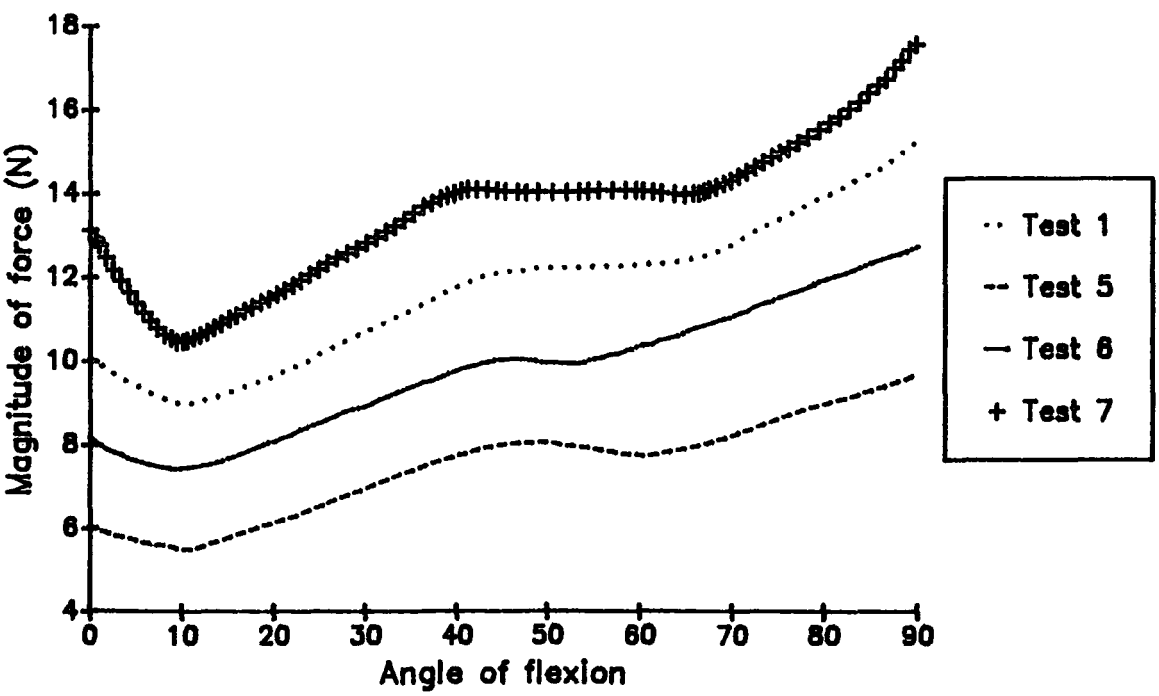

Fig 4.7 b) Variation of magnitude of force with load.

restore the correct 'tendon' balance after any interruption to a test) and compares well to the Weightman & Amis model. For tests 1 - 7 the static force applied was found to be very consistent for a particular test, with slight variability between tests (Table 4.1). The force applied was 180 - 190 N acting at 25° - 34° to the phalanx compared to the predicted angle of 26°.

The results of the initial trials were felt to be successful and on this basis tests on the Swanson Silastic implant were performed.

4.3 TESTS ON THE SWANSON SILASTIC IMPLANT

Tests were performed on two Swanson Silastic implants of greatly different sizes (size 2 and size 7). These were chosen to be the limiting sizes generally used in surgery although eleven sizes are manufactured with the size range extending from 00 to 9. Bone replicas of a suitable size were chosen for each prosthesis and prepared in the following manner, according to the recommendations made by Swanson & de Groot Swanson in 1984 (37).

The head of the metacarpal was removed up to the flare of the metaphysis but no resection was performed on the phalanx. A rectangular, slightly tapered hole was opened in each bone using a hot broach and to imitate the reaming of the medullary canals, deep holes were drilled into the cylindrical bone shafts. The hole in the metacarpal was placed 3 mm dorsally from the centre of rotation, as measured by Unsworth & Alexander in 1979 (20).

To prevent any damage from sharp bone edges the replicas were filed and rounded to make all points of contact with the prosthesis as smooth as possible. Each prosthesis was tested in the holes for goodness of fit and modifications were made with a rat-tailed file until the midsections rested comfortably against the bone heads and a sliding movement was easy without too much slackness. The implants could resist rotation due to the rectangular nature of the holes (Fig 4.8).

The replica bones and Swanson prosthesis were placed in the simulator and the 'tendons' adjusted to give a smooth cycle with the cams turned

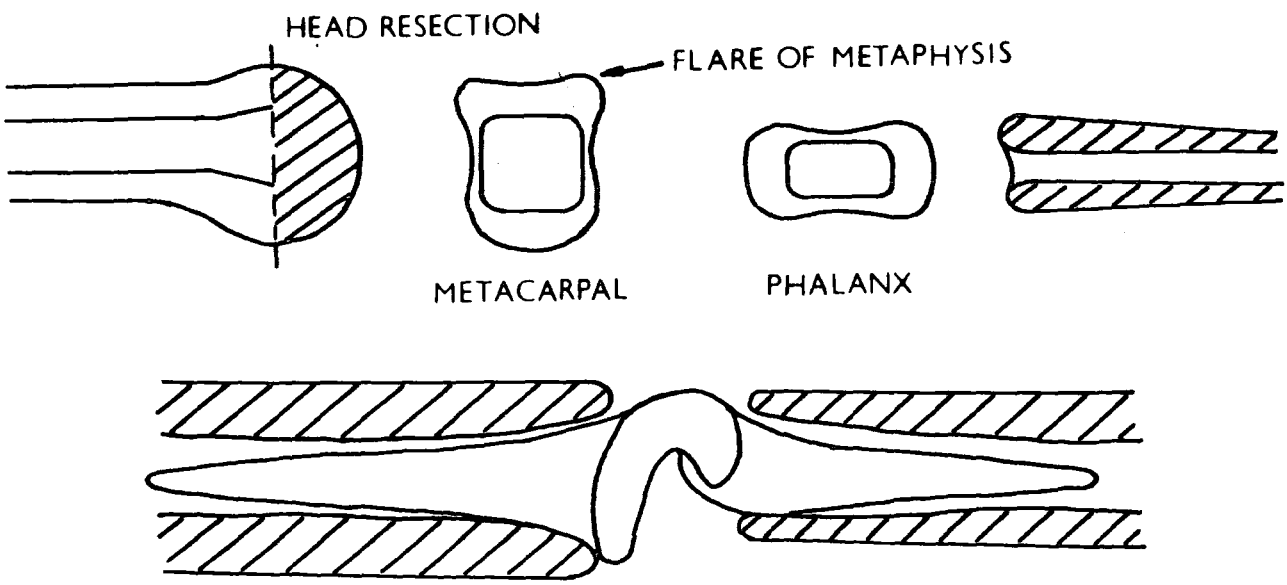

Fig 4.8 Preparation of replicas for Swanson tests.

by hand. The equipment, other than the motor, was switched on and left for a period of two hours to achieve a steady state 37°C. The tests began after a recalibration of the system.

The simulator ran almost continuously throughout the duration of each test, only being stopped for necessary cleaning or tendon replacement at approximately four-day intervals. Measurements of both static and dynamic loading were recorded regularly to keep a check on simulator consistency and typical results are shown in Figs 4.9 & 4.10.

Both the angle and the magnitude of the joint force exhibit the expected trends, in that both the magnitude of the force and its shear component increase with increasing flexion. In particular it can be seen that the subluxing force through both Swanson joints was consistently larger than any observed during the replica bone trials. Since the Swanson implant can carry more shear force across the joint than could be transferred through friction between two surfaces, this could be caused, in the first instance, when setting up an experiment if the 'tendons' were inadvertently adjusted to give a greater differential between the flexor and extensor 'tendons'. A smooth cycle could be achieved where in a replica test it would not. However, this is unlikely to be the explanation in this case since, for this very purpose, great care was taken to ensure that the smoothing spring lengths were adjusted to be the same as those in the replica bone tests. It would seem then that this effect was occurring as a direct result of the nature of the implant itself. Fig 4.11 shows what happens to the joint in the simulator. During flexion there is some compression at the midsection of the joint but the distal stem slides within the phalanx and bending occurs at C' - the intersection of the distal stem with the hinge. The

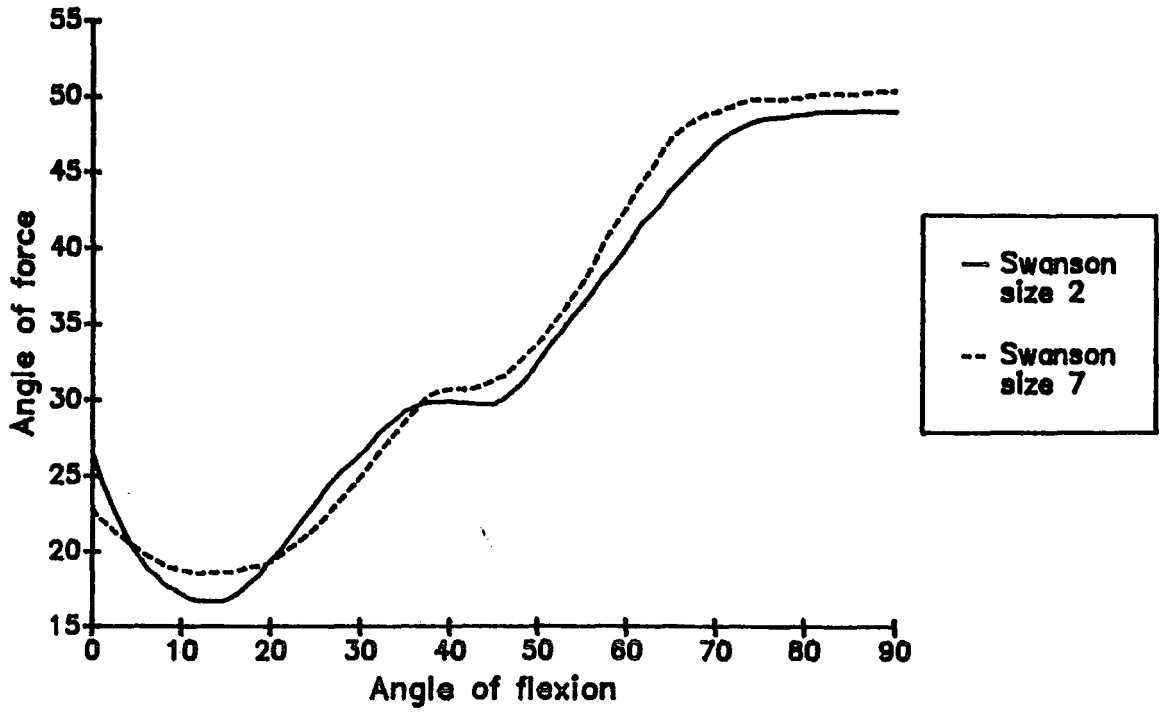

Fig 4.9 Swanson tests - variation of angle of force with flexion.

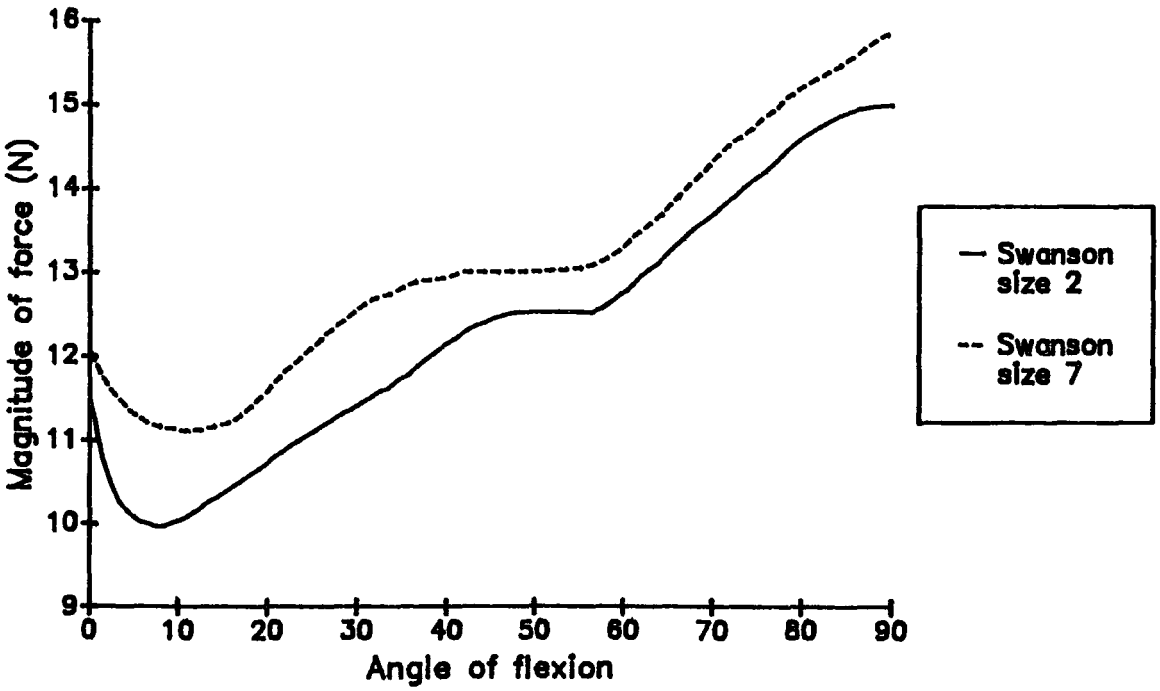

Fig 4.10 Swanson tests - variation of magnitude of force with flexion.

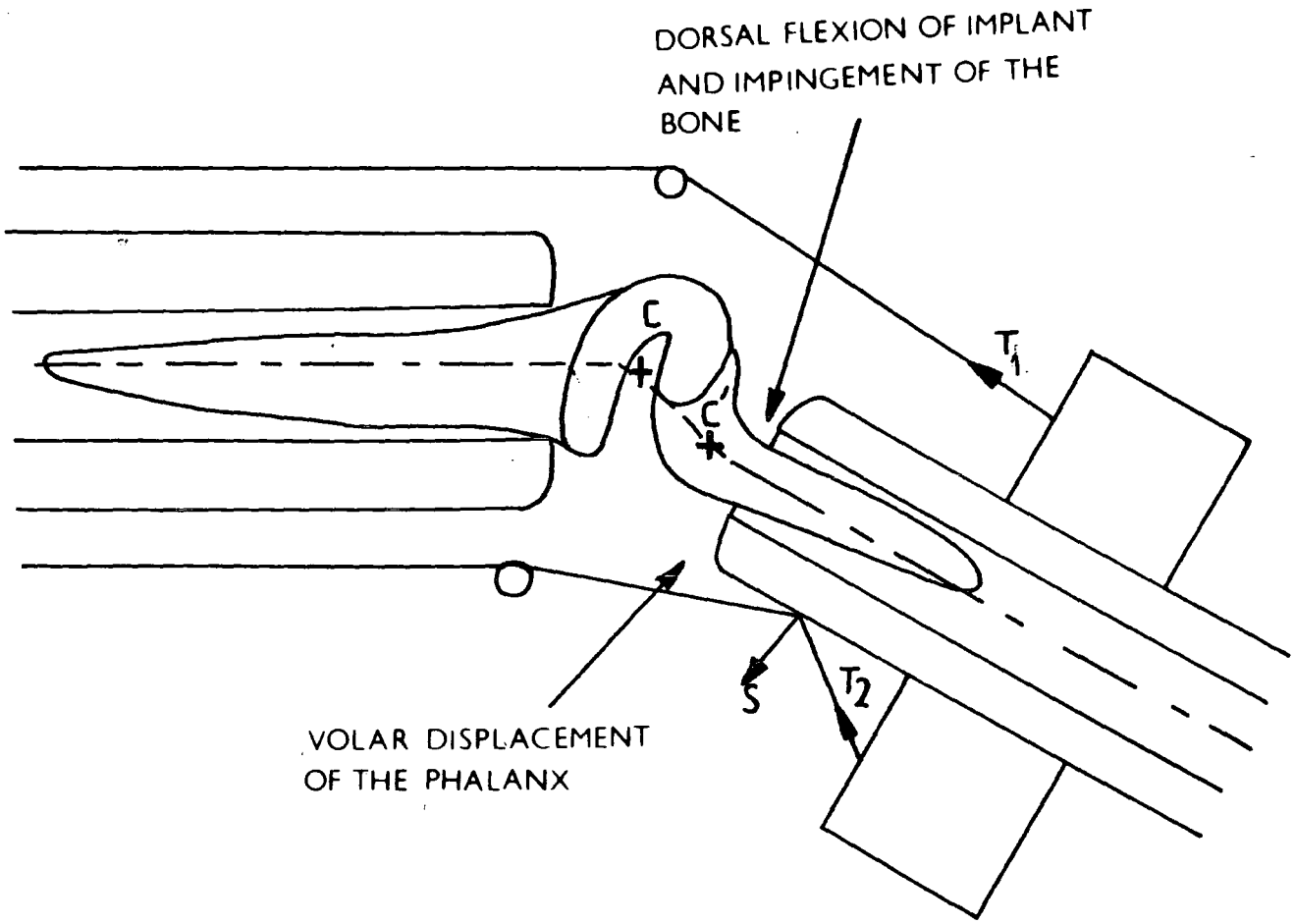

Fig 4.11 Volar subluxation of the Swanson implant in the simulator.

subluxing joint force causes a volar displacement of the phalanx as a consequence of the pliable nature of the implant. This displacement is limited by the stiffness of the silicone elastomer but is sufficient to alter the angles of the 'tendon' actions with respect to the joint, resulting in a larger subluxing component of the joint force for the same balance in 'tendon' tensions. An important consequence of this is the potentially damaging impingement of the bone against the implant during flexion.

The performance of the Swanson implant in patients is well documented (Beckenbaugh et al, 1976 (53), Hagert et al, 1975 (56), Swanson, 1972 (105)) and the basic mechanisms of failure are clear: failures usually occur within the first two years of surgery but this does not always indicate removal if function is maintained. Fracture most commonly occurs at the head of the distal stem and, less frequently, at the proximal stem. Sometimes fragmentation of the midsection occurs. The situation is complicated by lipid absorption, which may weaken the polymer system (Carmen & Mutha, 1972 (106)), and implant migration due to bone resorption, but initial surface damage propagated by stress cycling is the basic cause of failure.

The idea behind the Swanson implant was said to be that it can act as a joint spacer and provide some stability during the early stages of healing after surgery. The stems are allowed to slide so that the implant will find the best position with respect to the centre of rotation thereby distributing the stresses more evenly. The architecture of the implant is felt to encourage the encapsulation and bone reformation process which will in time render the implant, and the joint itself, more stable. However, it would seem that if the

encapsulation process is compromised by recurrent degenerative synovitis, the sliding motion of the implant promotes an adverse bone reaction resulting in the growth of bony spurs and cortical erosion. The implant is not strong enough to withstand deviating forces which produce volar subluxation and ulnar drift: thus failure eventually occurs through pinching of the material and tear propagation. This process is partly imitated by the simulator where no encapsulation can occur. The ensuing bone resorption and spur growth are not present either and it might be expected, therefore, that implant failure would take longer than in-vivo. Failures would probably be manifested as stem fractures since it is unlikely that midsection fragmentation could occur, as this is probably a consequence of ulnar deviation which again is absent in the simulator. Volar subluxation is present, as demonstrated previously (Fig 4.11), and impingement of the phalanx replica on the distal stem of the prosthesis does occur.

The size 2 Swanson test ran for a period of one month at 1.92 Hz. After one million cycles (equivalent to approximately six months normal use) the implant was removed for inspection and showed some evidence of abrasion on both stems, but especially over a region of about 7 mm in length on the dorsal surface at the head of the phalanx stem. These scars had arisen as a result of the stems sliding in their holes. There was also some permanent deformation on each side of the implant midsection presumably occurring as a result of the large compression applied during the heavy static loads. The implant was replaced and inspected again after two million cycles when a crack could clearly be seen at the head of the phalanx stem directly above the point of maximum bending C' (Fig 4.11). The crack had a depth of approximately 3 mm and extended over three quarters of the width of the stem. The depressions

visible on the implant midsection did not appear any more pronounced although the wear scars were more developed on both stems. The implant was again replaced and the crack could be seen to open and close during cycling. The prosthesis eventually failed due to stem fracture after only approximately 3.2 million flexions and 1048 static loads of 185 N at 34° to the phalanx (Fig 4.12). This is equivalent to approximately nineteen months of normal use.

The size 7 implant, though significantly greater in thickness, was not subjected to significantly larger forces than the size 2 (Fig 4.10). It ran at 1.92 Hz for a period exceeding three months and was examined at one million cycle intervals. Up to three million cycles very little damage was evident apart from some wear scarring on the volar and dorsal surfaces of the stems. At five million cycles the wear region on the dorsal surface of the distal stem head was well developed over a region of around 5 mm in length and a very small crack was visible at the distal edge of this region. A slight discolouration was visible in several areas of severe wear. The compression marks seen in the size 2 hub were now clearly visible in the size 7 though they were by no means as deep. At seven million cycles the initial crack had grown to a depth of 3 mm extending across the whole width of the stem and another small crack had initiated at the proximal end of the wear region at the intersection of the distal stem with the midsection. The discolouration in this region was now more pronounced although there seemed to be little change in the wear scarring of other regions. The test was stopped after 10 million cycles and 2582 static loads of 192 N at 36° to the phalanx. The prosthesis still had not failed although the crack had propagated to a depth of 5 mm. Directly beneath this, on the volar aspect of the distal stem, the wear damage was localised and had a depth

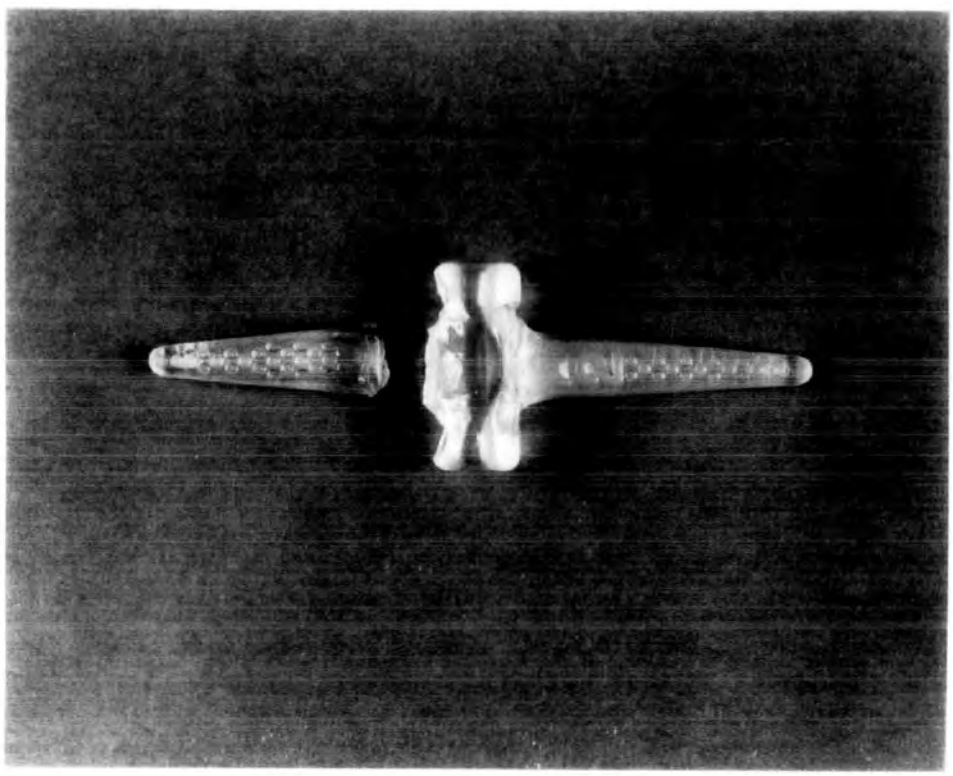

Fig 4.12 Swanson size 2 implant after failure at 3,200,000 cycles.

of some 2 mm. Very little damage could be seen in the metacarpal stems and the compression marks on the implant midsection had progressed no further (Figs 4.13 a) & b)). There is a photograph in a paper by Beckenbaugh et al in 1976 (53) which depicts two Swanson implants removed from patients after failure. The similarity between these and the damage received by the two test implants in the simulator is striking. Undoubtedly the simulator imitates the finger function very well and will provide an exacting and thorough test for any prosthesis design, producing results comparable to those which could be found in-vivo, to highlight any potential problems. The problems associated with the Swanson prosthesis are well understood and measures have been taken to improve the tear resistance of the material. Also over the past few years titanium grommets have been available which reduce the risk of implant damage from sharp bony edges and also prevent prosthesis migration. These however are not as widely used as they might be since they double the cost of the operation, which is very considerable already (Evans, 1989(48)).

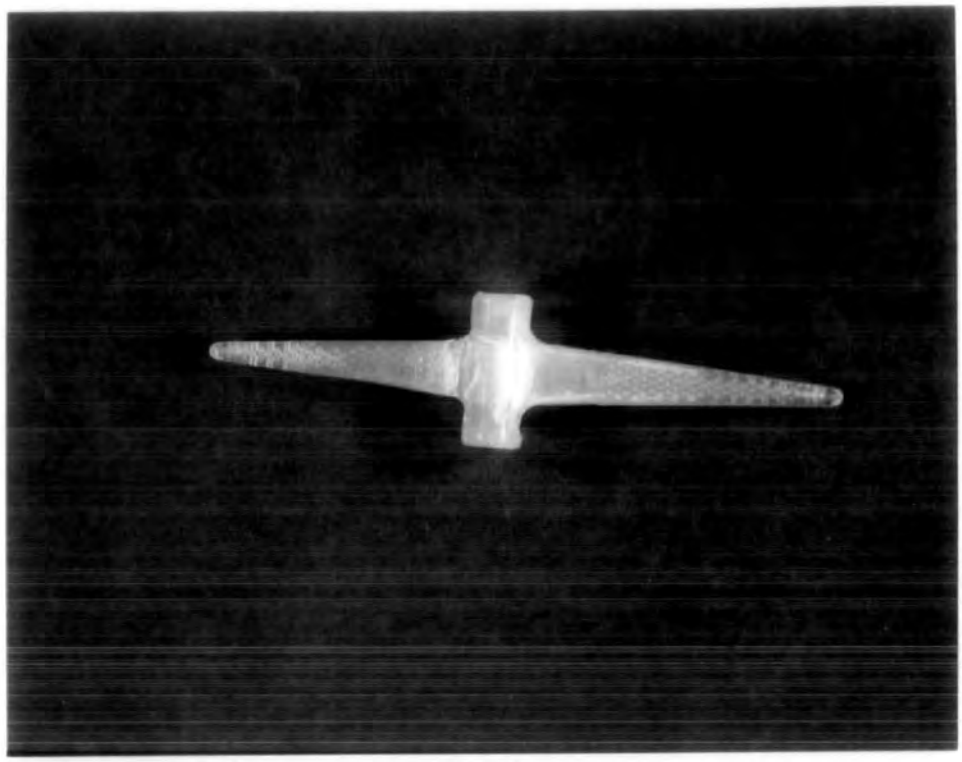

a)

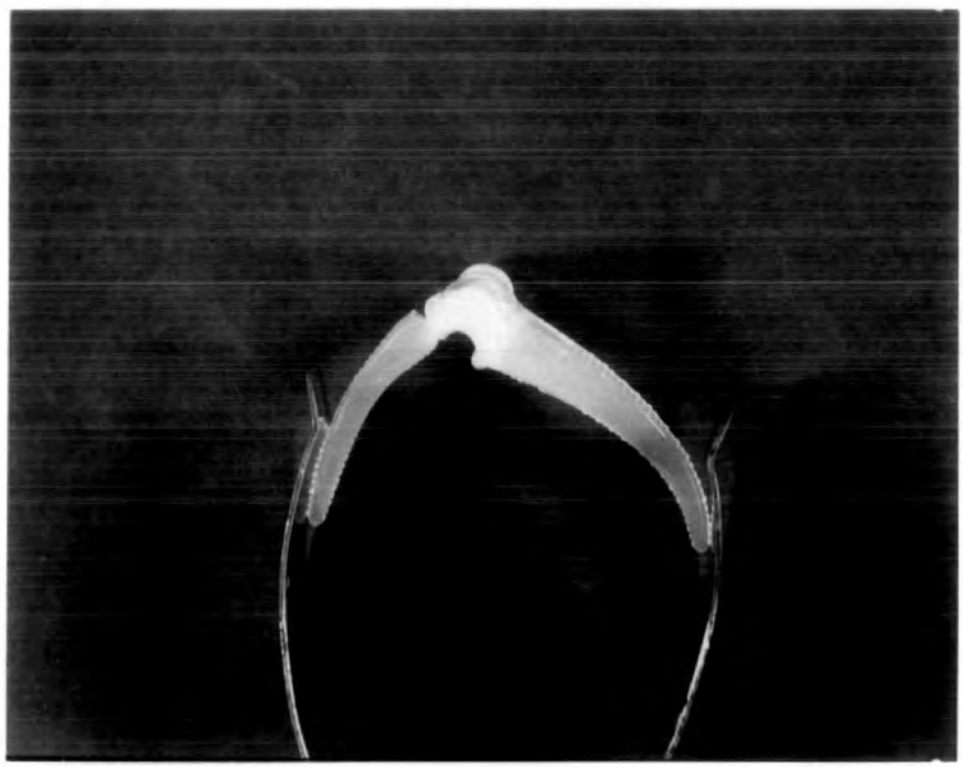

b)

Fig 4.13 Swanson size 7 implant after 10,000,000 cycles.

CHAPTER 5

LUBRICATION AND WEAR

5.1 LUBRICATION

5.1.1 Introduction

Bio-tribology is the study of the lubrication, friction and wear of sliding surfaces as applied to biological systems. For very low friction to be achieved between surfaces some kind of element is generally needed to separate them such as balls, rollers or fluid. There are two main types of lubrication - boundary and fluid film - which are very different in nature.

In boundary lubrication a chemically reactive substance between the two surfaces modifies the friction. This substance may promote oxide formation or its molecules may attach to the surfaces. In this way, during sliding, the surfaces are protected by another layer in which most of the shearing takes place. Engineering bearings of this kind yield friction coefficients no lower than 0.01. Friction is independent of sliding speed (even starting from rest) and the coefficient of friction is independent of load.

Fluid film lubrication can take several forms which all involve the total separation of the bearing surfaces with a pressurised layer of fluid in which the shearing takes place: they differ in the way in which the film thickness is maintained.

In hydrodynamic lubrication, a viscous liquid is drawn by the moving surface through a converging inlet into the load-carrying region. This generates a high pressure in the fluid while the surface motion persists

and friction coefficients well below 0.01 can be achieved. This is a very popular type of bearing but the relative motion of the surfaces is essential. If the bearing slows the film gets thinner and friction rises with the contact of surfaces. For this reason motor oils have been developed with a boundary lubricating ability.

Classical hydrodynamic lubrication assumes that the surfaces are rigid and do not deform under the generated pressures. However the surfaces are commonly compliant and the elasticity is such that the shape of the film is modified through the deformation of the surfaces. This is known as elastohydrodynamic lubrication and for a given load and sliding conditions the film is generally thicker than that of classical hydrodynamics.

A very important form of fluid film lubrication is the squeeze film effect. Here the two surfaces approach each other - not necessarily sliding - and to permit this approach viscous fluid is expelled from between the surfaces. This generates a pressure within the fluid which again can carry a considerable load. Because the film thickness is extremely small compared to the contact width the outward flow of fluid is severely restricted so that it may be a long time before boundary conditions are reached. The squeeze film effect is important in dynamically loaded bearings such as human joints.

Finally, fluid film lubrication can be produced indefinitely in a stationary bearing by pumping fluid into the film. This is known as hydrostatic or externally pressurised lubrication.

In any bearing it is unusual for one mode of lubrication to act in

isolation and commonly several will act at certain times during the duty cycle. The extent to which these mechanisms contribute to human joint lubrication is a controversial issue and the subject of much research since the 1930's. It is interesting to look at the history of this work and the consequences for implant design.

5.1.2 Historical Review

In 1932 MacConaill (107) proposed that human joints were hydrodynamically lubricated mainly on the basis of their anatomical features. This was disputed when Jones, in 1936 (108) and later Charnley, in 1959 (109) measured joint friction experimentally and found that friction coefficients of 0.02 or less persisted even down to zero speed. In their experiments these men used human joints as the fulcrum of a pendulum and looked at the rate of decay of swing amplitude due to friction. In Jones's experiment the decay in amplitude appeared exponential and he concluded that he was seeing hydrodynamic lubrication which turned into a very efficient boundary lubrication at low speeds. However, in Charnley's experiment the decay was linear indicating, it would seem, boundary lubrication only. The reported coefficients of friction were as low as 0.005 which is unheard of in boundary lubrication and researchers began to look for a more complex description to explain the observations. It was commonly felt that joints were fluid film lubricated and that either the escape of the film was very slow or that it was somehow being replaced.

In 1959 McCutchen (110) proposed that joints were lubricated by a mechanism which he called 'weeping lubrication' which was basically a self-pressurising hydrostatic mechanism. Cartilage is porous and

impregnated with fluid. Pressing on its surface initially raises the pressure of the fluid in its pores until it almost equals the applied pressure. Once the squeeze film has thinned so that asperities on opposite surfaces touch, they assume some of the bearing load which slightly lowers the pressure in the film. The pore pressure is then higher than the film pressure so pore fluid flows into the film and makes up the loss. As time passes the cartilage becomes more compressed and its skeleton carries more load. This lowers the pore pressure and also the film pressure leaving more load to be carried in solid contact: the friction rises slowly. Resoaking of the cartilage occurs regularly during joint cycling and some areas of cartilage do not touch at all. McCutchen's theory was supported by experimental tests in which he slid porous rubber (McCutchen, 1959 (110)) and later cartilage (McCutchen, 1962 (111)) against a glass surface. In these tests he saw a very slow increase in friction with time as the deformation of the slider increased, and if he removed the load and allowed the cartilage to resoak for a short time, the friction coefficient dropped and some deformation recovered. However, the permeability of cartilage is very low and the resulting fluid flow rates are minute (Maroudas, 1967 (112)) which led researchers to doubt whether this mechanism could maintain the fluid film.

In 1969 Maroudas (113) proposed the ultrafiltration theory. As two cartilages approach each other and before they touch some of the squeeze film liquid will escape by entering the cartilages and flowing through them. Because the pores in cartilage are about 60 Å in diameter the larger molecules cannot enter and accumulate on the cartilage surfaces to provide lubrication when the surfaces come into contact. Maroudas calculated that a layer of gel 225 Å thick will remain between the

surfaces with the film being stabilised by osmotic flow in. Opponents of this theory noted that no inflow took place with the surfaces at more than 2000 Å but the roughness of cartilage is several times larger than this and the approach of the surfaces may be arrested before ultrafiltration can take place. Maroudas's theory requires synovial fluid but water is also a good joint lubricator.

In 1968 Walker et al (114) performed some experiments similar to those of McCutchen in 1962 (111) and looked at the recovery of friction following each separation of the surfaces. This was too slow to be accounted for by an ordinary squeeze film and they proposed that the viscosity of the film must be higher than that of normal synovial fluid. To explain this they called on the Maroudas ultrafiltration mechanism aided by the trapping of pools of synovial fluid within depressions in the rough cartilage surface. This they called 'boosted' lubrication which was a squeeze film mechanism rather than McCutchen's hydrostatic mechanism, but both could largely be supported by the same experimental results with a difference of interpretation. It is possible that both mechanisms may occur in human joints under different conditions and this was demonstrated by Ling in 1974 (115).

Hydrodynamic lubrication and in particular elastohydrodynamic lubrication still has its proponents. Synovial fluid is thixotropic - its viscosity rises as the shear rate falls - and in 1953 Ogston & Stanier (116) suggested that human joints could be hydrodynamically lubricated. In 1959 Tanner (117) pointed out that the film would be so thin that the shear rate would be above the thixotropic range of synovial fluid causing it to act more like a thin Newtonian fluid. He returned to this point again (Tanner, 1966 (118)) after

making elastohydrodynamic calculations for the hip from which he concluded that a film thickness of 1000 Å was possible. This is still rather smaller than the surface roughness of cartilage and it would seem unlikely, therefore, that elastohydrodynamic lubrication alone could explain human joint lubrication. In 1967 Dowson (119) obtained similar results but pointed out the importance of squeeze film action which in dynamically loaded joints would act to increase film thickness.

Though it is generally acknowledged that human joints are fluid film lubricated in some way, it cannot be denied that intermittent use is a common phenomenon and boundary lubrication can be the only mechanism to combat cartilage damage on starting or stopping. Also, during a duty cycle several mechanisms can take place sequentially and during a walking cycle it is suggested that hydrodynamic, squeeze film, and elastohydrodynamic lubrication all occur.

5.1.3 The Lubrication of Prostheses

An artificial surface replacement prosthesis must give low friction and low wear in service. While patients do not notice high friction in their prostheses, it does give rise to increased stresses on the implant fixation and hence can cause loosening. Low wear obviously leads to a longer life for the prosthesis, and also reduces the possibility of an inflammatory reaction to debris. The question of lubrication in artificial joints must be addressed if they are to be designed able to withstand the demands placed upon them.

In 1969 Scales et al (120) measured the friction in artificial hip joints lubricated with bovine serum, and they concluded that no form of

fluid film lubrication could be produced in these joints. This point was contested in 1978 when Unsworth (121) saw evidence of mixed and fluid film lubrication in a Muller prosthesis which he tested in a pendulum using silicone fluid of different viscosities as the lubricant. The viscosities needed for fluid film lubrication were in excess of 0.5 Pas which certainly would not be found in pathological synovial fluid from an arthritic joint, values of 0.01 Pas being much more likely. Since artificial joints are generally made of fairly stiff impervious materials, they would not be likely to generate elastohydrodynamic films and hence film thicknesses between their surfaces would be three to four times smaller than between compliant surfaces. For most practical purposes it would seem then that the artificial joint must rely solely on the boundary lubricating ability of synovial fluid. For this reason, extensive wear test programmes are carried out to determine the hardest wearing materials available for use, with a view to making implants with a lifetime in excess of fifteen to twenty years at normal wear rates. In this research also, wear tests have been performed on the polyethylene/polyethylene system to ensure that wear rates in the MCP surface replacement prosthesis will be acceptable. It might be noted, however, in view of the very light loading and fast movement of the finger, that fluid film lubrication may indeed be possible in this implant, though this is not assumed. When the finger is under a large load there is little relative movement of the surfaces in general.

5.2 WEAR

5.2.1 Introduction

Durability of implants is an area of increasing concern since total joint replacement procedures are being performed increasingly in the young patient population who are very active. Indeed, patients as young as fourteen (Cole, 1979 (122)) have undergone this type of surgery.

Materials need a low coefficient of friction to allow functioning of a joint without excessive energy expenditure, and wear rates need to be low to allow a long service with minimum release of debris. It is commonly felt that laboratory bench-testing of the friction and wear properties of biomaterials and joint replacements should be a necessary and routine procedure prior to trials in a patient. At least two materials, PTFE and polyester were used in prostheses after insufficient or inappropriate laboratory evaluations with disastrous clinical results (McKellop, 1981 (123)). As yet there is no agreement about whether a simple material test rig or a complex physiological simulator should be used. Either way, proper consideration must be given to the wear measurement method, the test duration, and the criteria for judging a material's performance (Clarke, 1981 (124)). In general it is more common to perform wear studies using standard, simple wear testing rigs (eg. pin-on-plate, pin-on-disc, cylinder-on-cylinder), the type being chosen to be the most suitable for the kind of motion under consideration. The reciprocating pin-on-plate method is the most suitable choice for a finger joint since the track length can be accurately controlled and it provides more opportunities for debris to

act as abrasive particles between the surfaces, as probably occurs in situ. Due to lack of confidence in accelerated wear tests, the majority of experiments should be run close to the physiological velocities.

There are four main types of wear: adhesive, abrasive, corrosive and fatigue. In general they do not act in isolation: commonly two or more will occur together or sequentially.

Adhesive wear is the most common. As two surfaces slide over each other intimate contact is made with opposing asperities, which causes very high local stresses. These stresses lead to a cold welding at the junction. If the welded junction is then stronger than the corresponding junctions between the asperities and their respective surfaces, the weaker asperity/surface junction will be severed. This process causes the transfer of material from one surface to the other. If it is continued, a transfer film is formed which may be destroyed to cause loose wear debris. In 1953 Archard (125) proposed a model for adhesive wear in which he said that the volumetric adhesive wear V is directly proportional to the real area of contact A, and the sliding distance x:

$$V = k A x \qquad \ldots(1)$$

where k is known as Archard's constant. k is a statistical factor: Archard said that each time two asperities come into contact there is a constant probability k that an adhesive fragment will be formed.

Now A = N/H where N is the normal load and H is the hardness of the softer material. Thus:

$$V = \frac{k N x}{H} \qquad \ldots(2)$$

and if k/H = K then

$$V = K N x \qquad \ldots(3)$$

where K is the wear rate coefficient with the units mm^3/Nmm.

This is the simplest representation of wear and is particularly good for polymeric materials (Dowson & Wright, 1976 (126)).

Dividing by the apparent area of contact, equation (3) can be expressed alternatively as:

$$d = K P x \qquad \ldots(4)$$

where d is the depth of wear and P is the nominal contact pressure.

Two-body abrasive wear occurs when a rough hard surface (or a surface containing hard particles) slides on a softer surface. This type of wear is characterised by long deep scratches in the softer surface lying in the direction of the motion, and is minimised when the surfaces are smooth, especially with the metal/plastic system. For this reason it is commonly seen at the start of a wear test, when surfaces are rough from machining marks. When the surfaces have smoothed it may disappear but reappear later as three-body abrasive wear if loose debris becomes trapped between the surfaces.

Corrosive wear is mainly a problem with metallic surfaces. During sliding, should a natural protective coat such as an oxide film be rubbed off, exposing the bare material, then corrosion will occur. The

products of this chemical reaction are rubbed off with further sliding to again expose bare surface, and hence the process continues. This is known as corrosive wear and the corrosion products may well go on to cause three-body abrasive wear.

Fatigue occurs after many sliding cycles due to the continual loading and unloading of a material. Eventually surface and subsurface cracks will appear, leading to the removal of material from the surface. This type of wear is characterised by surface cracking and pitting with the cracks often occurring across the sliding direction. It is particularly common in heavily loaded, non-conforming joint implants such as those used for the knee.

5.2.2 The Wear of Prostheses

Wear is a very complex phenomenon and not only are the material properties important but also the implant design and the prosthesis forming technique. The conformity of the surfaces is a very important consideration. If contact occurs over a large area and the lubricant does not have good access to the surfaces, then wear will be high because the real area of micro-contact will be high (increasing adhesive wear) and the debris cannot readily escape (increasing three-body abrasive wear). A less conforming design, while tending to reduce these types of wear, will increase local contact stresses and so promote creep and fatigue problems. A compromise has to be made appropriate to the desired function of the prosthesis.

There are three types of wear test reported in the literature:

1) High speed tests in which there is no attempt to simulate physiology.
2) Tests where there is no simulation of dynamic joint loading profiles but in which other parameters such as stroke amplitude, frequency and contact stress are controlled.
3) Tests using complex joint simulators in which both the material and the design are evaluated.

A well-designed simulator has the capacity to provide very accurate and detailed information about the behaviour of a prosthesis but simulator tests are very time consuming and standard bench tests therefore do have a place. In this research programme tests have been performed using both methods and it is hoped in this way to give a fuller picture about the suitability of the material choice and the design features of the prototype implant in respect of wear and fatigue. The wear of an implant material is expressed as the amount of wear per year of equivalent use, with one year representing an estimated fixed sliding distance under load. This provides a wear factor that can be readily interpreted in terms of the potential clinical performance of the material.

The wear of biomaterials can be assessed by recording either dimensional changes or weight loss of specimens. The majority of wear studies have relied on dimensional changes to define wear (Clarke, 1981 (124)). However, dimensional changes generally give results showing considerable scatter. This problem arises principally because of the tendency of many polymers, particularly polyethylene, to creep under load. Creep of a polymer specimen is a function of material, geometry, temperature and loading conditions and may result in dimensional changes much larger

than those produced by wear (Rose et al, 1980 (127), Atkinson et al, 1980 (128)). The measurement protocol must be able to distinguish between creep and wear. Weight measurements too are not without their drawbacks. Polymers have a tendency to absorb or adsorb fluid and thereby gain weight. If the wear rate is low the specimens may be heavier after the test than before. The error due to fluid absorption can be minimised by the use of soak control specimens.

One of the problems in obtaining significant wear data is the time factor. Since it is important to run wear tests close to physiological velocities (approx. 40 cycles/min), one wear test will take more than one month to complete even with twenty-four hours of testing per day, because machine down-time is required for wear measurements and cleaning operations. In addition replicate tests must be performed to increase confidence. However, this represents an impossible time commitment with any single channel machine. A multiple-channel test capability is therefore of paramount importance in overcoming this limitation. With a simulator this is not possible and hence the necessity for standard wear testing.

The wear test duration is a very important consideration. In 1976 Rostoker & Galante (129) compared the wear rates of polyethylene at two contact stresses at both short- and long-term wear durations. They concluded that a sliding distance of at least 25.4 km was required to establish the long-term wear behaviour of materials such as polyethylene. On the basis of laboratory tests, Atkinson et al in 1978 (130) predicted that surface fatigue will occur in polyethylene in-vivo after eight to nine years of use for the metal/plastic joint. If this fatigue mechanism changes the observed wear rates substantially,

the laboratory tests will need to be long enough to encompass this regime. For a finger joint a sliding distance of around 70 km is equivalent to approximately five years use assuming, as a rough estimate, that a metacarpal with an 8 mm diameter head will perform 100 cycles per hour through 60° flexion. This would seem a reasonable distance over which to run bench wear tests for a surface replacement prosthesis for the MCP joint.

5.3 A FOUR-STATION BENCH WEAR TEST RIG

The wear test rig was adapted from an existing piece of apparatus used at Durham University since 1978. Basically the rig consisted of a mild steel sledge moving in a reciprocating motion along two fixed, parallel bars. This sledge provided the base for the plate holder and heating bed (Fig 5.1) and was driven by a 0.125 hp DC motor via a 10.5:1 reduction gear box. The gear box provided a slow speed, high torque motion and prevented any changing frictional forces from having a significant effect on the speed of the sledge. A slow speed of 41 cycles/min and path length of 56 mm were chosen to imitate the motion of a finger joint in normal use.

Heating was provided by a small cartridge heater placed within a centrally drilled hole in the mild steel heating bed. Temperature measurements were made of the under-side of the plates via thermocouples, and the lubricant temperature was periodically recorded during each test such that the pin and plate wear surfaces were held at ~37°C. The test plates were clamped to the heating bed by a retaining brass plate in which were milled four slots to provide a firm seating for each plate and which also formed wells over the plates for the lubricant. In this experiment the lubricant was distilled water drip-fed to the plates through rubber capillary tubing.

The wear pins were held in aluminium holders (Fig 5.2) which fitted into brass bushes supported by cantilevers (Fig 5.3). This arrangement meant that each wear pin rested on its plate and was restrained to move

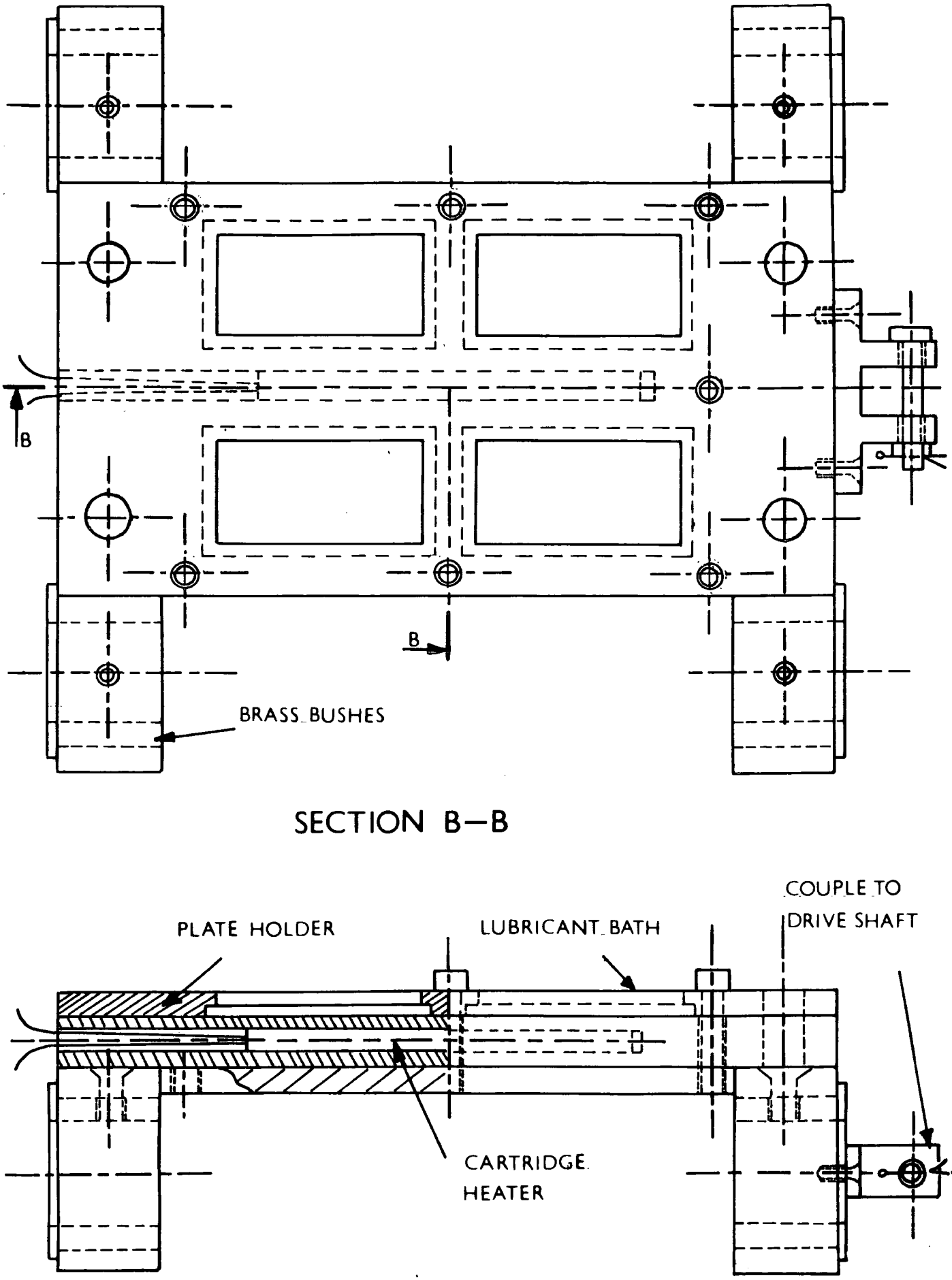

Fig 5.1 Wear rig sledge, heating bed and plate holder.

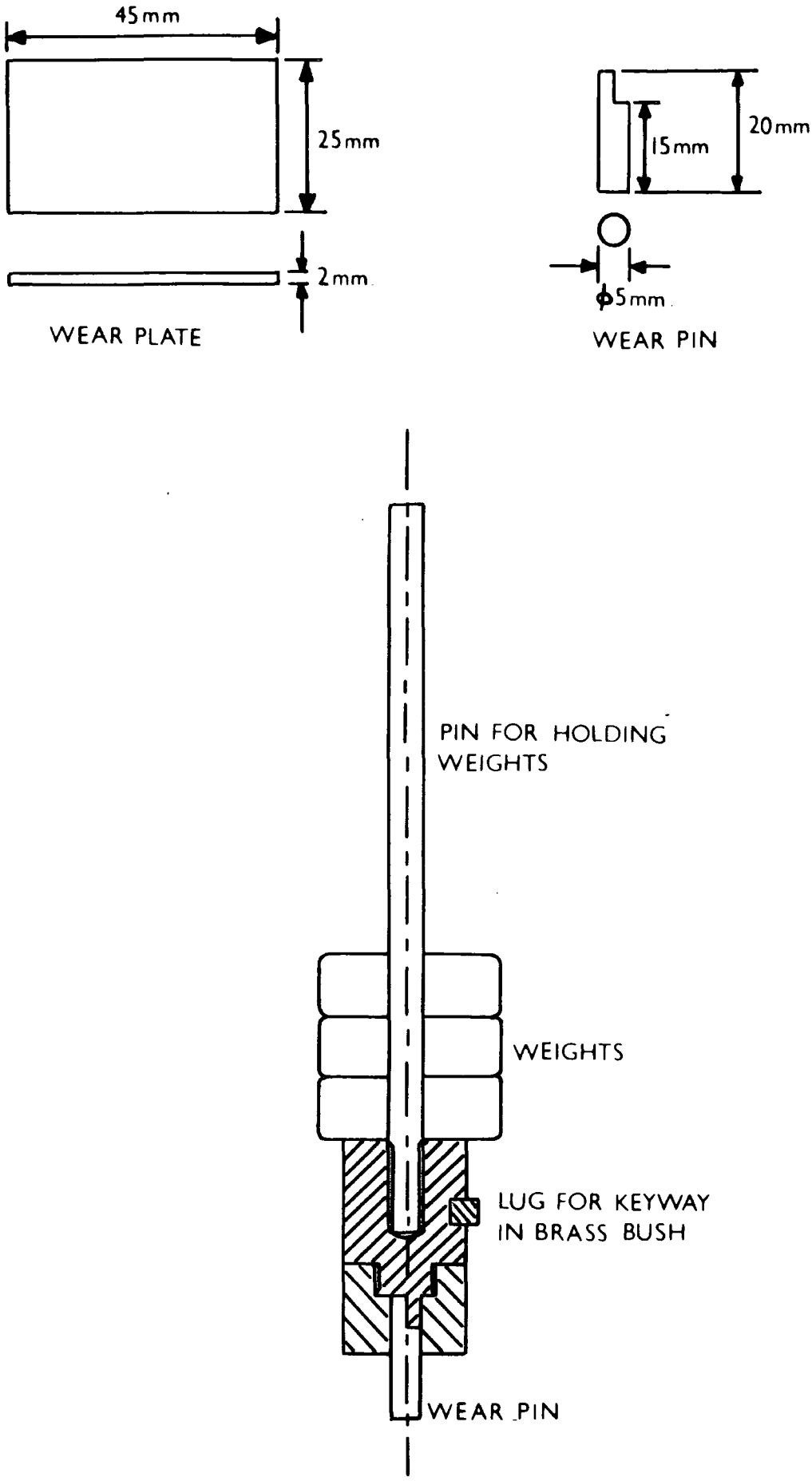

Fig 5.2 Wear test pin, plate and pin holder.

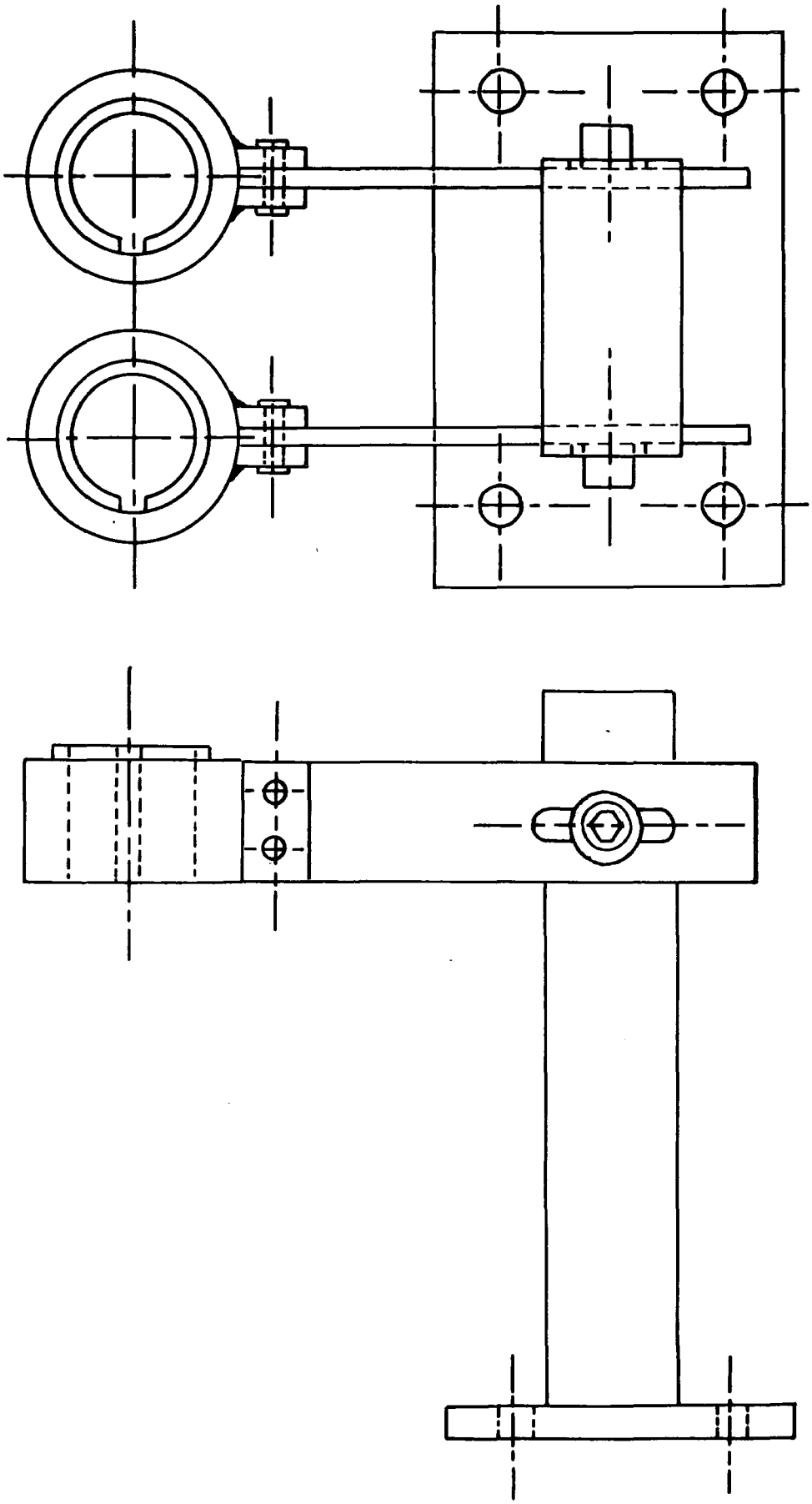

Fig 5.3 Wear rig cantilever support and bushes to hold test pins stationary above the plate sledge.

vertically. It was loaded by placing weights over the long stem attached to the pin holder. The design of the pin holder was such that a pin was always replaced in the same orientation to the plate after cleaning.

5.4 MATERIALS AND METHOD

5.4.1 Test Material

All the tests were carried out using ultra-high molecular weight polyethylene (density 0.954 g/cm^3) supplied by Chas F Thackray & Sons Ltd. This was block material, tested before cross linking which is thought to improve wear properties somewhat. Since the cross linked material is under development by the company it was not available at the time of these tests. However, the prototypes used in the simulator wear tests were cross linked and the wear rates will be compared with the raw material tested here. The purpose of the study was to look at wear mechanisms occurring when polyethylene is rubbed against itself.

The wear pins were solid cylinders of length 20 mm and diameter 5 mm, turned from a block of UHMWP. A notch was cut out for positioning (Fig 5.2). The polyethylene counterfaces were rectangular, 45 mm long and 25 mm wide, and were also machined from solid blocks of UHMWP. The counterface surface itself was milled. Lubrication of the surfaces was maintained by distilled water.

The initial roughnesses of the pin and plate surfaces were measured using a Taylor Hobson Talysurf Mark IV and the results are shown in Table 5.1. The average roughness of the pins was ~0.695 μm, and of the plates was ~0.782 μm longitudinally and ~0.656 μm transversely. Fig 5.4 shows electromicrographs of an unused counterface at x37.7 and x310 magnification using a Cambridge Stereoscan 600 SEM. On completion of each test the surfaces of both pin and plate were examined in this way.

Pin & Counterface Number		Roughness Ra (μm)		
		Plate Longitudinal	Plate Transverse	Pin
Test A	1	0.821	0.646	0.712
	2	0.797	0.621	0.694
	3	0.840	0.671	0.695
	4	0.799	0.708	0.609
Test B	1	0.814	0.630	0.803
	2	0.764	0.629	0.698
	3	0.766	0.664	0.711
	4	0.705	0.663	0.697
Test C	1	0.839	0.600	0.659
	2	0.801	0.690	0.689
	3	0.702	0.626	0.677
	4	0.733	0.721	0.704
Overall mean		0.782	0.656	0.696

Table 5.1 Initial roughness of the pins and plates.

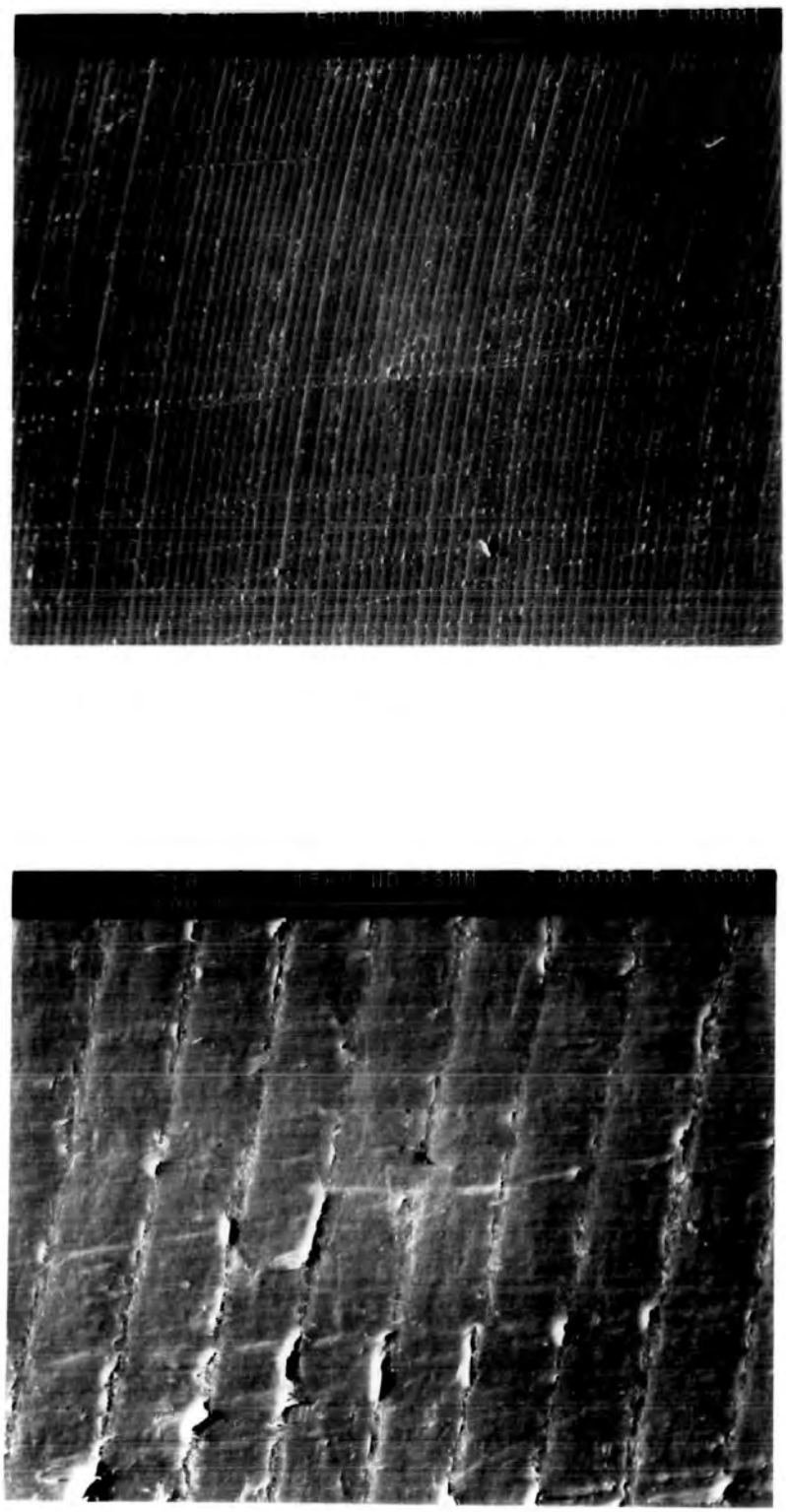

Fig 5.4 Micrographs of an unworn counterface.

Specimens were mounted on Dural stubs and coated with gold/palladium in an evaporation unit before being placed in the SEM. Since the polyethylene has a tendency to blister under the electron beam, a relatively low accelerating voltage of 15 kV was chosen.

5.4.2 Test Procedure

Wear is a very complex phenomenon dependent upon many variables and it is essential, therefore, to maintain a strict standard procedure during testing. Prior to the start of each test the sledge, wear pins, control pin and counterfaces were cleaned with alcohol and dried using a hairdryer. The wear and control pins were then carefully weighed and the average of five readings recorded. The counterfaces were loaded under the retaining plate and the reservoirs filled with lubricant from the drip-feed. Without the pins in place, the motor and cartridge heater were turned on for a warming up period of ~2 hours during which time the lubricant temperature and the motor speed were regularly monitored. When the motor speed had stabilised it was stopped briefly to allow the pin holders, loaded with the pins and the appropriate weights, to be placed in their brass bushes. The motor was started to begin the wear test after the control pin was placed in the lubricant.

During a test the ambient and lubricant temperatures were recorded such that 37°C could be maintained at the plate surface. However, since the cartridge heater was manually controlled, it proved to be better to maintain a stable temperature than to try to compensate for a drop in temperature, for instance, on an unusually cold day. The mean temperature over a whole test was 37°C.

Periodically, during a test, the motor was stopped for the weighing of the pins. This was performed rather frequently early in the test when the results were quite variable due to the presence of machining marks on the surfaces. Later in the test the interval between weighings was increased to about 48 hours. The plates were not weighed since the changes in weight would be very small compared to their original weight. Also, it would be difficult to replace them under the retaining plate at the correct orientation. The weighing of the pins obeyed the following procedure.

Firstly, the motor was stopped and the pins removed from their holders. They were tissue dried, ultrasonically cleaned and then washed in alcohol and dried using a hairdryer. Each pin, including the control, was weighed carefully and the average of five readings was recorded along with the accumulated sliding distance. The weight loss of the wear pins was converted into a volume loss, taking into account any weight changes in the control pin. This then removed any fluctuations in weight due to water absorption or instrument variability, to reveal the amount of wear that had actually taken place. After a set time of one hour the pins were replaced in their holders and loaded against the plates. The test resumed when the motor was switched on. The test ended after a sliding distance of around 70 km (or 23 days) and was repeated twice more to give an indication of reproducibility of results.

5.5 RESULTS

5.5.1 Volume Losses

The load conditions in each test are shown in Table 5.2 and the results for each are recorded in Tables 5.3 - 5.5 which present the values of volume loss due to wear after different sliding distances. Volume losses were calculated from the mean weight change using a density of 0.954 gcm^{-3} for the polyethylene. The measurement error in the weighings was ±0.5 mg which was equivalent to ±0.52 mm^3 in volume. Not surprisingly, during the course of the tests, some volume changes appeared positive (starred in the Tables) but these only occurred in the initial 10 km during the wearing-in period. They were seen to be unimportant in the final analysis. Graphs were plotted of the volume loss due to wear V (10^{-2} mm^3) against sliding distance L (km) (Fig 5.5). The slope of any straight line portion of the graph, divided by the normal force P (N) on each pin, is defined as the wear rate coefficient K (mm^3/Nm) at that time (equation (3)). The gradients were calculated using the method of least squares and are shown in Table 5.6 for each of the four loads. Since the results were found to be reproducible,

All Tests Pin & Plate	Load (N)	Stress (MPa)
1	19.0	0.968
2	8.5	0.433
3	5.0	0.255
4	14.0	0.713

Table 5.2 Test load conditions.

Time (hrs)	Distance (km)	T_{AMB} (°C)	T_{SAMP} (°C)	δV_1 ($10^{-2}mm^3$)	δV_2 ($10^{-2}mm^3$)	δV_3 ($10^{-2}mm^3$)	δV_4 ($10^{-2}mm^3$)
0.00	0.00	20	35	0.00	0.00	0.00	0.00
7.24	0.997	18	37	-10.48	-10.48	-10.48	-21.00
19.24	2.65	19	36	-41.90	-31.40	-21.00	-21.00
67.50	9.30	18	38	-52.40	-41.90	+21.00*	+10.50*
113.70	15.66	18	37	-155.70	-52.40	+10.50*	-103.40
165.20	22.76	17	38	-294.60	-88.60	-41.90	-189.80
209.10	28.80	17	36	-426.50	-128.40	-52.40	-270.10
255.10	35.14	17	35	-632.20	-163.10	-59.90	-344.70
290.40	40.00	20	38	-909.40	-202.40	-73.70	-471.00
326.00	44.91	16	38	-1179.50	-297.80	-80.90	-628.60
393.40	54.20	18	36	-1701.60	-481.20	-130.80	-932.90
448.80	61.83	17	37	-2163.70	-646.30	-170.00	-1195.40
497.20	68.50	17	37	-2503.10	-781.60	-212.30	-1410.80
540.70	74.49	18	37	-2807.90	-908.10	-249.50	-1622.10

Table 5.3 Volume changes in test A.

Time (hrs)	Distance (km)	T_{AMB} (°C)	T_{SAMP} (°C)	δV_1 ($10^{-2}mm^3$)	δV_2 ($10^{-2}mm^3$)	δV_3 ($10^{-2}mm^3$)	δV_4 ($10^{-2}mm^3$)
0.00	0.00	17	37	0.00	0.00	0.00	0.00
12.00	1.65	17	36	0.00	-10.48	-10.48	-10.48
23.57	3.25	18	37	-20.96	-20.96	-10.48	-10.48
35.57	4.90	19	35	-60.30	-10.90	+10.90*	-10.90
55.17	7.60	19	38	-39.60	-24.30	-30.40	+5.20*
84.20	11.60	16	39	-87.50	-26.60	-26.00	-69.70
109.61	15.10	19	37	-138.10	-53.10	-29.90	-101.90
148.81	20.50	18	38	-271.10	-92.80	-22.20	-173.60
207.61	28.60	16	36	-412.80	-134.40	-61.10	-264.80
242.45	33.40	17	37	-559.40	-179.50	-73.80	-340.20
281.65	38.80	17	36	-764.70	-221.30	-62.70	-469.80
325.91	44.90	20	36	-1233.40	-320.00	-63.80	-661.90
368.03	50.70	19	38	-1498.20	-435.90	-124.30	-859.10
435.90	60.05	18	37	-2119.60	-641.50	-172.70	-1177.30
489.98	67.50	18	37	-2402.40	-780.00	-187.20	-1402.60

Table 5.4 Volume changes in test B.

Time (hrs)	Distance (km)	T_{AMB} (°C)	T_{SAMP} (°C)	δV_1 ($10^{-2}mm^3$)	δV_2 ($10^{-2}mm^3$)	δV_3 ($10^{-2}mm^3$)	δV_4 ($10^{-2}mm^3$)
0.00	0.00	19	36	0.00	0.00	0.00	0.00
12.00	1.65	17	37	0.00	-10.48	+10.48*	-20.96
21.39	2.95	18	37	-10.48	0.00	-20.96	-10.48
33.39	4.60	16	39	+10.90*	-5.60	+10.90*	-10.90
53.72	7.40	16	37	-5.90	-30.40	-10.60	-40.60
71.86	9.90	18	38	-30.10	-50.60	-20.90	-48.30
95.82	13.20	17	38	-99.90	-51.20	-24.10	-69.70
137.92	19.00	17	36	-209.20	-72.70	-38.60	-113.80
178.57	24.60	15	37	-373.70	-133.60	-70.00	-238.20
233.01	32.10	18	36	-467.50	-117.90	-69.20	-270.10
258.42	35.60	17	38	-740.20	-190.10	-43.50	-376.80
299.07	41.20	17	37	-1074.60	-251.00	-95.10	-555.40
368.76	50.80	16	37	-1591.40	-397.40	-86.70	-801.20
422.47	58.20	17	36	-1846.20	-539.50	-132.90	-1033.10
460.95	63.50	18	37	-2280.60	-725.30	-206.60	-1288.70

Table 5.5 Volume changes in test C.

All Tests Pin & Plate	Load P (N)	V/L (10^{-5} mm^3/m)			Wear Rate Coeff. K (10^{-6} mm^3/Nm)			Depth (mm)
		Low	High	Mean	Low	High	Mean	
1	19.0	20.33 ±0.72	55.37 ±0.95	35.71 ±1.54	10.7 ±0.38	29.1 ±0.50	18.8 ±0.81	1.16
2	8.5	5.89 ±0.42	20.03 ±0.61	10.55 ±0.58	6.9 ±0.5	23.6 ±0.7	12.4 ±0.68	0.37
3	5.0	2.01 ±0.40	5.94 ±0.70	2.78 ±0.16	4.0 ±0.8	11.9 ±1.4	5.6 ±0.32	0.105
4	14.0	12.32 ±0.56	32.49 ±0.59	19.91 ±0.89	8.8 ±0.4	23.2 ±0.4	14.2 ±0.6	0.656

Table 5.6 Wear rate results.

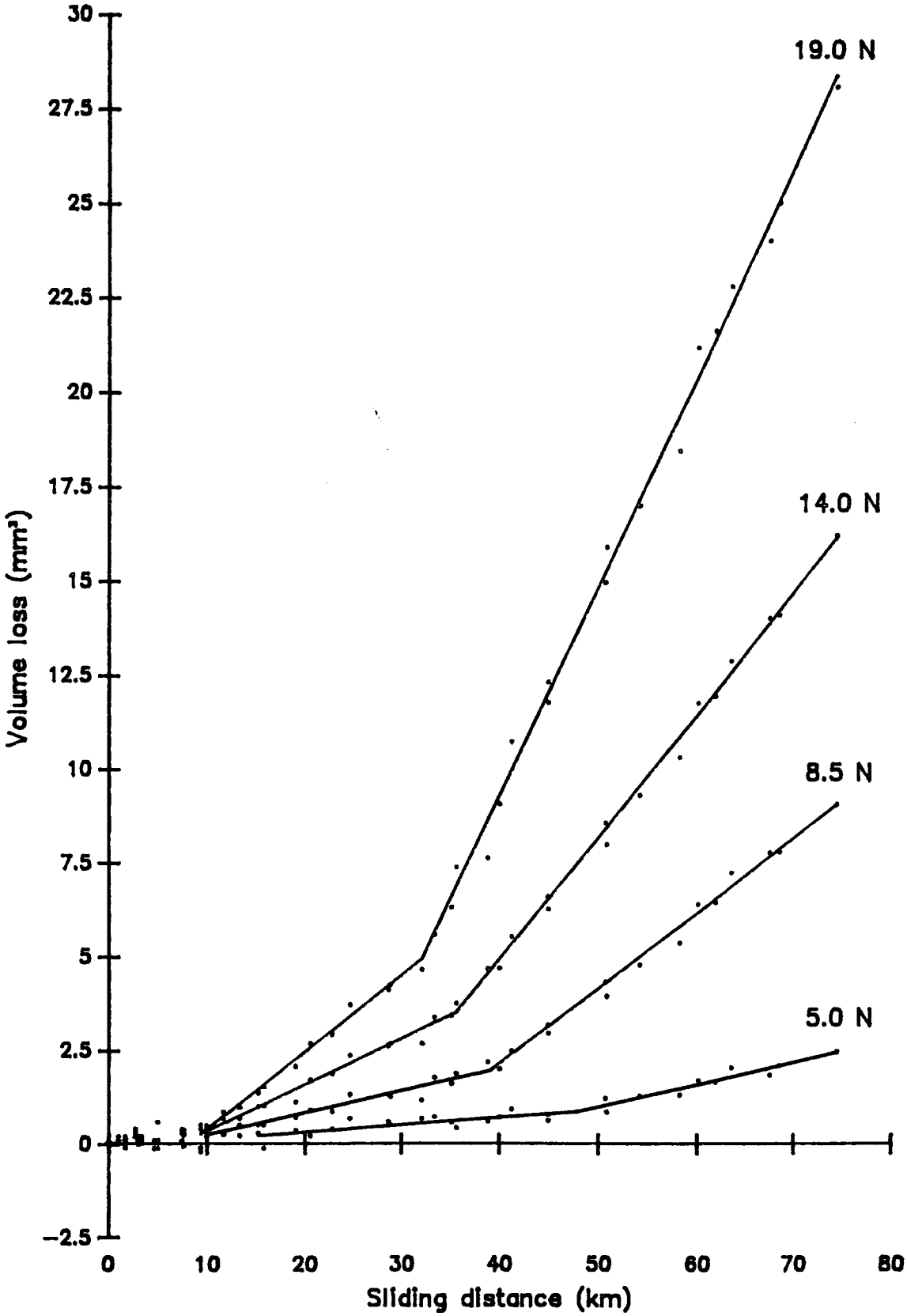

Fig 5.5 Graph of volume loss vs sliding distance.

tests A, B & C at each load were taken together. For each load three wear rates are given since in each case it was clearly apparent that a higher wear regime was taking over after a certain sliding distance, even for the 5 N load test. The wear rates of both regimes are given along with the mean wear rate for the whole test. Also given in Table 5.6 are the expected wear scar depths for the components (total volume lost / area of contact). Fig 5.6 shows how the volume lost per unit sliding distance varies with the applied load.

5.5.2 Electron Microscopy

Fig 5.7 shows the wear scar cross-section for one plate of each of the four loads tested using a magnification of x5. The depth of wear clearly increases with load and, from photographs, the mean wear depths for the pins were measured to be 1.2, 0.4, 0.1 & 0.6 mm for tests 1 - 4 respectively, which are largely in agreement with the expected values given in Table 5.6. The plates, however, did not seem to have worn quite as much as the pins and the mean scar depths were 0.8, 0.2, 0.1 & 0.4 mm.

Fig 5.8 shows evidence of abrasive wear with clear grooves marking the plates in the direction of travel. In general the wear surfaces of both the pin and plate took on a polished appearance with the surfaces of the high load tests being very much smoother than those of the low load tests. Figs 5.8 a) - c) show the progression of smoothness as the load increases. This would imply that abrasion is a more important wear mechanism in lightly loaded tests and is superseded by other mechanisms for higher loads. For two-body abrasion the surface asperities will quickly wear away under a heavy load. In fact, none of the initial

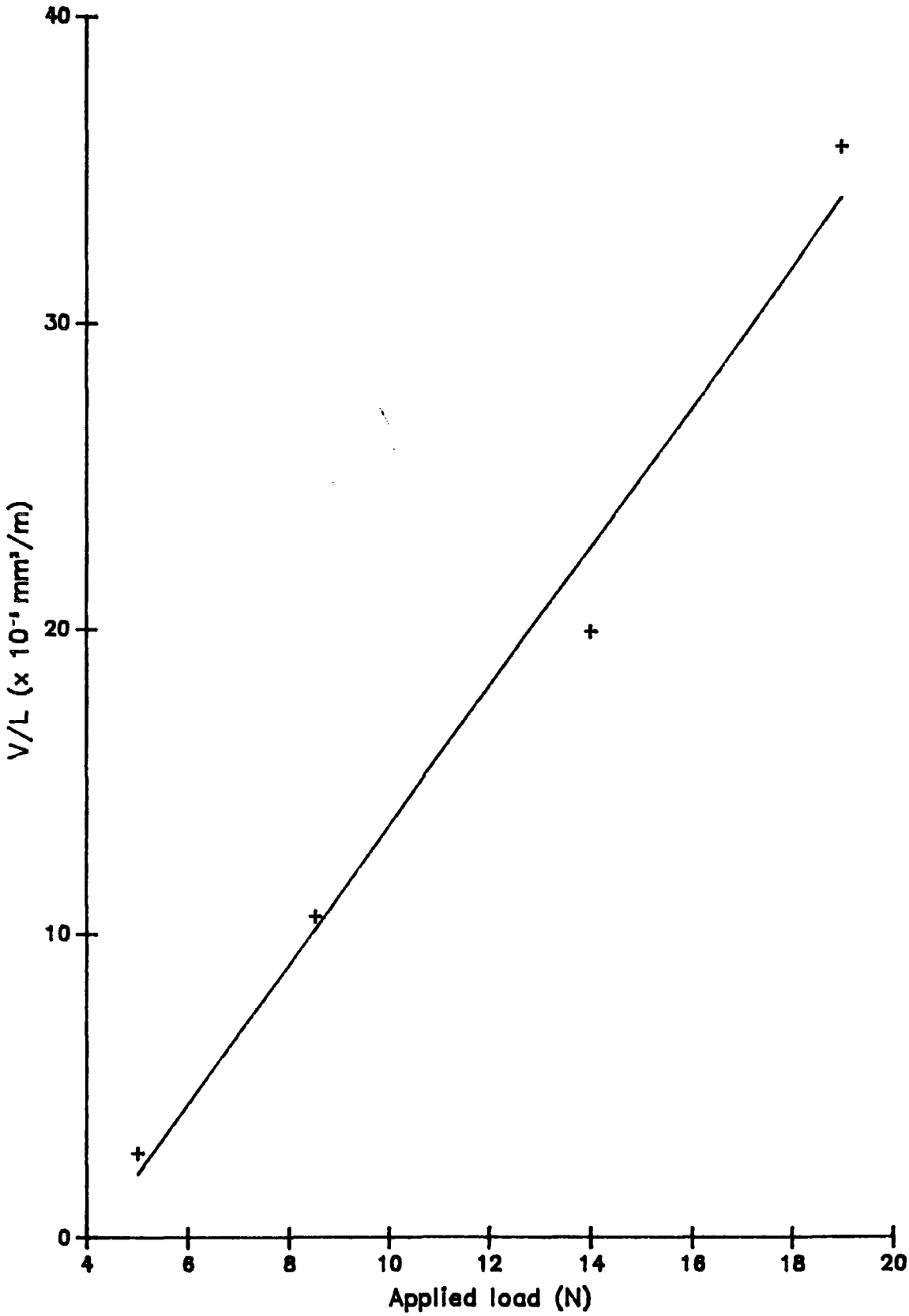

Fig 5.6 Graph of volume lost per unit sliding distance vs applied load.

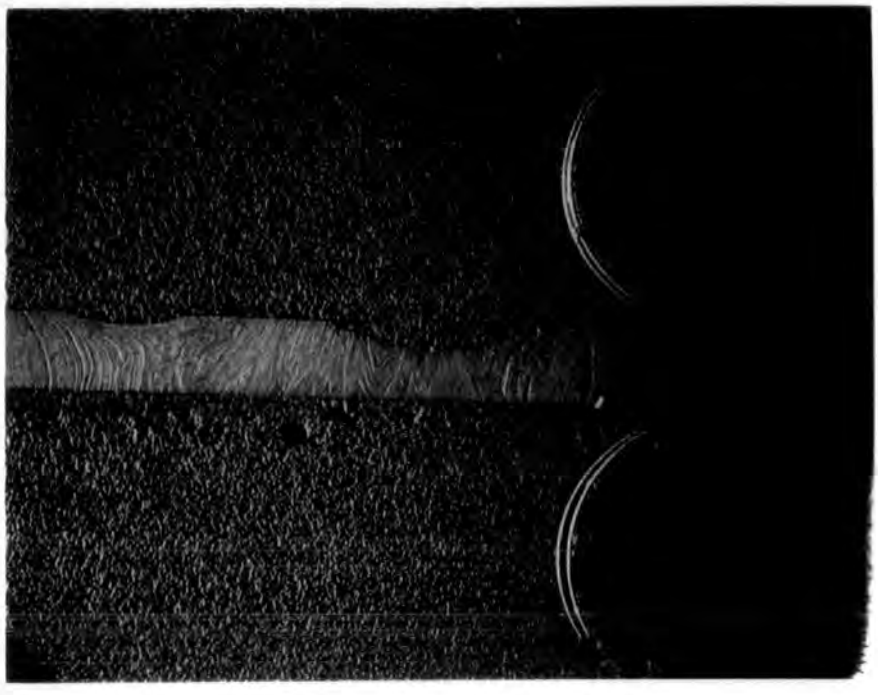

Fig 5.7 a) Wear scar cross-section for plate 1 test A.

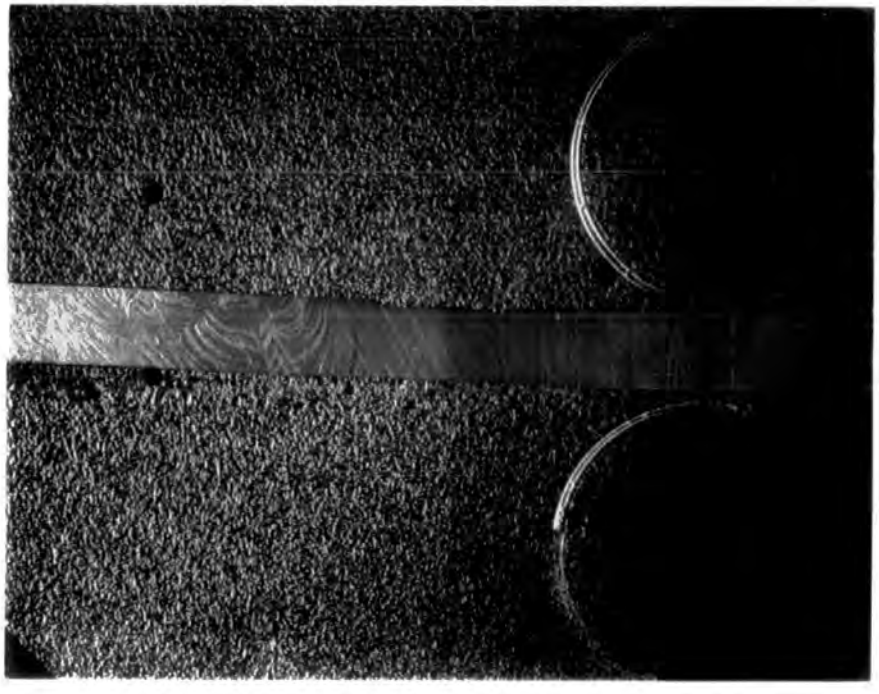

Fig 5.7 b) Wear scar cross-section for plate 2 test A.

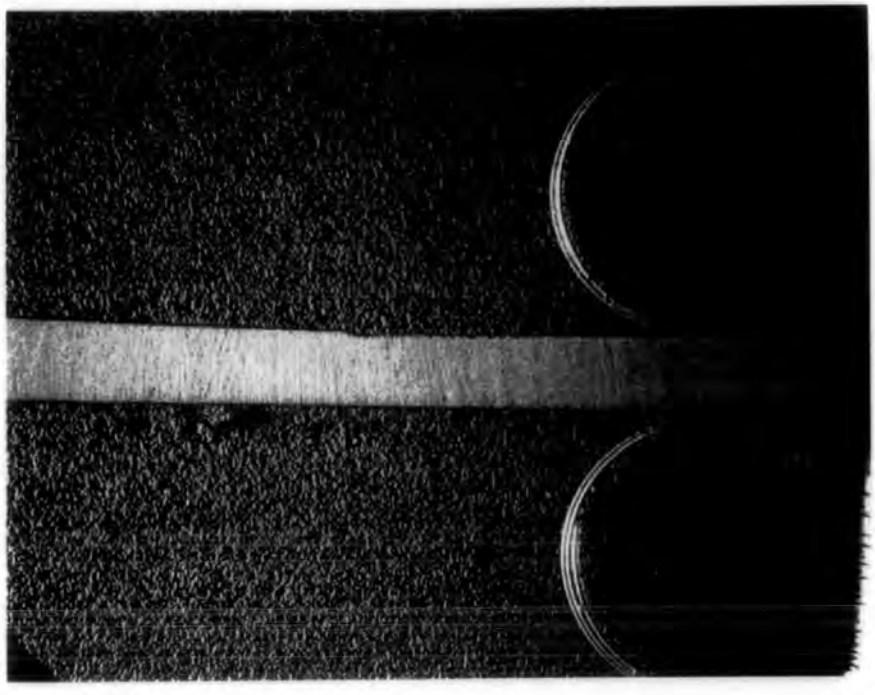

Fig 5.7 c) Wear scar cross-section for plate 3 test C.

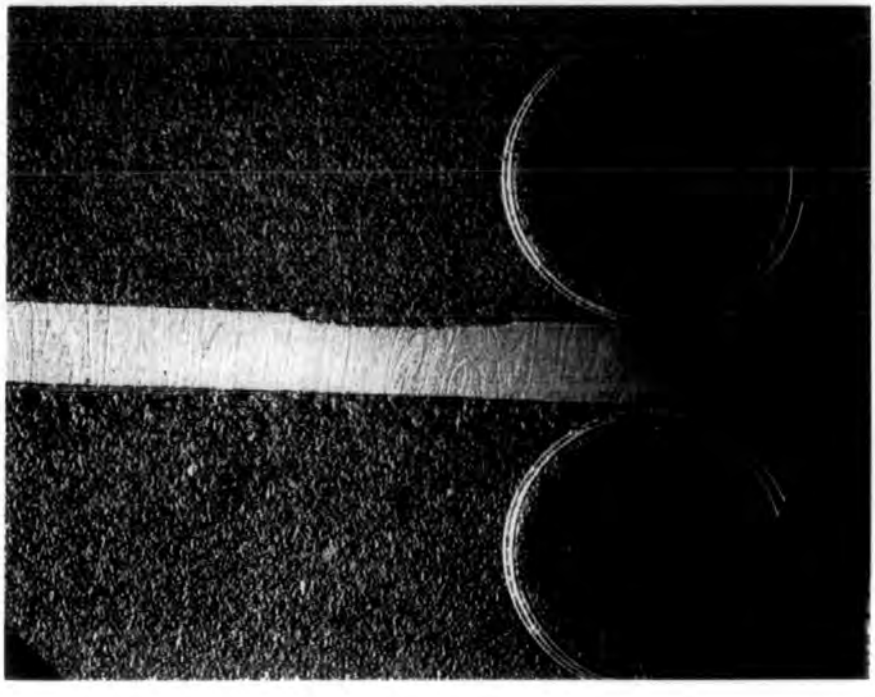

Fig 5.7 d) Wear scar cross-section for plate 4 test B.

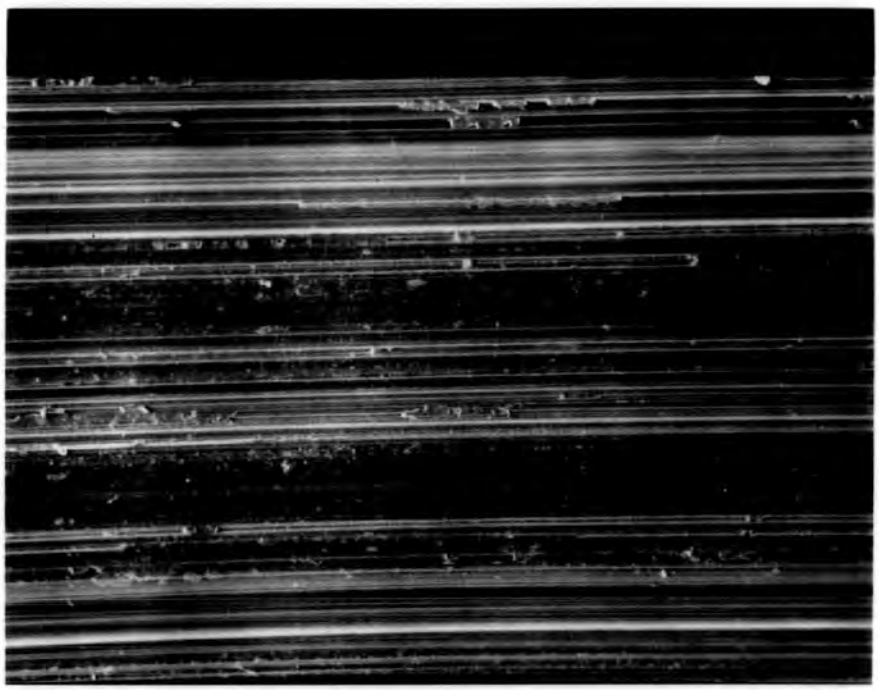

Fig 5.8 a) General view of worn surface - plate 3 test B.

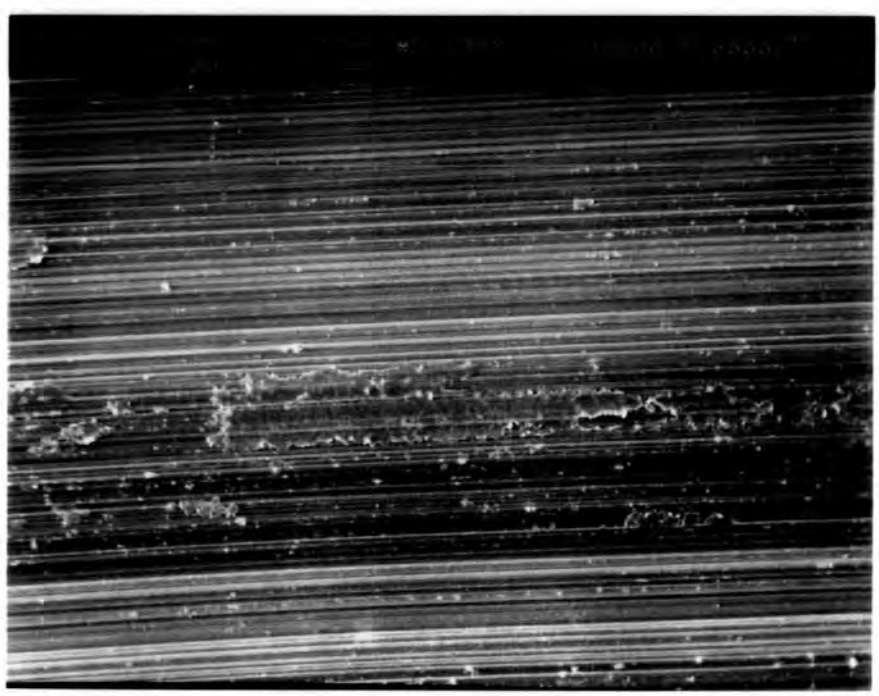

Fig 5.8 b) General view of worn surface - plate 2 test B.

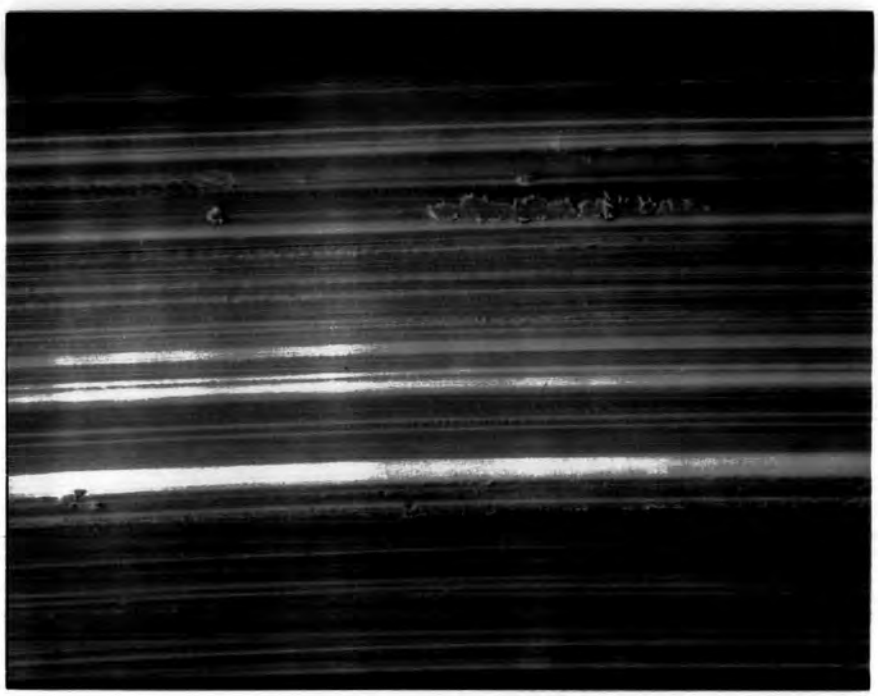

Fig 5.8 c) General view of worn surface - plate 1 test C.

machining marks could be seen on any pin or plate after the tests. Debris fragments can be clearly seen on all three photographs of Fig 5.8 with particle sizes ranging from a few microns to over 0.5 mm. These will have resulted in three-body abrasion trapped between conforming surfaces.

Some material is passed from one surface to the other through adhesion. This is film transfer where the material is smeared (or cold welded) onto the opposing surface. Examples of this are shown in Fig 5.9. In time the transfer film may be removed again and remain loose to cause three-body wear.

Figs 5.10 a) & b) show very clearly the extensive fine surface rippling that could be seen on all pins and plates. The ripples lie perpendicular to the direction of travel and are the result of adhesion and cold flow during the reciprocating motion.

Fig 5.10 b) is interesting in that small round particles appear to have been pressed deeply into the surface of the plate. Analysis revealed them to be NaCl and Fe particles which may have been impurities in the lubricant. If small bone particles were to become embedded in this way, severe abrasive wear to the prosthesis would result.

Fig 5.11 shows the two types of surface cracking visible in areas of each sample after the tests. Fig 5.11 a) shows brittle cracks up to 5 μm in length which run along the surface ripples perpendicular to the sliding direction. These are undoubtedly fatigue cracks propagated by the repeated change in direction of the motion. Fig 5.11 b) also shows cracks perpendicular to the sliding direction but these appear to be

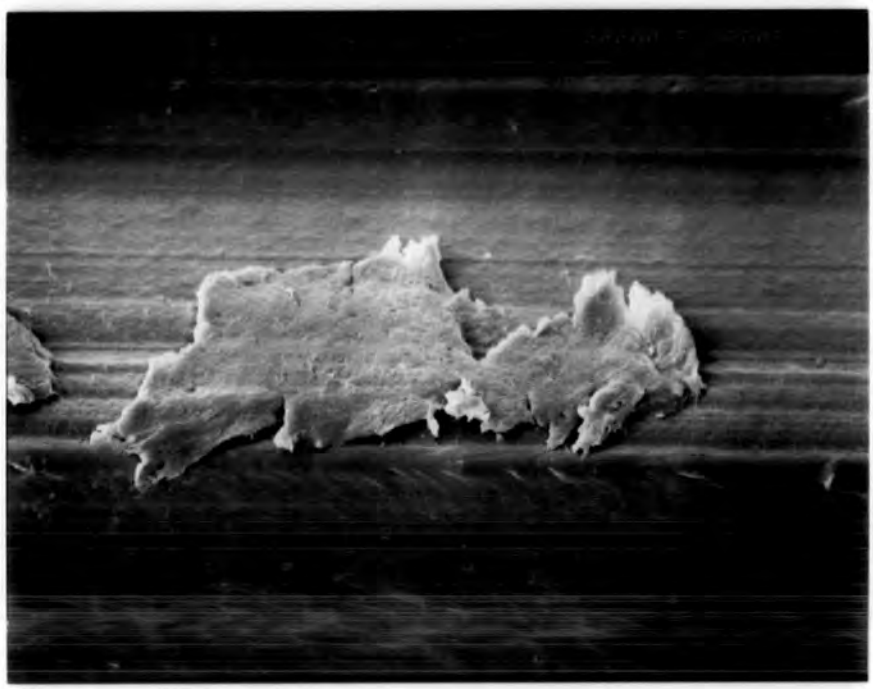

Fig 5.9 a) Film transfer and adhesion - pin 1 test A.

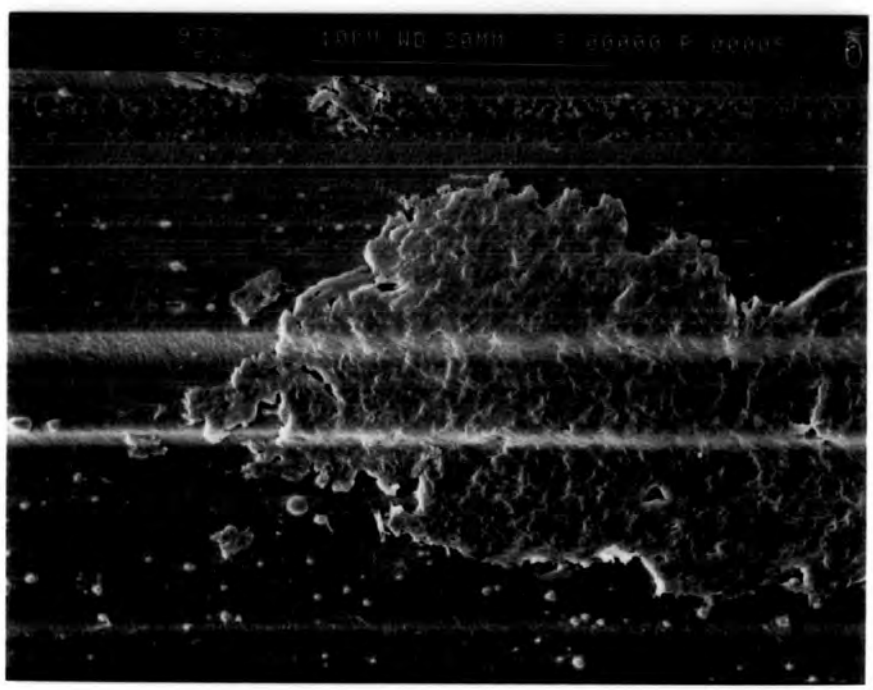

Fig 5.9 b) Film transfer and adhesion - plate 1 test A.

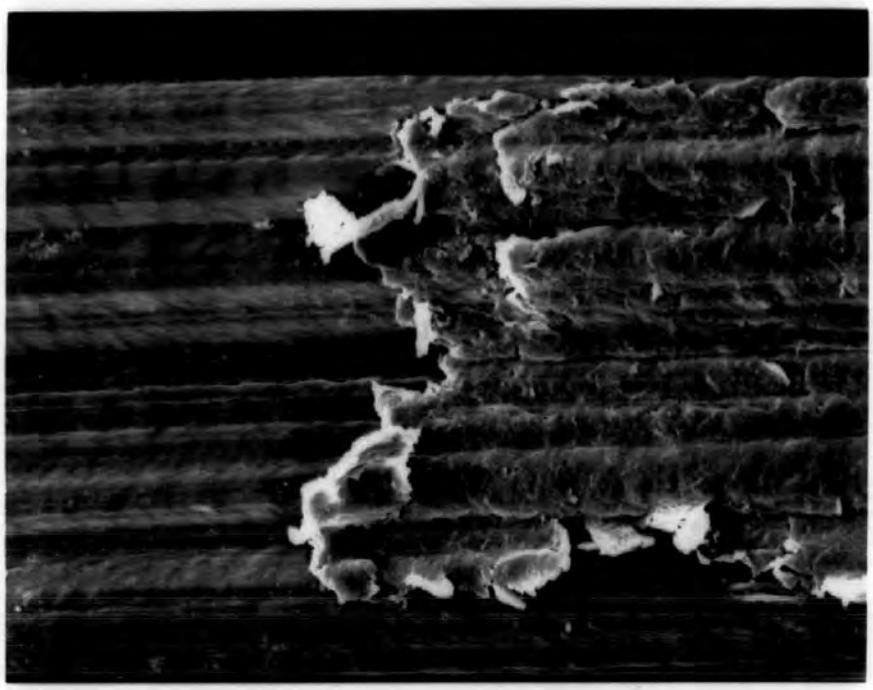

Fig 5.9 c) Film transfer and adhesion - pin 2 test C.

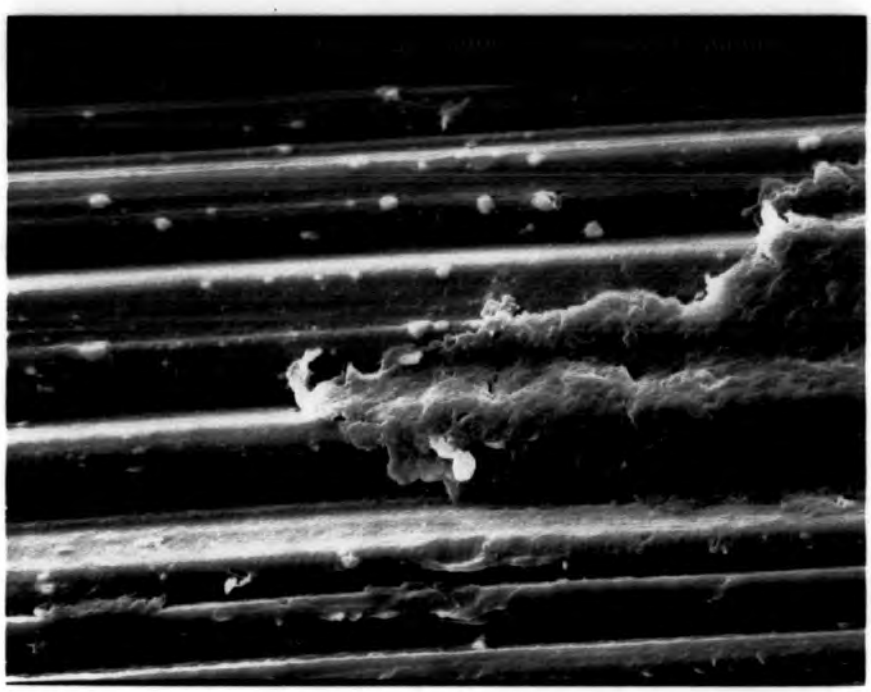

Fig 5.9 d) Film transfer and adhesion - plate 2 test C.

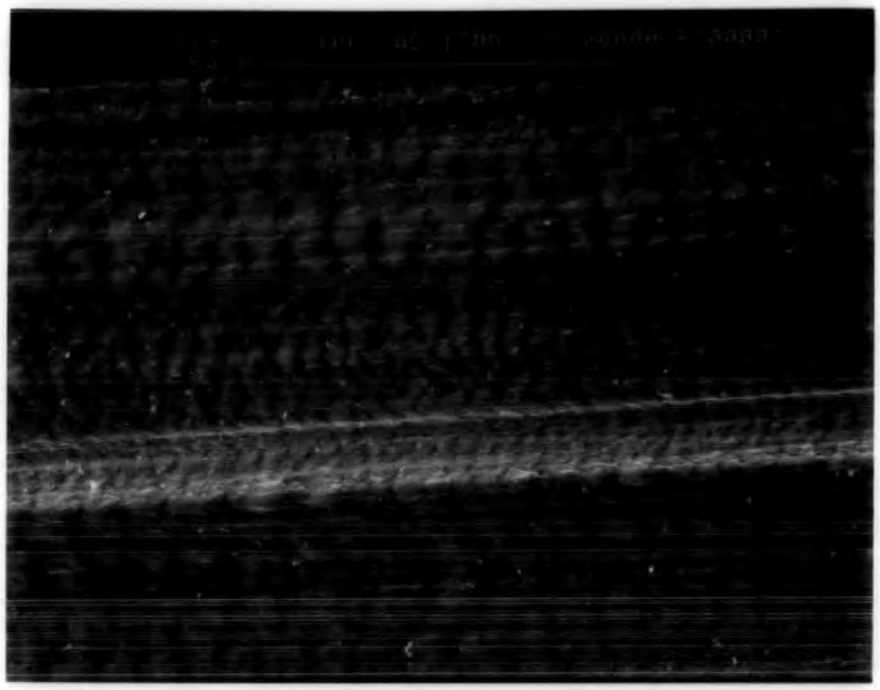

Fig 5.10 a) Surface rippling perpendicular to wear track pin 3 test A.

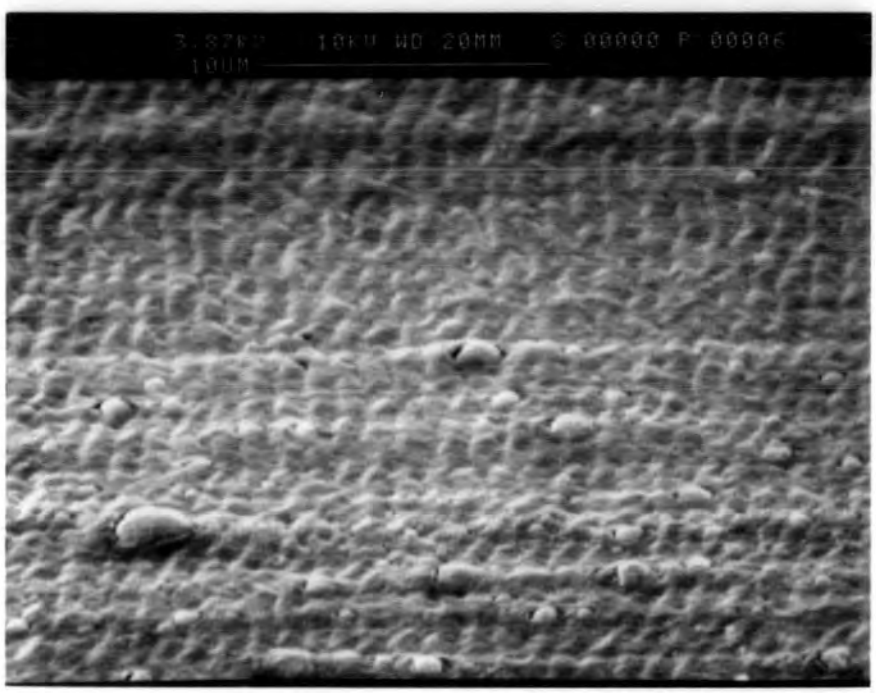

Fig 5.10 b) Surface rippling with embedded NaCl and Fe plate 1 test B.

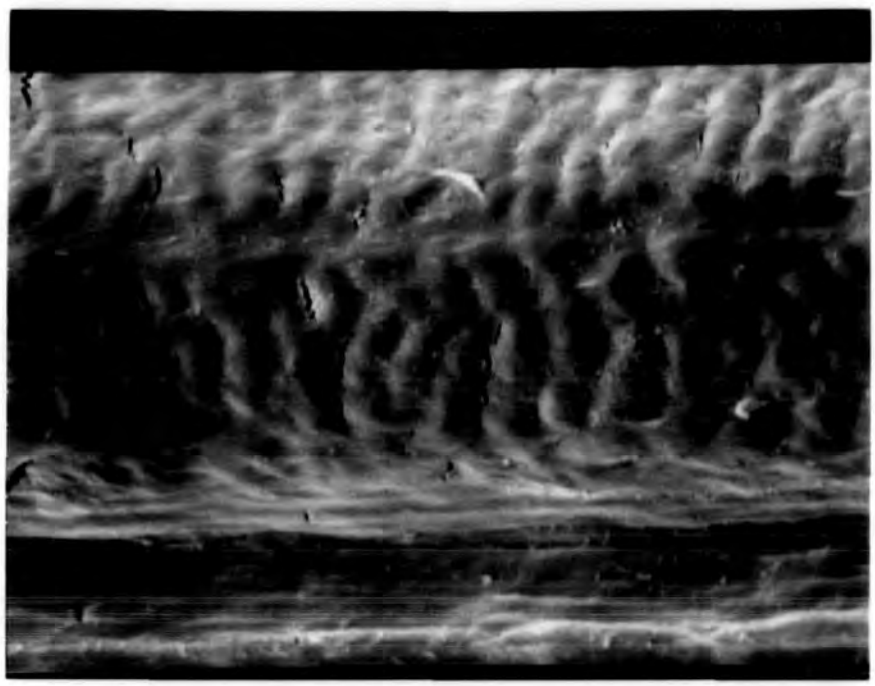

Fig 5.11 a) Fatigue damage parallel to ripples pin 1 test B.

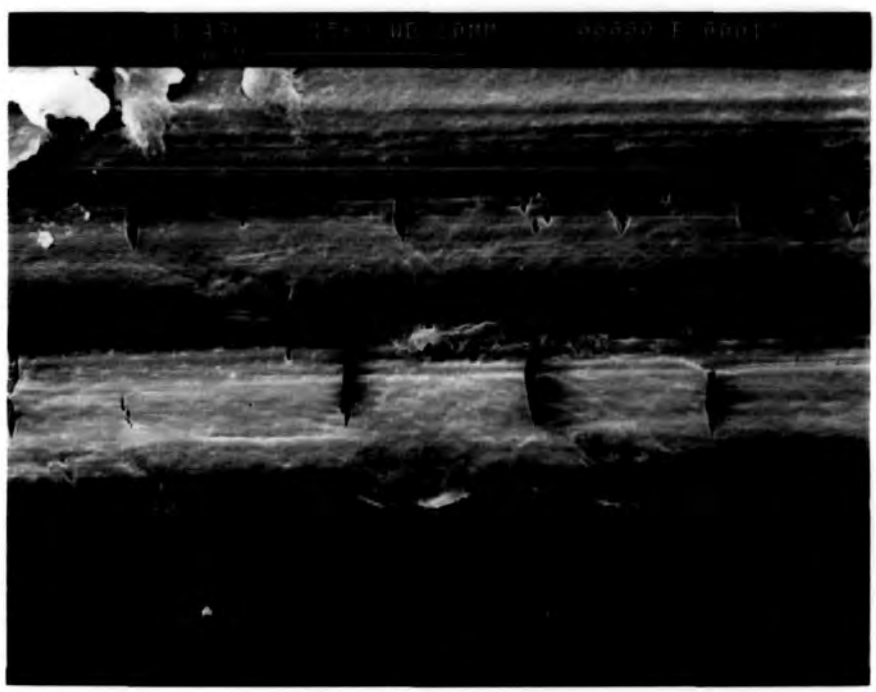

Fig 5.11 b) Fatigue damage in the absence of ripples plate 4 test A.

different in nature. The cracks are some 10 μm in length, larger and apparently deeper than the brittle cracks, and are situated in a smooth unrippled area of the wear scar. They do not appear to be brittle cracks, taking on more of an appearance of surface tears, but are likely also to be attributable to surface fatigue mechanisms. In general, the brittle type cracks were more common on the pins whereas the tear-like cracks were usually on the plates. The pins were often more rippled than the plates.

More evidence of adhesive wear is given in Figs 5.12 a) & b). The surfaces look scuffed through material being pulled or plucked away by bonding to the opposing surface. These areas will result in enhanced abrasive wear until they come loose altogether and escape the wear zone.

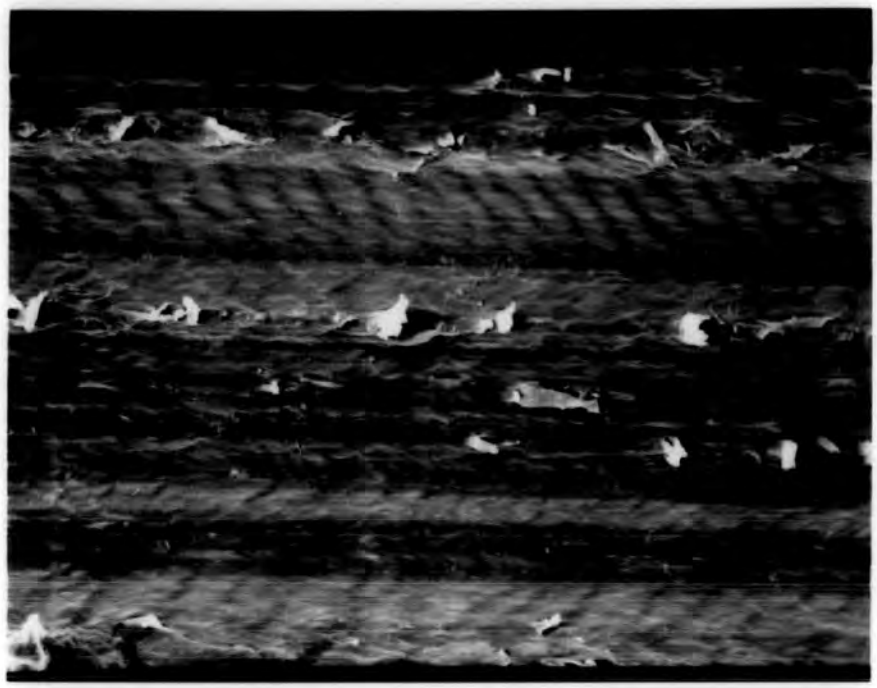

Fig 5.12 a) Evidence of adhesion - plate 1 test A.

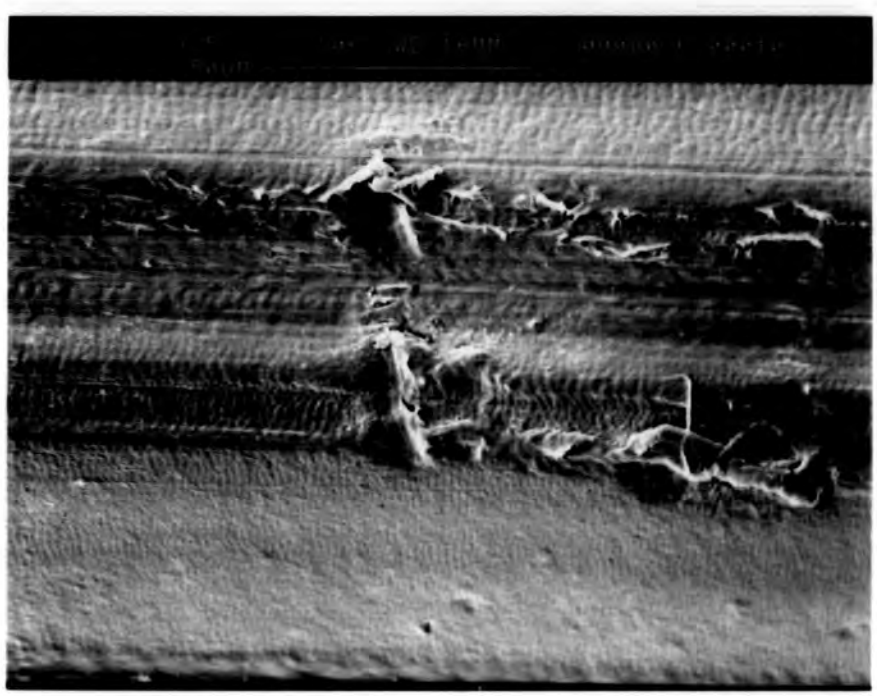

Fig 5.12 b) Adhesion and abrasion - plate 1 test B.

5.6 DISCUSSION AND CONCLUSIONS

Looking at Fig 5.5 the graphs for each of the four loads tested show that initially there is rather variable behaviour during a 'wearing-in' period of up to 10 km before the wear graph for each test settles into a steady state straight line. In these early stages there is some two-body abrasion, resulting in fine score marks of width ~10 μm, enhanced by the presence of the machining marks. Adhesive wear is the predominant mechanism at this stage and causes surface polishing, film transfer and some three-body abrasion through loose debris being trapped between the conforming surfaces. Evidence for these effects was seen in Figs 5.8 - 5.12. It is probable that the positive volume changes recorded in Tables 5.3 - 5.5 were the result of film transfer from the plate to the pin. While film transfer has been a strong feature of these wear tests this may not be the case for a prosthesis in-vivo. Polymer transfer layers have been seen in metal-polymer bench wear tests using distilled water or saline but have not been seen in tests using serum (McKellop, 1981 (123)). Neither have they been seen on prosthetic joints after removal (Charnley, 1975 (131)). This was thought to be due to the boundary lubricating ability of synovial fluid. However it isn't certain whether an all-polyethylene surface replacement would behave in the same way.

All the wear graphs show a distinct change in slope to a higher wear rate regime after a sliding distance of between 32 and 47 km, which depends upon the applied load. In each case the higher wear rate is some three times the lower rate and this has a strong effect on the overall mean value (Table 5.6), which highlights the importance of

running laboratory wear tests for a sufficient duration. This kind of behaviour is commonly seen in metal-polyethylene systems and can be attributed to the onset of a fatigue wear mechanism (Dowson et al, 1974 (132)). The cracking seen in Fig 5.11 is undoubtedly a feature of this fatigue wear mechanism and has been seen, along with the surface rippling effect, by other researchers in metal-polyethylene wear tests (Atkinson, 1976 (100), Walker, 1977 (133)).

Much of the wear testing that has already been performed concerns the wear of plastics on metals using a variety of lubricants under running conditions that are applicable to the design of lower limb prostheses. Very little work has been done on the wear of the polyethylene-polyethylene system since it has not yet been utilised in joint prostheses. However, in 1976, Atkinson (100) performed some such tests at the request of ICI over sliding distances of around 30 km. These tests revealed wear rates of between 6.3×10^{-6} and 28.2×10^{-6} mm^3/Nm for a load range of 6 - 32 N. These values compare very well with the results reported here in which wear rates between 5.6×10^{-6} and 18.8×10^{-6} mm^3/Nm were found for loads of 5 - 19 N. In a private communication in 1990 Dowson (134) reported rather worse wear performance for UHMWP, quoting $\sim 10^{-4}$ mm^3/Nm, though the sliding distance of each test was only 1 km, which is very low indeed.

In experiments to measure the wear rate of UHMWP against stainless steel, Seedhom et al in 1973 (135) recorded values of 0.9×10^{-7} to 8.7×10^{-7} mm^3/Nm. In 1974 Dumbleton et al (136), and later Shen & Dumbleton (137), recorded wear rates of between 1.0×10^{-7} and 5.0×10^{-7} mm^3/Nm. From the results obtained here, the wear rate of the metal-polyethylene system is up to 250 times lower than the all-plastic

system in terms of single component durability. In terms of the amount of debris released into the joint cavity this value is doubled.

Consider an MCP surface replacement prosthesis with a contact area of ~80 mm^2 and radius 8 mm which undergoes 100 cycles per hour through an arc of 57° flexion under a load of 12 N. One year of motion of such a joint represents a sliding distance of 13.9 km which, for an all-polyethylene design, means a loss of ~3.32 mm^3 in volume or 0.04 mm in depth for each component per year beyond the first two or three years (wear rate coefficient = 19.88 x 10^{-6} mm^3/Nm). For a polyethylene-metal design this means a loss of 0.08 mm^3 in volume or 0.001 mm in depth for the polyethylene component per year (wear rate coefficient = 0.5 x 10^{-6} mm^3/Nm).

In terms of debris released into the joint cavity, the all-polyethylene system will yield 6.64 mm^3 of material or 6640 particles of size 10 x 1 x 1 μm yearly compared with only 80 for the metal-polyethylene system. It is this aspect of the wear problem that is cause for most concern for the reasons discussed earlier. While implant durability does not seem a problem the debris produced in wear must be minimised and it is hoped that cross linking of the UHMWP will reduce this problem significantly. An indication of the success of this technique will be given in the report of the prototype simulator tests.

CHAPTER 6

PROTOTYPE TESTS USING THE FINGER FUNCTION SIMULATOR

6.1 INTRODUCTION

The most important work performed in this research programme was the extensive testing of the Durham surface replacement prosthesis in the finger function simulator. This major test series ran twenty-four hours per day for more than eight months and effectively completed the laboratory evaluation of the new prosthetic device.

The aim of the simulator tests was to subject the prosthesis to a programme of motion equivalent to a lifetime (some ten or twenty years) of normal service in-vivo. In the time available it was possible to test five prostheses in this way. The extensive commissioning trials and, in particular, the Swanson implant tests have shown clearly that any prosthesis will be severely tested in the finger function simulator. More importantly, since the common mode of failure in the Swanson device was successfully reproduced, it can be seen that the simulator accurately reproduces the physiological load patterns of the MCP joint.

Prior to clinical trials, simulator experiments give the best indication of the performance and durability of a prosthesis and highlight potential problems for consideration in the future. They have been used extensively for hip and knee prostheses and have an important contribution to make in the development of such devices in the laboratory. Of course, cadaveric studies and clinical trials must be performed if questions of implant migration, biocompatibility and stability in-vivo are to be addressed, but these are beyond the scope of the laboratory programme.

The main aims of the Durham surface replacement trials were:

i) To look for modes of fatigue failure or any damage that would be likely to result in premature failure.

ii) To assess whether an uncemented, square cross-section stem would be sufficient to hold each component in position adequately by looking for evidence of stem deformation and observing the direction of the wear marks.

iii) To look for evidence of cold flow deformation, which is commonly a problem with polyethylene components, and to decide whether this is prohibitive.

iv) To assess the extent of wear both from the point of view of component durability, and also considering the amount of debris released into the joint cavity. Comparisons with the standard bench wear tests were useful here.

6.2 MATERIALS

The five tests were carried out using cross linked UHMWP prototype components manufactured by Chas F Thackray and Sons Ltd of Leeds (Fig 6.1) of the design described in Chapter 2. In the first test the metacarpal component was a mark 1 prototype in which the dorsal aspect was considerably narrower than in the final mark 2 design.

For all five tests the components were of size 3 (out of the range of seven given in Tables 2.1 & 2.2). The components were implanted into two acrylic bone replicas, moulded from a suitable pair of matched bones using the technique described in Chapter 4. As with the Swanson tests these replicas were mounted on cylindrical stems for ease of grip in the simulator and the heads were carefully prepared by hand to receive the implant components. The bone heads remained intact and a square, slightly tapered hole was opened in each bone using a hot broach. To imitate the reaming of the medullary canals, deep holes were drilled into the cylindrical shafts. The hole in the metacarpal was placed 3 mm dorsally from the centre of rotation as reported by Unsworth & Alexander in 1979 (20). The articulating surface of the phalanx was filed out such that the component might sit inside a shallow ellipsoidal recess. That of the metacarpal was smoothed to conform with the back of the implant. Later in the development of the prosthesis, cutting tools will be designed such that the surgeon can quickly prepare each bone head and medullary canal.

To prevent any damage from sharp bone edges the replicas were filed and rounded to make all points of contact with the prosthesis as smooth as

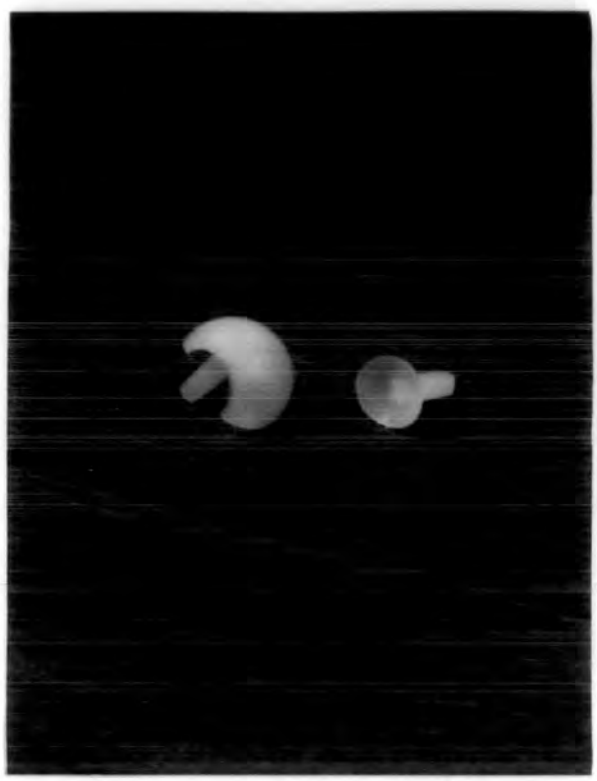

Fig 6.1 Durham surface replacement prosthesis
- crosslinked prototypes.

possible and the components were tested for rotation to ensure that the bone holes were not too large. For consistency, the same acrylic replica pair was used for each test and this is shown, with two implanted components, in Fig 6.2.

The main aims of the tests were to reveal fatigue failure mechanisms and to assess the wear resistance of the polyethylene prototypes. For this reason the results were assessed in comparison with the standard bench test wear data. The initial roughness of the prototypes appeared less than that of the bench test samples since they were injection moulded and not machined. However, they were still not very smooth compared to the highly polished metal surfaces used in hip prostheses. The metacarpal component heads appeared to have small rounded protuberances distributed across the articulating surface, whereas the phalangeal components displayed quite definite circular markings. Fig 6.3 shows electron micrographs of an unused pair of components at a magnification of x36, taken using a Cambridge Stereoscan 600 SEM. On the completion of each test the surfaces were all examined in this way and the components were studied generally using macrophotography.

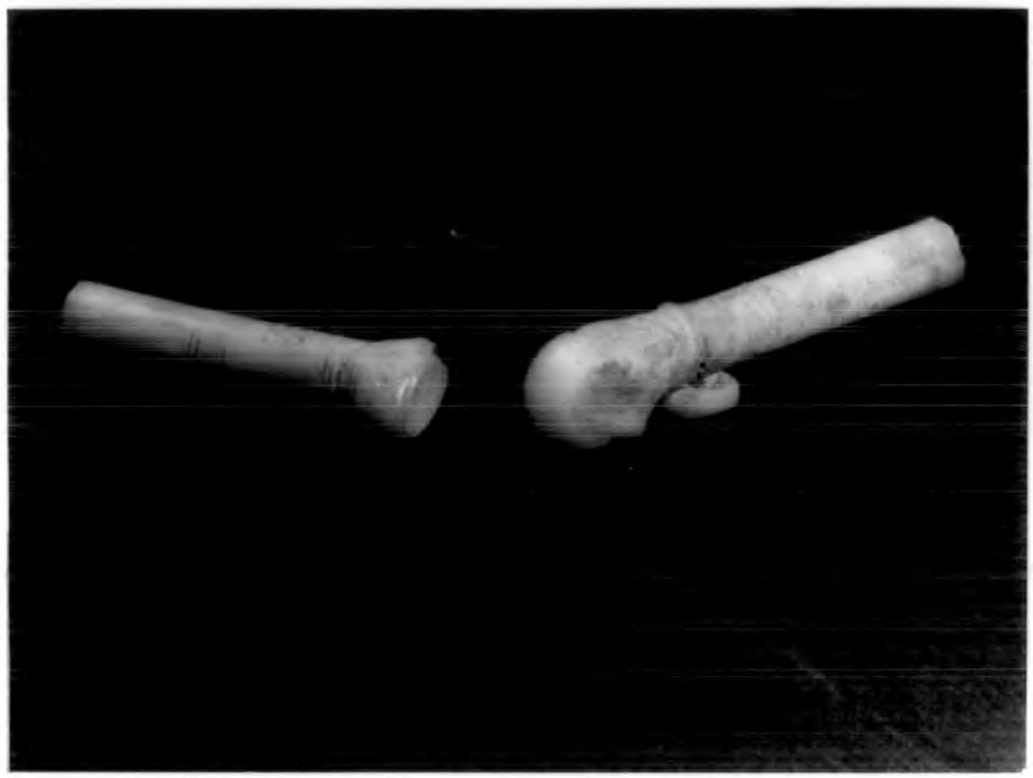

Fig 6.2 Prototype components mounted on replica bones for the simulator trials.

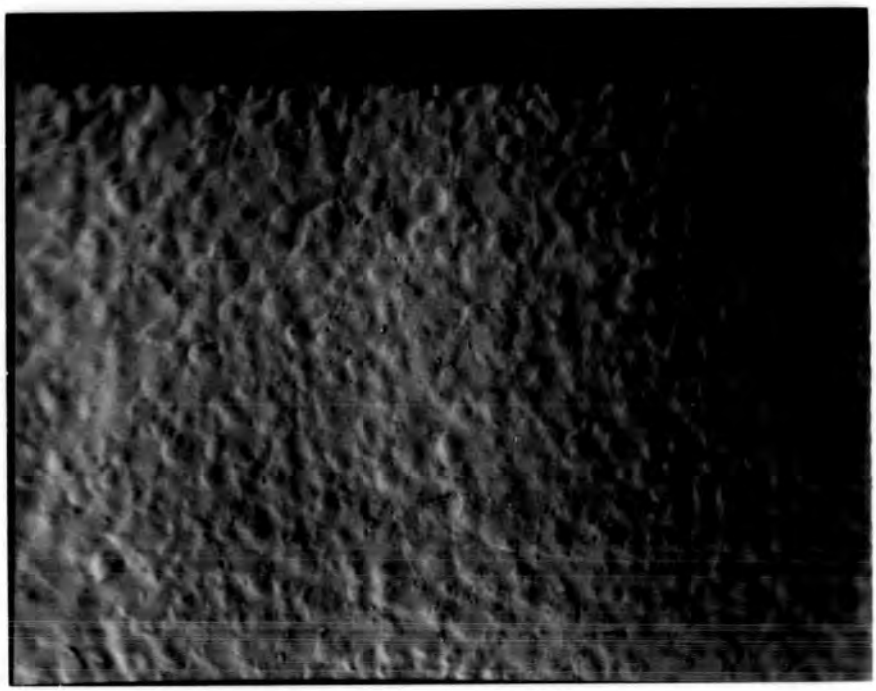

a) Metacarpal component.

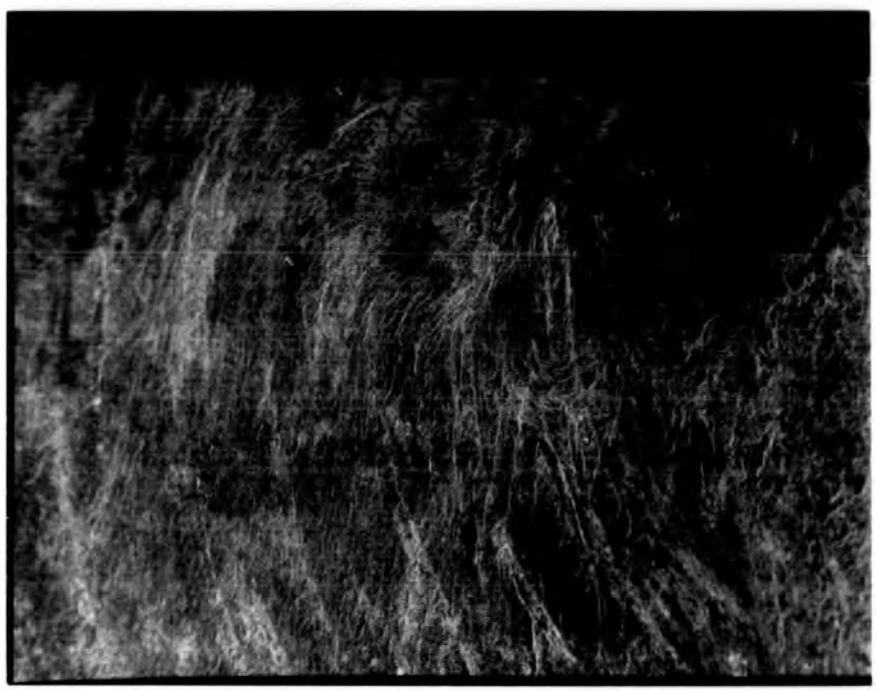

b) Phalangeal component.

Fig 6.3 Electron micrographs of the unused prototype surfaces.

6.3 METHOD

The replica bones and prototypes were carefully placed in the simulator and the tendons adjusted to give a smooth cycle with the cams turned by hand. For this series, unlike the Swanson trials, the volar plate pulley was in position.

The equipment, other than the motor, was switched on and left for a period of two hours in which to achieve a steady state 37°C in the saline bath. The tests began after recalibration of the data collection system. For each test the simulator ran almost continuously for a period of five to eight weeks, with short interruptions for cleaning, tendon replacement and sample weighing. Tendons were replaced as necessary and this could be performed in fifteen minutes. Cleaning and sterilisation of the rig was undertaken weekly and took three hours. The samples were weighed at least twice weekly and always while the simulator was being cleaned - this took one hour. A record of stoppage times was kept as far as possible but when tendon or motor failure occurred during the night it was estimated that the simulator had not functioned for 50% of the unattended period. This means that in any twenty-four hour operating period the uncertainty could be eight hours which over the duration of the tests would be equivalent to between 5 and 10 km error in the quoted sliding distance. During each test measurements of both static and dynamic loading were recorded periodically to ensure simulator consistency.

Since the study of wear was the most important aspect of this work, great care was taken that a strict standard procedure was maintained in

weighing the samples. Prior to the start of each test the components and their respective controls were cleaned with alcohol and dried using a hairdryer. They were then carefully weighed and the average of five readings recorded. The test components were mounted on the replica bones which were then carefully aligned in the simulator clamps. The controls were weighted and placed at the bottom of the simulator bath which was then filled with saline and heated until steady state conditions were achieved. Throughout the test the motor speed and temperature were carefully monitored. At no time, after the start of a test, were the replica bones removed from their clamps. For cleaning and sample weighing the tendons were released and the test components were gently removed from the replicas. This precaution was to ensure a consistent sliding direction. The weighing of the samples followed the same procedure as was used for the bench wear tests described in Chapter 5. Then they were replaced in the simulator and the tests continued. Three of the five tests ran for 130 km and two ran for ~300 km. These distances are equivalent to ~10 and 20 years normal use assuming that a finger joint performs 100 cycles per hour through 60° flexion. It had been hoped to allow test 5 to run on but the phalangeal component was badly damaged in a simulator failure after 300 km sliding distance.

6.4 RESULTS

A summary of the test conditions is given in Table 6.1 and the ranges of the dynamic force response curves are shown in Fig 6.4. Both the angle and the magnitude of the joint force were seen to exhibit the expected trends (Chapter 4) and were generally consistent throughout the test series.

Test No.	Mean Load		Angle of Load (°)	Mean Stress (MPa)	Cycle Speed (Hz)	Test Duration (days)
	Dynamic (N)	Static (N)				
1*	12.163	181.33	30	0.152	1.78	33.1
2	11.830	180.97	32	0.148	1.76	33.6
3	11.860	180.96	32	0.148	1.78	32.4
4	12.190	181.18	28	0.152	1.77	65.8
5	11.990	180.96	30	0.150	1.77	77.8

* Mark 1 prototype with a narrow metacarpal component

Table 6.1 The test details for the prototype tests.

The volume losses for each test are recorded in Tables 6.2 to 6.6 along with the mean load and temperature readings, the cycle count and the sliding distance. As in Chapter 5, volume losses were calculated from the weight changes using a density of 0.954 gcm^{-3} for the polyethylene. Again the error in a weight measurement was equivalent to ± 0.52 mm^3 in volume.

Graphs were plotted of the volume loss due to wear V (mm^3) versus sliding distance L (km) for each of the five tests (Figs 6.5 to 6.9) with the phalangeal and metacarpal components given by different

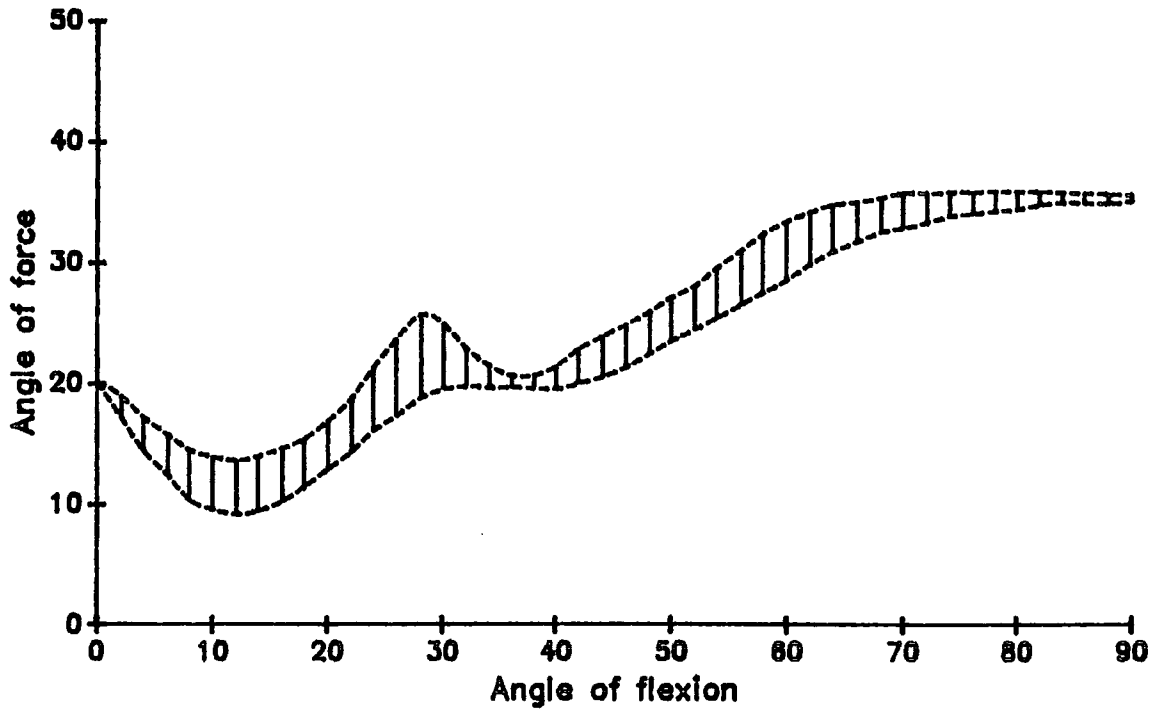

Fig 6.4 a) Angle of force vs angle of flexion.

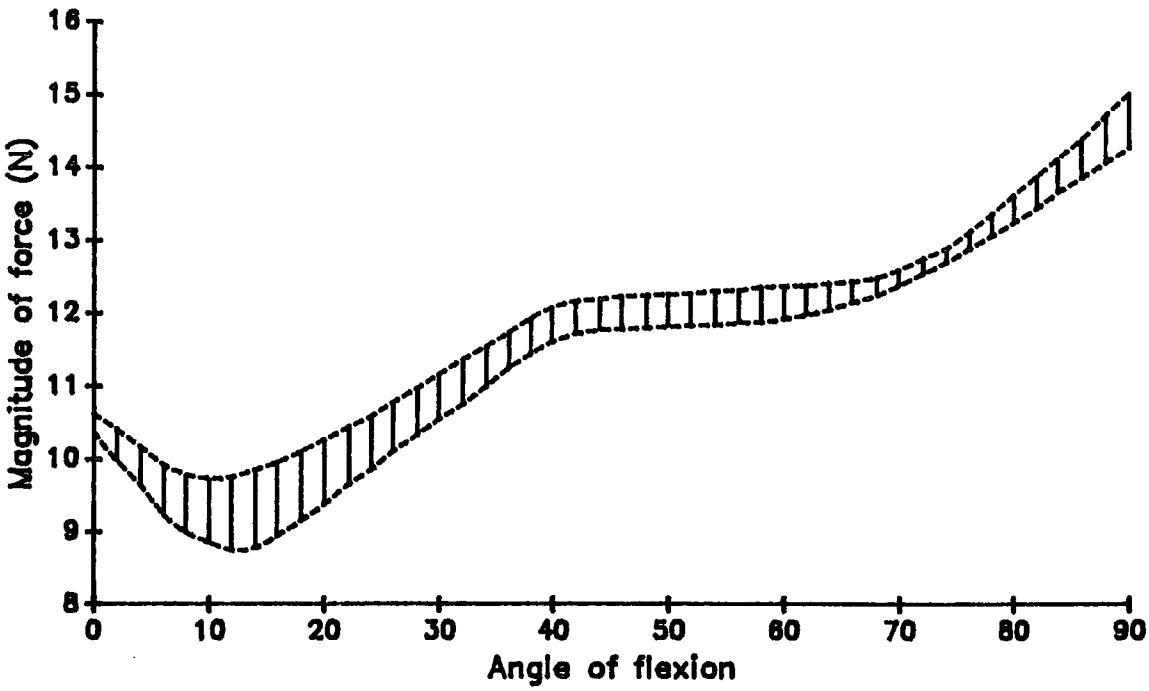

Fig 6.4 b) Magnitude of force vs angle of flexion.

Time (hrs)	Dist. (km)	Temp (°C)	Number of cycles	Dynamic load (N)*	No. of loads	Static load (N)*	Vol.loss Phalanx (mm^3)	Vol.loss Metacarp (mm^3)
8.99	1.45	36	57,857	12.050	18	181.50	-0.105	0.056
18.47	2.99	36	118,928	12.050	37	181.50	0.105	0.240
25.94	4.20	36	167,142	12.325	52	181.50	0.520	0.240
49.88	8.08	37	321,428	12.675	100	181.75	0.670	0.960
73.82	11.96	37	475,714	11.850	148	181.00	0.980	0.720
91.78	14.86	37	591,428	11.525	184	180.50	1.580	0.940
102.75	16.64	38	662,142	12.075	206	181.25	1.890	1.025
126.70	20.52	36	816,428	13.025	253	182.00	2.350	1.950
140.66	22.78	36	906,428	12.450	281	181.50	2.760	1.990
164.60	26.66	34	1,060,714	12.100	329	181.25	3.105	2.200
194.28	31.47	37	1,251,964	12.575	389	181.75	3.805	3.000
218.23	35.34	37	1,406,250	11.425	436	180.50	4.600	3.710
237.18	38.41	37	1,528,393	11.675	474	180.75	5.102	4.105
261.12	42.29	34	1,682,679	12.800	522	181.75	5.605	4.215
283.07	45.84	34	1,824,108	13.350	566	182.25	5.980	4.810
288.06	46.65	36	1,856,251	12.550	576	181.75	6.000	5.400
297.04	48.11	38	1,914,108	12.050	594	181.25	6.405	5.805
325.97	52.79	38	2,100,537	11.975	652	181.00	6.890	6.102
333.95	54.08	37	2,151,966	11.600	668	181.00	7.570	6.600
357.89	57.96	37	2,306,252	12.450	716	181.75	8.105	7.015
381.83	61.84	38	2,460,538	12.225	764	181.50	8.906	7.890
405.78	65.72	38	2,614,824	13.025	812	182.50	9.606	8.105
422.74	68.46	37	2,724,110	11.875	845	181.75	10.102	8.809
446.68	72.34	37	2,878,396	12.450	893	181.50	10.400	9.503
485.09	78.56	37	3,125,896	12.000	970	181.25	11.280	10.204
509.03	82.44	36	3,280,182	12.275	1018	181.25	11.672	10.986
525.24	85.07	30†	3,384,646	11.075	1050	180.00	12.000	11.103
634.99	102.84	36	4,091,875	11.250	1270	180.50	15.450	13.679
657.82	106.54	36	4,239,013	12.400	1316	181.50	15.860	14.100
676.91	109.63	37	4,361,986	11.875	1354	181.00	16.205	15.086
754.91	122.26	37	4,864,618	11.650	1510	181.00	18.665	16.540
794.91	128.74	37	5,122,378	12.550	1590	181.75	19.890	18.252

† Blocked pump or heater failure.

* Mean value for the period.

Table 6.2 Volume loss and load details for test 1.

Time (hrs)	Dist. (km)	Temp (°C)	Number of cycles	Dynamic load (N)*	No. of loads	Static load (N)*	Vol.loss Phalanx (mm^3)	Vol.loss Metacarp (mm^3)
20.75	3.36	38	133,713	11.050	42	180.25	0.201	-0.152
24.42	3.95	37	157,362	11.175	49	180.25	0.102	0.150
161.92	26.22	36	1,043,412	12.000	324	181.00	2.150	2.240
259.92	42.10	37	1,674,924	12.225	520	181.25	4.421	4.012
277.42	44.93	37	1,787,694	11.650	555	181.00	4.692	4.194
279.17	45.21	36	1,798,971	12.100	558	181.00	4.579	4.301
298.42	48.33	37	1,923,018	11.525	597	180.75	5.410	4.617
322.42	52.22	32†	2,077,674	12.850	645	181.75	5.990	5.115
394.17	63.84	32†	2,540,031	12.125	788	181.50	7.843	6.814
419.17	67.89	37	2,701,131	11.550	838	181.00	8.027	6.905
441.42	71.49	37	2,844,510	11.775	883	181.00	9.105	8.021
489.92	79.35	37	3,157,044	12.100	980	181.25	10.345	8.654
495.92	80.32	29†	3,195,708	11.200	992	180.50	10.906	8.801
559.17	90.56	37	3,603,291	12.675	1118	181.75	11.210	10.025
584.17	94.61	36	3,764,391	11.050	1168	180.00	12.302	11.651
606.42	98.21	37	3,907,770	13.025	1213	182.00	12.650	11.920
638.42	103.39	37	4,113,978	11.175	1277	180.25	13.397	12.612
657.42	106.47	39	4,236,414	11.650	1315	180.75	13.982	13.011
726.17	117.61	37	4,679,439	12.250	1452	181.50	15.242	14.219
734.17	118.90	37	4,730,991	12.000	1468	181.50	15.612	13.914
750.17	121.49	37	4,834,095	12.475	1500	181.50	16.141	15.010
773.42	125.26	37	4,983,918	11.275	1547	180.50	16.571	15.050
781.42	126.56	38	5,035,470	11.750	1563	180.75	17.331	15.513
805.42	130.44	37	5,190,126	11.350	1611	180.25	17.901	15.992

† Blocked pump or heater failure.

* Mean value for the period.

Table 6.3 Volume loss and load details for test 2.

Time (hrs)	Dist. (km)	Temp (°C)	Number of cycles	Dynamic load (N)*	No. of loads	Static load (N)*	Vol.loss Phalanx (mm^3)	Vol.loss Metacarp (mm^3)
7.00	1.13	37	45,108	11.975	14	181.00	0.118	0.006
46.75	7.57	37	301,257	12.400	94	181.50	0.627	0.593
96.00	15.55	37	618,624	11.250	192	180.50	1.241	1.483
141.75	22.96	37	913,437	11.000	284	180.00	2.218	2.016
165.25	26.76	26†	1,064,871	12.275	331	181.25	2.913	2.421
213.00	34.50	36	1,372,572	12.100	426	181.25	3.601	3.201
235.50	38.14	36	1,517,562	11.350	471	180.50	4.231	3.921
307.25	49.76	38	1,979,919	11.400	615	180.50	5.986	6.201
315.25	51.06	37	2,031,471	-	631	-	6.401	6.021
338.00	54.74	37	2,178,072	-	676	-	7.022	6.813
361.75	58.59	36	2,331,117	13.025	724	182.00	7.413	7.001
387.25	62.72	37	2,495,439	-	775	-	7.702	7.564
457.50	74.09	36	2,948,130	-	915	-	9.904	8.901
481.25	77.94	36	3,101,175	11.150	963	180.50	10.871	10.017
487.75	78.99	38	3,143,061	-	976	-	10.804	10.121
505.00	81.79	38	3,254,220	-	1010	-	11.246	10.200
528.75	85.63	37	3,407,265	12.050	1058	181.00	11.964	10.882
531.75	86.12	37	3,426,597	-	1064	-	11.871	10.901
719.50	116.53	37	4,636,458	12.075	1439	181.00	16.987	15.002
767.50	124.30	37	4,945,770	-	1535	-	17.800	16.841
777.50	125.92	37	5,010,210	12.175	1555	181.50	18.605	17.272

† Blocked pump or heater failure.

* Mean value for the period.

Table 6.4 Volume loss and load details for test 3.

Time (hrs)	Dist. (km)	Temp (°C)	Number of cycles	Dynamic load (N)*	No. of loads	Static load (N)*	Vol.loss Phalanx (mm^3)	Vol.loss Metacarp (mm^3)
9.00	1.45	37	57,996	13.150	18	182.00	-0.002	0.204
52.75	8.54	37	339,921	-	106	-	0.521	0.102
112.45	18.21	37	724,628	-	225	-	1.306	1.310
150.17	24.32	37	967,695	12.675	300	182.00	2.703	1.914
201.40	32.62	37	1,297,822	12.150	403	181.00	4.117	3.001
209.40	33.91	36	1,349,374	-	419	-	3.907	3.421
301.17	48.78	32†	1,940,739	12.075	602	181.00	6.831	6.245
349.17	56.55	36	2,250,051	12.025	698	180.75	7.923	6.674
403.75	65.39	37	2,601,765	-	808	-	9.871	8.002
427.75	69.28	38	2,756,421	-	856	-	10.246	8.682
472.45	76.56	37	3,046,401	12.675	945	182.00	11.992	9.490
521.10	84.39	37	3,357,968	12.550	1042	181.50	12.712	10.481
555.45	89.96	38	3,579,320	-	1111	-	13.861	11.782
624.10	101.08	38	4,021,700	11.050	1248	180.00	15.620	13.910
689.75	111.71	37	4,444,749	11.675	1380	180.75	17.812	15.005
720.50	116.69	37	4,642,902	-	1441	-	18.619	16.217
727.50	117.82	36	4,688,010	-	1455	-	18.810	16.349
804.60	130.31	37	5,184,842	12.000	1609	180.75	21.740	17.879
867.17	140.44	37	5,588,043	12.125	1734	181.00	21.360	18.891
912.50	147.78	37	5,880,150	-	1825	-	22.645	19.602
995.45	161.22	37	6,414,680	13.050	1991	181.75	24.421	21.984
1041.75	168.72	36	6,713,037	12.400	2084	181.50	26.609	23.001
1102.25	178.52	37	7,102,899	-	2205	-	28.698	24.862
1113.25	180.30	38	7,173,783	-	2227	-	29.041	26.013
1118.75	181.19	37	7,209,225	-	2238	-	29.502	26.002
1265.17	204.90	38	8,152,755	12.150	2530	181.25	30.621	27.914
1327.50	214.99	37	8,554,410	12.550	2655	181.25	32.781	29.681
1397.20	226.28	37	9,003,557	11.650	2794	181.25	35.602	31.256
1453.60	235.42	37	9,366,998	-	2907	-	36.400	31.656
1465.10	237.28	30†	9,441,104	-	2930	-	36.394	32.524
1502.50	243.34	26†	9,682,110	11.550	3005	180.75	37.998	34.021
1536.75	248.88	37	9,902,817	12.050	3074	181.00	38.771	34.391
1578.50	255.65	37	10,171,854	12.125	3157	181.00	41.514	35.812

† Blocked pump or heater failure.

* Mean value for the period.

Table 6.5 Volume loss and load details for test 4.

Time (hrs)	Dist. (km)	Temp (°C)	Number of cycles	Dynamic load (N)*	No. of loads	Static load (N)*	Vol.loss Phalanx (mm^3)	Vol.loss Metacarp (mm^3)
23.75	3.85	36	153,045	12.050	48	181.00	0.308	0.219
72.61	11.77	37	467,899	12.250	145	181.25	0.502	0.201
131.40	21.30	37	846,742	-	263	-	1.241	1.641
187.75	30.44	37	1,209,861	12.700	376	181.75	3.461	3.024
231.91	37.59	37	1,494,428	11.950	464	181.00	3.941	3.416
252.00	40.85	37	1,623,888	-	504	-	4.510	4.066
270.50	43.85	38	1,743,102	-	541	-	5.117	4.671
314.15	50.93	38	2,024,383	11.200	628	180.50	6.210	5.667
363.75	58.97	36	2,344,005	12.275	728	181.50	7.692	6.244
392.10	63.56	37	2,526,692	-	784	-	8.702	6.791
408.50	66.22	37	2,632,374	-	817	-	8.910	6.991
521.40	84.52	37	3,359,902	12.475	1043	181.50	11.540	9.361
568.20	92.11	30†	3,661,481	11.050	1136	180.00	12.670	10.761
610.50	98.97	28†	3,934,062	-	1221	-	13.567	11.513
687.00	111.37	36	4,427,028	11.475	1374	180.25	15.401	12.946
706.60	114.54	26†	4,553,330	12.075	1413	181.00	15.324	13.002
778.00	126.12	37	5,013,432	-	1556	-	17.610	14.671
806.00	130.66	37	5,193,864	-	1612	-	18.471	15.902
851.25	137.99	37	5,485,455	12.650	1703	181.50	19.651	16.772
942.40	152.77	38	6,072,826	11.600	1885	180.75	20.698	18.960
1021.50	165.59	37	6,582,546	11.250	2043	180.25	23.501	20.301
1101.00	178.48	37	7,094,844	11.800	2202	180.75	24.603	21.902
1149.50	186.34	37	7,407,378	-	2299	-	26.320	23.604
1204.00	195.17	36	7,758,576	12.325	2408	181.50	27.514	24.912
1256.17	203.63	37	8,094,759	-	2512	-	28.712	26.006
1304.80	211.51	38	8,408,131	-	2610	-	30.614	26.712
1407.60	228.18	38	9,070,574	12.000	2815	180.75	33.010	28.991
1468.00	237.97	37	9,459,792	-	2936	-	34.813	31.321
1501.01	243.32	37	9,672,508	11.975	3002	180.75	35.912	32.001
1642.50	266.26	37	10,584,270	12.150	3285	180.75	39.601	33.993
1709.25	277.08	36	11,014,407	12.950	3419	182.00	43.441	36.201
1761.50	285.55	37	11,351,106	-	3523	-	44.012	37.021
1866.15	302.51	37	12,025,471	11.550	3732	180.50	45.667	39.011

† Blocked pump or heater failure.

* Mean value for the period.

Table 6.6 Volume loss and load details for test 5 before simulator failure.

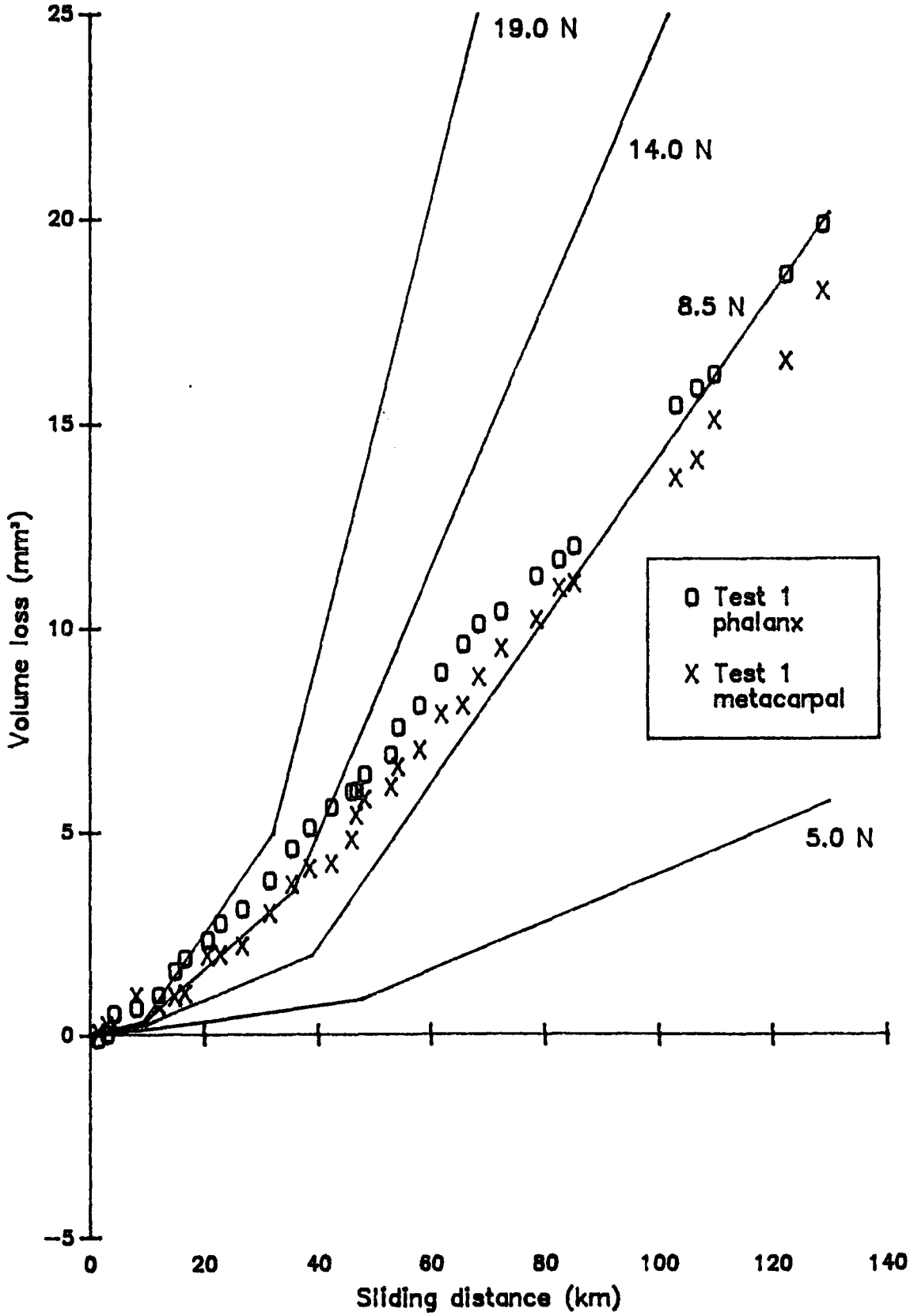

Fig 6.5 Test 1 prototype wear results.

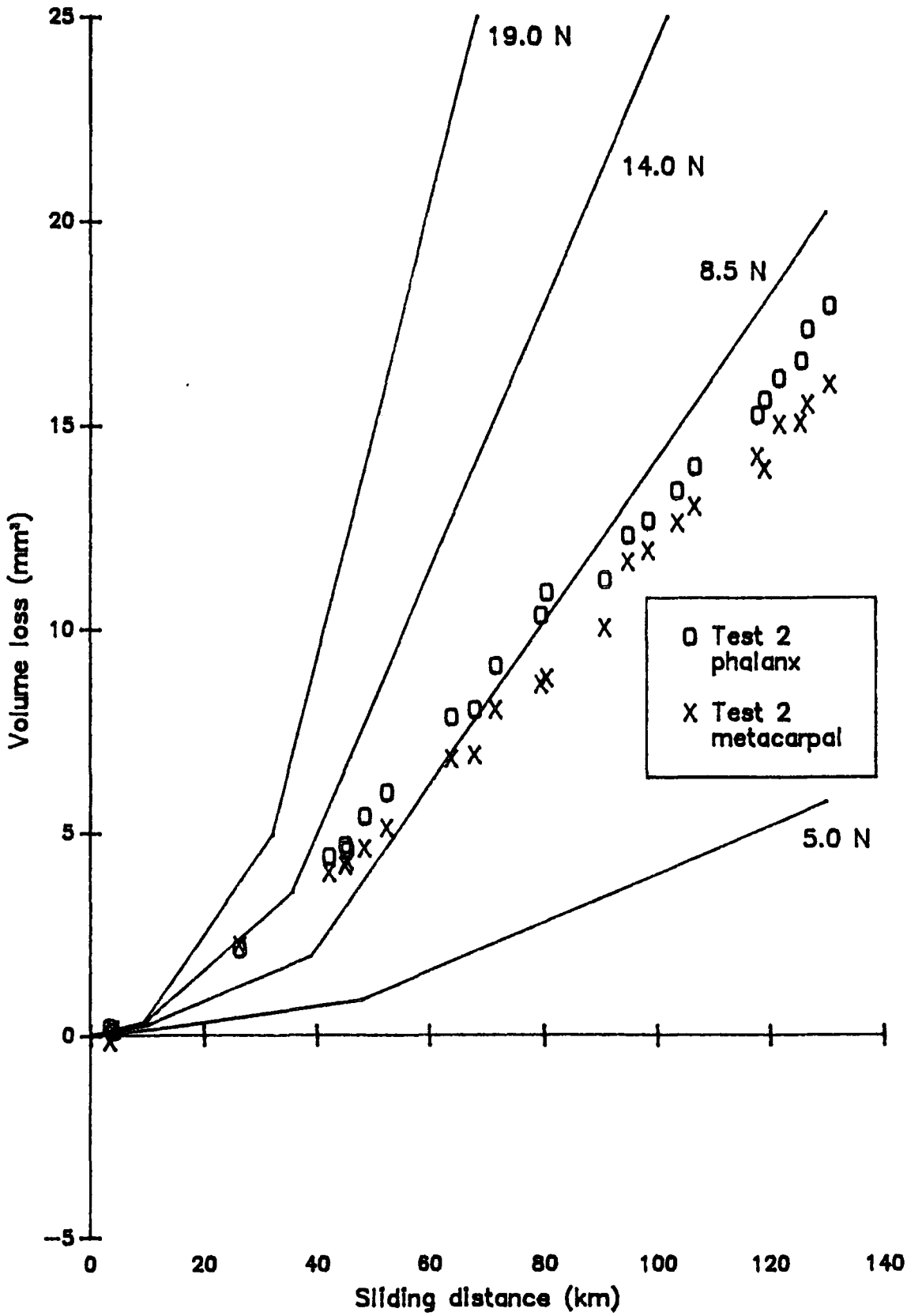

Fig 6.6 Test 2 prototype wear results.

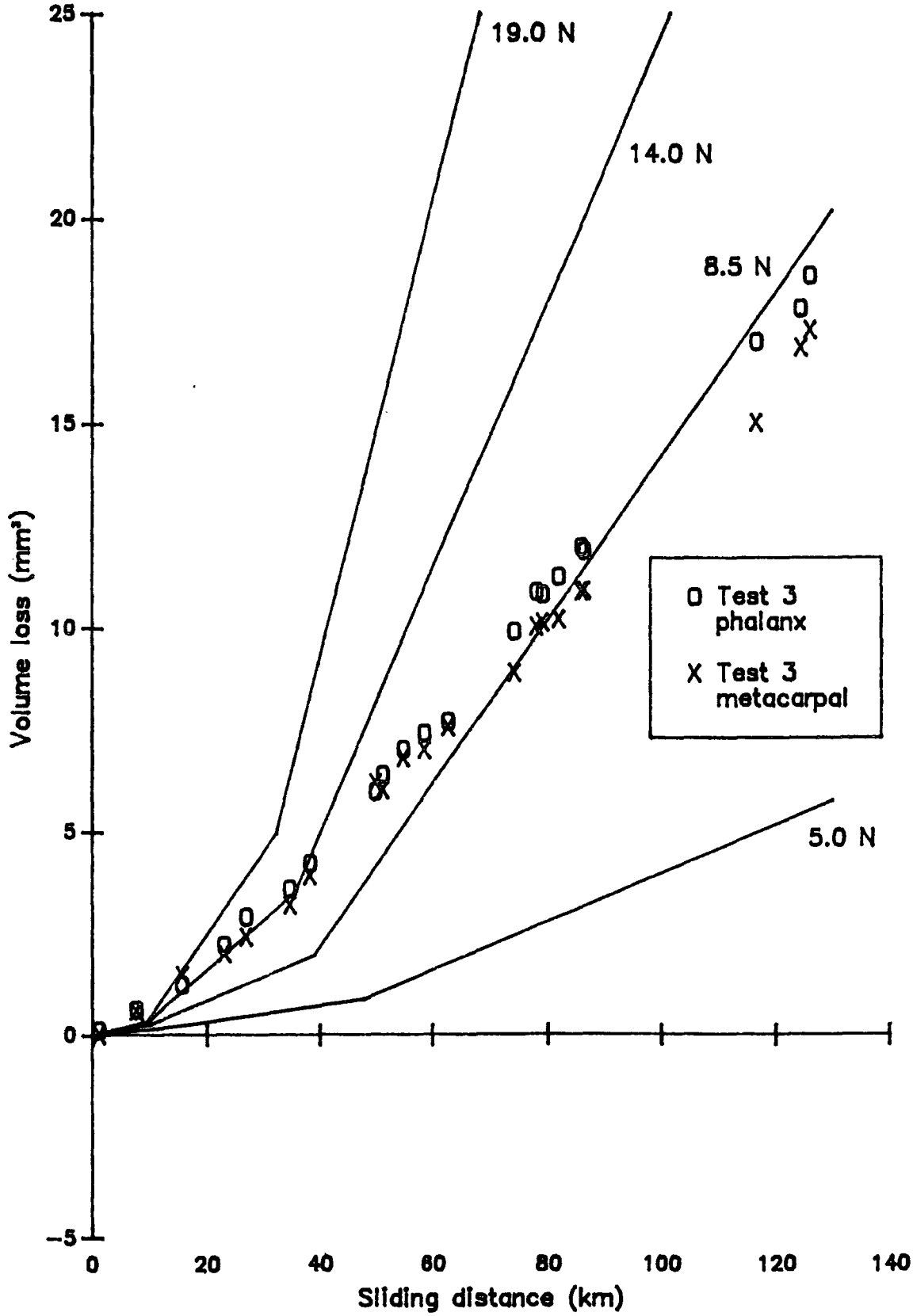

Fig 6.7 Test 3 prototype wear results.

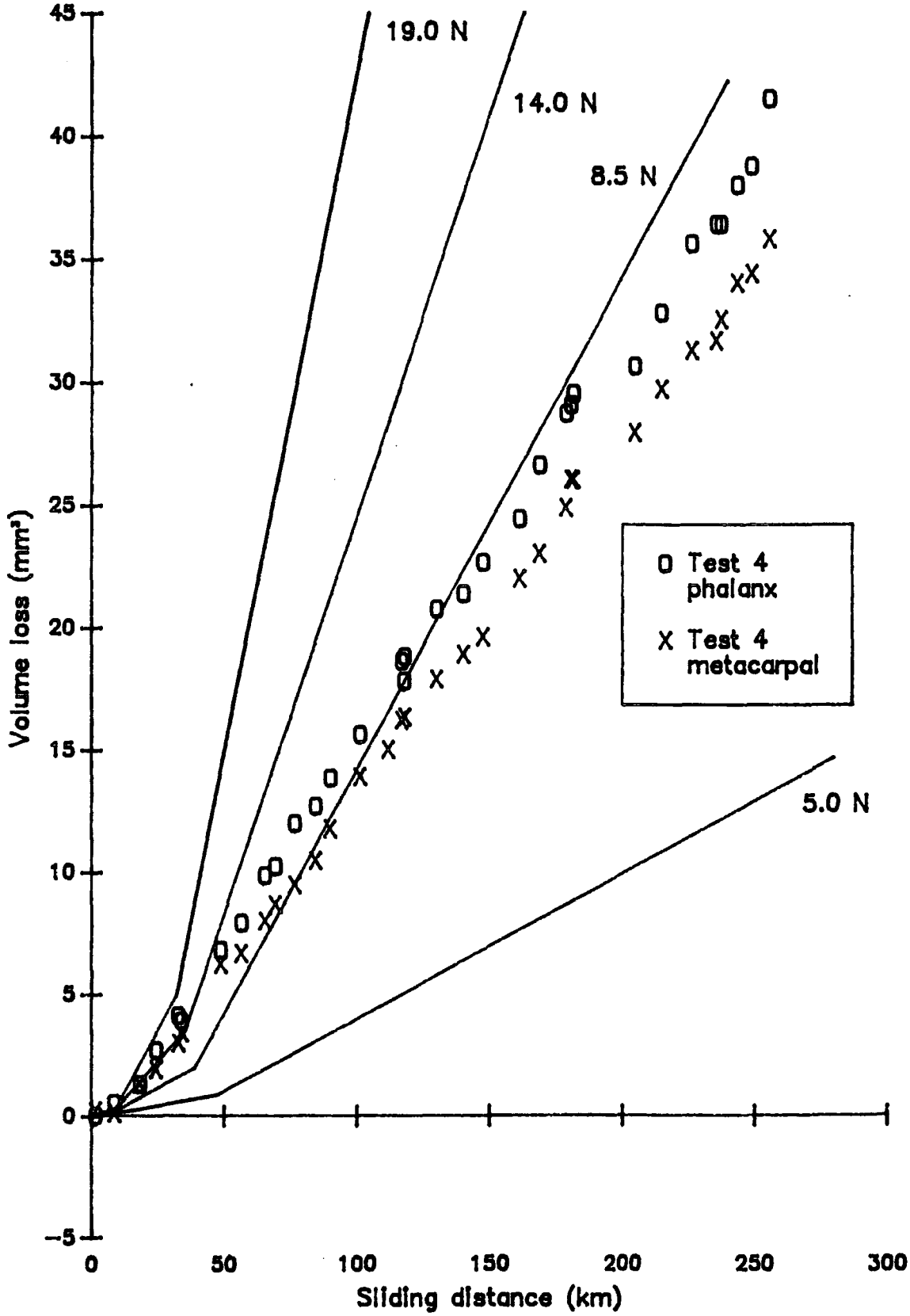

Fig 6.8 Test 4 prototype wear results.

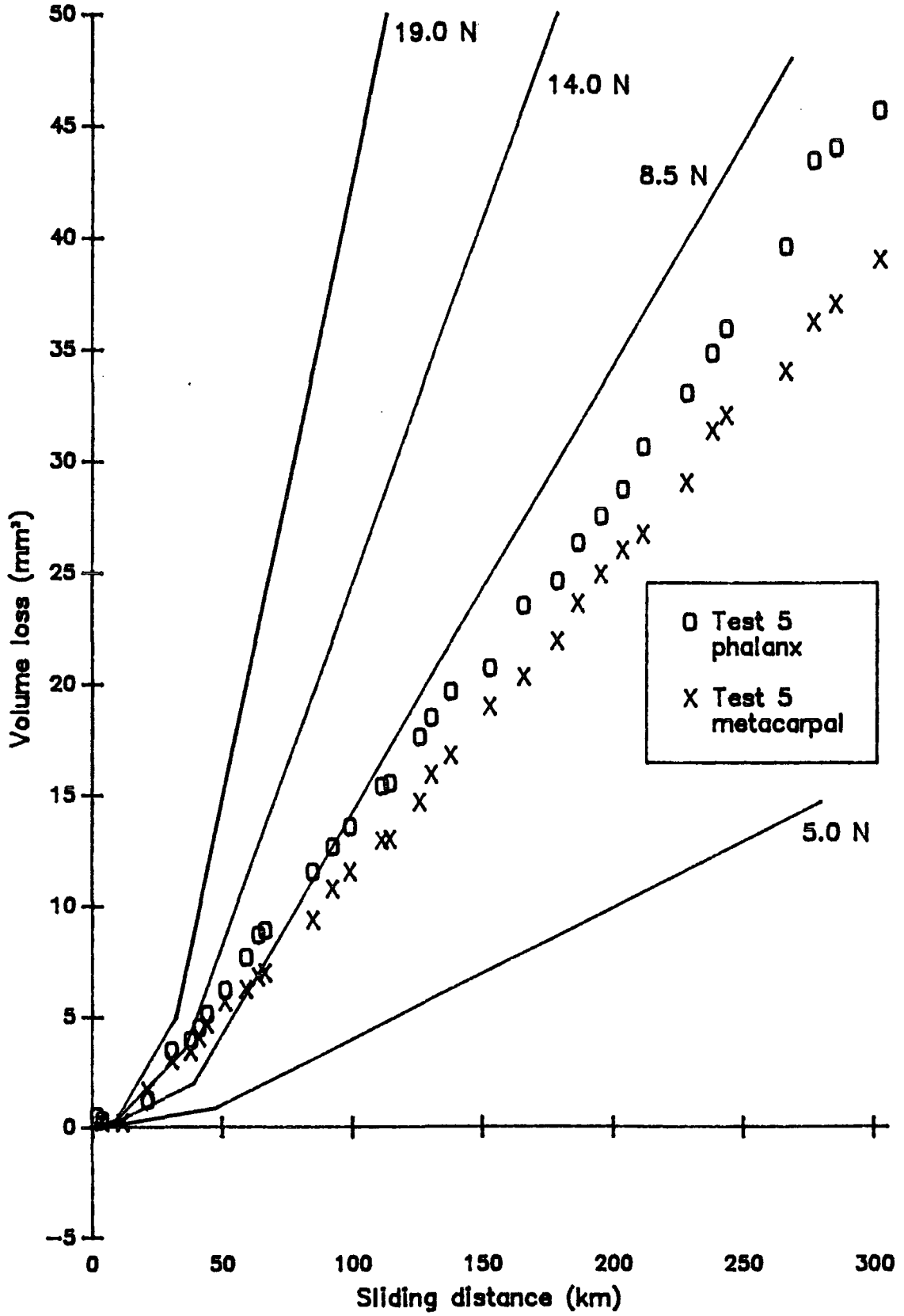

Fig 6.9 Test 5 prototype wear results.

symbols. Also shown on each graph are the extrapolations of the bench wear test results for reference. Fig 6.10 summarises the test series graphically, showing an upper and lower limit to the wear rate of the prototype under ~12 N normal load.

The mean wear rate (mm^3/m) and the wear rate coefficient (mm^3/Nm) were calculated in each case using the method of least squares and are shown for both the metacarpal and the phalangeal components in Table 6.7. The mean values for the whole series are also given.

Test No.	Phalanx			Metacarpal		
	Wear rate $10^{-5}mm^3/m$	Wear rate coeff. $10^{-6}mm^3/Nm$	Depth lost mm	Wear rate $10^{-5}mm^3/m$	Wear rate coeff. $10^{-6}mm^3/Nm$	Depth lost mm
1	15.58±0.15	12.81±0.12	0.25±0.002	14.33±0.23	11.78±0.19	0.07±0.001
2	14.21±0.24	12.01±0.20	0.23±0.003	13.07±0.24	11.05±0.20	0.07±0.001
3	15.20±0.27	12.82±0.23	0.24±0.004	13.95±0.25	11.76±0.21	0.07±0.001
4	16.07±0.15	13.18±0.12	0.51±0.002	14.36±0.12	11.78±0.10	0.15±0.001
5	15.38±0.17	12.83±0.14	0.58±0.006	13.44±0.09	11.21±0.08	0.16±0.001
All Mean	15.61±0.11	13.00±0.09		13.72±0.10	11.43±0.08	

Table 6.7 Test results summary.

6.4.1 Macrophotography

At the end of each test the samples were examined using macrophotography at magnifications of x4 to x10. Three sets of photographs are given in this section. The test 1 components are shown since the metacarpal component was a mark 1 prototype. Tests 2 & 3 were very similar in that they were mark 2 prototypes which both ran for a sliding distance of

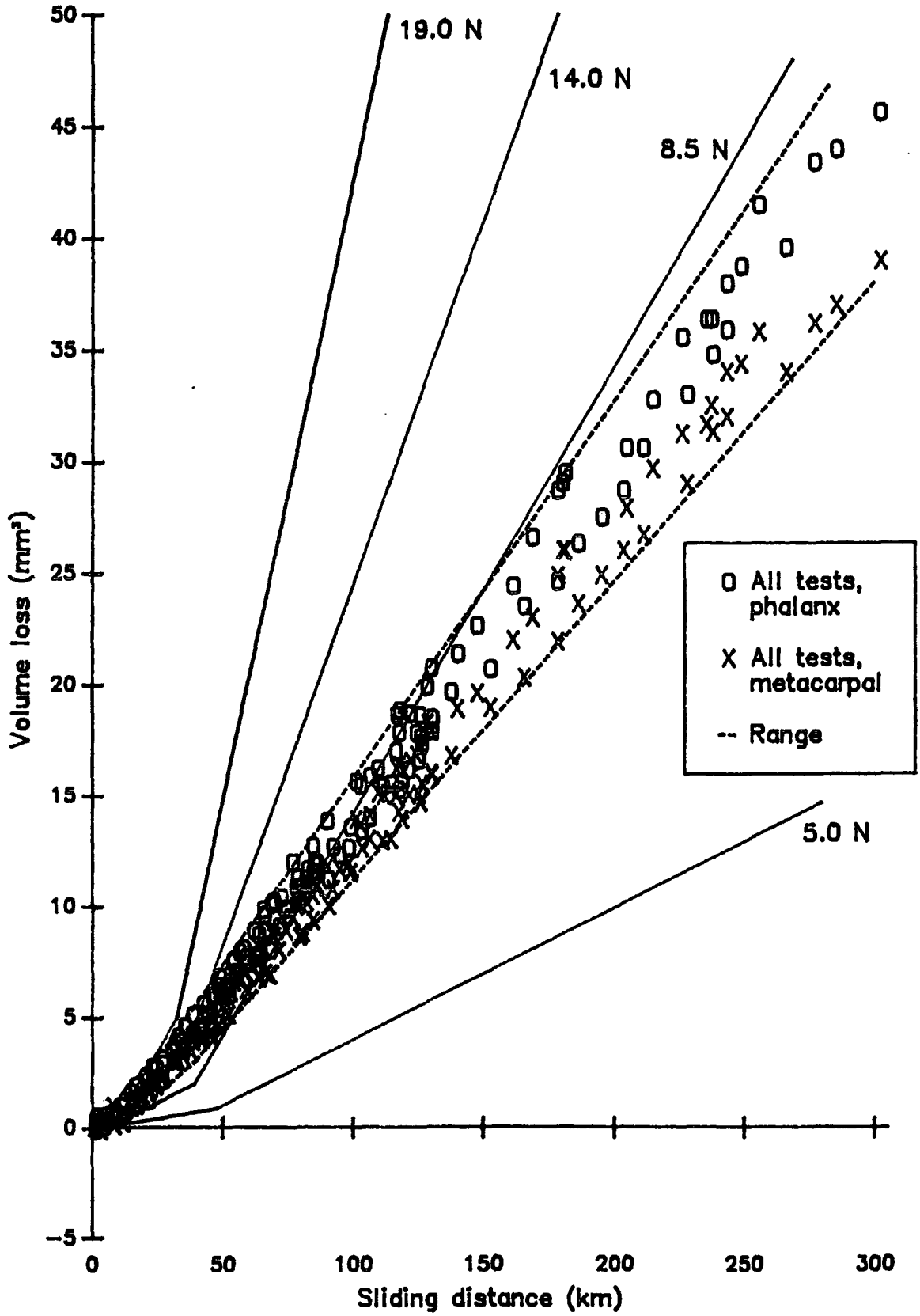

Fig 6.10 Summary of prototype wear results.

~130 km. The test 2 photographs are shown here since they contain some interesting features but comparisons are drawn with test 3 where differences were observed. Tests 4 & 5 again were similar, both running for about 300 km, but the test 5 components which were intended to undergo an extended trial were damaged in a simulator failure. The results recorded for test 5 are up to the last sample weighing before the failure and no photographs were taken.

Figs 6.11 a) & b) show the articulating surface and lower edge of the test 1 phalangeal component. The surface had a slightly polished appearance with a few wear marks running at an angle of ~20° to the dorsal, suggesting that the component may have rotated a little during the test. The circular marks originally present were still clearly visible, and the most important scar was a single deep scratch on the ulnar side, apparently corresponding to the edge of the metacarpal component. There was also some significant damage on the volar side of the articulating surface and material degradation and thinning were most marked here. There was some thinning of the component in general - possibly as much as 0.25 mm in depth - and it appeared more translucent than the control. There was no apparent gross deformation of the component attributable to cold flow of the polyethylene other than a noticeable smearing of the edge of the articulating surface. This effect has been seen in some polyethylene knee components. At the back of the component there was some very slight marking due to contact with the prepared bone surface but there was no stem damage of any kind.

Fig 6.12 shows the articulating surface of the test 1 metacarpal component which is significantly narrower in the dorsal aspect than the mark 2 design, shown in Fig 6.1. The surface had a very shiny

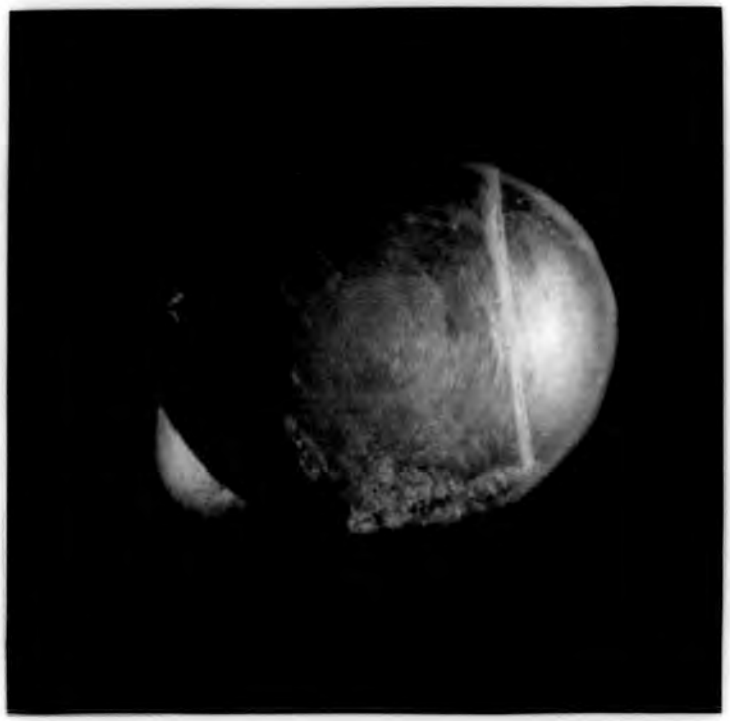

Fig 6.11 a) Surface of the test 1 phalangeal component.

Fig 6.11 b) Edge of the test 1 phalangeal component.

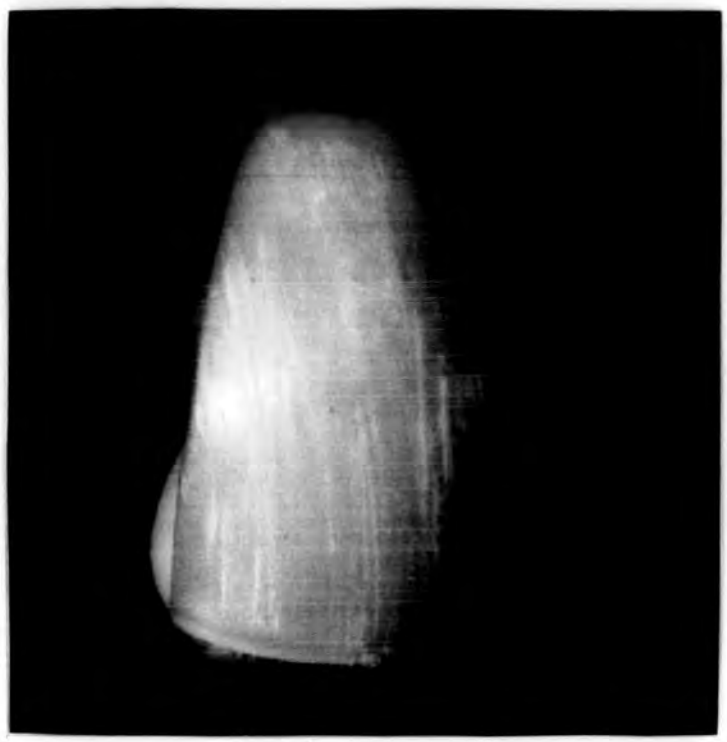

Fig 6.12 Surface of the test 1 metacarpal component.

appearance with clear abrasion marks running from 0° - 90° flexion, the deepest of which occurred at around 0° - 10° flexion on the ulnar side and at 60° - 90° flexion in the centre. There was a single impression mark at 10° hyperextension which was not associated with any abrasion, and there were some marks on the back of the component due to contact with the bone. There was no obvious thinning or cold flow deformation in the component, neither was there any stem damage.

Figs 6.13 a) & b) show the articulating surface and volar edge of the test 2 phalangeal component. Tests 2 & 3 ran for approximately the same duration as test 1 and their post-test appearance was generally very similar. The phalangeal components of tests 2 & 3 were noticeably thinned and more translucent than the controls, again perhaps 0.25 mm in depth. The surfaces showed clear evidence of abrasion with a loss of the pre-test circular marks which was not the case in test 1. The edges, and in particular the volar edge, were sharp and thinned, again indicating high stresses and cold flow. In both cases there was a definite material degradation at the palmar edge and this would appear to correspond with the moulding tool vent position. In contrast to test 1, neither test 2 or 3 displayed any deep marks in the surface of the phalangeal component since the mark 2 metacarpal component width exceeded that of the mating surface. There was no apparent stem damage or gross deformation in either case.

Figs 6.14 a) & b) show the upper and lower sections of the test 2 metacarpal component articulating surface. In tests 2 & 3 the metacarpal component surfaces were highly polished with abrasion marks that were particularly clear on the volar aspect. In test 3 these marks ran true but were at an angle of almost 45° to the dorsal on the test 2

Fig 6.13 a) Surface of the test 2 phalangeal component.

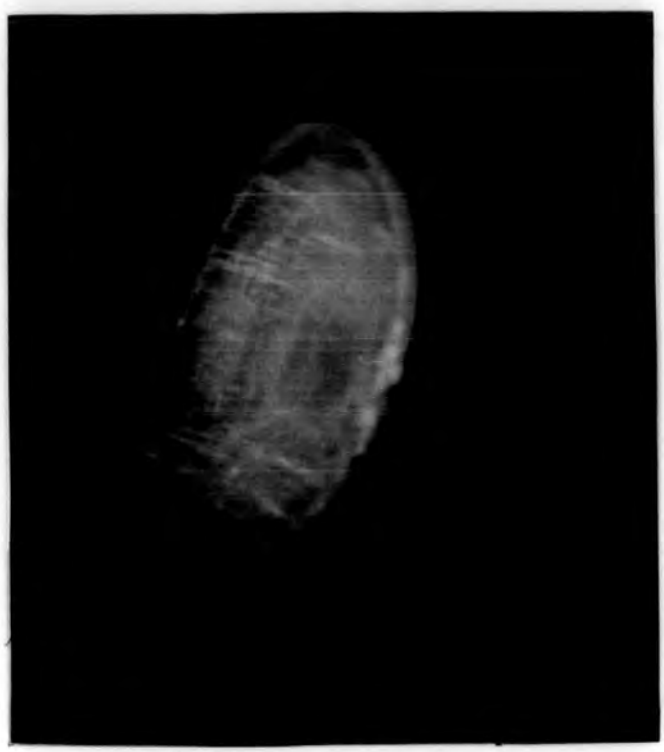

Fig 6.13 b) Edge of the test 2 phalangeal component.

Fig 6.14 a) Upper half of the test 2 metacarpal component surface.

Fig 6.14 b) Lower half of the test 2 metacarpal component surface.

component. In addition, while there was no gross deformation in the test 3 component, the stem was twisted in test 2 and bent towards the volar and ulnar edges. Looking from the back (Fig 6.15), the lower ulnar corner of the component was seen to be slightly displaced toward the stem. It was apparent that the deformation in the test 2 component was consistent with the angled abrasion marks and would seem to suggest that the component had twisted on the bone during the test and not that the bone was twisted in the clamp. In hyperextension there were again some impressions on both components not associated with abrasion marks. It would appear that under heavy static loading the components impinged on the adjacent pulley though it was not apparent at the time that this was occurring. On the test 2 component there was a single, quite wide, prominent scratch running from about 0° - 30° flexion which corresponded to the area of roughened material at the volar edge of the phalangeal component.

Figs 6.16 a) & b) show the surface and edge of the test 4 phalangeal component which had undergone ~10 million cycles in the finger function simulator. Thinning was considerable, with the component having lost in excess of 0.5 mm in depth. The abrasion marks were clear, some being quite deep, and the surface was very polished generally. The edges of the component were again smeared and this resulted in a 1.5 mm increase in the minor axis width. Surprisingly, perhaps, the palmar edge damage was not so severe. It is possible that the weak material had been worn away completely. There were some shallow marks on the back of the component but these were not noticeably worse than those of the shorter term tests.

Figs 6.17 a) & b) show the upper and lower sections of the test 4

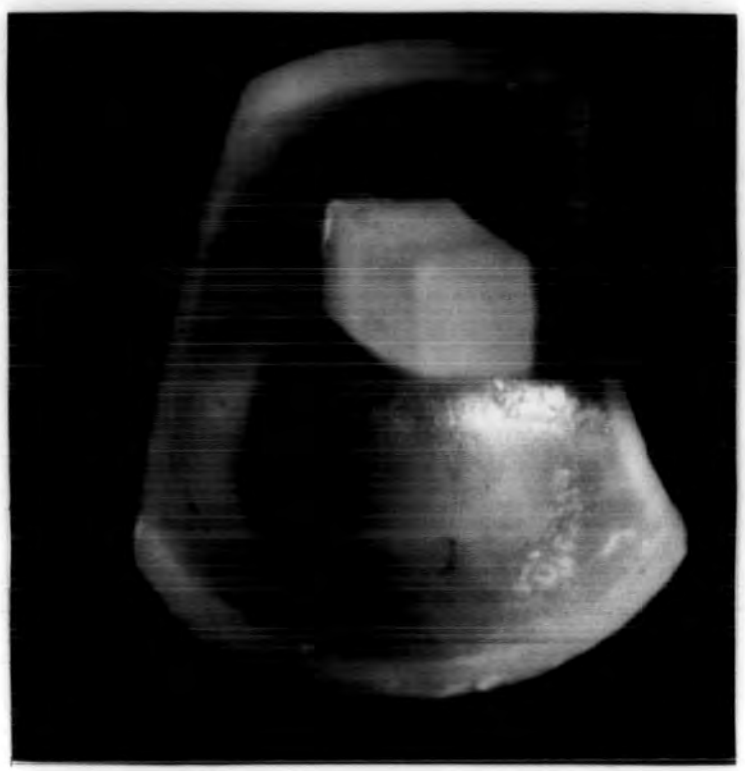

Fig 6.15 Rear view of the test 2 metacarpal component.

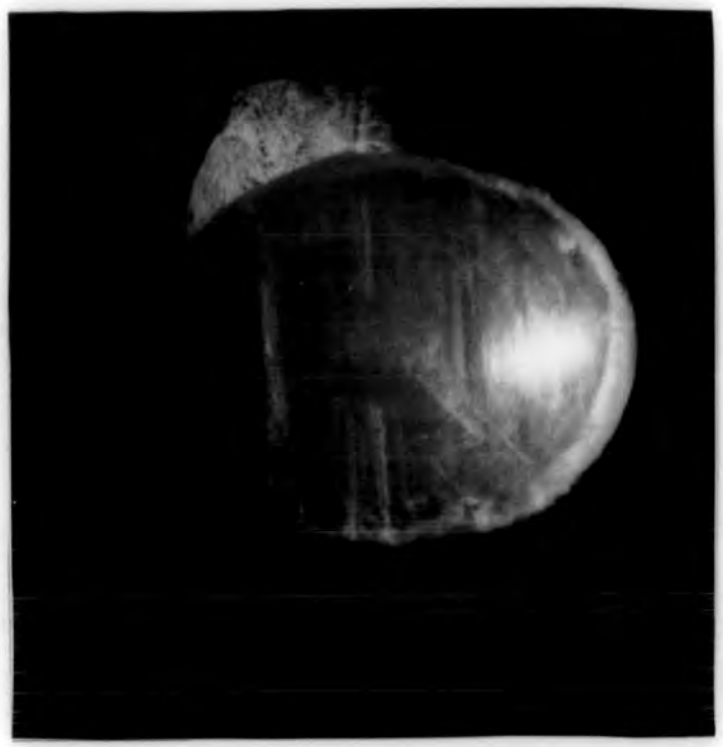

Fig 6.16 a) Surface of the test 4 phalangeal component.

Fig 6.16 b) Edge of the test 4 phalangeal component.

Fig 6.17 a) Upper half of the test 4 metacarpal component surface.

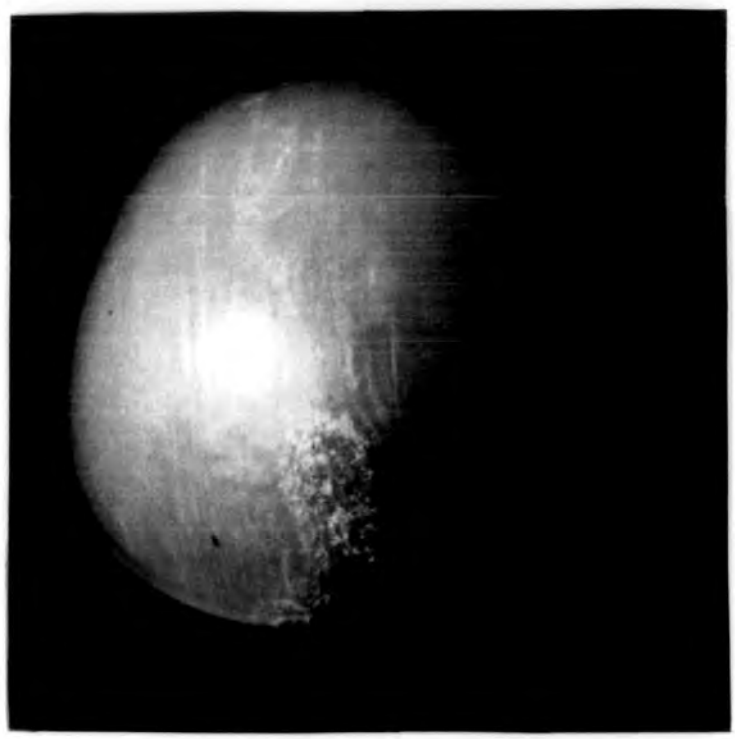

Fig 6.17 b) Lower half of the test 4 metacarpal component surface.

metacarpal component surface. The pulley mark could be clearly seen in hyperextension and abrasion was visible between 0 & 90° flexion. The most significant area of damage on this component was on the volar aspect of the articulating surface. A patch some 5 mm long and 2 mm wide was quite badly degraded. The appearance of this area was rather like the volar edge damage seen in the phalangeal components of tests 1 to 3, and would seem to be attributable to some surface fatigue mechanism rather than abrasion. The scar did not penetrate deeply. In this component and also that of test 5, there was some measurable thinning though only about 0.25 mm in depth. There was no damage or deformation in the stem or body of either component.

6.4.2 Electron Micrographs

Fig 6.18 shows a fairly low magnification view of the test 2 metacarpal component. The abrasion marks can be clearly seen with some indication of material plucking, but there are no debris fragments or transfer films visible. The most striking feature of this view is the series of small black spots scattered over the surface. On close inspection these were seen to be small pits in the surface, sometimes containing debris particles. Areas of pitting were seen on all the components examined and extensively on the volar aspect of the test 4 metacarpal component. They were less prominent on the phalangeal components.

At a similar magnification Fig 6.19 shows part of the area of severe damage on the volar aspect of the test 4 metacarpal component (shown earlier in Fig 6.17 b)). It would appear that a complete breakdown of the surface structure has occurred here and would no doubt have been associated with a significant loss of material. It is interesting to

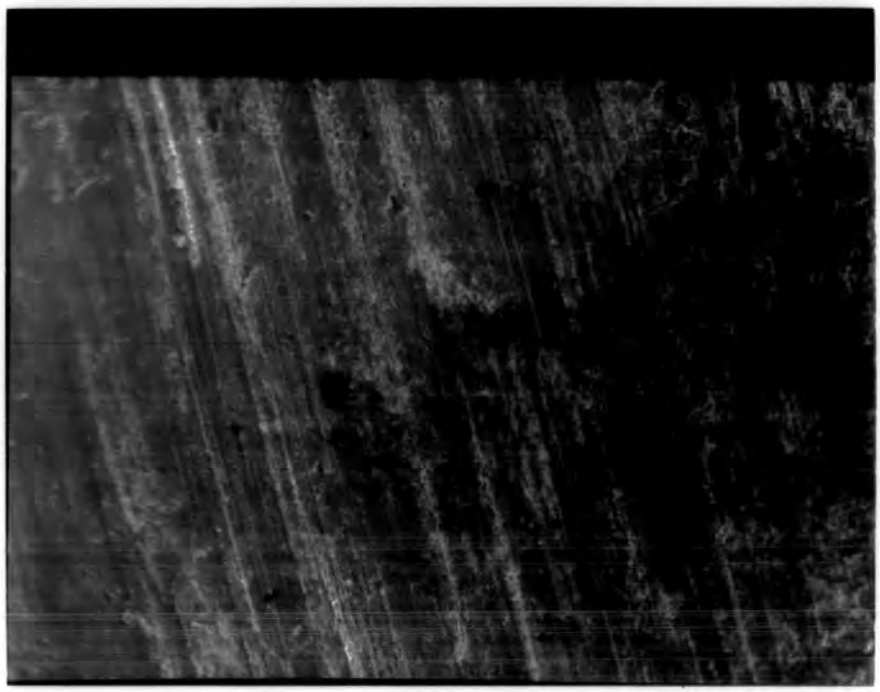

Fig 6.18 Onset of surface pitting - test 2 metacarpal component.

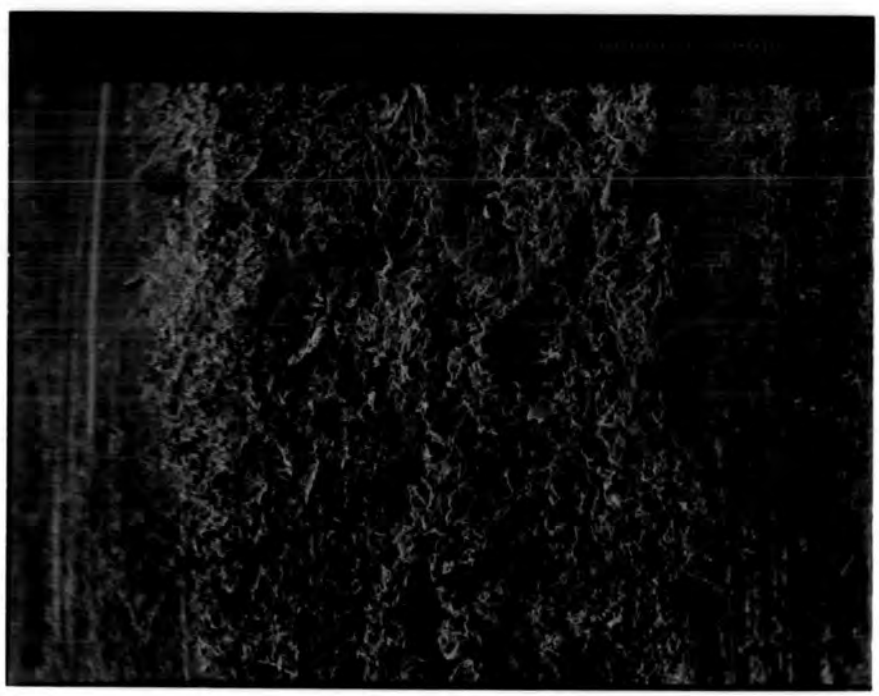

Fig 6.19 Gross surface degradation - test 4 metacarpal component.

note that at either side of this area there were large regions of pitting as shown in the previous micrograph. In Fig 6.19 these can just be seen in the upper right and lower left corners of the view. This would suggest that the fine pitting is a pre-cursor to the more severe surface failure seen here.

Surprisingly, the transverse surface rippling and cracking, so evident in the bench test specimens, were not observed at all in any of the prototype components examined. Fig 6.20, which is a high magnification view of the test 1 metacarpal component, shows just how smooth the wear surfaces were away from the degraded areas. There is some evidence of surface smearing here, and sub-micron sized pits are just visible on the right hand side of the view.

The phalangeal components generally showed more clear abrasion marks than the metacarpals and rather less surface degradation. This type of damage was only seen near to the vent sites on the volar edge, as shown in Figs 6.11 a) & 6.13 a). Surface plucking was commonly seen along the abrasion markings and a typical view is given in Fig 6.21.

At very high magnification, Fig 6.22 shows the edge of the damaged region of the test 4 phalangeal component. This area again shows a complete breakdown in the surface structure but in this case is not associated with the progression of a surface pitting mechanism. The appearance of the material is also quite different here and may actually be attributable to an as-manufactured material defect at the vent site.

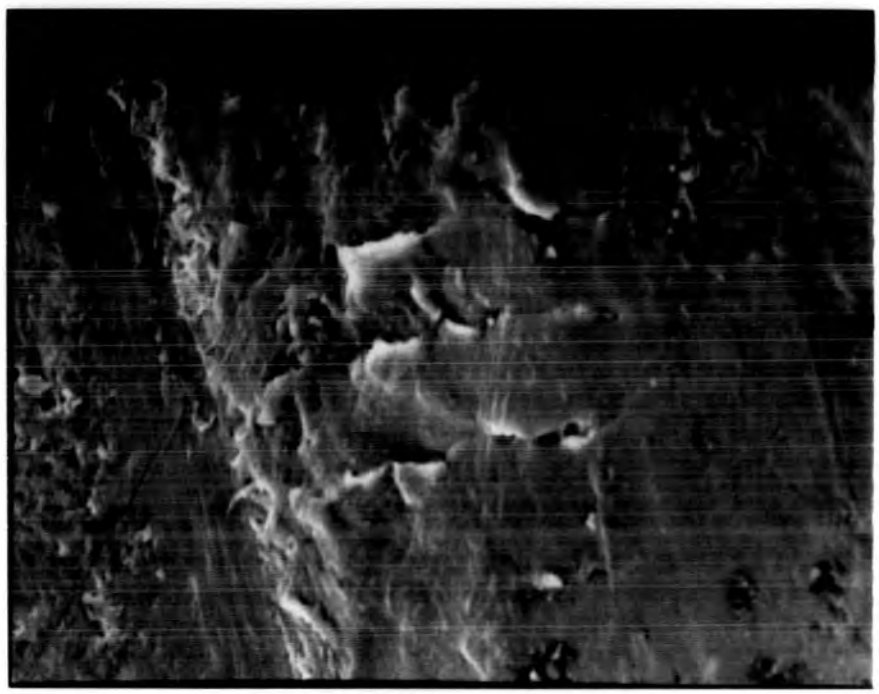

Fig 6.20 High magnification view of the test 1 metacarpal component.

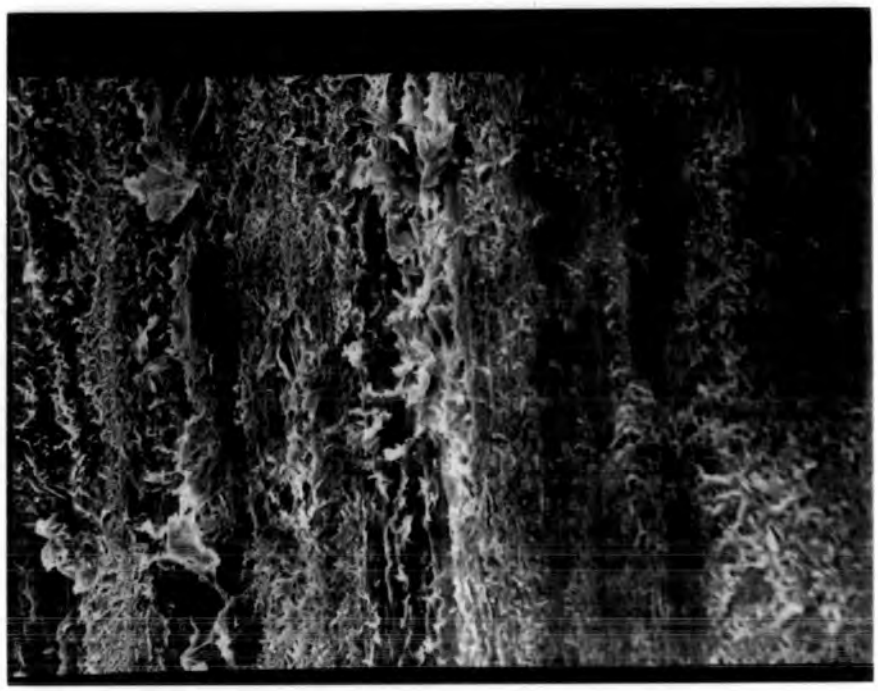

Fig 6.21 Surface plucking on the test 2 phalangeal component.

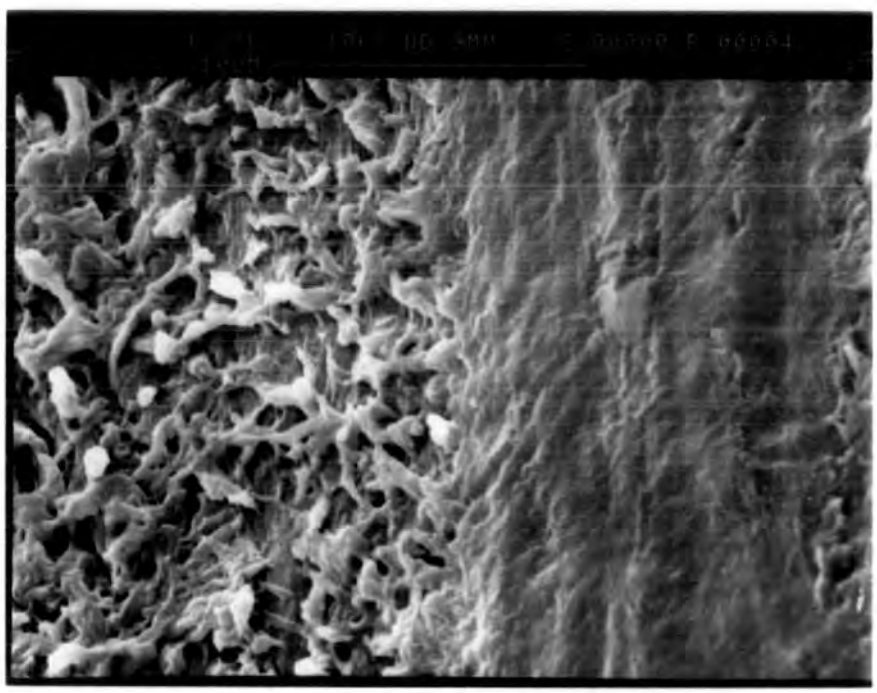

Fig 6.22 Surface degradation of the test 4 phalangeal component.

6.5 DISCUSSION AND CONCLUSIONS

6.5.1 General Comments

The five prototype pairs all survived severe testing in the finger function simulator with no indication of premature failure after cycling distances of some two to five times that required to fail the Swanson joint (Chapter 4). This is very encouraging. The bone cuts and stress fractures, so often a problem with finger joint implants, were not seen in this experimental programme other than some very minor markings at the back of the components. Cold flow was evident to a degree, particularly at the edges of the phalangeal component (Figs 6.11 b), 6.13 b) & 6.16 b)) and while this edge smearing was not too worrying, it has proved a severe problem in the polyethylene tibial components of surface knee replacements (Morrey et al, 1979 (138)). To reduce this problem it would be beneficial to seat the phalangeal component more deeply into the bone, perhaps filing the head back until it was flush with the polyethylene. Further evidence of cold flow was seen in the stem and volar edge of the test 2 metacarpal component (Fig 6.15). The twisting of the component on the bone head during testing has resulted in this permanent deformation. This is more worrying since it would seem that while the stem has held its orientation within the medullary canal the softness of the material has still allowed the component head to twist. The question was asked whether an uncemented, square cross-section stem would be sufficient to prevent rotation of the implant but clearly a stem of any geometry would suffer this problem. It is not known why rotation occurred in this case and indeed no other stems in the series showed any similar deformation. However, it should not be

taken too lightly and consideration may be given to strengthening the stem.

The wide metacarpal mark 2 design was undoubtedly more suitable than the mark 1 design used in test 1 which imparted a deep cut to the phalangeal component, possibly during heavy static loading (Figs 6.11 a) & b)).

One important feature in all the tests was the surface damage in the area surrounding the mould vent position (Figs 6.11 a) & 6.13 a)) which was particularly striking in the phalangeal components but also evident to some degree in the metacarpal components. These areas, when examined using the SEM, had a rather odd appearance compared with other worn areas (Fig 6.22) and, though it is not certain, it would seem likely that some as-manufactured defect is present here. It would be advisable to move the vent, if possible, onto the rear surface of each component.

6.5.2 The Wear Performance

The first observation to make on the wear behaviour of the prototypes is that the mechanisms occurring are **not** the same as for the non-cross linked material. Apart from the wear graphs lacking the distinctive dog-leg at ~40 km, the SEM micrographs show significant differences. As in the bench tests, abrasion is a prominent feature with clear wear scratches and a polished appearance of all the articulating surfaces. Some evidence of adhesion can also be seen (Fig 6.21) where material has been plucked from the surface as in Fig 5.12. However, film transfer does not seem to have occurred to any great extent at all, which is surprising. When two surfaces are totally conforming, as the prototypes are, it is more likely that wear debris will remain between the

surfaces, acting to enhance abrasion. In the case of the bench tests this was certainly true and transfer films were clearly present (Fig 5.9). It would seem that either the debris escaped, with the prototypes sliding at a greater speed than the bench tests, or that it did remain to cause three-body abrasion but was too hard to be smeared over the surfaces as a result of cross linking. The surface features of rippling and cracking (Figs 5.10 & 5.11), attributed to material fatigue in the bench tests, are also absent from the prototype micrographs. This would explain the absence of the dog-leg in the wear graphs. Even so, some form of fatigue is evident with the cross linked material (Figs 6.18 & 6.19) with surface pitting progressing to quite severe surface degradation in time. This mode of failure occurs after much greater sliding distances, probably in excess of 100 km (~7 years use) and severe damage was only seen in the test 4 metacarpal component which had performed in excess of 300 km. Its progression must have been rather gradual since there was no obvious change in wear rate as a result.

It is a pity that test 5 did not survive its intended duration since an upturn in the wear graph may eventually have appeared. Interestingly, the fatigue damage described here was only really seen on the metacarpal component surfaces on which a given area is repeatedly under tension and then compression during cycling. This is reminiscent of the situation in the knee joint though on a much smaller scale. In knees surface damage to the polyethylene tibial component is a common problem and damage very similar in appearance to that shown in Fig 6.19 was described by Wright & Bartel in 1986 (103) as 'delamination'. These authors reported that the severity of the surface damage was a function of patient weight, component thickness and duration of implantation.

While stresses in a finger joint are an order of magnitude less than in the knee, the component thickness is also very much less and it is possible that an increase in thickness may help. A fatigue mechanism for the creation of pits on the surface of polyethylene components was proposed by Rose et al in 1979 (139). Strictly it is not realistic to try to compare the wear performance of two materials from tests that are so different in nature, particularly as it is clear that the materials do not behave in the same way. However, it is instructive to do so if the conclusions are treated with due caution.

Fig 6.10 gives a graphical summary of the wear results for the prototype series along with the extrapolated bench test results for reference. The first observation to make is that the phalangeal components have worn slightly more than the metacarpal components in general. This difference was also seen in the bench tests with the pins wearing more than the plates.

The absence of the dog-leg in the prototype wear data has meant that the final volume loss at the end of each test at 12 N was below that expected for 8 N in the bench tests. In Chapter 5 it was stated that an MCP prosthesis made from non-cross linked polyethylene could be expected to lose ~3.32 mm^3 (or 0.04 mm in depth) per component per year after the first two or three years (wear rate coefficient = 19.88 x 10^{-6} mm^3/Nm). With regard to the debris released to the joint, this amounts to 66.4 mm^3 of material over ten years compared with only 0.8 mm^3 for a metal-polyethylene system (wear rate coefficient = 0.5 x 10^{-6} mm^3/Nm). On the same basis, a surface replacement made from cross linked polyethylene may be expected to release 38.1 mm^3 of debris into the joint over ten years (wear rate coefficient = 12 x 10^{-6} mm^3/Nm). This

is a significant improvement on the non-cross linked material.

6.5.3 Overall Performance

The results of the prototype test series are very pleasing indeed and, while some improvements could be made to increase component durability, no real problems are envisaged in continuing the development of the implant as an all-polyethylene system.

CHAPTER 7

FINITE ELEMENT ANALYSIS

7.1 INTRODUCTION

With more than half a million prosthetic joint implantations being performed annually and the increased life expectancy of these devices, progress is being directed towards mechanical optimisation to extend their functional life. The knowledge of the stress behaviour of orthopaedic implants and the supporting bone tissue is an important link to understanding the success or failure of such devices.

The mathematical tools available for stress analysis in classical mechanics are not really suitable for the highly irregular structural properties of bones and so researchers have moved to the finite element method, which has been employed in other areas of engineering for more than thirty years. In 1972 Brekelmans et al (140) wrote a paper on the use of finite elements to study stresses in healthy human bones. Since that time the numerical method has been used for bone/prosthesis structures, fracture fixation devices and soft tissues such as the heart and lungs. A description of its principles, possibilities and limitations, in orthopaedic biomechanics specifically, was published by Huiskes in 1983 (141). Also in 1983 a survey of the first decade of finite elements in biomechanics was reported by Huiskes & Chao (142) which included over one hundred references.

In the past five years the use of finite element techniques in bioengineering has really taken off even though, as yet, the methodology is still being explored and the results are largely qualitative and not quantitative. While this method has not yet had an enormous impact on the clinical orthopaedic community, it is likely to become increasingly

important over the next few years as the dialogue between clinicians and engineers improves. For this reason, and also for completeness, a brief finite element study of the Durham surface replacement prosthesis has been included here. While it is not intended to go into too much detail, it is hoped that this will demonstrate the potential of numerical stress analysis in the future development of this device. A thorough analysis could form the basis of a whole research programme.

7.2 METHOD AND ASSUMPTIONS

A finite element model is created by providing input data to describe the geometry of the structure, its material properties, and the applied loads. In biomechanics the essentially two-phase nature of the bone material, consisting of solid but porous matrix and an interstitial fluid, poses a problem of definition. Furthermore, bone is a living tissue and responds to stress by resorption or by forming cortical bone for strengthening. There is only sparse information available on the actual behaviour of bone and on the mechanical distinction between cortical and trabecular bone. While being anisotropic and non-homogeneous in nature, both behave approximately in a linear elastic way. Some very sophisticated models in two and three dimensions have been produced, especially on the femur, which have attempted to take non-homogeneity and anisotropy into account. However, in this study the bone is treated as a continuum material in two dimensions for simplicity. The solution follows a direct stiffness plane strain formulation with linearly elastic material properties using the computer package PAFEC 5.1. The material properties are given in Table 7.1.

Material	Young's Modulus (MPa)	Poisson's Ratio	Density (gcm^{-3})
Bone	14,000	0.30	1.4
UHMWP	1,100	0.43	0.954

Table 7.1 Material properties employed in the study.

The element meshes for both the metacarpal and phalangeal bones are shown in Fig 7.1. These were produced by hand but there are ways of automatically generating suitable meshes which are particularly useful for three dimensional and symmetrical systems. No attempt has been made to reproduce the true geometry of the bones but, compared to the polyethylene, the bones are effectively rigid bodies and the cylindrical geometry chosen will therefore have little effect on the stress calculations.

Each mesh is made up of isoparametric curvilinear elements for plane stress and plane strain, in which it is assumed that stresses do not vary through the thickness of an element (taken here to be 2 mm). The bone is represented by six-noded triangular elements and the implant components by eight-noded quadrilateral elements. The phalangeal mesh is made up of 420 elements and 1035 nodes compared to 427 elements and 1087 nodes in the metacarpal mesh.

In the majority of studies reported previously the prosthesis and bone have been taken to be solidly joined by a cement interface. In this study there is no cement involved and the component/bone interface is represented by a friction gap of $\mu = 0.5$ such that any relative movement normal to the interface is free and any parallel to the interface is subject to friction.

In the calculations performed the load applied to the joint was 200 N which is the maximum expected for the implant. This was uniformly distributed over the articulating surface of the phalangeal component and over an equivalent area for the metacarpal component.

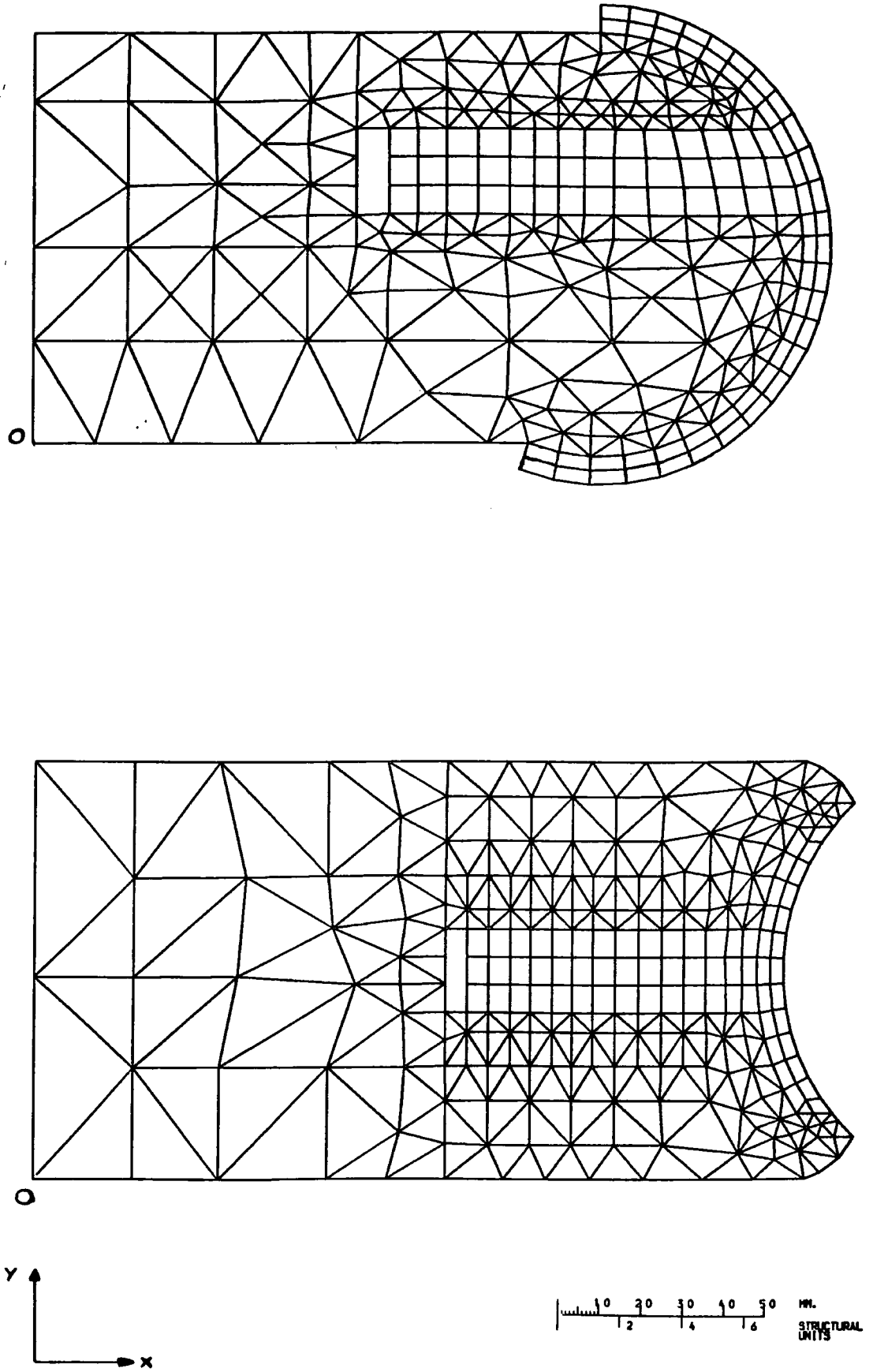

Fig 7.1 The finite element models used.

Finite element runs are time consuming and expensive and so a limited investigation was performed here. In the past researchers have spent a great deal of time and effort on detailed analysis without really gaining very much. It is important to define the aims before embarking on work of this nature. The aim of this work was to identify areas of stress concentration, assess the suitability of the stems, and suggest design changes in the light of the results. To this end four cases were run. For the first case the load was applied parallel to the x-axis of the phalanx. In general this is a reasonable test of the component since it has been shown (in Chapter 4) that the joint load will always stay within ~20° of the phalangeal axis. A trial performed with the load at 20° actually made very little difference to the stress pattern observed (results not shown). The other three cases were performed on the metacarpal at -30°, 0°, and 75° flexion respectively with the load acting through the centre of rotation of the bone. This again is not always the case in-vivo but the angle of flexion is much more important.

7.3 RESULTS

Fig 7.2 shows vector and contour plots for the principal stresses on the phalangeal system. Not surprisingly, stress concentrations can be seen at the head of the stem and at the rear edge of the articulating section of the component. In the prototype simulator trials very little damage was seen at the head of the stem, undoubtedly due to the way in which the stem canal was prepared. The head of the canal was slightly flared using a tapered broach, and the edges were rounded with a file. The result of this preparation was to reduce successfully the stress at the stem head.

The high stresses at the edge of the articulating section were actually enhanced in the simulator trials through the component protruding slightly beyond the bone surface. This resulted in cold flow of the polyethylene with the edges being thinned out.

Stresses in the stem can be seen to have diminished over a distance of ~5 mm - about half the stem length. This is shown more clearly in Fig 7.3 which is a graphical representation of the minimum principal stresses along the lower edge of the stem. From this it is established that the stem is of sufficient length.

Figs 7.4 to 7.6 show vector and contour plots for the principal stresses on the metacarpal system at positions of -30°, 0°, and 75° flexion. The first two positions show the expected stress concentration at the stem head which again was reduced in the simulator trials by careful canal preparation. At the 75° position, while the stem stresses are

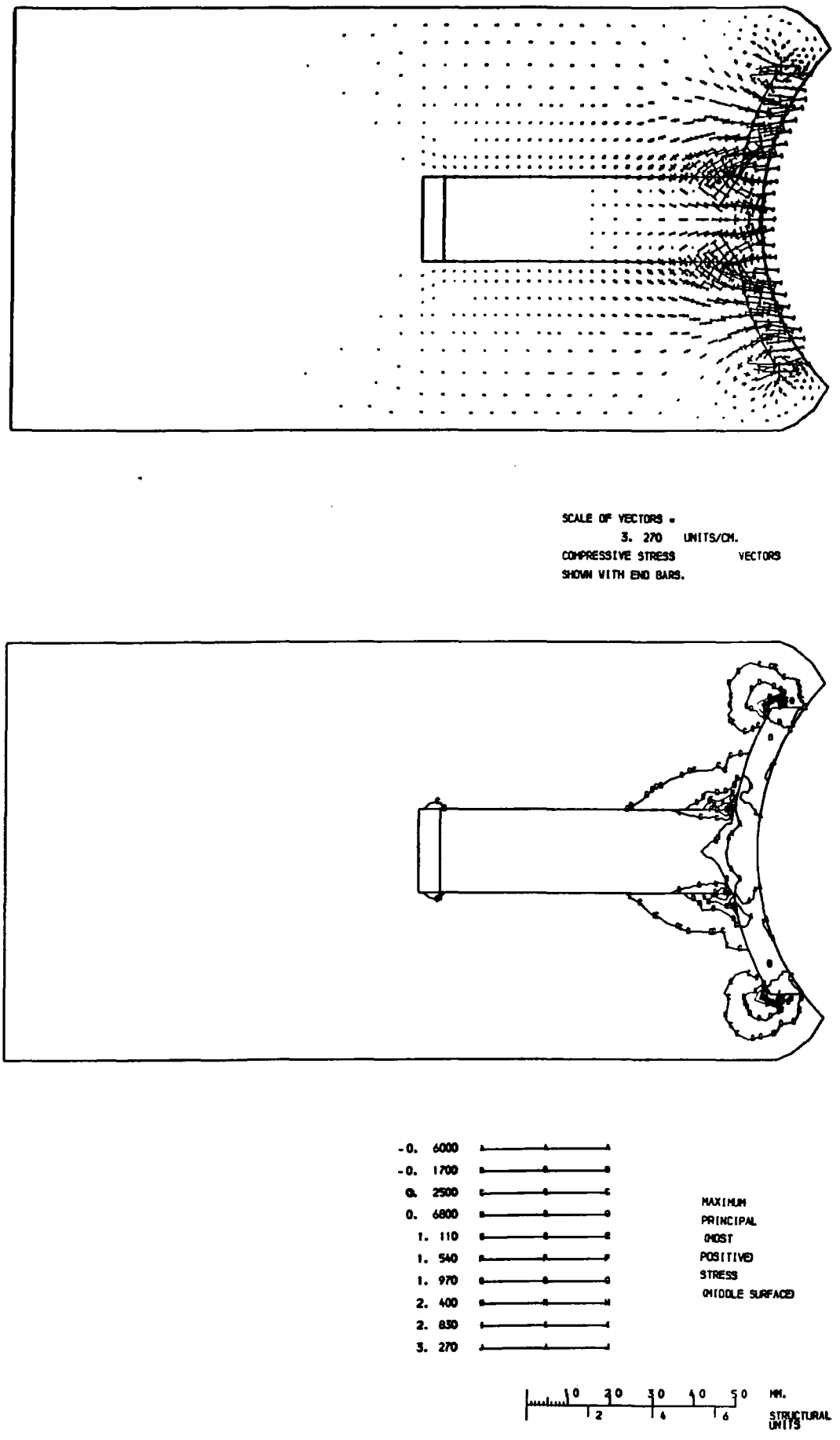

Fig 7.2 The stresses on the phalangeal system.

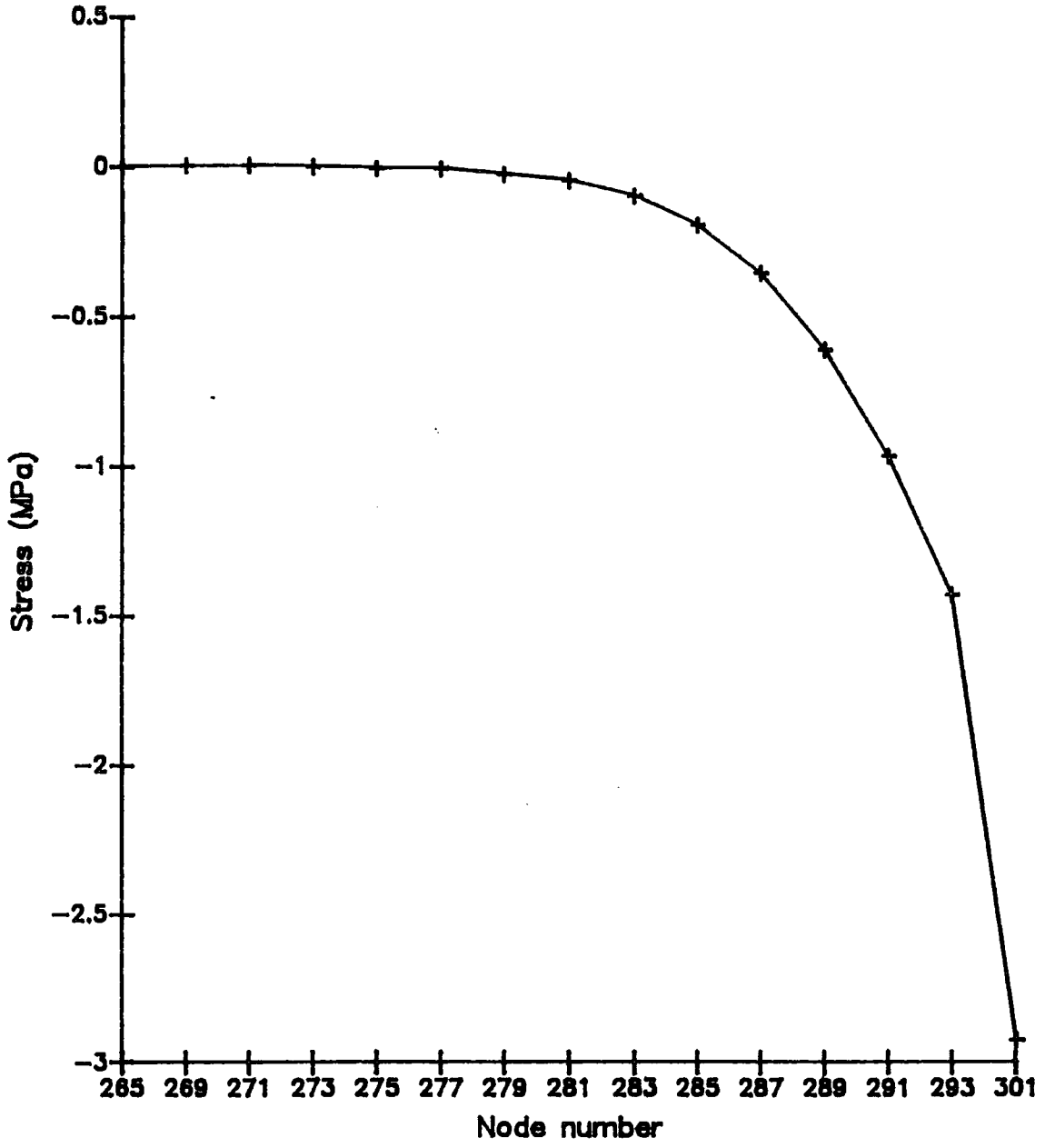

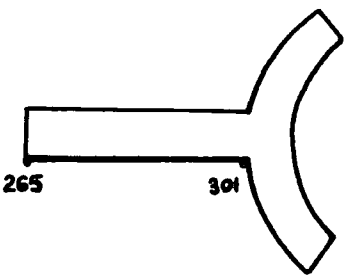

Minimum

Fig 7.3 Principal stresses along the phalangeal stem.

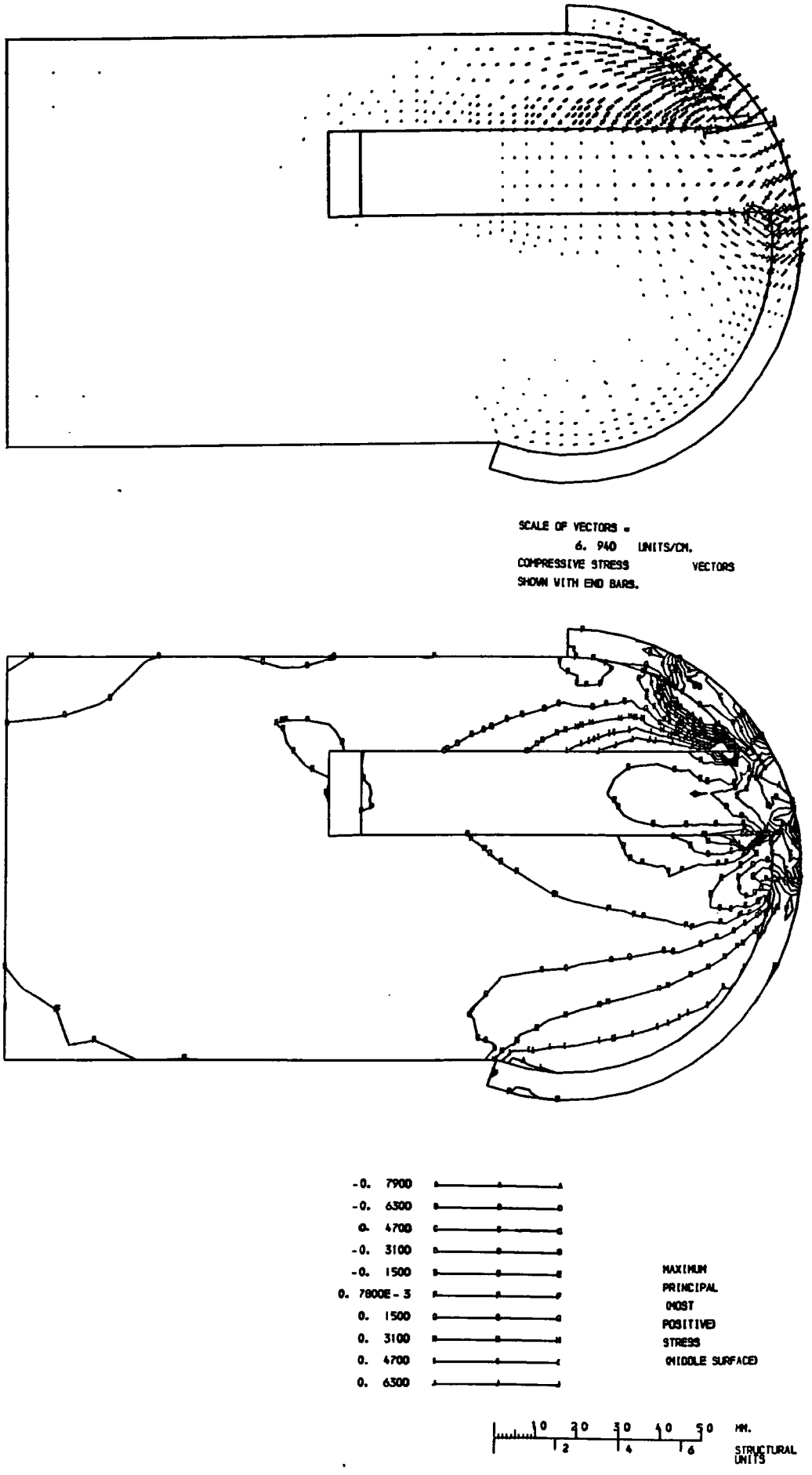

Fig 7.4 The stresses on the metacarpal system (-30° of flexion).

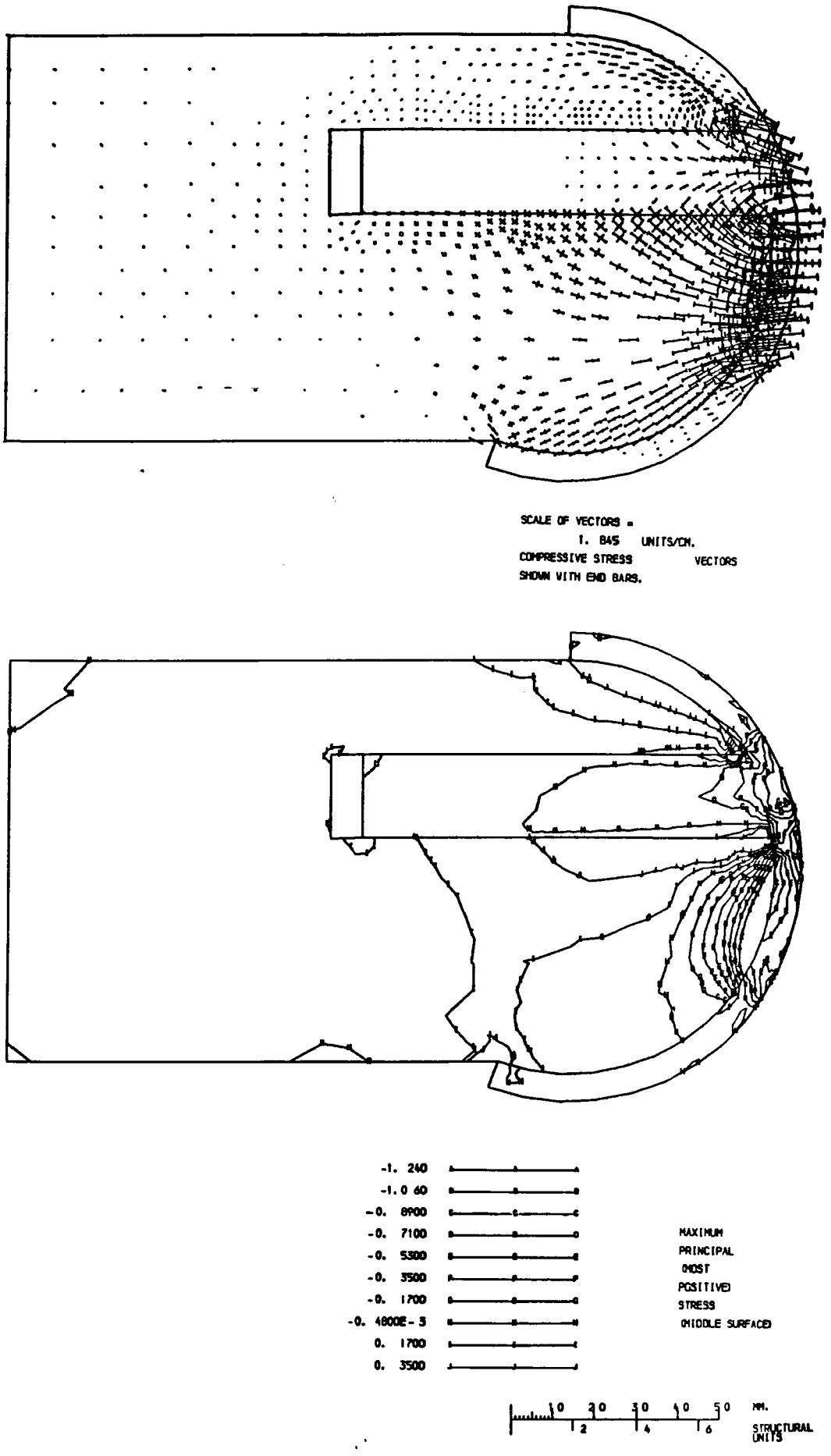

Fig 7.5 The stresses on the metacarpal system (0° of flexion).

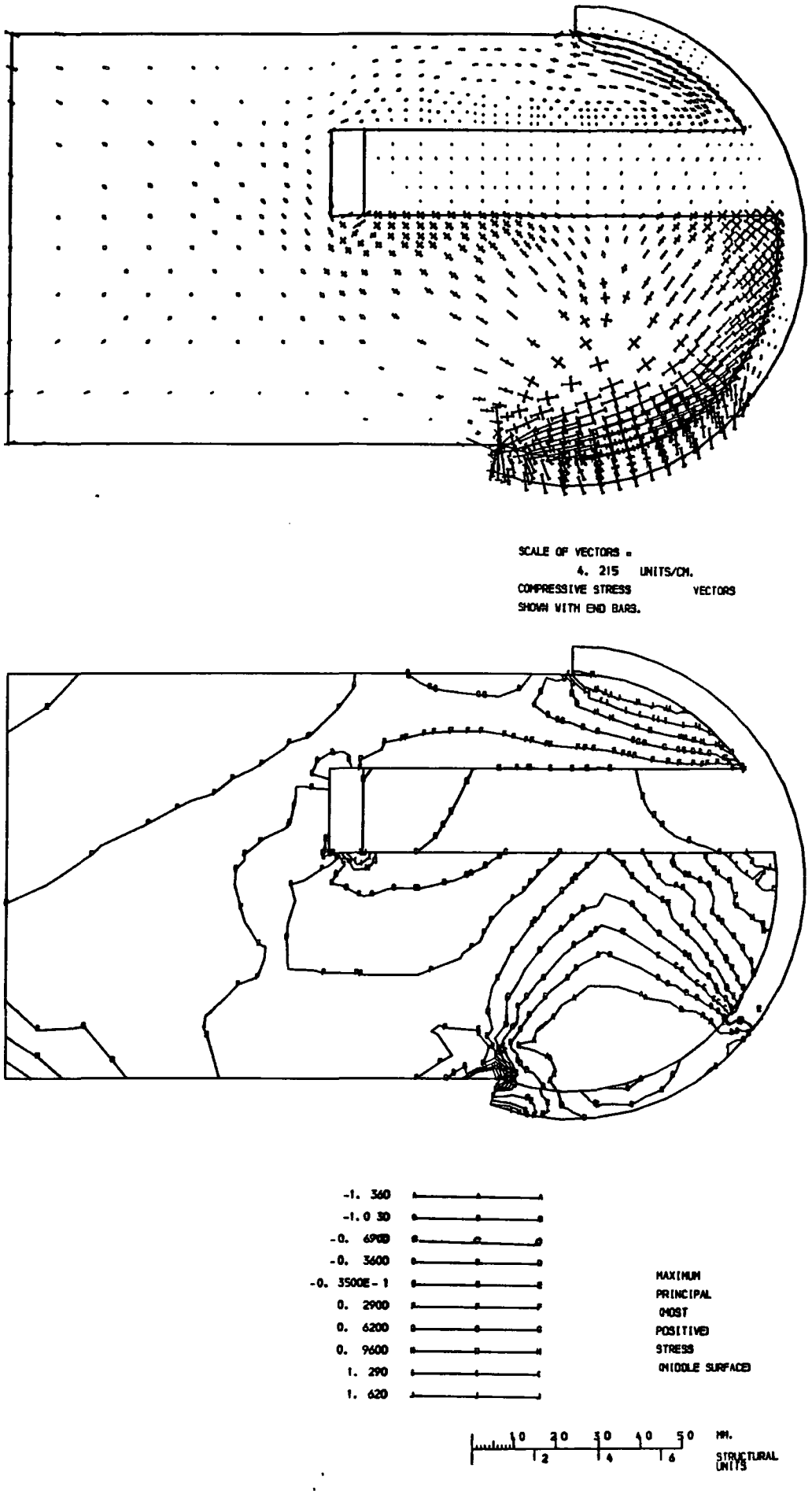

Fig 7.6 The stresses on the metacarpal system (75° of flexion).

significantly reduced, there is evidence of some stress concentration along the volar edge of the component which could result in cold flow of the polyethylene.

At positions of hyperextension there are high stresses through the dorsal section of the bone which is only some 2 to 3 mm in thickness close to the stem head. Fracture of this section of bone under heavy loading cannot be ruled out. Since the simulator trials involved the use of acrylic replicas the likelihood of this occurring could not be explored.

Potentially the most worrying aspect of the loading in the metacarpal component is the tension/compression cycling. This is shown in the contour plots of Figs 7.4 to 7.6 and is the consequence of the fact that the area of loaded contact is small and the loading pattern changes greatly as the phalanx moves around the metacarpal head. Over a long period of time this could result in fatigue damage, as seen in the tibial components of some knee prostheses. Indeed, some evidence of surface fatigue was seen in the simulator trials but, due to the relatively light dynamic loading in the finger, it would not be expected to cause premature failure.

The stem length is again shown to be adequate in distributing stress (Fig 7.7) but the stem head is seen to undergo quite severe cyclic stressing. This highlights the importance of moves to reduce stress at this point.

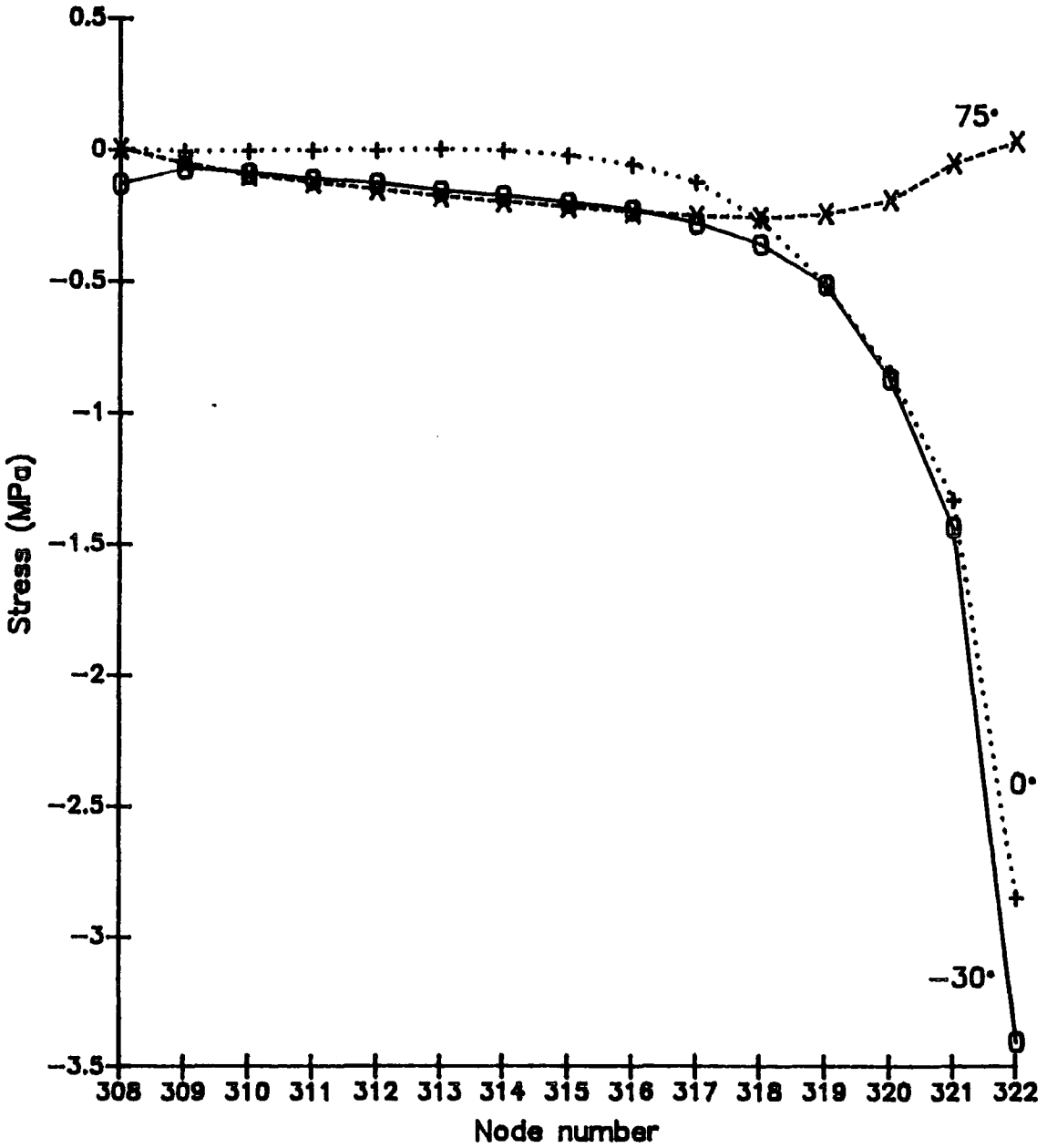

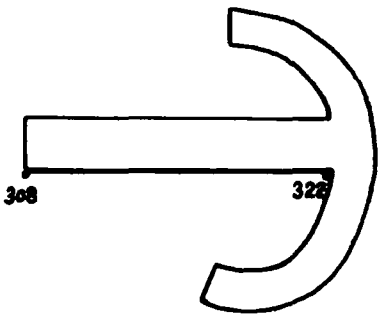

Minimum

Fig 7.7 Principal stress on the metacarpal stem.

7.4 CONCLUSIONS

Finite element analysis revealed areas of stress concentration in both components which can be reduced with careful bone preparation as demonstrated in the simulator trials. Some redundancy in stem length was highlighted which is also easily dealt with. Perhaps the most worrying discovery in this study was the possibility of fracture in the dorsal aspect of the metacarpal head where stresses are high in hyperextension. While this may turn out not to be a problem, it could not be seen in the simulator trials carried out so far since acrylic models were used. It would be advisable for tests to be performed using real bone to investigate the likelihood of failure in this region.

Fig 7.8 shows the recommended bone/implant configuration for the phalangeal system in the light of this work. The stem has been shortened, the stem canal flared, and the articulating section recessed a little deeper into the bone to prevent edge smearing.

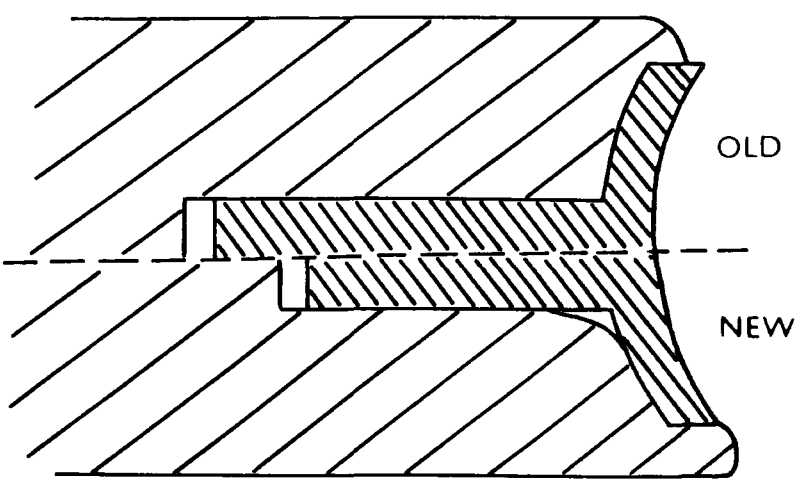

Fig 7.8 Recommended bone preparation for the phalangeal component.

Similar treatment of the stem and canal may be sufficient for the metacarpal system also. However, should fracture occur in the dorsal aspect of the metacarpal head, it may prove necessary to alter the component design as shown in Fig 7.9. Since the idea of the surface replacement is to cause as little disturbance to the bones as possible, this option should only be considered as a last resort.

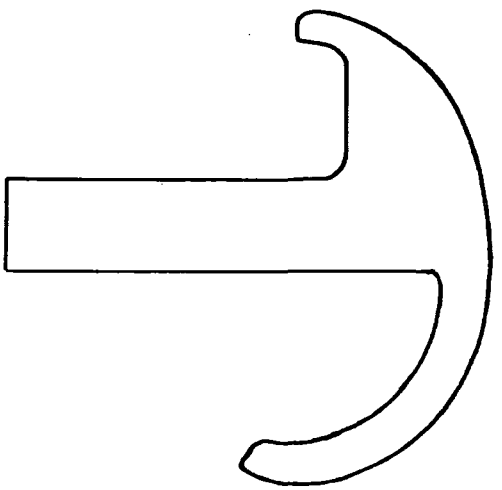

Fig 7.9 Possible modification to the metacarpal component.

While intended to be a demonstration of the potential of finite element studies in the development of prostheses, this work has augmented the laboratory experiments to some degree in assessing the Durham design. More detailed, perhaps three dimensional, studies could be performed later, perhaps in parallel with clinical trials, as minor modifications are made.

CHAPTER 8

CONCLUSIONS

8.1 SUMMARY OF ACHIEVEMENTS

The design of an uncemented two-component surface replacement prosthesis for the MCP joint has been undertaken. The development was based on a firm foundation of background investigations which are described in some detail in Chapter 1, and which are essential in work of this nature.

The component geometries, derived from a study of bone surface topologies (Chapter 2), are really very simple and, being made of cross linked UHMWP, are also easy to manufacture. The material was chosen for its inertness, wear resistance and its minimal effect on the bone. Its use in hip and knee joint implants has proved highly successful.

Increasingly, newly developed prostheses are being extensively tested in the laboratory before any clinical work is performed. For this reason a finger function simulator (described in Chapter 3) was built to test the prototypes. The design of the simulator was based on a careful biomechanical study of the MCP joint and its performance was assessed by testing the Swanson Silastic implant - Chapter 4. The failure of this implant in the laboratory has not previously been achieved. However, in the finger function simulator premature failure of the device did occur in a relatively short time and was seen to be very similar in nature to failures occurring in-vivo.

Five Durham surface replacement prototypes were tested in the simulator for periods estimated to be equivalent to 10 to 20 years use. None of the components failed or showed any tendency to premature failure which

was very encouraging indeed. Some cold flow was seen at the edges of the phalangeal component but this could be alleviated by a deeper insertion into the bone. Being a surface replacement the wear behaviour of the components is a very important consideration. Careful weight loss assessments were made on the test components during the simulator trials and electron micrographs were taken of the component surfaces afterwards (Chapter 6). In conjunction with the bench test results of Chapter 5, performed on non-cross linked UHMWP, a reasonable picture was built up about the wear mechanisms occurring in the implant, and the effects of cross linking on UHMWP. Release of debris into the joint cavity is cause for some concern.

Chapters 1 - 6 really fulfilled the aims of this research programme but for completion, and as a pointer for the future, a brief two dimensional finite element study of the prototype was described in Chapter 7.

8.2 FUTURE WORK

The development of the Durham surface replacement prosthesis has progressed now to the point where clinical investigations would be worthwhile. Clinical trials on patients will come much later but sizing trials on cadaveric specimens, and a study of the surgical techniques of implantation should be the next stage in the development. In addition to this, some aspects highlighted in this research programme should be addressed and the necessary action taken. In particular, questions raised in Chapter 6 about the suitability of the chosen material warrant further investigation. Certainly the components were seen to be durable enough to survive 10 to 20 years service, but the amount of debris released to the joint may prove prohibitive. It is recommended that further bench tests are undertaken to assess in more detail the surface fatigue mechanisms occurring in the cross linked UHMWP. Another important question remaining to be answered is that of the effect of the implant on the surrounding bone. Finite element analysis, detailed in Chapter 7, has suggested that there may be a problem with high stresses in the dorsal aspect of the metacarpal head. It would be advisable for a series of simulator trials to be performed using real bones such that any tendency to fracture will become apparent. Real bones were not used in the prototype trials of Chapter 6. Suggested design changes to the phalangeal and metacarpal components should be borne in mind but not necessarily employed until follow-up work has endorsed them.

8.3 CURRENT PHILOSOPHY

In correspondence with surgeons and researchers internationally it was interesting to learn the current philosophy regarding MCP joint replacement surgery. There has recently been a decided entrenchment in the work in this field and hence the lack of literature during the last decade. The reasons for this are:

i) A general dissatisfaction with the prosthetic designs over the last two decades.

ii) Decreased interest by manufacturers due to the high cost of development and the low rate of return on such materials.

iii) Widespread concern by many hand surgeons, particularly plastic surgeons, about the efficacy of cemented fixation in the hand and wrist.

iv) The difficulty of soft tissue balancing procedures following joint replacement.

v) In the medico-legal climate in the United States the continued use of unreliable devices is not justifiable and they are quickly withdrawn.

In recent years a trend back to the older resection arthroplasties has been evident. However, surgeons admit that the desire would be to have an anatomical resurfacing device, augmented by techniques to balance soft tissues which would diminish stresses and the tendency toward recurrent deformities. Currently this is not the case and researchers are tempted to add constraints to the design of implants which are associated with problems of loosening, fracture etc.

The way forward is undoubtedly the uncemented two-component resurfacing arthroplasty such as the one described in this thesis. The last five years have seen a renewed interest in this area particularly in the United Kingdom and the USA. It is true to say that the success of these devices lies not really in their design but in future progress in surgical techniques to repair the soft tissue structures of the joint. Without great improvements in this area a surface replacement is bound to fail and this should be the major consideration in the clinical stage of development. Having said this, researchers should not be deterred from their efforts in this field which looks to have great potential in the near future.

REFERENCES

1. Weightman B and Amis A A. Finger joint force predictions related to design of joint replacements. J Biomed Eng, **4**, 1982, 197-205.

2. Smith E M, Juvinall R C, Bender L F and Pearson J R. Role of the finger flexors in rheumatoid deformities of the metacarpophalangeal joints. Arthritis & Rheumatism, **7**, No 5, 1964, 467-480.

3. Long C, Conrad P W, Hall E A and Furler S L. Intrinsic-extrinsic muscle control of the hand in power grip and precision handling. J Bone Joint Surg, **52A**, 1970, 853-867.

4. Flatt A E and Fischer G W. Restraints of the metacarpophalangeal joints: a force analysis. Surg Forum, **19**, 1968, 459-460.

5. Berme N, Paul J P and Purves W K. A biomechanical analysis of the metacarpophalangeal joint. J Biomechanics, **10**, 1977, 409-412.

6. Purves W K, Berme N and Paul J P. Finger joint biomechanics. "Disability - Proc Seminar Rehab Disabled" (Eds. R M Kenedi, J P Paul and J Hughes), 1979, Macmillan, London, 318-332.

7. Chao E Y, Opgrande J D and Axmear F E. Three-dimensional force analysis of finger joints in selected isometric hand functions. J Biomechanics, **9**, 1976, 387-396.

8. Chao E Y and An K N. Determination of internal forces in human hand. J Eng Mechs Divn, ASCE, **104**, No EMI, 1978, 255-272.

9. Chao E Y and An K N. Graphical interpretation of the solution to the redundant problem in biomechanics. J Biomech Eng, **100**, 1978, 159-167.

10. An K N, Cooney W P, Chao E Y and Linscheid R L. Functional strength measurement in normal fingers. Adv Bioeng, 1978, ASME, New York, 89-90.

11. An K N, Chao E Y, Cooney W P and Linscheid R L. Forces in the normal and abnormal hand. J Orthop Res, **3**, No 2, 1985, 202-211.

12. Walker P S and Erkman M J. Laboratory evaluation of a metal-plastic type of metacarpophalangeal joint prosthesis. Clin Orthop Rel Res, **112**, 1975, 349-356.

13. Swanson A B, Matev I B and de Groot G. The strength of the hand. N Y Univ Med Sch Interclinic Bull, **13**, No 1, 1974, 1-8.

14. Walker P S and Erkman M J. Clinical evaluation of finger joints. "Human joints and their artificial replacements", 1977, C C Thomas, Springfield, Illinois, 348-351.

15. Opitz J L and Linscheid R L. Hand function after metacarpophalangeal joint replacement in rheumatoid arthritis. Arch Phys Med Rehabil, **59**, No 4, 1978, 160-165.

16. Jones A R, Unsworth A and Haslock I. A microcomputer controlled hand assessment system used for clinical measurement. Engineering in Medicine, **14**, No 4, 1985, 191-198.

17. Linscheid R L and Dobyns J H. Total joint arthroplasty - the hand. Mayo Clin Proc, **54**, 1979, 516-526.

18. Hagert C G. Advances in hand surgery: finger joint implants. Surg Ann, **10**, 1978, 253-275.

19. Unsworth A, Dowson D and Wright V. Cracking joints - a bioengineering study of cavitation in the metacarpophalangeal joint. Ann Rheum Dis, **30**, 1971, 348-357.

20. Unsworth A and Alexander W J. Dimensions of the metacarpophalangeal joint with particular reference to joint prostheses. Engineering in Medicine, **8**, No 2, 1979, 75-80.

21. Aleksandrowicz R, Pagowski S and Seyfried A. Anatomic-geometric and kinematic analysis of the metacarpophalangeal articulation of the III digit of human hand. Folia Morphol (Warsz), **XXXIII**, No 4, 1974, 353-361.

22. Pagowski S and Piekarski K. Biomechanics of metacarpophalangeal joint. J Biomechanics, **10**, 1977, 205-209.

23. Bartel D L, Fischer G W and Flatt A E. An investigation of human finger joint motion using the method of overdetermined collocation. Proc Annu Conf Eng Med Biol, **10**, No 26, 1968, A8.

24. Youm Y. Instantaneous centre of rotation by least square method. J Bioeng, **2**, 1978, 129-137.

25. Tubiana R and Toth B. Rheumatoid arthritis: clinical types of deformities and management. Clin Rheum Dis, **10**, No 3, 1984, 521-547.

26. Burke F. The effects of rheumatoid diseases of the hand. Clin Rheum Dis, **10**, No 3, 1984, 435-448.

27. Beckenbaugh R D and Linscheid R L. Arthroplasty in the hand and wrist. "Operative hand surgery" (Ed. D P Green), 2nd edition, 1989, Churchill-Livingstone, New York, 141-184.

28. Minami A, An K N, Cooney W P, Linscheid R L and Chao E Y. Ligamentous structures of the metacarpophalangeal joint: a quantitative anatomic study. J Orthop Res, **1**, No 4, 1984, 361-368.

29. Minami A, An K N, Cooney W P, Linscheid R L and Chao E Y. Ligament stability of the metacarpophalangeal joint: a biomechanical study. J Hand Surg, **10A**, No 2, 1985, 255-260.

30. Linscheid R L and Chao E Y. Biomechanical assessment of finger function in prosthetic joint design. Orthop Clin North Amer, **4**, No 2, 1973, 317-330.

31. Hakstian R W and Tubiana R. Ulnar deviation of the fingers - the role of joint structure and function. J Bone Joint Surg, **49A**, No 2, 1967, 299-316.

32. Smith R J and Kaplan E B. Rheumatoid deformities at the metacarpophalangeal joints of the fingers - a correlative study of anatomy and pathology. J Bone Joint Surg, **49A**, No 1, 1967, 31-47.

33. Harrison S H. The rheumatoid hand. Clin Rheum Dis, **4**, No 2, 1978, 403.

34. Gschwend N. Present trends in joint replacement. Private communication (transcript of presentation given 16 July 1987).

35. Urbaniak J R, McCollum D E and Goldner J L. Metacarpophalangeal and interphalangeal joint reconstruction: use of silicone rubber-Dacron prostheses for replacement of irreparable joints of the hand. Southern Med Journ, **63**, No 11, 1970, 1281-1290.

36. Nalebuff E A. Rheumatoid hand surgery - update. J Hand Surg, **8**, No 5, 1983, 678-682.

37. Swanson A B and de Groot Swanson G. Flexible implant arthroplasty in the rheumatoid metacarpophalangeal joint. Clin Rheum Dis, **10**, No 3, 1984, 609-629.

38. Flatt A E. "Care of the arthritic hand", 4th edition, 1983, St Louis, C V Mosby Co, London.

39. Flatt A E. Studies in finger joint replacement - a review of the present position. Arch Surg, **107**, 1973, 437-443.

40. Flatt A E. Prosthetic joints. "Symposium in reconstructive hand surgery" (Eds. Littler, Cramner and Smith), 1974, St Louis, C V Mosby Co, 229-232.

41. Brannon E W and Klein G. Experiences with a finger joint prosthesis. J Bone Joint Surg, **41A**, 1959, 87-102.

42. Girzadas D V and Clayton M L. Limitations of the use of metallic prosthesis in the rheumatoid hand. Clin Orthop Rel Res, **67**, 1969, 127-132.

43. Flatt A E and Ellison M R. Restoration of rheumatoid finger joint function - a follow-up note after fourteen years of experience with a metallic-hinged prosthesis. J Bone Joint Surg, **54A**, 1972, 1317-1322.

44. Blair W F, Shurr D G and Buckwalter J A. Metacarpophalangeal joint arthroplasty with a metallic hinged prosthesis. Clin Orthop Rel Res, **184**, 1984, 156-163.

45. Calnan J S and Reis N D. The development and use of an artificial finger joint. Biomed Eng, **3**, No 7, 1968, 314-319.

46. Nicolle F V and Calnan J S. A new design of finger joint prosthesis for the rheumatoid hand. Hand, **4**, 1972, 135-146.

47. Nicolle F V. Modified design of encapsulated metacarpophalangeal joint prosthesis for the rheumatoid hand. "Joint replacement in the upper limb", IMechE conf publications, C169/77, 1977, 133-135.

48. Evans D M. Private communication, 1989.

49. Niebauer J J, Shaw J L and Doren W W. Silicone-Dacron hinge prosthesis: design, evaluation, and application. Ann Rheum Dis, **28**(suppl), 1969, 56-58.

50. Hagert C G. Metacarpophalangeal joint implants - III: Roentgenographic study of the in-vivo function. Scand J Plast Reconstr Surg, **9**, 1975, 216-226.

51. Goldner J L and Urbaniak J R. The clinical experience with silicone-Dacron metacarpophalangeal and interphalangeal joint prosthesis. J Biomed Mater Res Symp, **4**, 1973, 137-163.

52. Derkash R S, Niebauer J J and Lane C S. Long-term follow-up of metacarpal phalangeal arthroplasty with silicone Dacron prostheses. J Hand Surg, **11A**, No 4, 1986, 553-558.

53. Beckenbaugh R D, Dobyns J H, Linscheid R L and Bryan R S. Review and analysis of silicone-rubber metacarpophalangeal implants. J Bone Joint Surg, **58A**, No 4, 1976, 483-487.

54. Blair W F, Shurr D G and Buckwalter J A. Metacarpophalangeal joint implant arthroplasty with a Silastic spacer. J Bone Joint Surg, **66A**, No 3, 1984, 365-370.

55. Fleming S G and Hay E L. Metacarpophalangeal joint arthroplasty: eleven year follow-up study. J Hand Surg, **9B**, No 3, 1984, 300-302.

56. Hagert C G, Eiken O, Ohlsson N M, Aschan W and Movin A. Metacarpophalangeal joint implants - I: Roentgenographic study on the Silastic finger joint implant, Swanson design. Scand J Plast Reconstr Surg, **9**, 1975, 147-157.

57. Walker P S, Nunamaker D, Huiskes R, Parchinski T and Greene D. A new approach to the fixation of a metacarpophalangeal joint prosthesis. Engineering in Medicine, **12**, No 3, 1983, 135-140.

58. Vahvanen V and Viljakka T. Silicone rubber implant arthroplasty of the metacarpophalangeal joint in rheumatoid arthritis: a follow-up study of 32 patients. J Hand Surg, **11A**, No 3, 1986, 333-339.

59. Swanson A B, Poitevin L A, de Groot Swanson G and Kearney J. Bone remodeling phenomena in flexible implant arthroplasty in the metacarpophalangeal joints - long-term study. Clin Orthop Rel Res, **205**, 1986, 254-267.

60. Beckenbaugh R D. Private communication, 1989.

61. Bieber E J, Weiland A J and Volenec-Dowling S. Silicone-rubber implant arthroplasty of the metacarpophalangeal joints for rheumatoid arthritis. J Bone Joint Surg, **68A**, No 2, 1986, 206-209.

62. Mannerfelt L and Andersson K. Silastic arthroplasty of the metacarpophalangeal joints in rheumatoid arthritis - long-term results. J Bone Joint Surg, **57A**, No 4, 1975, 484-489.

63. Linscheid R L. Private communication, 1989.

64. Stellbrink G, Zippel J and Englert H M. Fingergelenkprothesen Modell 'St Georg'. Handchirurgie, **3**, 1971, 83.

65. Gillespie T E, Flatt A E, Youm Y and Sprague B L. Biomechanical evaluation of metacarpophalangeal joint prosthesis designs. J Hand Surg, **4**, No 6, 1979, 508-521.

66. Englert H M. Nachuntersuchungsergebnisse von Swanson-Fingergelenkendoprothesen und den St Georger Modellen. Handchirurgie, **5**, 1973, 15-28.

67. Englert H M. Erfahrungen mit der Fingergrundgelensendoprothese Modell St Georg. Z Orthop, **113**, 1975, 487-491.

68. Devas M and Shah V. Link arthroplasty of the metacarpophalangeal joints - a preliminary report of a new method. J Bone Joint Surg, **57B**, No 1, 1975, 72-77.

69. Schetrumpf J. A new metacarpophalangeal joint prosthesis. Hand, **7**, No 1, 1975, 75-77.

70. Doi K, Kuwata N and Kawai S. Alumina ceramic finger implants: a preliminary biomaterial and clinical evaluation. J Hand Surg, **9A**, No 5, 1984, 740-749.

71. Minami M, Yamazaki J, Kato S and Ishii S. Alumina ceramic prosthesis arthroplasty of the metacarpophalangeal joint in the rheumatoid hand - a 2-4 year follow-up study. J Arthroplasty, **3**, No 2, 1988, 157-166.

72. Welsh R P, Hastings D E and White R. Resurfacing arthroplasty for the metacarpophalangeal joint. Acta Orthop Belg, **48**, 1982, 924-927.

73. Seedhom B B, Longton E B, Dowson D and Wright V. The Leeds knee. "Total knee replacement", 1975, Institution of Mechanical Engineers, London, 108-114.

74. Insall J, Ranawat C J, Scott W N and Walker P S. Total Condylar knee replacement: preliminary report. Clin Orthop Rel Res, **120**, 1976, 149-154.

75. Ewald F C, Scheinberg R D, Poss R, Thomas W H, Scott R D and Sledge C B. Capitellocondylar total elbow arthroplasty two to five year follow-up in rheumatoid arthritis. J Bone Joint Surg, **62A**, 1980, 1259.

76. Lowe L W, Miller A J, Allum R L and Higginson D W. The development of an unconstrained elbow arthroplasty. J Bone Joint Surg, **66B**, 1984, 243.

77. Cofield R H. Total shoulder arthroplasty with the Neer prosthesis. J Bone Joint Surg, **66A**, 1984, 899.

78. Williams D F. The properties and medical uses of materials - Part 2: effects of the environment on materials. Biomed Eng, **6**, 1971, 106-113.

79. Williams D F. The properties and medical uses of materials - Part 1: structure and mechanical properties of materials. Biomed Eng, **6**, 1971, 62-69.

80. Galante J O, Rostoker W and Doyle J M. Failed femoral stems in total hip prostheses. J Bone Joint Surg, **57A**, No 2, 1975, 230-236.

81. Cahoon J R and Paxton H W. Metallurgical analysis of failed orthopedic implants. J Biomed Mater Res, **2**, 1968, 1-22.

82. Laing P G. Compatibility of biomaterials. Orthop Clin North Amer, **4**, No 2, 1973, 249-273.

83. Ferguson A B, Laing P G, Hodge E S and Akahoshi Y. Characteristics of trace ions released from embedded implants in the rabbit. J Bone Joint Surg, **44A**, 1962, 362.

84. Evans E M, Freeman M A R, Miller A J and Vernon-Roberts B. Metal sensitivity as a cause of bone necrosis and loosening of the prosthesis in total joint replacement. J Bone Joint Surg, **56B**, 1974, 626.

85. Williams D F. The properties and medical uses of materials - Part 3.1: the reactions of tissues to materials. Biomed Eng, **6**, 1971, 152-156.

86. Hamblin D and Carter R L. Sarcoma and joint replacement. J Bone Joint Surg, **66B**, 1984, 625.

87. Penman H G and Ring P A. Osteosarcoma in association with total hip replacement. J Bone Joint Surg, **66B**, 1984, 632.

88. Swann M. Malignant soft-tissue tumor at the site of a total hip replacement. J Bone Joint Surg, **66B**, 1984, 629.

89. Cohen C A and Smith T C. The intraoperative hazard of acrylic bone cement: report of a case. Anaesthesiology, **35**, 1971, 547.

90. Judet R, Siguier M and Judet T. An uncemented total hip prosthesis. J Bone Joint Surg, **57B**, No 3, 1975, 396.

91. Hamaguchi T, Oonishi H, Okabe N, Nabeshima T and Shikita T. Total hip replacement with bioceram-type orthopaedic ceramic implants. Proc Jpn Soc Orthop Ceramic Implants, **1**, 1981, 165-171.

92. Oonishi H, Okabe N, Hamaguchi T and Nabeshima T. Cementless alumina ceramic total knee prosthesis. Proc Jpn Soc Orthop Ceramic Implants, **1**, 1981, 157-160.

93. Calnan J S and Reis N D. The development and use of an artificial finger joint. Biomed Eng, **3**, 1968, 314.

94. Bradley S A. Plastics in heart valves. "Prosthetic heart valves" (Ed. L A Brewer), 1969, C C Thomas, Springfield, Illinois.

95. Meester W D and Swanson A B. In-vivo testing of silicone rubber joint implants for lipid absorption. J Biomed Mater Res, **6**, 1972, 193-199.

96. Weightman B, Simon S, Rose R, Paul I and Radin E. Environmental fatigue testing of Silastic finger joint prostheses. J Biomed Mater Res Symp, **3**, 1972, 15-24.

97. Homsey C A. Biocompatibility in selection of materials for implantation. J Biomed Mater Res, **4**, 1970, 341-356.

98. Amstutz H C. Biomaterials for artificial joints. Orthop Clin North Amer, **4**, No 2, 1973, 235-248.

99. Charnley J. Factors in the design of an artificial hip joint. "Symposium on lubrication and wear in living and artificial human joints", April 1967, Institution of Mechanical Engineers, London.

100. Atkinson J R. An investigation into the wear of ultra-high molecular weight polyethylene when a polyethylene wear pin is loaded against a reciprocating polyethylene counterface lubricated by bovine synovial fluid at ambient temperature (18°C). Private communication, 1976.

101. Bruck S D and Mueller E P. Radiation sterilization of polymeric implant materials. J Biomed Mater Res: Applied Biomaterials, **22**, No A2, 1988, 133-144.

102. Skinner H B and Mabey M F. Soft-tissue response to total hip surface replacement. J Biomed Mater Res, **21**, 1987, 569-584.

103. Wright T M and Bartel D L. The problem of surface damage in polyethylene total knee components. Clin Orthop Rel Res, **205**, 1986, 67-74.

104. Banister A J, Gorrell I B and Roberts R S. The use of linear correlations, between sulphur-nitrogen bond distances and bond angles at NSN and SNS, in the prediction of minimum strain geometries of some sulphur-nitrogen species. J Chem Soc Faraday Trans 2, **81**, 1985, 1783-1794.

105. Swanson A B. Flexible implant arthroplasty for arthritic finger joints: rationale, technique and results of treatment. J Bone Joint Surg, **54A**, 1972, 435.

106. Carmen R and Mutha S C. Lipid absorption by silicone rubber heart valve poppets - in-vivo and in-vitro results. J Biomed Mater Res, **6**, 1972, 327.

107. MacConaill M A. The function of intra-articular fibrocartilages, with special reference to the knee and inferior radio-ulnar joints. J Anatomy (London), **66**, 1932, 210-227.

108. Jones E S. Joint lubrication. Lancet, **i**, 1936, 1043-1044.

109. Charnley J. The lubrication of animal joints. "Proceedings of the symposium on biomechanics", 1959, Institution of Mechanical Engineers, London, 12-22.

110. McCutchen C W. Mechanism of animal joints. Nature (London), **184**, 1959, 1284-1285.

111. McCutchen C W. The frictional properties of animal joints. Wear, **5**, 1962, 1-17.

112. Maroudas A. Hyaluronic acid films. Proc IMechE (London), **181**, Part 3J, 1967, 122-124.

113. Maroudas A. Studies on the formation of hyaluronic acid films. "Lubrication and wear in joints" (Ed. V Wright), 1969, Sector, London, 124-133.

114. Walker P S, Dowson D, Longfield M D and Wright V. 'Boosted lubrication' in synovial joints by fluid entrapment and enrichment. Ann Rheum Dis, **27**, 1968, 512-520.

115. Ling F F. A new model of articular cartilage in human joints. J Lube Tech, Trans ASME, 1974, 449-507.

116. Ogston A G and Stanier J E. The physiological function of hyaluronic acid in synovial fluids; viscous, elastic and lubricant properties. J Physiol (London), **119**, 1953, 244-252.

117. Tanner R I. Calculation of the shear rate in the hip joint lubricant. Appendix 4 of Charnley J, 1959 (109).

118. Tanner R I. An alternative mechanism for the lubrication of synovial joints. Phys Med Biol, **11**, 1966, 119-127.

119. Dowson D. Modes of lubrication in human joints. Proc IMechE (London), **181**, 1967, 45.

120. Scales J, Kelly P and Goddard D. Friction torque studies of total joint replacements - the use of a simulator. "Lubrication and wear in joints" (Ed. V Wright), 1969, Sector, London.

121. Unsworth A. The effects of lubrication in hip joint prostheses. Phys Med Biol, **23**, 1978, 253-268.

122. Cole W. Arthritis, new treatment, new drugs, new hope. Family Circle, **14**, 1979, 145-148.

123. McKellop H. Wear of artificial joint materials - II: twelve-channel wear-screening device: correlation of experimental and clinical results. Engineering in Medicine, **10**, No 3, 1981, 123-136.

124. Clarke I C. Wear of artificial joint materials - I: friction and wear studies: validity of wear-screening protocols. Engineering in Medicine, **10**, No 3, 1981, 115-122.

125. Archard J F. Contact and rubbing of flat surfaces. J Appl Phys, **24**, 1953, 981-988.

126. Dowson D and Wright V. Wear characteristics of prosthetic materials. "Biocompatibility of implant materials", 1976, Sector, London, 14-17.

127. Rose R, Nusbaum H, Schneider H, Ries S, Paul I, Crugnola A, Simon S and Radin E. On the true wear rate of ultra-high molecular weight polyethylene in the total hip prosthesis. J Bone Joint Surg, **62A**, 1980, 537-549.

128. Atkinson J R, Dowling J and Cicek R. Materials for internal prostheses: the present position and possible future developments. Biomaterials, **1**, 1980, 89-96.

129. Rostoker W and Galante J O. Some new studies of the wear behaviour of ultra-high molecular weight polyethylene. J Biomed Mater Res, **10**, 1976, 303-310.

130. Atkinson J R, Brown K J and Dowson D. The wear of high molecular weight polyethylene against dry stainless steel in unidirectional motion. J Lube Tech, Trans ASME, **100**, 1978, 208-218.

131. Charnley J. The wear of materials in the hip joint. "Plastics in medicine and surgery", 1975, Plastics and Rubber Institute, London, 3.1-3.10.

132. Dowson D, Atkinson J R and Brown K J. "Advances in polymer friction and wear" (Ed. L H Lee), 1974, Plenum Press, 533.

133. Walker P S. Friction and wear of artificial joints. "Human joints and their artificial replacements", 1977, C C Thomas, Springfield, Illinois, 368-422.

134. Dowson D. Private communication, 1990.

135. Seedhom B B, Dowson D and Wright V. Wear of solid phase formed high density polyethylene in relation to the life of artificial hips and knees. Wear, **24**, 1973, 35-51.

136. Dumbleton J H, Shen C and Miller E H. A study of the wear of some materials in connection with total hip replacement. Wear, **29**, 1974, 163-171.

137. Shen C and Dumbleton J H. The friction and wear behaviour of irradiated very high molecular weight polyethylene. Wear, **30**, 1974, 349-364.

138. Morrey B F, Stauffer R N, Cooney W P and Chao E Y. Total joint arthroplasty - the role of biomechanics. Mayo Clin Proc, **54**, 1979, 597-601.

139. Rose R M, Crugnola A, Ries M, Cimino W R, Paul I and Radin E L. On the origins of high in-vivo wear rates in polyethylene components of total joint prostheses. Clin Orthop, **145**, 1979, 277.

140. Brekelmans W A M, Poort H W and Slooff T J J H. A new method to analyse the mechanical behaviour of skeletal parts. Acta Orthop Scand, **43**, 1972, 301-317.

141. Huiskes R. Principles and methods of solid biomechanics. "Functional behaviour of orthopaedic biomaterials - Volume 1: Fundamentals" (Eds. P Ducheyne and G Hastings), 1983, CRC Press, Boca Raton, FL, Chapter 5.

142. Huiskes R and Chao E Y. A survey of finite element analysis in orthopedic biomechanics: the first decade. J Biomechanics, **16**, No 6, 1983, 385-409.

APPENDIX 1

SIMULATOR DESIGN CALCULATIONS

DC Motor Characteristics

Maxon DC motor

Nominal voltage	12 V
Max. power output	10.3 W
Max. continuous current	1.2 A
Max. permissible speed	9200 rpm
No load speed	4750 rpm
No load current	35 mA
Stall torque	87.5 mNm
Stall current	3.8 A

Spur gearbox

Reduction ratio	30:1
Max. continuous torque	0.2 Nm
Max. peak torque	0.6 Nm

Pneumatic System Characteristics

Enots K2305 00 0000 double action piston

Bore	40 mm
Area	1256 mm^2
Pressure:thrust ratio	1:125.6
Thrust at 5.5 bw	693 N
Stroke length	25 mm (max.)

Type 5/2 solenoid activation valve

Filter/drier/regulator unit type M2H-201-M3ED

Cam Disc Inertia

Need a flywheel effect but with reasonable acceleration from stationary.

Disc dimensions

Diameter	160 mm
Thickness	31 mm

Disc material

Duralumin, density	2800 kg/m^3

Mass of disc $M_D = \pi(0.08)^2 \times 0.031 \times 2800 = 1.745$ kg

Groove number 1

Inside radius	36 mm
Outside radius	51 mm
Depth	7 mm

Mass of removed material $M_{g1} = \pi(0.051^2-0.036^2) \times 2800 \times 0.007$

$= 0.08$ kg

Groove number 2

Inside radius	44.5 mm
Outside radius	59 mm
Depth	7 mm

Mass of removed material $M_{g2} = \pi(0.059^2-0.0445^2) \times 2800 \times 0.007$

$= 0.092$ kg

Total mass of cam disc $M = 1.745 - 0.08 - 0.092 = 1.573$ kg

Moment of inertia $I = \frac{1}{2}Ma^2 = 0.005$ kgm^2

Max. continuous torque $\Gamma = 0.2$ Nm (gearbox specification)

Therefore:

$$\text{Acceleration } \alpha = \frac{\Gamma}{I} = 40.0 \text{ s}^{-2}$$

which is not too slow.

Static Shaft Loading Calculations

Length of shaft = 150 mm

Centrally point-loaded by cam & 'tendons', P = 220 N

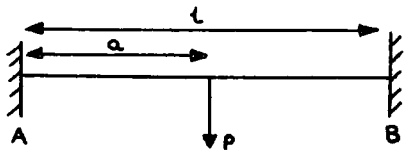

Consider fixed end moments.

At A: $M_{FA} = \dfrac{Pa(1-a)^2}{l^2}$ At B: $M_{FB} = \dfrac{Pa^2(1-a)}{l^2}$

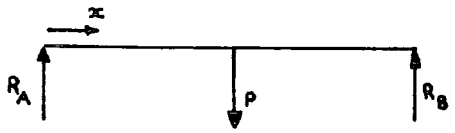

Consider free bending moments on the shaft.

Taking moments about A => $R_B = \dfrac{Pa}{l}$

Balancing forces vertically => $R_A + R_B = P$

Hence $R_A = \dfrac{P}{l}(1-a)$

Consider bending moment at x where $0 \leq x \leq a$:

$$M = R_A x = \frac{P}{l}(1-a)\,x$$

Adding fixed end moments:

$$M = -M_{FA} + (M_{FA}-M_{FB})\frac{x}{l} + \frac{P}{l}(1-a)\,x$$

=>

$$M = -\frac{Pa(1-a)^2}{l^2} + \left[\frac{Pa(1-a)^2}{l^2} - \frac{Pa^2(1-a)}{l^2}\right]\frac{x}{l} + \frac{P}{l}(1-a)\,x$$

=>

$$M = \frac{P(1-a)^2}{l^3}\left[x(1+2a) - al\right]$$

Maximum bending moment occurs at x = a:

$$M = \frac{2P(1-a)^2a^2}{l^3}$$

Substituting P = 220 N, l = 0.15 m, a = 0.075 m gives

$$M = 4.125 \text{ Nm}$$

Maximum stress $\sigma = MR/I$ where R = shaft radius = 6mm, and $I = \pi R^4/4$, so

$$\sigma = \frac{4M}{\pi R^3} = 2.43 \times 10^7 \text{ Nm}^{-2}$$

The yield stress of steel is 37.0×10^7 Nm^{-2}, hence there is no problem of failure.

Beam Deflection

$$M = EI \frac{d^2v}{dx^2}$$

=>

$$EI \frac{dv}{dx} = \frac{P(1-a)^2}{l^3} \left[\frac{x^2}{2} (l+2a) - alx \right] + A$$

=>

$$EIv = \frac{P(1-a)^2}{l^3} \left[\frac{x^3}{6} (l+2a) - \frac{alx^2}{2} \right] + Ax + B$$

Boundary conditions:

$$\frac{dv}{dx} = 0 \text{ at } x = 0 \Rightarrow A = 0$$

$$v = 0 \text{ at } x = 0 \Rightarrow B = 0$$

Hence at x = 75 mm,

$$EIv = -3.867 \times 10^{-3}$$

=>

$$v = \frac{-3.867 \times 10^{-3}}{2 \times 10^{11} \times 1.018 \times 10^{-9}} = 1.899 \times 10^{-5} \text{ m}$$

Hence the deflection is negligible.

Strain Gauge Calculations

Consider the strain-gauged cantilever beam of square cross-section, side b.

Light loading:

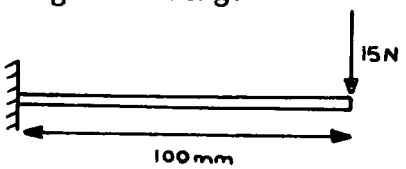

F = 15 N, l = 100 mm

b = 5 mm, E = 2×10^{11} N/m^2

Moment $M = F \times l = 1.5$ Nm

$$I = \frac{b^4}{12} = \frac{(0.005)^4}{12} = 5.2 \times 10^{-11}\ m^4$$

$$\text{Stress } \sigma = \frac{Mb}{2I} = \frac{1.5 \times 0.005}{2 \times 5.2 \times 10^{-11}} = 7.2 \times 10^{7}\ Nm^{-2}$$

=>

$$\text{Strain } \epsilon = \frac{\sigma}{E} = \frac{7.2 \times 10^{7}}{2 \times 10^{11}} = 360\ \mu\epsilon$$ -> suitable gauge chosen.

Heavy loading:

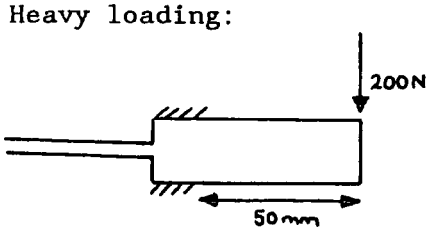

F = 200 N, l = 50 mm

b = 10 mm, E = 2×10^{11} N/m^2

Moment $M = F \times l = 10$ Nm

$$I = \frac{b^4}{12} = \frac{(0.01)^4}{12} = 8.33 \times 10^{-10}\ m^4$$

$$\text{Stress } \sigma = \frac{Mb}{2I} = \frac{10 \times 0.01}{2 \times 8.33 \times 10^{-10}} = 6.0 \times 10^{7}\ Nm^{-2}$$

=>

$$\text{Strain } \epsilon = \frac{\sigma}{E} = \frac{6.0 \times 10^{7}}{2 \times 10^{11}} = 300\ \mu\epsilon$$ -> suitable gauge chosen.

Deflection under light loading:

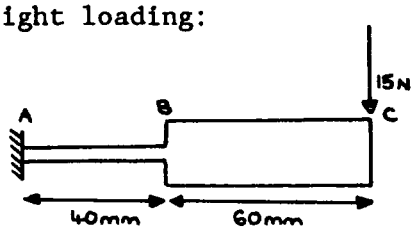

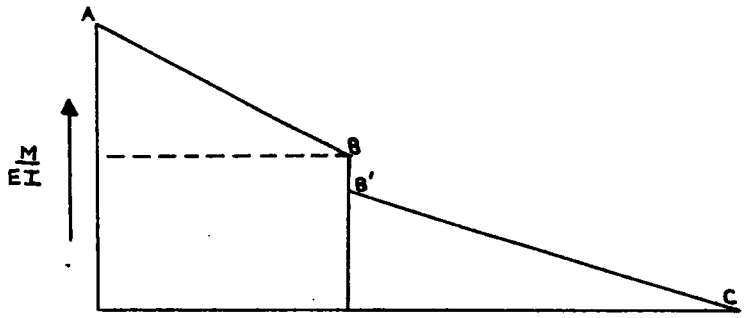

At A $\quad \frac{M}{EI} = \frac{15 \times 0.1}{2 \times 10^{11} \times 5.2 \times 10^{-11}} = 0.144 \text{ m}^{-1}$

At B $\quad \frac{M}{EI} = \frac{15 \times 0.06}{2 \times 10^{11} \times 5.2 \times 10^{-11}} = 0.0865 \text{ m}^{-1}$

At B' $\quad \frac{M}{EI} = \frac{15 \times 0.06}{2 \times 10^{11} \times 8.33 \times 10^{-10}} = 0.0054 \text{ m}^{-1}$

Sum of the moments of the M/EI diagram to calculate the deflection:-

$$\delta = \frac{(0.144-0.0865) \times 0.04}{2} \left[0.06 + \frac{2 \times 0.04}{3} \right]$$

$$+ (0.0865 \times 0.04) \, [0.06 + 0.02]$$

$$+ \frac{(0.0054 \times 0.06)}{2} \left[\frac{2 \times 0.06}{3} \right]$$

$$= 3.8 \times 10^{-4} \text{ m} \rightarrow \text{very small.}$$

Deflection under a heavy load:

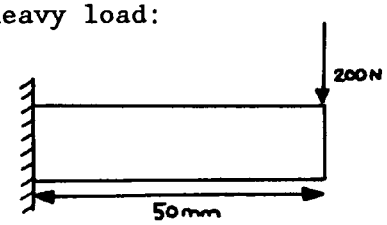

$$\delta = \frac{Fl^3}{3EI} = \frac{200 \times (0.05)^3}{3 \times 2 \times 10^{11} \times 8.33 \times 10^{-10}} = 5 \times 10^{-5} \text{ m} \rightarrow \text{very small.}$$

APPENDIX 2

SIMULATOR PROGRAMS

Simulator data collection program

```
 10 REM
 20 REM                  PROGRAM MENU
 30 REM
 40 DIM d%(20)
 50 DIM e%(20)
 60 DIM s%(20)
 70 DIM f%(20)
 80 DIM r%(20)
 90 DIM g%(20)
100 DIM w%(20)
110 DIM h%(20)
120 DIM s(20)
130 DIM d(20)
140 DIM r(20)
150 DIM w(20)
160 DIM H$(4)
170 DIM J$(5)
180 DIM T%(20)
190 DIM F$(3)
200 DIM F%(3)
210 DIM A(20)
220 DIM A%(20)
230 DIM binary%(12)
240 DIM sa$(20)
250 DIM sb$(20)
260 MODE 135
270 DIM D$(4)
280 D$(1)="Run Tests."
290 D$(2)="Display Data."
300 D$(3)="Display Graphs."
310 D$(4)="Help."
320 J$(1)="View the same data again."
330 J$(2)="Choose another file."
340 J$(3)="Look at the stored files."
350 J$(4)="Go back to the menu."
360 J$(5)="Get a hard copy of data."
370 H$(1)="Resultant Force against                Angle of Flexion/Time."
380 H$(2)="Angle of Force against                 Angle of Flexion/Time."
390 H$(3)="Lateral Force against                  Angle of Flexion/Time."
400 H$(4)="Forward Force against                  Angle of Flexion/Time."
410 *KEY3 CHAIN"MENU"¦M
420 VDU 23,1;0;0;0;0;
430 CLS
440 CLG
450 PRINT
460 REM
470 REM                      FIRST PAGE
480 REM
490 PRINT CHR$151;
500 FOR I=1 TO 37
510 PRINT CHR$175;
520 NEXT
530 PRINT TAB(5)CHR$141;CHR$151"FINGER FUNCTION SIMULATOR"
540 PRINT TAB(5)CHR$141;CHR$151"FINGER FUNCTION SIMULATOR"
550 PRINT CHR$151;
560 FOR I=1 TO 37
```

```
570 PRINT CHR$175;:NEXT
580 PRINT
590 PRINT "        Select program required-"
600 @%=6
610 FOR I=1 TO 4
620 PRINT I;".   ";D$(I)
630 NEXT
640 PRINT
650 PRINT
660 PRINT
670 PRINT CHR$151;:FOR I=1 TO 37:PRINT CHR$175;:NEXT
680 PRINT
690 PRINT SPC(1)CHR$137;CHR$135;"     Please ensure that the"
700 PRINT SPC(1)CHR$137;CHR$135;"     results disc is loaded"
710 PRINT SPC(1)CHR$137;CHR$135;"     into drive 1."
720 PRINT CHR$151;:FOR I=1 TO 37:PRINT CHR$175;:NEXT
730 REPEAT
740 *FX21,0
750 A=GET
760 UNTIL A>48 AND A<53
770 PRINT TAB(0,A-40-(-1)*(A-50))CHR$134;CHR$136;"]";CHR$137;
780 FOR I=1 TO 7000
790 NEXT
800 A=A-48
810 REM
820 REM                  TAKE CHOICE
830 REM
840 ON A GOTO 880,3670,5050,850
850 *MOUNT0
860 *DIR
870 CHAIN "$.HELP1"
880 REM
890 REM      CHOICE 1. RUN TEST
900 REM
910 CLS
920 CLG
930 VDU 26
940 PROCoption1
950 MODE 135
960 PROCstoredata
970 GOTO 2920
980 DEFPROCoption1
990 REM
1000 REM SET UP PAGE FOR OPTION 1.
1010 REM
1020 CLS
1030 VDU 23,1,0;0;0;0
1040 CLS
1050 CLG
1060 PRINT CHR$(135);CHR$(157);CHR$(132);CHR$(141)"         COLLECT DATA"
1070 PRINT CHR$(135);CHR$(157);CHR$(132);CHR$(141)"         COLLECT DATA"
1080 PRINT TAB(1,3) "File Name........."
1090 PRINT TAB(1,11) "Test Description...."
1100 PRINT TAB(1,7) "Which Bridge?....1) HALF  2) FULL"
1110 PRINT TAB(1,15) "Input Speed (1/100 s)...."
1120 VDU 23,1,1;0;0;0
1130 PRINT TAB(1,24) "                        "
1140 REM
```

```
1150 REM        INPUT FILE NAME
1160 REM
1170 PRINT TAB(18,3);
1180 INPUT""Ref$
1190 REM
1200 REM           INPUT BRIDGE
1210 REM
1220 PRINT TAB(18,7);
1230 REPEAT
1240 A$=GET$
1250 UNTIL A$="1" OR A$="2"
1260 IF A$="1" THEN L$="HALF"
1270 IF A$="2" THEN L$="FULL"
1280 PRINT TAB(18,7);L$;"               "
1290 REM
1300 REM       INPUT FILE INFORMATION
1310 REM
1320 PRINT TAB(20,11);
1330 INPUT""Des$
1340 REM            INPUT SPEED
1350 PRINT TAB(24,15);
1360 INPUT""P
1370 VDU 23,1,0;0;0;0;0
1380 PRINT TAB(1,18) "Do you wish to alter anything? (Y/N)"
1390 B$=GET$
1400 IF B$="Y" GOTO 1040
1410 IF B$="N" GOTO 1420 ELSE GOTO 1390
1420 ENDPROC
1430 REM
1440 REM            TAKE TWENTY READINGS
1450 REM
1460 DEFPROCstoredata
1470 *MOUNT 1
1480 *DIR
1490 PROCpage
1500 TIME=0
1510 Tr=TIME
1520 *IEEE
1530 cmd%=OPENIN("COMMAND")
1540 data%=OPENIN("DATA")
1550 PRINT£ cmd%,"BBC DEVICE NO",0
1560 PRINT£ cmd%,"CLEAR"
1570 PRINT£ cmd%,"REMOTE ENABLE"
1580 PRINT£ cmd%,"END OF STRING",CHR$(13)
1590 FOR I%=1 TO 20
1600 fwdbridge%=OPENIN("7,1")
1610 PRINT£ cmd%,"UNLISTEN"
1620 PRINT£ cmd%,"LISTEN",fwdbridge%,"EXECUTE"
1630 PRINT£ data%,"1000mstrain1"
1640 PRINT£ cmd%,"UNLISTEN"
1650 PRINT£ cmd%,"TALK",fwdbridge%
1660 INPUT£ data%,sa$(I%)
1670 PRINT£ cmd%,"UNTALK"
1680 CLOSE£ fwdbridge%
1690 sidbridge%=OPENIN("7,2")
1700 PRINT£ cmd%,"UNLISTEN"
1710 PRINT£ cmd%,"LISTEN",sidbridge%,"EXECUTE"
1720 PRINT£ data%,"1000mstrain2"
```

```
1730 PRINT£ cmd%,"UNLISTEN"
1740 PRINT£ cmd%,"TALK",sidbridge%
1750 INPUT£ data%,sb$(I%)
1760 PRINT£ cmd%,"UNTALK"
1770 CLOSE£ sidbridge%
1780 T%(I%)=TIME
1790 NEXT I%
1800 CLOSE£ data%
1810 CLOSE£ cmd%
1820 REM
1830 REM                CONVERT TO DECIMAL
1840 REM
1850 FOR I%=1 TO 20
1860 F$(1)=LEFT$(sa$(I%),1)
1870 F$(2)=MID$(sa$(I%),2,1)
1880 F$(3)=RIGHT$(sa$(I%),1)
1890 FOR number=1 TO 2
1900 FOR M=1 TO 3
1910 IF F$(M)="@" THEN F%(M)=0
1920 IF F$(M)="A" THEN F%(M)=1
1930 IF F$(M)="B" THEN F%(M)=2
1940 IF F$(M)="C" THEN F%(M)=3
1950 IF F$(M)="D" THEN F%(M)=4
1960 IF F$(M)="E" THEN F%(M)=5
1970 IF F$(M)="F" THEN F%(M)=6
1980 IF F$(M)="G" THEN F%(M)=7
1990 IF F$(M)="H" THEN F%(M)=8
2000 IF F$(M)="I" THEN F%(M)=9
2010 IF F$(M)="J" THEN F%(M)=10
2020 IF F$(M)="K" THEN F%(M)=11
2030 IF F$(M)="L" THEN F%(M)=12
2040 IF F$(M)="M" THEN F%(M)=13
2050 IF F$(M)="N" THEN F%(M)=14
2060 IF F$(M)="O" THEN F%(M)=15
2070 NEXT M
2080 A=F%(1)
2090 B=F%(2)
2100 C=F%(3)
2110 I=4
2120 N=8
2130 count=1
2140 D=A/N
2150 IF D>=1 THEN D=1 ELSE D=0
2160 binary%(count)=D
2170 A=A-(N*D)
2180 N=N/2
2190 count=count+1
2200 IF count<=I THEN GOTO 2140
2210 I=I+4
2220 N=8
2230 A=B
2240 B=C
2250 IF I<>16 THEN GOTO 2140
2260 N=2048
2270 IF number=2 THEN GOTO 2370
2280 d%=0
2290 FOR J=1 TO 12
2300 d%=(binary%(J)*N)+d%
```

```
 2310 N=N/2
 2320 NEXT J
 2330 F$(1)=LEFT$(sb$(I%),1)
 2340 F$(2)=MID$(sb$(I%),2,1)
 2350 F$(3)=RIGHT$(sb$(I%),1)
 2360 NEXT number
 2370 s%=0
 2380 FOR J=1 TO 12
 2390 s%=(binary%(J)*N)+s%
 2400 N=N/2
 2410 NEXT J
 2420 REM
 2430 REM              CHOOSE FULL OR HALF BRIDGE
 2440 REM
 2450 IF L$="FULL" THEN GOTO 2490
 2460 d%=d%/(4.095*0.1387)
 2470 s%=s%/(4.095*0.1835)
 2480 GOTO 2510
 2490 d%=d%/(4.095*0.01444)
 2500 s%=s%/(4.095*0.01348)
 2510 e%(I%)=d% MOD 100
 2520 f%(I%)=s% MOD 100
 2530 d(I%)=d%/100
 2540 s(I%)=s%/100
 2550 d%(I%)=d% DIV 100
 2560 s%(I%)=s% DIV 100
 2570 REM
 2580 REM                   CALCULATE RESULTANT FORCE
 2590 REM
 2600 r(I%)=(d(I%)*d(I%))+(s(I%)*s(I%))
 2610 r%=SQR(r(I%))*100
 2620 g%(I%)=r% MOD 100
 2630 r(I%)=r%/100
 2640 r%(I%)=r% DIV 100
 2650 REM
 2660 REM                       CALCULATE ANGLE OF FORCE TO MC
 2670 REM
 2680 IF d(I%)=0 THEN w(I%)=90 ELSE w(I%)=DEG(ATN(s(I%)/d(I%)))
 2690 w%=w(I%)*100
 2700 h%(I%)=w% MOD 100
 2710 w(I%)=w%/100
 2720 w%(I%)=w% DIV 100
 2730 @%=&0002020A
 2740 NEXT I%
 2750 REM
 2760 REM        PUT TIME, FORCE, ANGLE OF FORCE, ANGLE OF FLEXION,
 2770 REM        BOTH COMPONENTS OF FORCE AND A DESCRIPTION OF FILE.
 2780 REM
 2790 *ADFS
 2800 file=OPENOUT(Ref$)
 2810 FOR I%=1 TO 20
 2820 PROCconvert
 2830 IF I%<>1 THEN GOTO 2860
 2840 PRINT£ file,P,A$,Des$,A(I%),T%(I%),s(I%),d(I%),r(I%),w(I%),s%(I%),d%(I%)
,r%(I%),w%(I%),e%(I%),f%(I%),g%(I%),h%(I%)
 2850 GOTO 2870
 2860 PRINT£ file,A(I%),T%(I%),s(I%),d(I%),r(I%),w(I%),s%(I%),d%(I%),r%(I%),w%
(I%),e%(I%),f%(I%),g%(I%),h%(I%)
```

```
2870 NEXT I%
2880 CLOSE£ file
2890 *ADFS
2900 *MOUNT 0
2910 ENDPROC
2920 CLS
2930 VDU 23,1,0;0;0;0
2940 CLS
2950 CLG
2960 PRINT CHR$(135);CHR$(157);CHR$(132);CHR$(141)"          COLLECT DATA"
2970 PRINT CHR$(135);CHR$(157);CHR$(132);CHR$(141)"          COLLECT DATA"
2980 PRINT TAB(1,3) "FILE NAME........."
2990 PRINT TAB(1,7) "BRIDGE............"
3000 PRINT TAB(1,11) "TEST DESCRIPTION...."
3010 VDU 23,1,1;0;0;0
3020 PRINT TAB(1,24)"                      "
3030 PRINT TAB(18,3);Ref$
3040 PRINT TAB(18,7);L$
3050 PRINT TAB(20,11);Des$
3060 PRINT
3070 PRINT
3080 PRINT CHR$134;CHR$136;"          TESTING COMPLETED";CHR$137
3090 PRINT
3100 PRINT
3110 PRINT
3120 PRINT CHR$151;:FOR I=1 TO 37:PRINT CHR$175;:NEXT
3130 PRINT CHR$135;"          Would you like to:"
3140 PRINT
3150 PRINT "(1)Take more readings, (2)Go to menu."
3160 PRINT CHR$151;:FOR I=1 TO 37:PRINT CHR$175;:NEXT
3170 *FX21,0
3180 E$=GET$
3190 IF E$="1" THEN GOTO 940
3200 IF E$="2" THEN GOTO 420 ELSE GOTO 3180
3210 REM
3220 REM          CONVERT TIMES TO ANGLES OF FLEXION
3230 REM
3240 DEFPROCconvert
3250 IF T%(I%)<=P THEN A%(I%)=(90*T%(I%)/P)
3260 IF T%(I%)>P AND T%(I%)<=P*2 THEN A%(I%)=(180-(90*T%(I%)/P))
3270 IF T%(I%)>P*2 AND T%(I%)<=P*3 THEN A%(I%)=(-180+(90*T%(I%)/P))
3280 IF T%(I%)>P*3 AND T%(I%)<=P*4 THEN A%(I%)=(360-(90*T%(I%)/P))
3290 IF T%(I%)>P*4 AND T%(I%)<=P*5 THEN A%(I%)=(-360+(90*T%(I%)/P))
3300 IF T%(I%)>P*5 AND T%(I%)<=P*6 THEN A%(I%)=(540-(90*T%(I%)/P))
3302 IF T%(I%)>P*6 AND T%(I%)<=P*7 THEN A%(I%)=(-540+(90*T%(I%)/P))
3303 IF T%(I%)>P*7 AND T%(I%)<=P*8 THEN A%(I%)=(720-(90*T%(I%)/P))
3304 IF T%(I%)>P*8 AND T%(I%)<=P*9 THEN A%(I%)=(-720+(90*T%(I%)/P))
3305 IF T%(I%)>P*9 AND T%(I%)<=P*10 THEN A%(I%)=(900-(90*T%(I%)/P))
3310 A%(I%)=A%(I%)*100
3320 A(I%)=A%(I%)/100
3330 ENDPROC
3340 REM
3350 REM         DISPLAY PAGE WHILE TAKING READINGS
3360 REM
3370 DEFPROCpage
3380 VDU 23,1,1;0;0;0
3390 CLS
3400 CLS
```

```
3410 CLG
3420 PRINT CHR$(135);CHR$(157);CHR$(132);CHR$(141)"          COLLECT DATA"
3430 PRINT CHR$(135);CHR$(157);CHR$(132);CHR$(141)"          COLLECT DATA"
3440 PRINT TAB(1,3) "FILE NAME........."
3450 PRINT TAB(1,7) "BRIDGE............"
3460 PRINT TAB(1,11) "TEST DESCRIPTION...."
3470 VDU 23,1,1;0;0;0
3480 PRINT TAB(1,24)"                    "
3490 PRINT TAB(18,3);Ref$
3500 PRINT TAB(18,7);L$
3510 PRINT TAB(20,11);Des$
3520 PRINT
3530 PRINT
3540 PRINT
3550 PRINT CHR$151;:FOR I=1 TO 37:PRINT CHR$175;:NEXT
3560 PRINT
3570 PRINT SPC(1) CHR$137;CHR$135;"   Please ensure that the joint"
3580 PRINT SPC(1) CHR$137;CHR$135;"   is at 0 deg flexion as the"
3590 PRINT SPC(1) CHR$137;CHR$135;"   space bar is pressed!"
3600 PRINT CHR$151;:FOR I=1 TO 37:PRINT CHR$175;:NEXT
3610 VDU 23,1,0;0;0;0;0
3620 PRINT TAB(1,23) "    PRESS SPACE BAR TO START TEST"
3630 IF INKEY-99 GOTO 3650
3640 GOTO 3620
3650 PRINT TAB(1,23) CHR$134;CHR$136;"         TAKING READINS       ";CHR$137
3660 ENDPROC
3670 *MOUNT 1
3680 *DIR
3690 CLS
3700 CLG
3710 VDU 23,1,0;0;0;0
3720 CLS
3730 PRINT CHR$135;CHR$157;CHR$132;CHR$141"          VIEW DATA"
3740 PRINT CHR$135;CHR$157;CHR$132;CHR$141"          VIEW DATA"
3750 PRINT
3760 PRINT "Do you want to see stored files? (Y/N)"
3770 C$=GET$
3780 IF C$="Y" GOTO 3800
3790 IF C$="N" GOTO 3830 ELSE GOTO 3770
3800 PROCcat
3810 IF INKEY-99 GOTO 4010
3820 GOTO 3810
4010 CLS
4020 CLG
4030 VDU 23,1,0;0;0;0
4040 CLS
4050 PRINT CHR$135;CHR$157;CHR$132;CHR$141"          VIEW DATA"
4060 PRINT CHR$135;CHR$157;CHR$132;CHR$141"          VIEW DATA"
4070 PRINT
4080 PRINT TAB(1,3) "Filename?........."
4090 PRINT TAB(18,3);
4100 INPUT""File$
4110 that_one=OPENIN(File$)
4120 INPUT£ that_one,P,A$,Des$
4130 FOR I=1 TO 20
4140 INPUT£ that_one,A(I),T%(I),s(I),d(I),r(I),w(I),s%(I),d%(I),r%(I),w%(I),e
%(I),f%(I),g%(I),h%(I)
4150 NEXT
```

```
4160 CLOSE£ that_one
4170 PRINT "Speed...";P;"  Description....";Des$
4180 PRINT "ANG FLX(DEG)  FORCE(N)  ANG FORCE(DEG)"
4190 FOR I=1 TO 20
4200 IF g%(I)<10 AND h%(I)<10 GOTO 4290
4210 IF g%(I)<10 AND h%(I)>=10 GOTO 4270
4220 IF g%(I)>=10 AND h%(I)<10 GOTO 4250
4230 PRINT A(I),"      ",r%(I);".";g%(I);"      ";w%(I);".";h%(I)
4240 GOTO 4300
4250 PRINT A(I),"      ",r%(I);".";g%(I);"      ";w%(I);".0";h%(I)
4260 GOTO 4300
4270 PRINT A(I),"      ",r%(I);".0";g%(I);"      ";w%(I);".";h%(I)
4280 GOTO 4300
4290 PRINT A(I),"      ",r%(I);".0";g%(I);"      ";w%(I);".0";h%(I)
4300 NEXT
4310 IF INKEY-99 GOTO 4330
4320 GOTO 4310
4330 CLS
4340 CLG
4350 VDU 23,1,0;0;0;0
4360 CLS
4370 PRINT CHR$135;CHR$157;CHR$132;CHR$141"          VIEW DATA"
4380 PRINT CHR$135;CHR$157;CHR$132;CHR$141"          VIEW DATA"
4390 PRINT
4400 PRINT TAB(1,3) "Filename.........";File$
4410 PRINT " Description....";Des$
4420 PRINT "LAT FORCE(N) FOR FORCE(N) TIME(1/100s)"
4430 FOR I=1 TO 20
4440 IF e%(I)<10 AND f%(I)<10 GOTO 4530
4450 IF e%(I)<10 AND f%(I)>=10 GOTO 4510
4460 IF e%(I)>=10 AND f%(I)<10 GOTO 4490
4470 PRINT s%(I);".";f%(I),d%(I);".";e%(I),T%(I)
4480 GOTO 4540
4490 PRINT s%(I);".0";f%(I),d%(I);".";e%(I),T%(I)
4500 GOTO 4540
4510 PRINT s%(I);".";f%(I),d%(I);".0";e%(I),T%(I)
4520 GOTO 4540
4530 PRINT s%(I);".0";f%(I),d%(I);".0";e%(I),T%(I)
4540 NEXT
4550 IF INKEY-99 GOTO 4570
4560 GOTO 4550
4570 CLS
4580 CLG
4590 VDU 23,1,0;0;0;0
4600 CLS
4610 PRINT CHR$135;CHR$157;CHR$132;CHR$141"          VIEW DATA"
4620 PRINT CHR$135;CHR$157;CHR$132;CHR$141"          VIEW DATA"
4630 PRINT
4640 PRINT "CHOOSE FROM THE FOLLOWING OPTIONS:-"
4650 @%=6
4660 FOR I=1 TO 5
4670 PRINT I;".    ";J$(I)
4680 NEXT
4690 PRINT
4700 PRINT
4710 PRINT
4720 REPEAT
4730 K=GET
```

```
4740 UNTIL K>48 AND K<54
4750 PRINT TAB(0,K-41-(-2)*(K-50))CHR$134;CHR$136;"]";CHR$137;
4760 FOR I=1 TO 7000
4770 NEXT
4780 K=K-48
4790 ON K GOTO 4800,4010,4900,420,5210
4800 CLS
4810 CLG
4820 VDU 23,1,0;0;0;0
4830 CLS
4840 PRINT CHR$135;CHR$157;CHR$132;CHR$141"          VIEW DATA"
4850 PRINT CHR$135;CHR$157;CHR$132;CHR$141"          VIEW DATA"
4860 PRINT
4870 PRINT
4880 PRINT TAB(1,3)"FILENAME.........";File$
4890 GOTO 4170
4900 CLS
4910 CLG
4920 VDU 23,1,0;0;0;0
4930 CLS
4940 PRINT CHR$135;CHR$157;CHR$132;CHR$141"          VIEW DATA"
4950 PRINT CHR$135;CHR$157;CHR$132;CHR$141"          VIEW DATA"
4960 PROCcat
4970 IF INKEY-99 GOTO 4010
4980 GOTO 4970
4990 DEFPROCcat
5000 PRINT
5010 *CAT
5020 PRINT
5030 PRINT TAB(1,23) "    PRESS SPACE BAR TO CONTINUE"
5040 ENDPROC
5050 *MOUNT 1
5060 *DIR
5070 CLS
5080 CLG
5090 VDU 23,1,0;0;0;0
5100 CLS
5110 PRINT CHR$135;CHR$157;CHR$132;CHR$141"          VIEW GRAPHS"
5120 PRINT CHR$135;CHR$157;CHR$132;CHR$141"          VIEW GRAPHS"
5130 PRINT
5140 PRINT "Do you want to see stored files? (Y/N)"
5150 F$=GET$
5160 IF F$="Y" GOTO 5180
5170 IF F$="N" GOTO 5540 ELSE GOTO 5150
5180 PROCcat
5190 IF INKEY-99 GOTO 5540
5200 GOTO 5190
5210 CLS
5220 PRINT "Filename.......";File$
5230 PRINT "Speed...";P;"  Description....";Des$
5240 PRINT "ANG FLX(DEG)  FORCE(N)  ANG FORCE(DEG)"
5250 FOR I=1 TO 20
5260 IF g%(I)<10 AND h%(I)<10 GOTO 5350
5270 IF g%(I)<10 AND h%(I)>=10 GOTO 5330
5280 IF g%(I)>=10 AND h%(I)<10 GOTO 5310
5290 PRINT A(I),"      ",r%(I);".";g%(I);"      ";w%(I);".";h%(I)
5300 GOTO 5360
5310 PRINT A(I),"      ",r%(I);".";g%(I);"      ";w%(I);".0";h%(I)
```

```
5320 GOTO 5360
5330 PRINT A(I),"      ",r%(I);".0";g%(I);"      ";w%(I);".";h%(I)
5340 GOTO 5360
5350 PRINT A(I),"      ",r%(I);".0";g%(I);"      ";w%(I);".0";h%(I)
5360 NEXT
5370 *GDUMP
5380 CLS
5390 PRINT "LAT FORCE(N) FOR FORCE(N) TIME(1/100s)"
5400 FOR I=1 TO 20
5410 IF e%(I)<10 AND f%(I)<10 GOTO 5500
5420 IF e%(I)<10 AND f%(I)>=10 GOTO 5480
5430 IF e%(I)>=10 AND f%(I)<10 GOTO 5460
5440 PRINT s%(I);".";f%(I),d%(I);".";e%(I),T%(I)
5450 GOTO 5510
5460 PRINT s%(I);".0";f%(I),d%(I);".";e%(I),T%(I)
5470 GOTO 5510
5480 PRINT s%(I);".";f%(I),d%(I);".0";e%(I),T%(I)
5490 GOTO 5510
5500 PRINT s%(I);".0";f%(I),d%(I);".0";e%(I),T%(I)
5510 NEXT
5520 *GDUMP
5530 GOTO 4570
5540 CLS
5550 CLG
5560 VDU 23,1,0;0;0;0;0
5570 CLS
5580 PRINT CHR$135;CHR$157;CHR$132;CHR$141"          VIEW GRAPHS"
5590 PRINT CHR$135;CHR$157;CHR$132;CHR$141"          VIEW GRAPHS"
5600 PRINT
5610 PRINT TAB(1,3)"Filename?........"
5620 PRINT TAB(18,3);
5630 INPUT""File$
5640 PRINT TAB(1,3) "Choose from the following:-                                    "
5650 @%=6
5660 FOR J=1 to 4
5670 PRINT J;".   ";H$(J)
5680 NEXT
5690 PRINT
5700 PRINT
5710 PRINT
5720 REPEAT
5730 K=GET
5740 UNTIL K>48 AND K<53
5750 PRINT TAB(0,K-41-(-2)*(K-50))CHR$134;CHR$136;"]";CHR$137;
5760 PRINT TAB(0,K-40-(-2)*(K-50))CHR$134;CHR$136;" ";CHR$137;
5770 FOR I=1 TO 7000
5780 NEXT
5790 K=K-48
5800 ON K GOTO 5810,6260,6310,6400
5810 MODE 128
5820 PROCfile
5830 IF A$="2" GOTO 5870
5840 PROCaxis_one
5850 PROCplot_one
5860 GOTO 5890
5870 PROCaxis_one_a
5880 PROCplot_one_a
5890 PRINT TAB(14,3)"         Do you require a printout? (Y/N)"
```

```
5900 L$=GET$
5910 IF L$="Y" GOTO 5930
5920 IF L$="N" GOTO 6000 ELSE 5900
5930 PRINT TAB(14,3)"                                                    "
5940 *MOUNT 0
5950 *DIR
5960 *LOAD $.EPFX80M 900
5970 CALL &900
5980 *MOUNT 1
5990 *DIR
6000 MODE 135
6010 CLS
6020 CLG
6030 VDU 23,1,0;0;0;0
6040 CLS
6050 PRINT CHR$135;CHR$157;CHR$132;CHR$141"          VIEW GRAPHS"
6060 PRINT CHR$135;CHR$157;CHR$132;CHR$141"          VIEW GRAPHS"
6070 PRINT
6080 PRINT "   Would you like to:"
6090 PRINT
6100 PRINT "   1)View another graph."
6110 PRINT
6120 PRINT "   2)Choose another file."
6130 PRINT
6140 PRINT "   3)Go back to menu."
6150 E$=GET$
6160 IF E$="1" GOTO 6190
6170 IF E$="2" GOTO 5540
6180 IF E$="3" GOTO 420 ELSE GOTO 6150
6190 CLS
6200 CLG
6210 VDU 23,1,0;0;0;0
6220 CLS
6230 PRINT CHR$135;CHR$157;CHR$132;CHR$141"          VIEW GRAPHS"
6240 PRINT CHR$135;CHR$157;CHR$132;CHR$141"          VIEW GRAPHS"
6250 GOTO 5640
6260 MODE 128
6270 PROCfile
6275 IF A$="2" GOTO 6295
6280 PROCaxis_two
6290 PROCplot_two
6291 GOTO 6300
6295 PROCaxis_two_a
6296 PROCplot_two
6300 GOTO 5890
6310 MODE 128
6320 PROCfile
6330 IF A$="1" GOTO 6370
6340 PROCaxis_three_a
6350 PROCplot_three_a
6360 GOTO 6390
6370 PROCaxis_three
6380 PROCplot_three
6390 GOTO 5890
6400 MODE 128
6410 PROCfile
6420 IF A$="1" GOTO 6460
6430 PROCaxis_four_a
```

```
6440 PROCplot_four_a
6450 GOTO 6480
6460 PROCaxis_four
6470 PROCplot_four
6480 GOTO 5890
6490 DEFPROCaxis_one
6500 CLS
6510 CLG
6520 PRINT TAB(20,1)"           Filename.........";File$
6530 VDU 29,100;50;
6540 VDU 5
6550 MOVE 0,0
6560 DRAW 0,900
6570 MOVE 0,0
6580 DRAW 1000,0
6590 FOR J=100 TO 1000 STEP 100
6600 MOVE -10,J
6610 DRAW 10,J
6620 NEXT J
6630 FOR J=500/9 TO 1000 STEP 500/9
6640 MOVE J,10
6650 DRAW J,-10
6660 NEXT J
6670 FOR L=100 TO 1000 STEP 100
6680 W=1000/L
6690 Y=20/W
6700 IF Y>=10 MOVE -95,L+10
6710 IF Y<10 MOVE -80,L+10
6720 PRINT;Y
6730 NEXT L
6740 MOVE -50,950
6750 PRINT "RESULTANT FORCE (N)"
6760 FOR I=500/9 TO 1000 STEP 500/9
6770 X=(I*9) DIV 50
6780 MOVE I-10,-25
6790 IF X>90 GOTO 6820
6800 PRINT;X
6810 GOTO 6840
6820 X=180-X
6830 PRINT;X
6840 NEXT I
6850 MOVE 1000,10
6860 PRINT "ANG.FLEX
                (DEG)"
6870 VDU 4
6880 ENDPROC
6890 DEFPROCplot_one
6900 VDU 5
6910 FOR I%=1 TO 20
6920 T%(I%)=T%(I%) MOD (P*2)
6930 MOVE T%(I%)*500/P-7,r(I%)*50+10
6940 PRINT CHR$42
6950 NEXT
6960 VDU 4
6970 ENDPROC
6980 DEFPROCplot_two
6990 VDU 5
7000 FOR I%=1 TO 20
```

```
7010 T%(I%)=T%(I%) MOD (P*2)
7020 MOVE T%(I%)*500/P-7,w(I%)*10+10
7030 PRINT CHR$42
7040 NEXT
7050 VDU 4
7060 ENDPROC
7070 DEFPROCplot_three
7080 VDU 5
7090 FOR I%=1 TO 20
7100 T%(I%)=T%(I%) MOD (P*2)
7110 MOVE T%(I%)*500/P-7,s(I%)*50+10
7120 PRINT CHR$42
7130 NEXT
7140 VDU 4
7150 ENDPROC
7160 DEFPROCplot_four
7170 VDU 5
7180 FOR I%=1 TO 20
7190 T%(I%)=T%(I%) MOD (P*2)
7200 MOVE T%(I%)*500/P-7,d(I%)*50+10
7210 PRINT CHR$42
7220 NEXT
7230 VDU 4
7240 ENDPROC
7250 DEFPROCfile
7260 that_one=OPENIN(File$)
7270 INPUT£ that_one,P,A$,Des$
7280 I%=0
7290 REPEAT
7300 I%=I%+1
7310 INPUT£ that_one,A(I%),T%(I%),s(I%),d(I%),r(I%),w(I%),s%(I%),d%(I%),r%(I%
),w%(I%),e%(I%),f%(I%),g%(I%),h%(I%)
7320 UNTIL EOF£ that_one
7330 CLOSE£ that_one
7340 ENDPROC
7350 DEFPROCaxis_two
7360 CLS
7370 CLG
7380 PRINT TAB(20,1)"           Filename.....";File$
7390 VDU 29,100;50;
7400 VDU 5
7410 MOVE 0,0
7420 DRAW 0,900
7430 MOVE 0,0
7440 DRAW 1000,0
7450 FOR J=100 TO 1000 STEP 100
7460 MOVE -10,J
7470 DRAW 10,J
7480 NEXT J
7490 FOR J=500/9 TO 1000 STEP 500/9
7500 MOVE J,10
7510 DRAW J,-10
7520 NEXT J
7530 FOR L=100 TO 1000 STEP 100
7540 W=L/10
7550 MOVE -95,L+10
7560 PRINT;W
7570 NEXT L
```

```
7580 MOVE -50,950
7590 PRINT "ANGLE OF FORCE (DEG)"
7600 FOR I=500/9 TO 1000 STEP 500/9
7610 MOVE I-10,-25
7620 X=(I*9) DIV 50
7630 IF X>90 GOTO 7660
7640 PRINT;X
7650 GOTO 7680
7660 X=180-X
7670 PRINT;X
7680 NEXT I
7690 MOVE 1000,10
7700 PRINT "ANG.FLEX
                (DEG)"
7710 VDU 4
7720 ENDPROC
7730 DEFPROCaxis_three
7740 CLS
7750 CLG
7760 PRINT TAB(20,1)"           Filename.........";File$
7770 VDU 29,100;50;
7780 VDU 5
7790 MOVE 0,0
7800 DRAW 0,900
7810 MOVE 0,0
7820 DRAW 1000,0
7830 FOR J=100 TO 1000 STEP 100
7840 MOVE -10,J
7850 DRAW 10,J
7860 NEXT J
7870 FOR J=500/9 TO 1000 STEP 500/9
7880 MOVE J,10
7890 DRAW J,-10
7900 NEXT J
7910 FOR L=100 TO 1000 STEP 100
7920 W=1000/L
7930 Y=20/W
7940 IF Y>=10 MOVE -95,L+10
7950 IF Y<10 MOVE -80,L+10
7960 PRINT;Y
7970 NEXT L
7980 MOVE -50,950
7990 PRINT "LATERAL FORCE (N)"
8000 FOR I=500/9 TO 1000 STEP 500/9
8010 MOVE I-10,-25
8020 X=(I*9) DIV 50
8030 IF X>90 GOTO 8060
8040 PRINT;X
8050 GOTO 8080
8060 X=180-X
8070 PRINT;X
8080 NEXT I
8090 MOVE 1000,10
8100 PRINT "ANG.FLEX
                (DEG)"
8110 VDU 4
8120 ENDPROC
8130 DEFPROCaxis_four
```

```
8140 CLS
8150 CLG
8160 PRINT TAB(20,1)"           Filename.........";File$
8170 VDU 29,100;50;
8180 VDU 5
8190 MOVE 0,0
8200 DRAW 0,900
8210 MOVE 0,0
8220 DRAW 1000,0
8230 FOR J=100 TO 1000 STEP 100
8240 MOVE -10,J
8250 DRAW 10,J
8260 NEXT J
8270 FOR J=500/9 TO 1000 STEP 500/9
8280 MOVE J,10
8290 DRAW J,-10
8300 NEXT J
8310 FOR L=100 TO 900 STEP 100
8320 W=1000/L
8330 Y=20/W
8340 IF Y>=10 MOVE -95,L+10
8350 IF Y<10 MOVE -80,L+10
8360 PRINT;Y
8370 NEXT L
8380 MOVE -50,950
8390 PRINT "FORWARD FORCE (N)"
8400 FOR I=500/9 TO 1000 STEP 500/9
8410 MOVE I-10,-25
8420 X=(I*9) DIV 50
8430 IF X>90 GOTO 8460
8440 PRINT;X
8450 GOTO 8480
8460 X=180-X
8470 PRINT;X
8480 NEXT I
8490 MOVE 1000,10
8500 PRINT "ANG.FLEX
                (DEG)"
8510 VDU 4
8520 ENDPROC
8530 DEFPROCaxis_one_a
8540 CLS
8550 CLG
8560 PRINT TAB(20,1)"           Filename.........";File$
8570 VDU 29,100;50;
8580 VDU 5
8590 MOVE 0,0
8600 DRAW 0,942
8610 MOVE 0,0
8620 DRAW 1000,0
8630 FOR J=90 TO 900 STEP 90
8640 MOVE -10,J
8650 DRAW 10,J
8660 NEXT J
8670 FOR J=500/9 TO 1000 STEP 500/9
8680 MOVE J,10
8690 DRAW J,-10
8700 NEXT J
```

```
8710 FOR L=90 TO 900 STEP 90
8720 Y=2*L/9
8730 MOVE -95,L+10
8740 PRINT;Y
8750 NEXT L
8760 MOVE -50,950
8770 PRINT "RESULTANT FORCE (N)"
8780 FOR I=500/9 TO 1000 STEP 500/9
8790 MOVE I-85,-25
8800 X=(I*P)/5
8820 x%=X DIV 100
8830 PRINT x%
8860 NEXT I
8870 MOVE 1000,10
8880 PRINT "TIME
             (1/100s)"
8890 VDU 4
8900 ENDPROC
8910 DEFPROCaxis_three_a
8920 CLS
8930 CLG
8940 PRINT TAB(20,1)"           Filename.........";File$
8950 VDU 29,100;50;
8960 VDU 5
8970 MOVE 0,0
8980 DRAW 0,942
8990 MOVE 0,0
9000 DRAW 1000,0
9010 FOR J=90 TO 900 STEP 90
9020 MOVE -10,J
9030 DRAW 10,J
9040 NEXT J
9050 FOR J=500/9 TO 1000 STEP 500/9
9060 MOVE J,10
9070 DRAW J,-10
9080 NEXT J
9090 FOR L=90 TO 900 STEP 90
9100 Y=2*L/9
9110 MOVE -95,L+10
9120 PRINT;Y
9130 NEXT L
9140 MOVE -50,950
9150 PRINT "LATERAL FORCE (N)"
9160 FOR I=500/9 TO 1000 STEP 500/9
9170 MOVE I-85,-25
9180 X=(I*P)/5
9200 x%=X DIV 100
9210 PRINT x%
9240 NEXT I
9250 MOVE 1000,10
9260 PRINT "TIME
             (1/100s)"
9270 VDU 4
9280 ENDPROC
9290 DEFPROCaxis_four_a
9300 CLS
9310 CLG
9320 PRINT TAB(20,1)"           Filename.........";File$
```

```
9330 VDU 29,100;50;
9340 VDU 5
9350 MOVE 0,0
9360 DRAW 0,942
9370 MOVE 0,0
9380 DRAW 1000,0
9390 FOR J=90 TO 900 STEP 90
9400 MOVE -10,J
9410 DRAW 10,J
9420 NEXT J
9430 FOR J=500/9 TO 1000 STEP 500/9
9440 MOVE J,10
9450 DRAW J,-10
9460 NEXT J
9470 FOR L=90 TO 900 STEP 90
9480 Y=2*L/9
9490 MOVE -95,L+10
9500 PRINT;Y
9510 NEXT L
9520 MOVE -50,950
9530 PRINT "FORWARD FORCE (N)"
9540 FOR I=500/9 TO 1000 STEP 500/9
9550 MOVE I-85,-25
9560 X=(I*P)/5
9580 x%=X DIV 100
9590 PRINT x%
9620 NEXT I
9630 MOVE 1000,10
9640 PRINT "TIME
              (1/100s)"
9650 VDU 4
9660 ENDPROC
9670 DEFPROCplot_one_a
9680 VDU 5
9690 FOR I%=1 TO 20
9700 T%(I%)=T%(I%) MOD (P*2)
9710 MOVE T%(I%)*500/P-7,r(I%)*9/2+10
9720 PRINT CHR$42
9730 NEXT
9740 VDU 4
9750 ENDPROC
9760 DEFPROCplot_three_a
9770 VDU 5
9780 FOR I%=1 TO 20
9790 T%(I%)=T%(I%) MOD (P*2)
9800 MOVE T%(I%)*500/P-7,s(I%)*9/2+10
9810 PRINT CHR$42
9820 NEXT
9830 VDU 4
9840 ENDPROC
9850 DEFPROCplot_four_a
9860 VDU 5
9870 FOR I%=1 TO 20
9880 T%(I%)=T%(I%) MOD (P*2)
9890 MOVE T%(I%)*500/P-7,d(I%)*9/2+10
9900 PRINT CHR$42
9910 NEXT
9920 VDU 4
```

```
 9930 ENDPROC
 9940 DEFPROCaxis_two_a
 9950 CLS
 9960 CLG
 9970 PRINT TAB(20,1)"           Filename.........";File$
 9980 VDU 29,100;50;
 9990 VDU 5
10000 MOVE 0,0
10010 DRAW 0,900
10020 MOVE 0,0
10030 DRAW 1000,0
10040 FOR J=100 TO 1000 STEP 100
10050 MOVE -10,J
10060 DRAW 10,J
10070 NEXT J
10080 FOR J=500/9 TO 1000 STEP 500/9
10090 MOVE J,10
10100 DRAW J,-10
10110 NEXT J
10120 FOR L=100 TO 1000 STEP 100
10130 W=L/10
10140 MOVE -95,L+10
10150 PRINT;W
10160 NEXT L
10170 MOVE -50,950
10180 PRINT "ANGLE OF FORCE (DEG)"
10190 FOR I=500/9 TO 1000 STEP 500/9
10200 MOVE I-85,-25
10210 X=(I*P)/5
10220 x%=X DIV 100
10230 PRINT x%
10240 NEXT I
10250 MOVE 1000,10
10260 PRINT "TIME
               (1/100s)"
10270 VDU 4
10280 ENDPROC
10290 END
```

Simulator data collection help program

```
    5 MODE 135
   10 VDU 23,1,0;0;0;0;0
   20 VDU 14
   30 PRINT SPC 15"USER GUIDE"
   40 PRINT
   50 PRINT
   60 PRINT "INTRODUCTION"
   70 PRINT
   80 PRINT "The package you are using will enable   you to take force measure
ments at will  during cyclical testing of a finger     joint prosthesis in the
 simulator."
   90 PRINT "All the important data will be stored onthe results disc in drive
 1 and can be  viewed either in table form or graphicalform via this program."
   91 PRINT "It is also possible to obtain hard      copies of the data and th
e graphs but   the discs must first be transferred to aBBC connected to a prin
ter!"
   92 PRINT
```

```
   93 PRINT
   94 PRINT "     PRESS SHIFT TO SCROLL ON"
   95 PRINT
   96 PRINT
  100 PRINT "Set up the simulator and run it as usualmaking sure that the stra
in gauges,     amplifiers etc, have had ample time to  warm up and reach stead
y state          (about 1 hr)."
  110 PRINT "Load the systems disc into drive 0 and  the results disc into dri
ve 1 then pressshift/break to obtain the program menu."
  129 PRINT
  130 PRINT "MENU"
  140 PRINT
  150 PRINT SPC 10"1)Run Test"
  160 PRINT SPC 10"2)View Data"
  170 PRINT SPC 10"3)View Graphs"
  180 PRINT SPC 10"4)Help"
  190 PRINT
  200 PRINT "      When this appears type in                the number you req
uire."
  210 PRINT
  220 PRINT "RUN TEST"
  230 PRINT
  235 PRINT "It is important to note that this optionwill only run on this BBC
 which is      connected to an IEEE interface!"
  240 PRINT "The first screen asks for the following information:"
  250 PRINT
  260 PRINT SPC 10"Filename?"
  270 PRINT SPC 10"1)Half or 2)Full Bridge?"
  280 PRINT SPC 10"Test Description?"
  290 PRINT SPC 10"Speed (1/100 s)"
  300 PRINT
  310 PRINT "For the filename just type the name of  the file you wish to crea
te and press   return. It may be useful to call it by  the date or something."
  320 PRINT "For the bridge you must decide whether  you want to measure large
 static forces (Full) or small dynamic ones (Half or   Full). Check the amplif
ier connections  then type 1 or 2 followed by return."
  330 PRINT "For the description you may type        anything you wish that wi
ll describe thetest you are doing. For instance, you   may wish to include the
 date and the    name of the prosthesis. Again you must  type return on comple
tion."
  360 PRINT "For the speed you are required to input the time taken for the jo
int to flex    from 0 to 90 degrees. This must be in   1/100 s (EG.50) then pr
ess return."
  370 PRINT
  380 PRINT "When you have put in all the required   information the computer
will ask if youwish to alter anything. If you have mis-typed something it can
be altered at    this stage."
  390 PRINT "When you are happy with everything you  will be prompted to press
 the space bar when readings are to be taken."
  400 PRINT "Since the simulator is not computer     controlled the bar must b
e pressed as   the joint reaches 0 degrees flexion."
  410 PRINT "The computer will take and store the    readings and then ask if
you would like to:"
  420 PRINT
  430 PRINT "1)Take more readings, 2)Go back to menu."
  440 PRINT
  450 PRINT SPC 8"Type the required number."
  460 PRINT
```

```
  470 PRINT "VIEW DATA"
  480 PRINT
  490 PRINT "This will give you the opportunity to   view the files stored on
the results    disc and then ask you to choose a file  to view."
  500 PRINT "The data will be displayed over two     screens and then a furthe
r five options given. Type in the required number but  beware the hardcopy opt
ion needs a      printer."
  510 PRINT
  520 PRINT "VIEW GRAPHS"
  530 PRINT
  540 PRINT "This will give you the opportunity to   view the files stored on
the results    disc and then ask you to choose a file  to view."
  550 PRINT "You must choose from a choice of four   graphs (again hardcopies
can only be    made when connected to a printer)."
  560 PRINT "After each graph you may choose to view a different graph, choose
 another file  or go back to menu."
  565 PRINT
  566 PRINT "         PRESS SPACE BAR FOR MENU"
  567 IF INKEY-99 GOTO 580
  568 GOTO 567
  570 VDU 15
  580 CHAIN "$.MENU"
  590 END
```